# Characterization of the coiled-coil domain-containing protein 124 (Ccdc124) as a novel centrosome and midbody component involved in cytokinesis

A THESIS SUBMITTED TO
THE DEPARTMENT OF MOLECULAR BIOLOGY AND GENETICS
AND THE GRADUATE SCHOOL OF ENGINEERING AND SCIENCE OF
BILKENT UNIVERSITY
IN PARTIAL FULFILLMENT OF THE REQUIREMENTS FOR
THE DEGREE OF DOCTOR OF PHILOSOPHY

**BY**
**PELİN TELKOPARAN AKILLILAR**
**JUNE 2013**

I certify that I have read this thesis and that in my opinion it is fully adequate, in scope and in quality, as a thesis for the degree of Doctor of Philosophy.

Prof. Dr. Mehmet Öztürk (Advisor)

I certify that I have read this thesis and that in my opinion it is fully adequate, in scope and in quality, as a thesis for the degree of Doctor of Philosophy.

Assoc. Prof. Dr. Uygar H. Tazebay (Co-advisor)

I certify that I have read this thesis and that in my opinion it is fully adequate, in scope and in quality, as a thesis for the degree of Doctor of Philosophy.

Assist. Prof. Dr. A Elif Erson Benson

I certify that I have read this thesis and that in my opinion it is fully adequate, in scope and in quality, as a thesis for the degree of Doctor of Philosophy.

Assist. Prof. Dr. Nurhan Özlü

I certify that I have read this thesis and that in my opinion it is fully adequate, in scope and in quality, as a thesis for the degree of Doctor of Philosophy.

Assist. Prof. Dr. Ali O. Güre

I certify that I have read this thesis and that in my opinion it is fully adequate, in scope and in quality, as a thesis for the degree of Doctor of Philosophy.

Assist. Prof. Dr. Özlen Konu

Approved for the Graduate School of Engineering and Science

Prof. Dr. Levent Onural
Director of the Graduate School

# ABSTRACT

## CHARACTERIZATION OF THE COILED-COIL DOMAIN-CONTAINING PROTEIN 124 (CCDC124) AS A NOVEL CENTROSOME AND MIDBODY COMPONENT INVOLVED IN CYTOKINESIS

Pelin Telkoparan Akıllılar
Ph.D. in Molecular Biology and Genetics
Supervisor: Prof. Dr. Mehmet Öztürk
Co-advisor: Assoc. Prof. Dr. Uygar H. Tazebay
June 2013, 259 Pages.

Cytokinetic abscission is the cellular process leading to physical separation of two postmitotic sister cells by severing the intercellular bridge. During cell division several functional complexes accumulate at the bridge connecting the two sister cells. The most noticeable structural component of the intercellular bridge is a transient organelle termed as midbody. This novel organelle is localized at a central region, which marks the site of cytokinetic abscission. Despite its major role in completion of cell divison, our understanding of spatiotemporal regulation of midbody assembly is incomplete. In this thesis work, we first characterizated the coiled-coil domain-containing protein-124 (Ccdc124), a eukaryotic protein conserved from fungi-to-man, at the molecular level. We identified that at the sub-cellular level Ccdc124 is localized at centrosomes and the midbody depending on stages of the cell cycle. In interphase cells, as well as in mitosis, the protein is localized to centrosomes. However at later stages of cytokinesis (late-anaphase/telophase) Ccdc124 translocates to the midbody. Knockdown of Ccdc124 in human HeLa cells leads to accumulation of enlarged and multinucleated cells; however, centrosome maturation was not affected. Similarly, in preliminary *in vivo* assays involving down-regulation of Ccdc124-homologue in zebra fish early embryos, we observed multinuclear embryonic cells. Furthermore, we have validated a previously observed *in vitro* interaction in our laboratory between Ccdc124 and the Ras guanine nucleotide exchange factor 1B (RasGEF1B) by co-immunoprecipitation assays. As RasGEF1B is strictly a Rap2 GTP-binding protein specific nucleotide exchange factor, this result has suggested a possible involvement of Rap2 in cytokinesis related events. Thus, subsequently, we assessed the sub-cellular localization of Rap2 in synchronized cells during cytokinesis. We found that even though it does not play a role in cell division, Rap2 is localized to the midbody. This result establishes a functional link between cytokinesis and activation of localized Rap2 signaling at the midbody. Data presented in this thesis work indicate that Ccdc124 is a novel factor operating both for proper progression of late cytokinetic stages in eukaryotes, and for establishment of Rap2 signaling dependent cellular functions proximal to the abscission site.

***Keywords***: Ccdc124, Centrosome, Cytokinesis, Midbody, Rap2 signaling, RasGEF1B

# ÖZET

## COILED-COILED DOMAIN-CONTAINING PROTEIN 124 (CCDC124)'ÜN SİTOKİNEZDE ROL OYNAYAN YENİ BİR SENTROZOM VE ORTA-CİSİMCİK (MIDBODY) PROTEİNİ OLARAK TANIMLANMASI

Pelin Telkoparan Akıllılar
Moleküler Biyoloji ve Genetik Doktorası
Tez Yöneticisi: Prof. Dr. Mehmet Öztürk
Eş Danışman: Assoc. Prof. Dr. Uygar H. Tazebay
Haziran 2013, 259 Sayfa.

Sitokinetik ayrılma, hücre bölünmesinde iki hücre birbirinden ayrılırken hücreler arası köprünün fiziksel olarak kopmasını sağlayan hücresel süreçtir. Hücre bölünmesi sırasında pekçok işlevsel yapı hücreler arası köprüde bir araya gelerek bölünmeyi düzenlerler. Hücreler arası köprünün en belirgin parçası, köprünün orta bölgesinde lokalize olan ve kopuş noktasını belirleyen orta-cisimcik (midbody) adındaki geçici organeldir. Hücrelerin düzgün şekilde bölünmesi esnasındaki önemli rolüne rağmen, orta-cisimciği oluşturan proteinlerin tamamı ve bunların nasıl düzenlediği tam olarak bilinmemektedir. Bu tez çalışmasında, insandan mayaya kadar korunmuş yeni bir ökaryotik protein olan coiled-coil domain-containing protein-124 hücresel, moleküler, ve işlevsel olarak tanımlanmıştır. Çalışmada sunulan sonuçlar, Ccdc124'ün hücre döngüsünün evrelerine bağlı olarak sentrozom ve orta-cisimcikte konumlanan yeni bir protein olduğunu göstermektedir. Ccdc124 interfaz evresi ve mitozun erken safhalarında sentrozoma lokalize olurken, sitokinezin geç evrelerinde (geç-anafaz/telofaz) sentrozomdan ayrılarak orta-cisimciğe konumlanmaktadır. İnsan HeLa hücre modelinde yaptığımız çalışmalarda, Ccdc124 ifadesinin düşürülmesi sonucunda sentrozom sayısı ve oluşumu etkilenmezken, büyük ve çoklu sayıda çekirdeğe sahip (bi/multinuclear) hücrelerin sayısının arttığını belirledik. Aynı şekilde, zebra balığı erken embriyolarında yapılan öncü çalışmalarda, Ccdc124 gen ifadesinin baskılanması benzer şekilde çok-çekirdekli embriyonik hücre oluşumlarına sebep olmuştur. Bunlara ek olarak, bu tez çalışmasında, daha önce laboratuvarımızda *in vitro* olarak gösterilmiş olan Ccdc124'ün Ras-guanin nükleotid değişim faktörü proteini-1B (Ras-guanine nucleotide exchange factor-1B, RasGEF1B) etkileşimi birlikte çökeltme deneyleri ile valide edilmiştir. RasGEF1B sadece Rap2 GTP-bağlayan proteine özgü bir aktivatör değişim faktörü olduğu için, bu sonuç Rap2 proteininin de hücre bölünmesi sırasında veya sonrasında rolü olabileceğini düşündürmüştür. Bu nedenle, senkronize edilmiş hücrelerde sitokinez sırasında Rap2 G-proteinin hücresel konumunu araştırdık. Bunun sonucunda, Rap2'nin hücre bölünmesi sırasında rol oynamamasına rağmen, bölünme sırasında orta-cisimcikte konumlandığını bulguladık. Bu tez çalışması, aynı zamanda bir sentrozom proteini olan Ccdc124 proteininin orta-cisimcikte konumlanarak sitokinez ile, sitokinez sonrası hücresel işlevleri düzenleyen yeni bir moleküler faktör olarak işlev gördüğünü gostermektedir.

***Anahtar kelimeler***: Ccdc124, orta-cisimcik (Midbody), Rap2 sinyal yolu, RasGEF1B, sentrozom, sitokinez

*To my precious family…*

*Aileme...*

# ACKNOWLEDGEMENTS

First of all, I would like to offer my heartfelt thanks to my supervisor, Assoc. Prof. Uygar Tazebay for giving me the opportunity to work in his lab, for his guidance, for his endless support during years and for his friendship. He is not just a mentor for me; he is also my Life Coach.

I would like to thank Prof. Mehmet Öztürk for giving me a chance in Kaniltek project, for his interest and for his support.

I would like to offer my special thanks to Dr. Hani Alotaibi for teaching me how to be a graduate student, for sharing me his invaluable knowledge and for his friendship.

I am really grateful to my best friends Dilek and Ayşegül, life would not be full of fun without you. I also would like thank other Öztürk Lab present members Gökhan, Derya, French Muhtar Emre, Yusuf, Merve, Engin, Umur, Çigdem and past members Mustafa, Özge, Haluk, Nilgün.

I also want to thank all present and past MBG family especially Elif Yaman, Serap, Mutlu, Defne, Emre, Fuat, Verda, Fusun, Gulsah, Fusun Elvan, Abdullah Amca, Yavuz Abi, Bilge.

Morever I want to thank all Faculty members at MBG, Bilkent University

I would like to thank my advisors in Utrecht Medical Center Prof. Johannes L. (Hans) Bos, Assoc. Prof. Holger Rehmann and my friends Dr. Lars Meijer, Dr. Martijn Gloerich, Sarah Consonni, and Dr. Willem-Jan Pannekoek.

I would like to thank my family for their patience and endless support. I am living away from you and Eskisehir for years I hope it was worth it.

I would like to thank my husband Emre, for his support and for his patience. If you were not force me about coming Ankara, I would not be PhD.

I would like to thank Stefan Fuss and Xalid Bayramlı for Zebrafish studies in Bogazici University.
I am grateful to Greenfield Sluder for GFP-Centrin containing RPE1 cells, to Prasad Jallepalli for providing RPE1 cells with GFP-Plk1(WT), to Daniel Pak for Rap2-WT-HA, Rap2-G12V-HA, and Rap2-S17N-HA expression vectors

My graduate studies and this thesis work was supported by TÜBİTAK (TBAG-109T049 and 109T925)

Collaborative Research at the Laboratory of Prof. Dr. Johannes L. Bos, Utrecht University was supported by European Science Foundation (ESF), Frontiers of Functional Genomics Grant Programme.

# TABLE OF CONTENTS

# LIST OF TABLES

# LIST OF FIGURES

## ABBREVIATIONS

| | |
|---|---|
| Ab | Antibody |
| ATP | Adenosine triphosphate |
| CDK | Cyclin Dependent Kinase |
| C-terminus | carboxy terminus |
| $ddH_2O$ | Double distilled water |
| DMEM | Dulbecco's Modified Eagle's Medium |
| EDTA | ethylenediaminetetraacetic acid |
| FACS | Fluorescence-activated cell sorting |
| FBS | Fetal Bovine Serum |
| g | gram |
| hpf | hours postfertilization |
| IF | Immunofluorescence |
| IP | Immunoprecipitation |
| kb | Kilo base |
| kDa | Kilo Dalton |
| LB | Luria-Bertani media |
| LC-MS/MS | liquid chromatography-mass spectrometry |
| µg | microgram |
| mg | milligram |
| µl | microliter |
| ml | milliliter |
| N-terminus | amino terminus |
| OD | Optical Density |
| O/N | Over night incubation |
| PAGE | Polyacrylamide gel electrophoresis |

| | |
|---|---|
| PBS | Phosphate Buffered Saline |
| PBS-T | Phosphate Buffered Saline with Tween-20 |
| PCR | Polymerase chain reaction |
| PEI | polyethylenimine |
| RT | Room temperature |
| shRNA | short hairpin RNA |
| SILAC | Stable isotope labeling by amino acids in cell |
| siRNA | Small interfering RNA |
| TB | Transformation buffer |
| TBS | Tris Buffered Saline |
| TBS-T | Tris Buffered Saline with Tween-20 |
| WB | Western Blotting |

# CHAPTER 1. INTRODUCTION

## 1.1 The Cell Cycle

All living organisms starting from primitive unicellular bacteria to the most developed multicellular ones are generated by a repeated cycle mechanism, known as the cell cycle. The cell cycle is both a complex and a highly ordered process. During the process one cell duplicates its genome accurately, and it is divided into new but genetically identical two daughter cells. In addition to genomic duplication, cells also duplicate their other organelles and mass of proteins to maintain their size. Conversely, to maintain the nucleo-cytoplasmic ratio, duplication of DNA content and cytoplasmic content is viably bound to each other.

The eukaryotic cell cycle is divided into four sequential different phases: the first gap interval (G1), DNA synthesis phase (S), the second gap interval (G2), and the mitosis phase (M; *see below*). G1, S, and G2 phases are together known as the interphase, which altogether takes close to 23 hours in higher eukaryotes followed by 1 hour of M phase [1]. In the synthesis or S phase, DNA replicates itself, which nearly takes half of the cell cycle time. Following the S phase, generation of bipolar mitotic spindles, segregation of sister chromatids, and separation of cells occur during the M phase. Cytokinesis, or separation of two daughter cells can either be considered as the final part of the M phase, or it is also called as the cytokinesis phase (C phase) distinct from the M phase [2]. The G1 and G2 phases, which stand for “gaps” in the cell cycle, are intervals between DNA synthesis (S phase) and mitosis (M phase). These two gaps allow cell growth, and provide time to ensure cellular conditions suitable for progression of S and M phases. The cell is preparing for DNA synthesis during the G1 phase, and its length is determined by external conditions. If external conditions are not suitable for cell cycle progression, then cells may enter resting G-zero ($G_0$) state. $G_0$ cells do not actively go through the cell cycle (quiescent) until conditions are suitable for the growth [3]. Similarly, cells prepare for the M phase during G2, which is the second gap interval in the cell cycle.

The progression of the cell cycle depends on the external signals such as mitogens and growth factors. The cell responds to these extracellular signals via pathways regulated by cyclins through their associations with cyclin-dependent-kinase proteins

(CDKs), [4]. CDKs are serine/threonine kinases that are activated at specific times in the cell cycle (Fig. 1.1), [5].

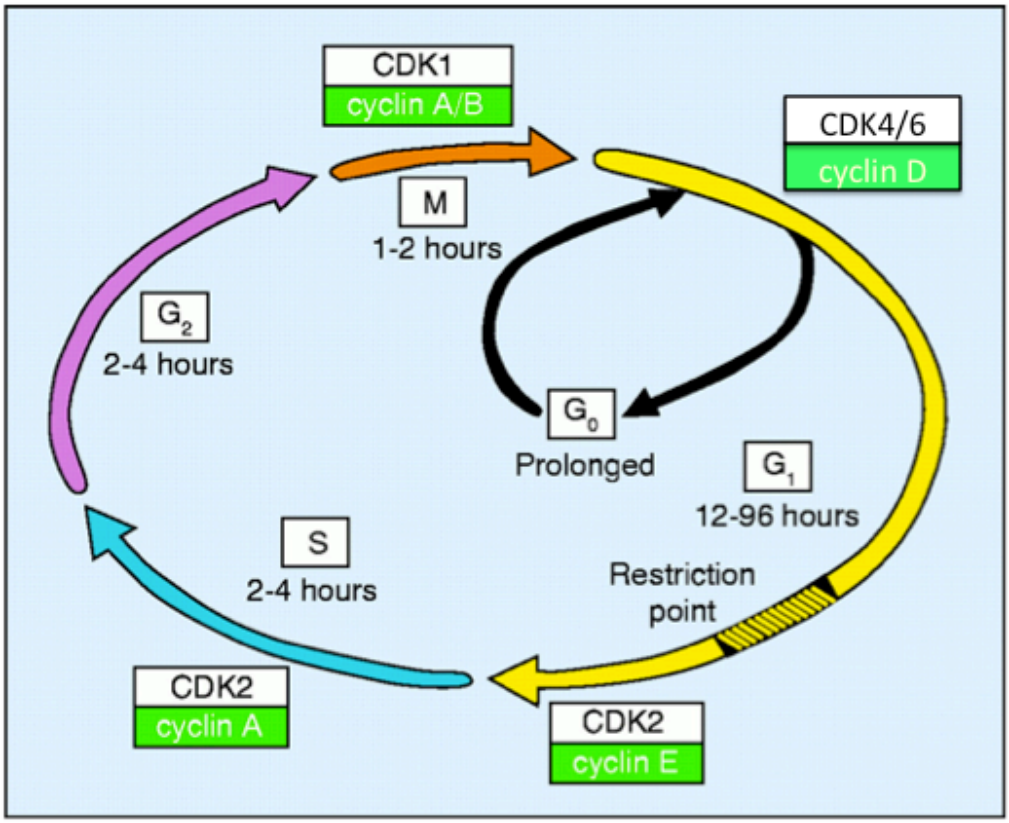


**Figure 1.1. The Cell Cycle.** Schematic drawing of cell cycle dependent activation of cyclins and CDKs. Modified from, Israels and Israels, 2000, The Cell Cycle, *The Oncologist* 5, 510-513, ©AlphaMed Press.

The constant activity of the CDKs during cell cycle progression is critical, because inhibition of their activities may cause disruption of mitosis [1]. CDKs are primarily regulated by interactions of specific cyclin molecules that are continuously synthesized or degraded in a stage dependent manner throughout the cell cycle. Typically, cyclins bind to CDKs, and via nuclear localization signals on cyclins, CDKs are targeted to the nucleus where they phosphorylate a variety of cell cycle regulatory substrates (*see below*). There are four main classes of cyclins: G1-cyclin

(cyclin D), G1/S-cyclin (cyclin E), S-cyclin (cyclin A) and M-cyclin (cyclin B). During G1 phase, cyclin D associates with Cdk4 and Cdk6 and formation of the cyclin/CDKs complexes results activation of CDKs by their phosphorylation [6]. Moreover, they phosphorylate a key protein, Retinoblastoma (Rb) protein that regulates G1 phase of the cell cycle by controlling the critical restriction point (R-point) of the G1. In fact, hypo-phosphorylated Rb forms complex with E2F, which is a transcription factor, and inhibits transcription of the target genes. After phosphorylation of Rb by the cyclinD/CDK4-6 complexes, Rb dissociates from E2F and allows transcription of target genes [5]. One of them is cyclin E, which complexes with Cdk2, and it is required for passage of restriction point. In the meantime, Rb stays in phosphorylated form until completion of mitosis. The cyclinE/CDK2 complexes are required for transition from G1 to S phase of the cell cycle. During G1/S transition the expression of cyclin A increases and stays stable through the S phase [4]. In the early S phase, cyclin A complexes with Cdk2 and then, in the late S phase, form complex with cdk1. Cyclin A/CDK2 complex initiates DNA synthesis and their activity remains high during G2 until that prevents excess DNA replication by binding site of replication site. Following to the completion of DNA replication, cell division occurs during M phase, and the activation of mitotic events is triggered by formation of cyclin B/CDK1 complexes [1]. When cells are ready to divide, cdc25 activates cdk1 by dephosphorylating this key kinase molecule. Cyclin B/CDK1 triggers chromosomal condensation, nuclear envelope breakdown, cytoskeleton rearrangement, and reorganization of Golgi and endoplasmic reticulum [1].

### 1.1.1. Cellular Aspects of Different Stages of Mitosis and Cytokinesis

M phase could be considered as the most complicated and highly regulated phase of the cell cycle, which is divided into six major stages: the first five stages involves nuclear division (mitosis) and the last one is known as the cytokinetic abscission (Fig. 1.2), [7]. Once the size of the cell increases, and chromosomes replicated concomitant to centrosome duplication, mitosis (M) begins with the prophase. At this initial stage, replicated chromosomes condense by recruiting specialized proteins called condensins [7] forming two identical sister chromatids. In the meantime the

mitotic spindles begin to be formed by the centrosomes translocating to two opposite cellular poles (*see below*). Prometaphase begins with the breakdown of the envelop into vesicles, which is an important step for spindle assembly, as it facilitates attachment of chromosome kinetochores to centrosomes (or spindle pole bodies in lower eukaryotes) that are located at two opposite poles of the cell. During metaphase, chromosomes are in their most compact form and can be easily visualized at this stage. Chromosomes are aligned at the center of the cell on the metaphase plate and sister chromatids are attached to spindles poles via microtubules of kinetochores.

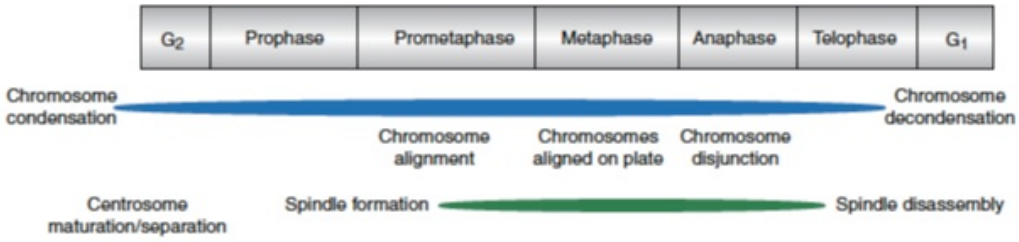


**Figure 1.2. Comparison of the phases of mitosis in terms of their chromosome condensation and alignment status.** Modified from Pines and Rieder, 2001, Re-staging mitosis: a contemporary view of mitotic progression. *Nature Cell Biology* 3, E3-E6, ©2001 Macmillan Magazines Ltd.

At anaphase microtubules of kinetochores start shortening and spindle poles move to outward. As a result, sister chromatids partition to dividing daughter cells. The last step of the mitosis is telophase, during which sister chromatids arrive to the spindle poles, and chromosomes start to decondensate. The nuclear membrane reassembles around each chromosome, and finally contractile ring begins to form to prepare the cell to cytokinesis; the process of separation of daughter cells from each other. The molecular requirements for cytokinesis are highly conserved among all major animal model systems (Fig. 1.3), [8]. Cytokinesis is initiated with assembly of antiparallel microtubules at the center of spindle midzone, which is called central spindle during anaphase [9]. At final stages of cytokinesis, separation of sister cells are completed by a process called abscission, which leads to irreversible fission of plasma membranes at the intercellular bridge between dividing cells.

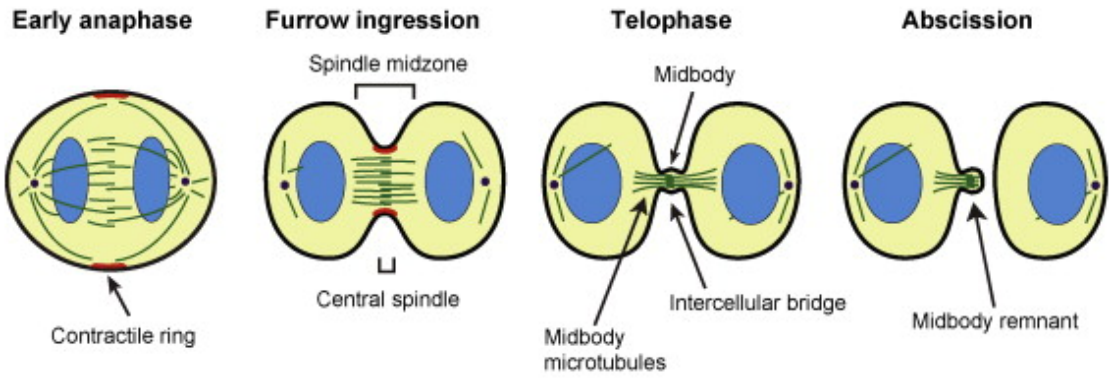


**Figure 1.3. Schematic diagram of the different stages of cytokinesis.** Microtubules, green; chromatin, blue; contractile actin ring, red; centrosomes, black dots. Modified from Guizetti and Gerlich, 2010, Cytokinetic abscission in animal cells. *Seminars in Cell and Developmental Biology*, 21, 909-916, ©2010 Elsevier Ltd.

### 1.1.2. Molecular Regulation of Cytokinetic Abscission

In dividing animal cells, cytokinesis initiates with the assembly and constriction, organized by signaling from the anaphase spindle of an equatorial contractile ring. Two main components of the cytoskeleton, actin and tubulin are essential structural proteins for successful cytokinesis in eukaryotes. Together with spindle asters, the central spindle determines the position of the cleavage plane by directing localization and activation of the key G protein, Ras-homologue A (RhoA), at the cell cortex [10]. RhoA GTP-binding proteins are lipid-modified molecules, and this modification allows association with the plasma membrane at the ingressed cleavage furrow close to the midzone. Like all Ras-superfamily of GTP-binding proteins, RhoA bound to guanosine triphosphate (GTP) is in its active form, while when it is bound to guanosine diphosphate (GDP) it is inactive [10]. GDP/GTP re-exchange, and thus activation of RhoA is carried-out by the translocation of a RhoA-specific guanine nucleotide exchange factor (GEF) named as Ect2 to the midzone. Then, RhoA directly activates formins, and active formin proteins elongate the linear actin filaments for formation of contractile ring. Also, RhoA indirectly activates myosin II motor activity by phosphorylation of myosine light chain with the help of ROCK and citron kinases [11]. Subsequently, activated myosin II binds to actin filaments, and triggers constriction of the contractile ring. In fact, Ect2 is itself recruited to the central spindle by binding to Centralspindlin complex component CYK-4 [10].

Centralspindlin is mostly important for animal central spindle assembly, which is a hetero-tetrameric complex consisting of homodimers of both CYK-4 (RhoGAP) and MKLP1 (mitotic kinesin-like protein) proteins. Importantly, the interaction between CYK-4 and Ect2 is regulated by Plk1 (polo-kinase-1), and Plk1 is recruited to central spindle through microtubule-associated protein PRC1 [8]. On the other hands, Cdk1 negatively regulates these interactions, and it inactivates Ect2, MKLP1, and PRC1 by phosphorylating these effectors in early stages of mitosis, and thus it prevents premature cytokinesis. During anaphase after segregation of chromosomes, the activity of Cdk1 begins to decline and inhibitory sites of multiple spindle components are dephosphorylated [12] and cytokinesis is triggered (cytokinetic furrow formed). Aurora B is another key mitotic regulator kinase, which is involved in establishment of the timing of cytokinetic abscission [13]. Aurora B targets a number of proteins that localize to the cleavage furrow. Therefore, it has been proposed that phosphorylation of intermediate filaments at the cleavage furrow destabilizes the filaments in preparation for cytokinesis [14, 15]. Aurora B also phosphorylates myosin II regulatory light chain at the cleavage furrow. Inhibition of Aurora B activity prevents proper myosin II localization to the cleavage furrow and disrupts spindle midzone organization [16]. Mutation of Aurora B target sites in intermediate filament proteins leads to defects in filament deformation and prevents the final stage of cytokinesis [15].

After completion of cleavage furrow formation, two daughter cells remain connected to each other with a thin intracellular bridge, which contains dense antiparallel microtubule bundles that overlap at a central region called midbody. The cytoplasmic bridge between two daughter cells must be cleaved to form genetically identical two cells. This terminal stage of cytokinesis is known as the abscission stage [17]. Abscission occurs by removal of cytoskeletal structures from intracellular bridge, followed by constriction of cell cortex and plasma membrane fission. Following the ingression of the intracellular bridge until actomyosin ring reaches to 1-2 μm diameter, Golgi and recycling endosome-derived vesicles accumulate at the midbody region during late-telophase (*see below*). Vesicles in intracellular bridge fuse with plasma membrane, and they increases surface of the membrane before abscission. In addition, midbody accumulation of many different vesicle targeting and tethering

factors, including centriolin and exocyst complex, Rab35, Rab11-FIP3, v- and t-SNARES and BRUCE are required for efficient abscission [18].

### 1.2 The Role of Centrosome in Cell Division

Microtubules (MT) are highly dynamic tubular polymers and they are essential component of cytoskeleton proteins in all eukaryotic organisms. MTs have critical roles in many cellular processes such as intracellular transport of proteins and organelles, motility of motor proteins, establishment of cell polarity and cell division [19, 20]. MTs are hollow tubes with fast growing plus ends and slowly growing minus ends, and they are composed of α- and β-tubulin proteins. These proteins form heterodimers when bound to GTP and come together with lateral and longitudinal contacts [20]. The structure of MTs is not stable, and in dividing cells MT dimers reorganize to form bipolar mitotic spindles in a cell cycle dependent manner [19]. The organizations of all these properties of MTs are arranged by microtubule organizing centers (MTOCs). Major MTOCs in eukaryotes are centrosomes in animal cells, and spindle pole bodies in fungi [19]. The centrosome is a subcellular non-membrane bound organelle that regulates the MT spatial organization and nucleation [21]. Thus it influences many cellular activities including maintenance of cell shape, motility, cell polarity, spindle formation, chromosomal segregation, and cell division [22].

The centrosome consists two cylindrical centrioles and pericentriolar material (PCM) that surrounds the centrioles (Fig. 1.4). Centrioles are cylinders made of nine MT triplets found in many eukaryotes and organize two important organelles; cilia and centrosome. The older centriole is known the mother or mature centriole, and the younger one is known as the daughter centriole [23]. They are polarized through proximal- and distal-axis, and while both of them recruits MTs in their vicinity, only mother centriole can bind MTs at the subdistal apandages [24]. Centrioles are surrounded by electron dense material, pericentriolar matrix (PCM) that contains many coiled-coil domain containing centrosomal proteins and γ-tubulin together with γ-TuRC. PCM associated with centriols and regulate their assembly [22].

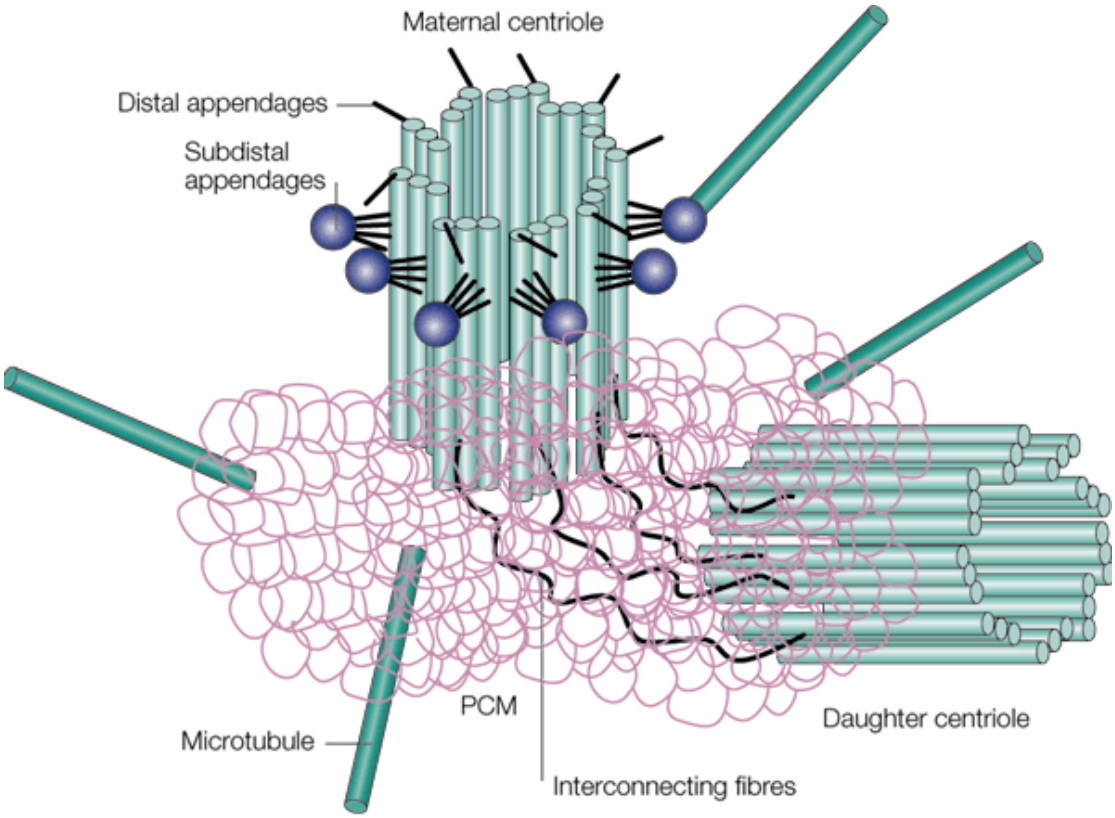


**Figure 1.4. The centrosome is composed of two centrioles, connected by interconnecting fibers and surrounded by the pericentriolar material (PCM).** Microtubules are nucleated from the pericentriolar matrix and the appendages of the maternal centriole. Figure adapted from *Nature Rev. Mol. Cell Biol*. 2, 688-698. © 2001 Macmillan Magazines Ltd.

Centrosomes are duplicated once per cell cycle, and there are four main phases of centrosome duplication: centriole disengagement, nucleation of daughter centriols, elongation of procentrioles and separation of centrosomes [21]. Disengagement of centrioles occurs during G1/S and it is important for limiting duplication of centrioles once per cell cycle. The disengagement of centrioles is catalysed by proteolytic activity of separase proteins [25]. Under cell cycle regulation by the kinase Plk1, separase enzyme cleaves cohesin that bind two centrioles to each other [22]. During S phase, centriole assembly factors accumulate and the newly synthesized daughter centrioles remain tightly bound to mother centriole, which elongate throughout S and G2 phases. At the last step of the centriole cycle at the G2/M transition, centrioles accumulate more PCM and duplicated centrosomes are separated and form the bipolar mitotic spindlepoles [25].

In early studies, one of the components of centrioles was thought to be microtubule-organizing structures for assembling the mitotic spindles. However, many eukaryotes such as fungi and higher plants do not contain centrioles, yet they could still organize bipolar mitotic spindles. Interestingly, when centrioles were removed by laser ablation, mitotic spindles still formed [26, 27]. Furthermore, to obtain direct experimental support, Renata *et al.* [28] inhibited centrioles formation in flies and mutant flies were developed normally, but they were suffered from defects in their sensory organelle cilia. These studies clearly indicated that centrioles are not essential for microtubule organization, and the components that promote the formation and organization of microtubules were mostly found in the surrounding dynamic proteinaceous material, PCM [19]. The exact composition of PCM is still not known, even though several high throughput proteomics studies have addressed this issue [29,30]. Among proteins associated with PCM, γ-tubulin is found as an essential factor for microtubule nucleation, and microtubule organization in all eukaryotic organisms. It was firstly found in the filamentous fungus *Aspergillus nidulans,* and it was identified as an essential factor for formation of microtubules from the spindle pole body [31, 32]. γ-tubulin nucleates polymerization of the microtubules form α- and β-tubulin monomers. Early studies on biochemistry of γ-tubulin show that it forms complex with members of gamma complex proteins (GCPs), which coming together with γ-tubulin, they form the γ-TuRC complex [19]. In addition to nucleation and organization features of γ-TuRC, it also stabilizes microtubules by capping minus ends and prevents depolimerization of the microtubules [19].

### 1.3 The Midbody Composition and Formation at the Cytokinetic Abscission

The midbody is an electron dense transient organelle formed at the mid-space between dividing cells, first described by German biologist Walther Flemming in 1891. The mammalian midbody is formed after furrow ingression from tightly packed antiparallel microtubules at the spindle midzone during cytokinesis [33, 34]. In order to understand its exact composition during cytokinesis, Skop *et al.* [33] isolated midbodies from Chinese hamster ovary (CHO) cells, and they studied its

composition by LC-MS associated multidimensional protein identification methods. They identified 160 novel candidate proteins, 57 of them (36%) was previously shown to play roles in cytokinesis [33]. Also, by using immunofluorescence methods in HeLa cells, clear midbody localization of these 10 novel proteins (RACK1, IQGAP1, Keap1, Endplasmin/GRP4, RAB GDI, KIF4, AnnexinII, BIP, Glut1, Novel/CGI-49, and GM130) during cytokinetic abscission were validated [33]. Despite having a list of midbody proteins, knowledge about the organization and localization of these proteins to the midbody region is still limited. The midbody proteins could be categorized into three major groups, as bulge proteins, dark zone proteins, and flanking proteins [34]. The bulge (stem body) at the center of the midbody (Fig. 1.5) accumulates centralspindlin proteins and its interacting partners, such as CEP55, ARF6 and the Rho-GEF protein Ect2 [35, 36]. A narrow region onto microtubule bundle in the center of the midbody, where γ-tubulin staining is blocked, accumulates the known interacting pairs PRC1 and KIF4 [34]. In reference to antibody-excluding characteristics, this localization is described as the

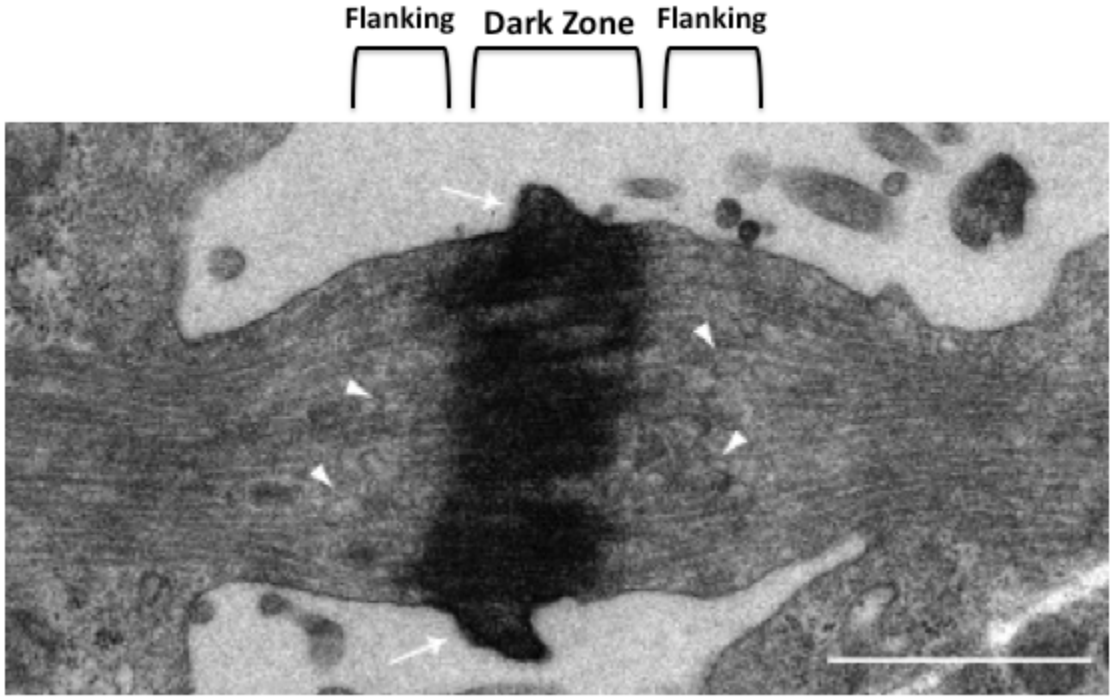


**Fig. 1.5. Midbody is formed of various zones with different molecular compositions.** The upper and lower 'bulge regions' are indicated by white arrows, and flanking zones were marked with multiple white arrow-heads. Dark zone area,

and flanking zones were also indicated on top of the electron-micrograph. Bar represents 1 μm. Figure modified from Guizetti and Gerlich, 2010, Cytokinetic abscission in animal cells. *Seminars in Cell and Developmental Biology*, 21, 909-916, ©2010 Elsevier Ltd.

"dark zone". Two broader bands on microtubules outside the dark zone (known as the "flanking zone") accumulates midbody forming factors such as CENPE, MKLP2 and Aurora B [34], whose relocalizations to the midbody is concomitant with the midbody maturation. The dark zone protein PRC1 localizes microtubule overlaps and stabilizes these overlapping regions [34]. The other dark zone protein, KIF4, binds to plus end of microtubules and it inhibits elongation of microtubules. Midbody assembly and function are regulated by three different kinases: Cdk1, Aurora B and Plk1 [34]. During initiation of cytokinesis at telophase, cyclin B is degraded by anaphase promoting complex (APC) and inhibits activation of Cdk1. This inhibition of Cdk1 on its turn activates Plk1. Active Plk1 phosphorylates centralspindlin complex and recruits Ect2, and initiates cleavage furrow formation and cell contractility [37]. During metaphase/anaphase transition Plk1 also inhibits abscission factor CEP55 by phosphorylating it and thus preventing its untimely recruitment to the anaphase spindle [38]. In anaphase, degradation of Plk1 by APC activates CEP55, a protein with a coiled-coil domain (CCD) motif, leading to the initiation of cytokinetic abscission [39, 38]. On the other hand, the flanking zone kinase, Aurora B, functions as the factor determining the precise site of abscission by negatively regulating RhoA and annilin proteins [34]. Previous studies have also indicated the presence of microtubule nucleation-related proteins that are shared between the centrosome and the midbody, which is characterized by anti-parallel microtubule bundles emanating from the central spindle [9]. These include for instance γ-tubulin, and because of this the midbody is also considered as a secondary MTOC associated with the contractile ring forming at the site of cleavage furrow ingression [40].

Importantly, membrane traffic is now established to have the central role in successful completion of cytokinetic abscission. During abscission, the midbody ring serves as the recruitment site for secretory vesicules [41], which are essential in formation of multivesicular bodies forming the site of abscission (Fig. 1.6). In

addition to secretory membrane trafficking, it is clear that endosomal traffic also contributes remarkably to cytokinesis [10].

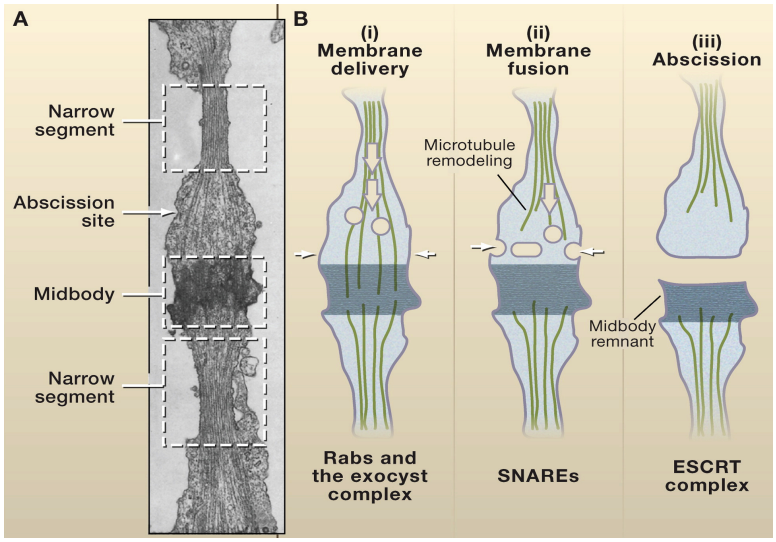


**Figure 1.6. Abscission in animal cell cytokinesis. A**, intracellular bridge and the midbody structure showing microtubules entering the dense midbody matrix containing the kinesin-like factor, Mklp1. **B**, a model for membrane trafficking during cytokinesis in animal cells. (i), Late in telophase, membrane vesicles are delivered along microtubules down the intracellular bridge. These vesicles may be delivered from the Golgi or endocytic compartments in the cell body (open arrows) or may arise directly by endocytosis adjacent to the midbody (filled arrows), or from both sources. Initial tethering of these vesicles is expected to be dependent on both a Rab GTPase and the exocyst-tethering complex. Abscission is an asymmetric process, preferentially occurring on one side of the midbody, perhaps controlled by the centrosomes and a subset of centrosomal proteins such as centriolin [40, 88]. (ii) Retraction of microtubules from the midbody allows these membranes to fuse both with one another and with the plasma membrane. (iii) Abscission occurs once this membrane network completely fills this space and creates a new section of plasma membrane. Recent evidence suggests that this involves the ESCRT complex [42]. Microtubules, green; midbody, dark blue. Figure and legends modified from Barr and Gruneberg, 2007, Cytokinesis: Making and Placing the Final Cut. *Cell*, 131: 847-860. © 2007 Cell Press.

The key factor for completion of membrane fission events is Endosomal Sorting Complex Required for Transport III (ESCRT-III) [42]. ESCRT-III is an important abscission factor, which mediates membrane deformation in various important biological processes (e.g. virus budding, autophagy). A centrosome protein CEP55 interacts with ESCRT proteins Tsg101 and ALIX and recruits ESCRT-III to the midbody while it translocates there at late telophase (Figs. 1.6 and 1.7), [39, 42, 10].

The final step of the abscission is membrane cleavage for which first actin-myosin ring should be disassembled on one side of the midbody narrow [10]. Disassembly of midbody microtubules is mediated by recruitement of an ESCRT interacting partner protein, spastin [43, 44]. Subsequently, spastin depolymerizes microtubules introducing the final cut in cytokinetic abscission [44].

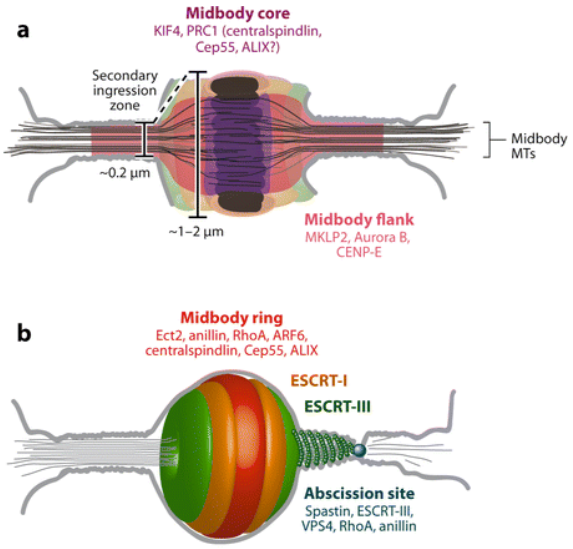


**Figure 1.7. Organization of the intracellular bridge and the midbody.** Schematics show (a) central plane and (b) surface views of the intracellular bridge. Major protein complexes were indicated. Figure taken from Green *et al*., [10] Cytokinesis in Animal Cells. *Annual Rev. Cell. Dev. Biol.* 28, 29-58. © 2012 by Annual Reviews.

### 1.4 Involvement of Ccdc Proteins in Centrosome and Midbody Functions

The centrosome is a dynamic non-membranous organelle with PCM assembled around centrioles, as mentioned above. It organizes microtubules that regulate cell shape, polarity, adhesion and mobility [45, 46]. In addition, it also facilitates intracellular transport and positioning of the organelles. To understand dynamic composition and localization of centrosome proteome, recently Jakobsen *et al*. have characterized the human centrosome by using a mass spectrometry-based proteomics approach combined with an antibody based subcellular screen of candidate proteins. In this work, 116 known and 40 novel candidate centrosome proteins were identified, of which 22 were validated as entirely novel centrosome components, and 5 turned out to associate preferentially either with mother or daughter centrioles [30]. Interestingly, these analyses also indicated that the majority (%60) of centrosomal proteins contain CCD (coiled-coil domain) type oligomerization motifs as their predominant structural features, which seem to be important for proper centrosome

assembly. In addition they compared localization of these candidate proteins between interphase and mitotic stages by stainings methods. Most of the CCD containing (CCDC) proteins localized differentially to centrosomes, spindles, and midbody during cell cycle, in a way similar to CEP55 and γ-tubulin, which are also coiled coil domain containing proteins [39], (Pelin Telkoparan and Uygar Tazebay, unpublished observations). When the expression levels of these candidate proteins were downregulated using RNAi methods, multiple types of cell division defects were observed [30]. Similarly, previous studies of Skop *et al*. [33] also indicated the predominant roles of CCDC proteins in midbody establishment and cytokinesis. Two major proteins involved in formation of the midbody and establishment of the abscission site, PRC1 and MKLP1, are CCDC type proteins, and absence of their CCD motifs perturbs subcellular localizations, and thus, functions of these factors [34]. Therefore, it must be clearly stated that CCDC proteins form the backbone of PCM and the midbody, possibly forming a docking platform for several factors (such as, SNARE complexes, ESCRT machinery proteins, G-protein activator GEFs, and Rab family docking regulators, etc.) involved in completion of cytokinetic abscission.

### 1.4 RasGEF1 Family of Guanine Nucleotide Exchange Factors (GEFs)

During their functional cycle, Ras-superfamily of G proteins cycle between an active GTP-bound conformation and an inactive GDP-bound form. This cycle of G proteins is regulated by guanine nucleotide exchange factors (GEFs) and GTPase activating proteins (GAPs). GEFs activate G-proteins by stimulating the binding of GTP, and in reverse, GAPs lead to their inactivation due to the catalysis of GTP hydrolysis to GDP [47]. Briefly, GEFs catalyze the dissociation of the GDP nucleotide from the G protein by affecting the nucleotide-binding residues so that the nucleotide affinity is diminished and, therefore, the nucleotide is released and subsequently replaced by GTP. In fact, mostly the affinity of the G proteins for GTP and GDP is similar, and the GEF does not directly favor binding of GTP over GDP. Thus the resulting increase in GTP-bound over GDP-bound forms is due to remarkably higher cellular concentration of GTP as compared to GDP [47].

Active small G proteins control diverse signaling networks important for the regulation of cell proliferation, survival, differentiation, vesicular trafficking, and gene expression [48]. Best-studied examples of small G-proteins belong to the Ras-family, which comprises H-Ras, N-Ras, K-Ras. These small G proteins are also known to be oncogenic proteins, and they have functions in many signaling events that control processes like proliferation, differentiation, morphogenesis and apoptosis [49]. Remarkably, each small G proteins family has its own non-homologous GEFs and GAPs proteins. RasGEFs have CDC25 homology domain (CDC25 HD), which is essential for the activity of these proteins. CDC25 HD is an ancient domain and its origins date back to the last eukaryotic common ancestor [50]. GEFs that have CDC25 HD regulate Ras, Rap and Ral family of G proteins, which are altogether named as Ras proteins. The smart database platform (http://smart.embl-heidelberg.de/smart) lists 28 RasGEF-CDC25 domains, most of which, occur in tandem with an N-terminal extension of Ras-Exchange Motif (REM) domain, which are in close contact with each other [51].

*RasGEF1* genes encode a subgroup of highly conserved Ras guanine nucleotide exchange factors [51]. The combined data generated from EST projects and genome-scanning gene-prediction programs suggest that vertebrates have three distinct *RasGEF1* (1A, 1B, and 1C) genes. Phylogenetic analysis of the predicted RasGEF proteins show that the fish and mammalian proteins have only slightly diverged during evolution [50].

Previous *in vitro* studies carried-out by Elif Yaman have clearly indicated that RasGEF1 family of GEFs are specific activators of Rap2, while they do not affect exchange of nucleotides on Rap1 [51]. Same authors have also found residues on Rap2 contributing to the recognition of this G protein by RasGEF1 family, and proposed that Phe-39 is the key residue in establishing the specificity of interaction between RasGEF1 and Rap2 [51].

### 1.5 The Significance of Rap Signaling in Cell Biology

Ras-Proximal (Rap) family proteins are Ras-like small G-proteins, which act as molecular switches, typically cycling between a GDP-bound inactive and a GTP-bound active state, as mentioned above. In fact, Rap1 was originally identified as a

suppressor of Ras-induced transformation, on the basis of similarity in effector-binding regions, which were proposed to compete with Ras in effector recognition [52]. It is now widely accepted that Rap could also function independently of Ras, and it could signal via its own set of effectors [53]. Functions attributed to Rap1 comprise the control of establishment of cell polarity [54, 55], activation of integrin-mediated cell adhesion [56, 57, 58, 59] and the regulation of cell–cell contacts [60, 61]. Additionally, Rap1 has been implicated in cell proliferation [62] and secretion [63, 64]. There are five known mammalian Rap proteins; Rap1A, Rap1B, Rap2A, Rap2B, Rap2C. There is about 95% sequence identity between Rap1A and Rap1B, and about 90% identity between Rap2A, Rap2B, and Rap2C. In addition Rap2 proteins share %60 similarities between Rap1 [51, 53]. Effectors of Rap GTP-binding proteins consist of Ras/Rap-binding domain (RBD) or Ras/Rap-association (RA) domain to interact with active Rap protein. In addition it was shown that citron homology domain (CNH) bind only active Rap2, and not Rap1 proteins, and therefore it is a discriminative domain between these two groups of related G proteins [65]. Following the interaction of active Rap proteins, effectors play role in different biological processes, such as integrin mediated cell adhesion, cell-to-cell junctions, cell polarity, exocytocis and cell proliferation [53]. In addition, endogenous Rap proteins were visualized by fluorescence protein-tagging methods, and they are found to localize many subcellular membrane compartments of the mammalian cells including the perinuclear Golgi apparatus, endoplasmic reticulum, endocytic vesicles, secretory vesicles and the nuclear envelope [53]. It is now revealed that in different membrane compartments, there exists different Rap interacting effector proteins that could induce different downstream pathways [53, 66].

### 1.6 Aim of This Study

Intrigued by its strict conservation in all eukaryotic species, we decided to functionally characterize the human counterpart of the coiled-coil domain-containing protein 124 (Ccdc124). We propose that it is a novel component of the centrosome during interphase and at the G2/M transition. We then decided to study the subcellular localization of Ccdc124 during cell division. We found that Ccdc124 relocated to the midbody at

telophase, and acted as an essential molecular component in cytokinetic abscission. It was previously proposed by members of our group that Ccdc124 is an interaction partner of the Ras-guanine nucleotide exchange factor 1B (RasGEF1B; Elif Yaman, PhD. Thesis, 2009). We aimed to further validate this interaction, and identified that these two proteins interact at the midbody where this GEF could activate the small G protein Rap2 [51] at pre-abscission stages. We then decided to knock-down Ccdc124 in embryos of the vertebrate model organism *Danio rerio* (zebrafish) by using specific morpholino oligonucleotides, and observed enlarged cells with compromised genetic stability in various tissues, thereby validating our observations on the role of Ccdc124 in cellular abscission. We propose that the coiled-coil protein Ccdc124 on one hand contribute to the regulation of cytokinetic abscission at the midbody, and on the other hand it recruits RasGEF1B to the midbody where this exchange factor activates the small G protein Rap2. Data presented in this thesis work propose a mechanistic link between cytokinetic abscission and Rap signaling that is mainly linked to the formation of cell-cell junctions, regulation of cell-extracellular matrix adhesion, and establishment of cell polarity [53], i.e., molecular processes that must follow cell division while tissues are formed.

# CHAPTER 2. MATERIALS AND METHODS

## 2.1 MATERIALS

### 2.1. 1. Bioinformatics Tools

Amino acid sequence of the Ccdc124 and its homologue gene sequences were downloaded from NCBI homologene. The conservation pattern of the novel gene among all eukaryotic species was analysed using ClustalW2 (version 2.1) multiple alignment program and sequence similarities between the species were investigated via FASTA. Phylogenetic tree of Ccdc124 was done using neighbor joining (NJ) method in MEGA4 bioinformatic tool. Coiled coild domain of Ccdc124 was analyzed in COILS (www.ch.embnet.org/software/COILS_form.html) bioinformatics platforms. Canditate functional sites of the Ccdc124 protein was searched in ELM bioinformatics tool (http://elm.eu.org/about.html) .

### 2.1.2. Agarose gel solutions

**Ethidium bromide:** 10 mg Etidium bromide was dissolved in 1 ml deionized water ($ddH_2O$) and diluted into 1mg/ml.

**Agarose gel, 1%:** 1g agarose was dissolved in 100 ml TAE.

**TAE, 50X:** Tris base, 242 g; Tritiplex III (EDTA), 37.2 g; glacial acetic acid, 57.1 ml were mixed and completed volume to 1 L with $ddH_2O$. Dilute 1X for working solution and store at room temperature.

**6X Loading dye:** 0.05 g bromophenol blue were dissolve in 10 ml $ddH_2O$ water, and added into 30% glycerol solution.

### 2.1.3. Microbiology Strains

Escherichia coli (*E. coli)* DH5α and BL21 bacterial strains were used in this study.

### 2.1.4 Microbiology Solutions

**LB medium:** 10 g tryptone, 5g yeast extract and 5g NaCl were prepared in 1 $ddH_2O$ and autoclaved immediately after preparation.

**Agar medium:** Bacto agar was added 1.5 % into LB buffer then autoclaved and poured onto plates, waited at room temperature overnight for solidification of agar plates.

**Glycerol stock solution:** 25 ml %100 (sterile) glycerol were mixed with 25ml autoclaved LB near fire.

**SOB Liquid medium:** 2% tryptone, 0.5% yeast extract, 10mM NaCl 2.5mM KCl were prepared in $ddH_2O$. Then 10mM $MgCl_2$ and 10mM $MgSO_4$ were added into solution.

**SOC Liquid medium:** SOB with 20mM Glucose**.**

**Transformation Buffer (TB):** 10mM PIPES, 15mM $CaCl_2$ and 250mM KCl were added, pH is adjusted to 6.7 with KOH then 55mM $MnCl_2$ was put into solution and sterilized with 0.45 mm filter.

**Miniprep Solution I:** 50mM Glucose, 25mM Tris-HCl (pH 8.0), 10mM EDTA (pH 8) are dissolved in $ddH_2O$.

**Miniprep Solution II:** 0.2N NaOH, 1% SDS were used freshly.

**Miniprep Solution III:** 5M Potassium acetate and 11.5 ml Glacial acetic acid were completed to 100ml with $ddH_2O$.

**RNase (20mg/ml):** 1M Tris pH 8.0 and 5M NaCl were combined with 20 mg RNase, then solution was boiled for 15 minutes and store at -20$^0$C.

**Ampicillin:** 100mg/ml stock solution were prepared in dd$H_2O$ then sterilized by filtration and stored at -20$^0$C. Working solution is 100µg/ml.

**Kanamycin:** 40mg/ml kanamycin stock solution prepared in dd$H_2O$ then sterilized by filtration and stored at -20°C. Working solution is 40µg/ml.

### 2.1.5 Western Blot Solutions

**Protein lysis buffer:** 50mM Tris-HCl (pH 8.0), 250mM NaCl, 1% NP-40, 1x Protease Inhibitor Cocktail were dissolved in dd$H_2O$.

**IP buffer:** 50mM Tris-HCl (pH 7.5)**,** 5mM $MgCl_2$, 150mM NaCl, 1 tabl/50ml Complete Protease Inhibitor Cocktail (Roche 1460500), 0.5 ml/50ml Phosphotase Inhibitor Cocktail 1 (SIGMA P2850-5ml), 0.5 ml/50ml Phosphotase Inhibitor Cocktail 2 (SIGMA P5726-5ml) were mixed in dd$H_2O$.

**Ral Buffer**: % 10 glycerol, 200mM NaCl, 50mM Tris 7.5 pH, %1 NP40 5mM $MgCl_2$ were prepared in dd$H_2O$ and 50ul Apoprotinin, 50ul Leupeptin, 50ul Na3VO4, pipette point NaF inhibitors were added for 50ml final volume.

**Semi-dry Transfer Buffer, 1X:** 39mM Glycine, 48mM Trizma base, 0.037% SDS and 200ml Methanol were mixed. Then volume was completed to 1L with dd$H_2O$.

**Running Buffer, 5X:** 15.1 g Trizma base, 95 g Glycine, 50 ml 10% SDS were completed to 1L with $ddH_2O$.

**Wet transfer buffer, 10X:** 30.3 g Tris base and 144 g Glycine were dissolved in 1L $ddH_2O$. Dilute 1X for working solution with $ddH_2O$ and add 20% Methanol store at 4C° (use freshly).

**TBS, 10X:** 12.1 g Trizma base and 87.6 g NaCl were dissolved in 1 L $ddH_2O$ and pH was adjusted to 8.0. Tween-20 was added into 1X TBS to a final 0.1%.

**Gel staining solution:** Coomassie brilliant blue G.250, 100 mg; absolute ethanol, 50 ml; phosphoric acid (85%), 100 ml were prepared in $ddH_2O$ volume was completed to 1 L with and solution was filtered.

**Gel de-stain solution:** 20% methanol and 7% acetic acid were mixed in $ddH_2O$.
**40% acrylamide** was purchased from Millipore. (Cat no. 800804)

**Gel formulations (10 ml):** Mix tris buffer, SDS and 40% acrylamide in $ddH_2O$ according to the gel percentage as described in the Table 2.1. Immediately prior to pouring the gels, add 10% APS and TEMED shake gently to initiate polymerization

Table 2.1: SDS-PAGE Gel Formulations

| **Running Gel** | **7.5%** | | **10%** | | **12%** | | **15%** | |
|---|---|---|---|---|---|---|---|---|
| | 1 | 2 | 1 | 2 | 1 | 2 | 1 | 2 |
| **1.5 Tris HCl pH 8.8** | 2500 | 5000 | 2500 | 5000 | 2500 | 5000 | 2500 | 5000 |
| **dd$H_2O$** | 5415 | 10830 | 4790 | 9580 | 4290 | 8580 | 3540 | 7080 |
| **40% Acryl/bis 37.5:1** | 1875 | 3750 | 2500 | 5000 | 3000 | 6000 | 3750 | 7500 |
| **10% SDS** | 100 | 200 | 100 | 200 | 100 | 200 | 100 | 200 |
| **10% APS** | 100 | 200 | 100 | 200 | 100 | 200 | 100 | 200 |
| **TEMED** | 10 | 20 | 10 | 20 | 10 | 20 | 10 | 20 |

| **Stacking Gel** | **4%** | | | |
|---|---|---|---|---|
| | 1 | 2 | 3 | 4 |
| **0.5 Tris HCl pH 6.8** | 1250 | 2500 | 3750 | 5000 |
| **dd$H_2O$** | 3145 | 6290 | 9435 | 12580 |
| **40% Acryl/bis 37.5:1** | 500 | 1000 | 1500 | 2000 |
| **10% SDS** | 50 | 100 | 150 | 200 |
| **10% APS** | 50 | 100 | 150 | 200 |
| **TEMED** | 5 | 10 | 15 | 20 |

**APS, 10% (w/v):** 0.1 g ammonium persulfate was dissolved in 1 ml dd$H_2O$, filtered and stored at -20°C.

**Gel loading buffer, 5X** (20ml) was purchased from Fermentas (#R0891).
Protein ladders were purchased from Fermentas (#26616) and BIO-RAD (#161-0373). As well as gel loading buffer was prepared manually; 50 mM Tris-HCl pH 6.8, 1% SDS, 0.02% bromophenol blue, 10% Glycerol and 5% 2-mercaptoethanol.

**1.5 M Tris-HCl, pH 8.8:** 121.1 g Trisma base were prepared in 200ml dd$H_2O$ and pH was adjusted 8.8 with HCl.

**0.5 M Tris-HCl, pH 6.8:** 121.1 g Trisma base were prepared in 200ml dd$H_2O$ and pH was adjusted 6.8 with HCl.

**Blocking solution (w/v):** 2.5 g milk powder was prepared in 1x TBS-Tween.

**Stripping solution** was used commercially. (Milipore, Lot: PS01795976)

### 2.1.6 IP reagents

GFP beads were used from Chromotek (lot :120420001A). Flag beads(A2220-5ml) and HA beads (E6779-1ml) were acquired from SIGMA**.** Protein G Sepharose 4 (10054549) and Protein A Sepharose (10043746) beads were purchased from GE Healthcare.

### 2.1.7 Polymerase chain reaction (PCR) and reagents and cDNA synthesis reagents

RevertAid First Strand cDNA synthesis Kit was used from Fermentas (#K1622). Pfu polymerase (#EP0502), 10mM dNTP Mix (#R0192) and taq polymerase (#EP0402) were also from Fermentas.

### 2.1.8 Vectors

DNA ladder were from Fermentas (1kb #SM0313, 100BP #SM0313). pEGFP-N2 (Clonetech), pEGFP-C3 (Clonetech), pmCherry-C1 (Clonetech), pEYFP-C1(Clonetech), pcDNA4/TO/Myc/his A,B,C (Invitrogen), p3xFlag-CMV10/14(Sigma) were obtained commercially.
pRFP-Rab11, pRFP-Rab5, pYFPTNIK, GFP-RalGDS constructs were provided from Hans Bos laboratory (UMC, Utrecht, Netherlands). The Ccdc124 esiRNAs and control esiRNAs were from SIGMA.

### 2.1.9 Oligonucleotides

Oligonucleotides in the table 2.2 were synthesized by IONTEK (Istanbul, Turkey).

Table 2.2: List of primers used in this thesis work.

| Primer ID | Sequence (5'-3') |
|---|---|
| LocSeq-F | TGGCCACGTCCAGCAAGGTC |
| LocSeq-R | TCCGCCACGCTGAGCACTGCA |
| HlocF0 | GAGACGGACTCTTGCTATGTTG (Tm62) |
| HllocR0 | AGCCTTGCCGCCACCTTTATTGG (Tm66) |
| RAP2A_RT_F | TCTACCGCAAGGAGATCG AG |
| RAP2A_RT_R | TCTGCCTTCGCTGGACGATA |
| RAP2AF | GGATCCAAGCTTATGCGCGAGTACAAAGTGGTG |
| RAP2Arev | GAATTCGATATCCTATTGTATGTTACATGCAG |
| RAP2A6HisR | GAATTCGATATCCTAATGGTGATGGTGATGATG TTGTATGTTACATGCAGAACAGC |
| RASGEF1B-F1 | AAGCTTGCGGCCGCATGGAACAAAAACTCATCTCAGAAGA GGATCTGATGCCTCAGACTCCTCCCTTTTCAT |
| RASGEF1B-F2 | AAGCTTGCGGCCGCATGCCTCAGACTCCTCCCTTTTCAG |
| RASGEF1B-R1 | GGATCCTCTAGAAACTCTGCCTAAGAGGCTCGACCTT |

| | |
|---|---|
| RASGEF1B-R2 | GGATCCTCTAGATATCCCTTTGAAGTGGGATGGTATA |
| RASGEF1B-RT-F | GAGCACCAGAGACTAAGTGA |
| RASGEF1B-RT-R1 | CCCTTTGTATAGACTGTGGC |
| RASGEF1B-RT-R2 | AACAGAGAGGAAGCAGTGGA |
| RASGEF1B 1. Iso pmCherry-C1-F | AGATCTCGAGTGATGCCTCAGACTCCTCCCTTTTCAG |
| RASGEF1B 1. Iso pmCherry-C1, pEGFP-C3 R | GTCGACGAATTCTTAAACTCTGCCTAAGAGGCTCGACC |
| RASGEF1B 1. Iso pEGFP-C3 F | TCAGATCTCGAGATGCCTCAGACTCCTCCCTTTTCAG |
| RAP2A pEYFP-N1-F and pmCherryC1-F | GAGCTCAAGCTTATGCGCGAGTACAAAGTGGTG |
| RAP2A pmCherryC1R | GGTACCGTCGACCTATTGTATGTTACATGCAG |
| RAP2A pEYFP -N1 R | GGTACCGTCGACTGTTGTATGTTACATGCAGAA CAGCA |
| L-HA-R | GGATCCTCTAGATCAAGCGTAATCTGGAACATCGTATGGGT ACTTGGGGGC |
| HALNG-F1 | GAATTCAAGCTTATGCCCAAGAAGTTCCAG |
| T103A-F | GCCCAGATCGAGGACGCGCTGCGCGCGAGACCATCAG |
| T103A-R | CTGATGGTCTCGGCGCAGCGCGTCCTCGATCTG GGC |
| T103D-F | GCCCAGATCGAGGACGACCTGCGCCGAGACCATCAG |
| T103D-R | CTGATGGTCTCGGCGCAGGTCGTCCTCGATCTGGGC |
| T103E-F | GCCCAGATCGAGGACGAGCTGCGCCGAGACCAT CAG |
| T103E-R | CTGATGGTCTCGGCGCAGCTCGTCCTCGATCTGGGC |
| S141A-F | GTGCTGGAGGAGGGCGCCGTGGAGGCGCGCGACC |
| S141A-R | GGTGCGCGCCTCCACGGCGCCCTCCTCCAGCAC |
| S141D-F | GTGCTGGAGGAGGGCGACGTGGAGGCGCGC ACC |
| S141D-R | GGTGCGCGCCTCCACGTCGCCCTCCTCCAGCAC |
| S141E-F | GTGCTGGAGGAGGGCGAGGTGGAGGCGCGC ACC |
| S141E-R | GGTGCGCGCCTCCACCTCGCCCTCCTCCAGCAC |

| | |
|---|---|
| S122A –F | GCCGAGAAAGCCAAGGCCCATCTGGAGGTGCCG |
| S122A –R | CGGCACCTCCAGATGGGCCTTGGCTTTCTCGGC |
| S122D –F | GCCGAGAAAGCCAAGGACCATCTGGAGGTGCCG |
| S122D –R | CGGCACCTCCAGATGGTCCTTGGCTTTCTCGGC |
| S122E –F | GCCGAGAAAGCCAAGAGCATCTGGAGGTGCCG |
| S122E –R | CGGCACCTCCAGATGCTCCTTGGCTTTCTCGGC |
| Ccdc124GFP-Full_F | AAGCTTGAATTCATGCCCAAGAAGTTCCAGGGTGAG |
| Ccdc124_L64M_GFP_F | AAGCTTGAATTCATGGAACGTAAGAAGGAGACG |
| Ccdc124V142M_GFP_F | AAGCTTGAATTCATGGAGGCGCGCACCATCGAG |
| Ccdc124GFP_N2_REV | GGTACCGGATCCTCTTGGGGGCATTGAAGGGCAC |
| Ccdc124_M1L-F | CCCTGCTGAGGGCTGCCCAAGAAGTTCCAGGGTG |
| Ccdc124_M1L-R | CACCCTGGAACTTCTTGGGCAGCCCTCAGCAGGG |
| Ccdc124_M47L-F | CAAACACGTCCTGAGGAAGGAGCAGCGCAAGGAG |
| Ccdc124_M47L-R | CTCCTTGCGCTGCTCCTTCCTCAGGACGTGTTTC |
| GAPDH–F | GGCTGAGAACGGGAAGCTTGTCAT |
| GAPDH–R | CAGCCTTCTCCATGGTGGTGAAGA |

### 2.1.10 Cell culture reagents

100X non-essential amino acids was acquired from GIBCO (#11140), penicillin/streptomycin was purchased from Biochrom AG (A2213) and 100X (200mM) L-glutamine was purchased from GIBCO (#25030).

**PBS 10x:** NaCl, 80 g; KCl, 2 g; $KH_2PO_4$, 2.4 g, $Na_2HPO_4$, 14.4 g; were dissolved in 1 L of dd$H_2O$ and adjust to volume pH 7.2–7.4.

**Geneticin-G418**: It was purchased from GIBCO (#10131) and 500 mg/ml solution was prepared in dd$H_2O$ after filtration it was stored at -20°C (stock solution). 200-800 µg/ml (working solution).

**Puromycin:** 2 mg/ml solution was prepared in dd$H_2O$ in then was sterilized by filtration and was stored at -20°C (stock solution). 2µg/ml (working solution).

**Polyethylenimine (PEI#23966) transfection reagent:** 200mg PEI was dissolved in pure etanol.

**DMEM and DMEM/F12** was purchased from GIBCO and prepared by adding 10% FBS, 1% L-glutamine, 1% penicillin/streptomycin and 1 % non-essential amino acids.

### 2.1.11. Immunofluorescence reagents

**Blocking solution**: 2% BSA, 0.1% Triton-X in 1x PBS.

**Washing Solution:** 0.1% Trition-X in 1x PBS

**DAPI (4', 6-diamino-2-phenylindole):** 0.1-1 µg/mL working solution in double-distilled water.

**Mounting medium** was purchased from DAKO (#10053437).

### 2.1.12. Antibodies

All of the antibodies were purchased from different companies. Name of the companies and dilutions are depicted in table 2.3.

Table 2.3 List of antibodies used in this thesis work.

| Antibody ID | Origin species | Company | Lot | WB | IF |
|---|---|---|---|---|---|
| CCDC124-Cter | Rabbit(100-150) | BETHYL | A301-834 | 1/1000 | 1/100 |
| CCDC124-Middle | Rabbit(173-223) | BETHYL | A301-835 | 1/1000 | 1/200 |
| Anti-Nter CCDC124 | Rabbit | Cambrige Research Biochemicals | | 1/5000 | |
| Anti-Rap2 | Rabbit | Genetax | GTX108831 | 1/2500 | 1/250 |
| Anti-Rap2 | Mouse | BD-biosciences | 610215 | 1/1000 | 1/100 |
| Anti-RasGEF1B | Rabbit | Cambrige Research Biochemicals | | 1/1000 | 1/100 |
| Anti-Plk1 | Rabbit | Nurhan Ozlu | | 1/100.000 (IP) | 1/10.000 |
| Anti-Plk1 | Rabbit | Abcam | 109777 | 1/1000 | 1/200 |
| Anti-Flag | Mouse | Sigma | F3165 | 1/5000 (IP) | |
| Anti-alpha tubulin | Mouse | Santa Cruz Biotec. | Sc-5286 | 1/5000 | 1/500 |
| Anti-beta tubulin | Rabbit | Santa Cruz Biotec. | Sc-9104 | | 1/100 |
| Anti-gama tubulin | Mouse | Abcam | 11316 | 1/1000 | 1/200 |
| HA ab. | Mouse | Santa Cruz Biotec. | Sc-7392 | 1/1000 | 1/200 |

| | | | | | |
|---|---|---|---|---|---|
| HA-HRP | Mouse | Cell signaling | 29993 | 1/5000 | |
| Anti-mouse | Goat | Sigma | A2304 | 1/5000 | |
| Anti-Rabbit | Goat | Sigma | A9169 | 1/5000 | |
| Anti-FlagHRP | Mouse | Sigma | A8592 | 1/240.000 (IP) | |
| Alexa 488 | Mouse | Invitrogene | 898236 | | 1/500 |
| Alexa 488 | Rabbit | Invitrogene | A11034 | | 1/500 |
| Alexa 568 | Mouse | Invitrogene | A11031 | | 1/500 |
| Alexa 568 | Rabbit | Invitrogene | 898234 | | 1/500 |
| Anti-GFP | Rabbit | Sigma | G1544 | 1/1000 | |
| Anti-RACK1 | Rabbit | Sigma | R1915 | 1/5000 | 1/200 |

### 2.1.13 Cell Syncronization Reagents

**Nocodazole** (Sigma #M1404): 10mg/ml stock solution was prepared in DMSO. 200ng/µl were used as working dilution.

**Thymidine** (Sigma #T1895): 100mM stock solution was prepared in ddH20. Working solution was 2.5uM.

### 2.1.14 Mass spectrometry reagents

Stable N-ter Flag Ccdc124, C-ter Flag Ccdc124, YFP-RasGEF1B and EV (3Xflag-CMV-14 and EYFP-N1 plasmids) expressing HEK293 cell lines were generated and used in experiments (*see below*). DMEM cell culture medium (Gibco) was routinely used in experiments. Cell culture medium lacked arginine, lysine or methionine. Dialyzed fetal bovine serum (Gibco) without essential amino acids for SILAC labeling were commercially obtained and used in all experiments. Antibiotics

(penicillin and streptomycin, 100X Invitrogen), and Glutamine (100X, Invitrogen) were supplied when necessary. For immunoprecipitations GFP antibody bound commercial beads (Chromotek, #120420001A) and Flag antibody bound commercial beads (Flag beads, A2220-5ml) were used. L-Arginine monohydrochloride (Sigma, #A6969), L-Lysine (Sigma #L9037), L-Methionine (Sigma #M5308) were used in light SILAC media.

SILAC amino acids L-arginine-$^{13}C_6$ monohydrochloride (Cambridge Isotope Laboratories, CLM-2265); L-arginine-$^{13}C_6{}^{15}N_4$ hydrochloride (Sigma-Isotec, #608033); L-lysine-$^{13}C_6{}^{15}N_2$ hydrochloride (Sigma-Isotec, #60804); L-methionine-$^{13}C,{}^{2}H_3$ (methyl-$^{13}C,{}^{2}H_3$) (Sigma-Isotec, # 299154) were used in heavy SILAC media preparation.

8 M urea (Sigma, U5128) in 0.1 M Tris/HCl pH 8.5 (UA) was prepared as 1 ml per 1 sample. 0.5M NaCl was in dd$H_2O$ (Prepare 0.25 ml per 1 sample). Trypsin was used from 0.4 µg/µl stock. 0.05M Iodoacetamide (IAA) was prepared in UA. 0.05M Ammonium bicarbonate was dissolved in dd$H_2O$ (ABC).

Trifluoroacetic acid (TFA), Formic acid (FA) and Complete protease inhibitor tablets (Roche Diagnostics) were also used in these assays.

### 2.1.15 Mass-spectrometry Equipment used in Analysis

LTQ-Orbitrap Mass spectrometer (Thermo Fisher Scientific) was used in analysis. Agilent 1200 series Nano-flow HPLC system was attached to apparatus. Protein and peptide identification software tools were used a served in analysis (Mascot-version 2.2.03, Matrix Science). Scaffold (version 2.05.02, proteome Software Inc.) was used for peptide validation. Raw mass spectrometric data were analyzed by MSQuant software package (version 1.0.13.12). Thermo-mixer set to 20$^{\circ}$C. Micrococon YM-30 filter (Milipore, Cat no. 42410).

### 2.1.16 Zebrafish injection reagents

Ccdc124 morpholino (5'- CTGGGACTTTCCTTTTCCTGAGCCA-3'), RasGEF1B morpholino (5'-GGGTGGCGTCTGAGGCATTTTGTC), chordin positive control (5'-ATCCACAGCAGCCCCTCCATCATCC-3') , and standard control morpholino

(5'-CCTCTTACCTCAGTTACAATTTATA-3') were purchased from GeneTools, Philomath, OR, USA). 1x Danieau solution; 58 mM NaCl, 0.7 mM KCl, 0.4 mM $MgSO_4$, 0.6 mM Ca $(NO_3)_2$ , 5.0 mM HEPES pH 7.6.

## 2.2 METHODS

### 2.2.1. General methods

#### 2.2.1.1 Bacterial strains storage

Bacterial strains were stored by "Glycerol-Stock" method. A single colony was picked from agar plate then it was inoculated into 3 ml LB in 15 ml cononical tube. Falcons were incubated O/N at 37°C and at 225 rpm. For glycerol stock, 500µl bacterial culture was added into 500 µl of sterile 50% glycerol-50%LB mix. This mix was frozen at -80°C.

#### 2.2.1.2 Competent cell preparation

DH5α (or another suitable strain) strains were grown in SOB medium at 20°C for 5-7 hours until to reach from $OD_{600}$ of 0.2 to $OD_{600}$ of 0.5-0.6 (logarithmic growth range) by shaking at 225 rpm. When the optical density was reached, the flask was cooled down on ice for 10 minutes. Then cells poured into sterile 50 ml tubes. Cells were harvested by centrifugation at 2500xg for 10 minutes. (rotor must be prechilled). Supernatants were discarded and pellets were resuspended in ice-cold transformation buffer and kept on ice for 10 minutes. The suspension was then centrifuged at 2500xg for 10 minutes. The pellet was gently resuspended in ice-cold TB containing 7% DMSO and left on ice for 10 minutes. 0.2 ml aliquots were pipetted into cold microcentrifuge tubes.
Tubes were immediately put into liquid nitrogen to freeze rapidly and stored at –80°C.

#### 2.2.1.3 Transformation of *E.coli*

Competent cells were taken from –80°C stock thawed on ice. 200 µl of cells were put into 15ml polypropylene tubes and placed on ice. Appropriate amount of plasmid

was added onto competent cells. Then cells were incubated with plasmid on ice for 30 minutes. Then heat-shocked for 30 seconds at 42°C, then the tubes were transferred to an ice bath for 2 minutes and 800 µl SOC was added. Following incubation for 1 hour at 37°C with vigorous shaking, 50-100 µl cells were plated out on LB-agar with selective antibiotics and incubated at 37°C O/N.

#### 2.2.1.4. Plasmid DNA purification

##### 2.2.1.4.1. Small Scale Plasmid DNA preparation by Alkaline Lysis Method

Transformed bacterial cells were grown in 3 ml selective antibiotics contaning LB medium O/N at 37°C by shaking at 225 rpm. 1.5 ml bacterial culture was taken and centrifuged for 1 minute at 13,000 rpm in a micro centrifuge. Then the supernatant was discarded, and the pellet was resuspended in 100 µl Solution I. Freshly prepared 200 µl of Solution II was added and inverted 2-3 times. Bacterial chromosomal DNA and proteins (cell debris) were precipitated by addition of 150 µl of Solution III. This mixture was left on bench for 2-3 minutes, and then centrifuged for 15 minutes at 13,000 rpm. The supernatant was transferred to another 1.5 ml tube. The plasmid DNA was mixed with two-volume ice-cold absolute ethanol. The plasmid was precipitated by centrifugation at 13,000 rpm, at room temparature for 15 minutes. The supernatant was discarded and the pellet was washed 1-2 times with 500 µl of 70% ethanol and centrifuged at 13,000 rpm for 15 minutes. Then supernatant was discarded and the pellet was left at room temperature for 15 minutes to air dry and resuspended in 20-50 µl of sterile dd$H_2O$ containing 20 µg/ml RNaseA. Samples were stored at 4°C for short term or at –20°C for long term. The quality of the miniprep was checked by agarose gel electrophoresis and the amount of plasmid was measured by using spectrophotometer (Nanodrop ND-100, ND100.V3.1.1 software).

##### 2.2.1.4.2 Purification of plasmid with Fermentas GeneJET Plasmid Miniprep Kit

This plasmid isolation method was used for cloning and sequencing procedures. To isolate plasmid DNA by using Fermentas GeneJET Plasmid Miniprep Kit (#K0503) 1.5 ml bacterial culture was used following manufacturer's instructions.

#### 2.2.1.4.3 Large Scale Plasmid DNA preparation

This plasmid isolation method was preferred because it facilated the use of plasmids in cloning and mammalian cell transfection assays by using "Promega Pureyield Plasmid Midiprep kit (#A2495)" following manufacture's instructions.

### 2.2.1.5. Quantification of Nucleic Acids

Nucleic acid concentrations and purities were determined by using ND-1000 V3.7.1 software in the Nanodro model from Thermoscientific Company.

### 2.2.1.6. Restriction enzyme digestion of plasmid DNA

1-10 μg plasmid DNA was routinely used during restriction enzyme digestion and performed in 20-100 μl reaction volume. Reaction was done in appreciate conditions by following suggestion of manufacturers. Restriction enzymes were used from Fermentas Company.

### 2.2.1.7 Vector construction

The C-ter HA epitope tagged Ccdc124 (L-HA) was cloned into XbaI/HindIII sites of pcDNA4/TO/MYC/HIS-B plasmid vector by PCR method. LHA-forward and LHA-reverse primers (Sequences was shown in table 2.1) were used. The S122A, S122D, T103A, T103D, S141A, S141D, T96A, T96D Ccdc124 phospho sites mutation containing plasmids were prepared on L-HA plasmid by site directed mutagenesis as mentioned in methods.

The RAP2Awt construct was cloned into HindIII/EcorV sites of pcDNA4/TO/MYC/HIS-B by PCR method with RAP2A-F and RAP2A-R primers.

The RAP2A-His plasmid was cloned into HindIII/EcorV sites of pcDNA4/TO/MYC/HIS-B plasmid by PCR cloning using RAP2A-F and RAP2AHis-R primers.

For identification of an alternative translation start site in Ccdc124 ORF methionine residue (Met-47) in Ccdc124 ORF was mutated to Leu amino acids in Ccdc124-HA

vector construct using Ccdc124_M47L-F and Ccdc124_M47L-R primers by site directed mutagenesis method (*see below*).

To prepare Full-Cter-GFP-Ccdc124 and Truncated-Cter-GFP-Ccdc124 plasmid constructs, Ccdc124-GFP-Full-F, Ccdc124-L64M-GFP-F, Ccdc124V142M-GFP-F and GFP-N2-R primers were used and Ccdc124 constructs were cloned into EcorI/BamHI sites of pEGFP-N2 plasmid via PCR cloning method.

The RasGEF1B constructs were cloned into XhoI/EcorI sites of pmCherryC1, pECFP-C1, pEGFP-C3, pEYFP-N1 plasmids (cloning primers were shown in the *Table 2.1*).

The RAP2A was cloned into HindIII/SalI sites of pmCherryC1, pEYFP-N1 plasmids (Primers were shown in the *Table 2.1*).

**2.2.1.8 Site directed mutagenesis**

Ccdc-124 Ser, Thr, Tyr putative phosphorylation site mutants were generated on the plasmid vector containing C-ter HA-linked version of Ccdc124 (L-HA) using the sense and antisense primers were shown in the *table 2.2*.

40 ng template DNA and 10 pmol of sense (S) and anti-sense (AS) primers were used in mutagenesis PCR reactions which involved 5 min. initial denaturation at 95°C followed by 18 cycles of 1 min 60°C, 6 min 68°C, 1 min 95°C, and the final extension step of 10 min 68°C. Then, samples were subjected to DpnI digestion and transformed into E.coli DH5a competent cells. The plasmids were isolated and their sequences were verified by sequencing.

**2.2.1.9. Agarose gel electrophoresis of DNA**

Agarose was dissolved in 1X TAE buffer (DNA samples < 1kb were separated in 1-2% agarose gel, > 1kb were loaded 0.8% agarose gel.) in microwave and ethidium bromide was added to a final concentration of 10 μg/ml. The DNA samples were prepared with 1x loading dye and were loaded onto gels. The gel was run in 1x TAE at different voltage and time depending on the size of the DNA fragments.

### 2.2.2. Cell culture methods

#### 2.2.2.1. Cell lines and Stable clones

Human embryonic kidney (HEK293), Human cervical cancer cell line (HeLa), Human osteosarcoma (U2OS) cell line, Huh7, MCF7N, HepG2, Snu449, Retinal Pigment Epithelial-1 (RPE-1) cell line, and RPE1-GFP-Centrin, RPE1-GFP-Plk1 cell lines were used in this study. Cell lines having Trex in their names are similar to those explained above, except that they contain a constitutively expressed bacterial tetracycline repressor (TetR) gene.

To obtain stably N-ter-Flag-Ccdc124, C-ter-Flag-Ccdc124, and N-ter-GFP –Ccdc124 expressing HEK293 cell lines, a cytotoxicity curve was performed with Geneticin-G418. 600 μg/ml G418 was chosen for selection. HEK293 cells were transfected with Flag-Ccdc124, Ccdc124-Flag, GFP-Ccdc124 plasmid constructs and their controls by using Fugene6 transfection reagent as mentioned *table 2.4*. 1-2 day later, transfected cells were seeded onto 150mm plates. After 24 hours growth medium were changed with selection antibiotic containing medium. We waited 7-14 days for formation of colonies. Then colonies were transferred into 6 well plates and cell pellet of the colonies were used to perform immunoblotting. Positive colonies were selected and preserved by freezing for future experiments.

#### 2.2.2.2 Growth conditions of cell lines

HEK293, Trex-293, Huh7, HepG2, Trex-HepG2 U2OS cells, and HeLa cells were maintained in high glucose DMEM, MCF7N, Trex-MCF7, Snu449, Trex-Snu449 cell lines were grown in RPMI, C2C12 in %20 FBS containing DMEM, differentiated C2C12 was grown in DMEM (high glucose + glutamine, no Sodium Pyruvate) Donor equine serum, insulin and Retinal Pigment Epithelial-1 (RPE1) cells were grown in DMEM/F12 (1:1) supplemented with 10% FBS, 1% penicillin/streptomycin (P/S) and 1% L-glutamine and kept at 37 $^{\circ}$C in a humidified 5% CO2 atmosphere. RPE1 cells were obtained from Nurhan Özlü (Koç University, Istanbul), and RPE1 lines stably expressing GFP-Centrin, and GFP-Plk1 were gifts

from Greenfield Sluder (U. Mass. Medical School, MA), and Prasad Jallepalli (Memorial Sloan-Kettering, NY), respectively.

#### 2.2.2.3 Cell cycle synchronization

Cells were synchronized by a first thymidine block (2,5 mM) for 16 hours, released for 8 hours, and then blocked a second time with thymidine for 16 hours, followed by 200 nM nocodazole treatment/12 hours. Mitotic arrested cells were collected by "mitotic shake-off", and either analyzed directly (0 min.), or recultured for 15, 30, 45, 60, 120, 150, and 180 mins. At the beginning of the experiments cell cycle status of samples were established by FACS analysis as described in Fabbro *et al*. [39] and at each time point cells were processed for Immunofluorescence.

#### 2.2.2.4 FACS analysis of the cells

$1x10^6$ unsynchronized or synchronized cells were collected as samples, and resuspended in 0.3 ml of PBS buffer. Cells were fixed by addition of 0.7 ml cold ethanol (70%), left on ice for 1hr, and then washed and resuspended in 0.25 ml of PBS in which they were treated with 0.5mg/ml RNAse-A for 1 hr at 37°C. Cellular DNA is then stained with 10 μg/ml propidium iodide (PI) solution, and cytometric analysis was performed by FACS at 488 nm. Data was analyzed by using Accuri C6 C flow plus software.

#### 2.2.2.5. Cryopreservation of stock cells

Exponentially growing cells in 100mm cell culture plate were harvested by trypsinization and collected in 5 ml growth medium. Then, cells were precipitated at 1500 rpm for 3 min. The pellet was suspended in a freezing medium (10% DMSO, 10% FCS and 80% DMEM). Pellets were resuspended in 1ml freezing medium in cryotubes and they were left at -20°C O/N. The next day cells were stored-80°C for 1 day to 1 month. Finally, the tubes were transferred into the liquid nitrogen storage tank for future experiments.

#### 2.2.2.6. Thawing of frozen cells

The frozen cell line was taken from the liquid nitrogen tank and immediately put on ice and then placed into a 37°C water bath for 1-2 minutes. The cells were transferred into 15ml tubes and resuspended in 5ml growth medium. The cells were centrifuged at 1500 rpm for 3 minutes. Supernatant was discarded and the pellet was resuspended in 10 ml culture medium to be plated into 100 mm dish. After overnight incubation culture mediums were replenished.

#### 2.2.2.7. Transient transfection of eukaryotic cell lines

##### 2.2.2.7.1. Transfection of cell lines using FuGene-6 and PEI

Cell lines were transfected with plasmid DNAs using FuGENE-6 reagent (Roche) and PEI. FuGENE:DNA and PEI:DNA ratios were determined experimentally to be 3:1 for, HeLa and U2OS, 1:2,5 for HEK293 cells. In general, appropriate amount of cells were seeded onto tissue culture dishes the day before the transfection, so that they reached 80-90% confluency on the day of transfection. Before the transfection, growth medium was aspirated and replaced with growth medium without antibiotics. Serum and antibiotic free medium were mixed with plasmid DNA in 1.5 ml tubes and appreciate transfection reagent were added on the mix, incubated at RT 30 minutes for Fugene and 20 minutes for PEI. Transfection reagent/DNA mix was added dropwise to the plate of cells. Transfected cells were incubated for 24 hr at 37°C in an incubator with an atmosphere of 5% $CO_2$ in air. 1 day after transfection medium was refreshed with growth medium and placed back to incubator for a further 24 hours. The transfection reagents and appropriate amounts of DNA used for transfection in different cell lines and different culture plates were given in Table 2.4.

Table 2.4. The amounts of reagents and media that were used in Fugene and PEI transfection methods.

| Reagents \ Type of plate | | 150mm plate | 100mm plate | 6 well plate | 12 well plate |
|---|---|---|---|---|---|
| **FUGENE** | HEK293 | 90 µl | 15µl | 2.5µl | 1.5µl |
| | HeLa | 108 µl | 18µl | 3µl | 1.5µl |
| | U2OS | 108 µl | 18µl | 3µl | 1.5µl |
| **PEI** (HEK293) | | 37.5µl | 15µl | 2.5µl | - |
| **DMEM W/O** | | 1ml | 0.5ml | 0.1ml | 0.1ml |
| **DNA** | | 18µg | 6 µg | 1µg | 0.5µg |
| **Culture medium** | | 20 ml | 10ml | 2ml | 1ml |

**2.2.2.7.2. Transfection of cell lines using Lipofectamine RNAiMax**

50 nM of Mission® esiRNA from Sigma-Aldrich (cat. EHU004061) was used for silencing Ccdc124 in HeLa cells by using Lipofectamine RNAiMax (Invitrogen) as transfection reagent.

500 µl of optiMEM was added in 6 well plates, 50ng siRNA was added on top of optiMEM, and mixed gently. 5µl Lipofectamine RNAiMax was added to each well

containing diluted RNAi molocule, mixed and they incubated at RT for 10-20 min. Cells were diluted in 2.5 ml complete medium without antibiotics, added onto RNAi-lipofectamine mix and mixed gently by rocking the plate back and forth. Cells were analysed 48-72 hours later by WB, IF.

### 2.2.3 RNA extraction

The expression level of Ccdc124 and GAPDH in different cell lines was monitored by semiquantitative RT-PCR. RNA was prepared from cell pellets using the NucleospinRNA II kit (Macherey-Nagel #740955) as recommended by the manufacturer. The RNA preparation protocol included on-column Dnase treatment step, minimizing the presence of genomic DNA in the RNA samples. RNA concentrations were determined by spectrophotometry.

### 2.2.4 cDNA synthesis and RT-PCR assay

Revert-Aid first Strand cDNA Synthesis Kit (MBI Fermantas #K1622, Germany) was used for preparation of first strand cDNA from 2ug of total RNA. Semi-quantitative RT-PCR primers amplified two or more exonic sequences. –RT control was prepared to ensure the amplification from cDNA only.

PCR amplification was done in 25 µl reaction volumes containing 1X PCR buffer, 1.5 mM MgCl2, 200 µM dNTP, 10 pmoles of each primer, and 1 unit of *Taq* DNA polymerase (Fermentas). Thermal cycler conditions consisted of an initial denaturation step at 95°C for 5 min; a loop cycle of 95°C, 20sec / 60°C, 20sec / 72°C, 30sec; and a final extension at 72°C for 5 minutes. The cycle number varied for each transcript amplified, for Cdc124 and RAP2A 30 it was 30 cycles, for RasGEF1B (1.iso) it was 35 cycles, and cycle number for GAPDH was 21 cycles. PCR products were run on 2% agarose gel.

### 2.2.5 Western blotting

Cells collected from 6 well culture plates were lysed in 50 µl lysis buffer. Protein concentrations were determined by Bradford assay. 40 µg of whole cell extracts were

denatured in gel loading buffer at 95°C for 5 min, resolved by SDS-PAGE using a 12% gel, and electrotransferred onto PVDF membranes (Millipore).

### 2.2.6 Immunoprecipitation (IP)

For RasGEF1B/Ccdc124 co-immunoprecipitation experiments, HEK293 cells were transfected with Flag-Ccdc124 and YFP-RasGEF1B vectors. 48 hours later, cells were lysed in NP-40 lysis buffer, flag-tagged agarose beads (A2220, Sigma-Aldrich) were used to precipitate proteins for two hours, followed by a centrifugation for 30 sec. at 8800 rpm, then beads were washed three times with NP-40 lysis buffer. 50µl sample buffers were added to lysates and incubated at 95°C for 5 min, fractionated by SDS-PAGE for immunoblot analysis and transferred onto PVDF membranes (Millipore). Anti-GFP (G1544, Sigma-Aldrich) and anti-Flag-HRP M2 (A8592, Sigma-Aldrich) were used in Western blot analysis. Blotted proteins were visualized using the ECL detection system (Amersham).

### 2.2.7 Immunofluorescence (IF)

HeLa cells on cover slips were fixed by ice cold 100% Metanol for 10 min at -20, washed three times with PBS-T; blocked in 2% BSA for 1 hour and incubated 1 hour with primary, washed again three times with PBS-T and incubated for 1 hour with suitable secondary antibodies. Fluorescent images were taken by Zeiss Imager-A1 microscope with a Zeiss Acroplan 40X objective. Images were captured on the Zeiss Axia Cam MRc 5- CCD camera for fixed samples. Microscope control and image processing were done through Axiovision version 4.6 software program (Universal Imaging).

### 2.2.7 *In vitro* CKII Kinase Assay

CKII kinase was purchased from NEB Biosciences (New Jersey, USA). In CKII phosphorylation analysis of Ccdc124, in each experimental set-up 1.5 µg nickel column purified his-tagged Ccdc124 (kindly provided by Elif Yaman) was used. For detection of phosphorylation, ATP (100 µM) was replaced by ATP-γ-S (100 µM; Epitomics, #3701-1), and thiophosphorylate its substrate. Then thiophosphorylation

site on the substrate is alkylated with p-nitrobenzyl mesylate (PNMB, Epitomics, #3700-1) and following tagged kinase substrate was detected by a specific antibody (Thiophosphate Ester RabMAb, Epitomics, #2686-1). In control experiments, CKII activity was inhibited by addition of 10 μM of 4,5,6,7-Tetrabromo-2-azabenzimiddazole (TBB; Calbiochem # 218697) to *in vitro* assay reactions. *In vitro* kinase reaction was carried-out for 30 min. at 30°C using CKII protein (100 U) incubated with pure 1.5 μg his-tagged Ccdc124 protein as substrate using ATP-γ-S followed by alkylation 2 hours with PNBM at RT.

### 2.2.8 Mass spectrometry

Stable N-terminal (N-ter) and C-ter-Flag tagged Ccdc124, YFP-RasGEF1B, Empty Vector control (3xFlagCMV14), and YFP (control) expressing monoclonal HEK293 cell lines were prepared by Fugene transfection method. Then, these stable clones were selected, and they were maintained in DMEM containing 1% penicillin/ streptomycin, 10% FBS, and 0.6mg/ml Geneticin. Stable isotope labeling by amino acids in cell culture (SILAC) was performed for six doublings in SILAC medium containing light or heavy lysine and arginine aminoacids, 1% penicillin/ streptomycin, 10% FBS and 0.6mg/ml Geneticin. Following the collection of the cells by scraping, the cells lysed in NP-40 buffer and cleared by centrifugation. The supernatants were transferred to new eppendorf tubes and protein concentrations of were calculated using Bradford assay. The light amino acids and heavy amino acid containing lysates were mixed in 1:1 ratio. After that, lysates were bound to Flag beads or GFP beads for two hours to allow precipitation. There are two methods to convert them into peptides with suitable sizes for MS analysis. The first one is based on the solubilization of proteins in SDS gel, whereas the second one is the detergent free digestion of proteins in solution using filter-aided sample preparation (FASP) methods. We performed both of the methods for Ccdc124 and only FASP method for RasGEF1B analysis. For the first method, we added 2x sample buffer onto washed beads following IP and we loaded proteins into commercial Nu-Page gel (Invitrogen). Then, bands were cut and isolated from the gel. Following this step, these gel slices were digested with trypsin at 37°C, and supernatants were put into

new eppendorf tubes. Subsequently, we acidified the digestion mixture with TFA (1%) to stop digestion reaction, and we added 2-gel volumes of 1% TFA/30% ACN for extraction of peptides. Finally the extraction solution and digestion mixture were combined and the organic component was evaporated in a vacuum centrifuge.

MS samples were also prepared with FASP method in some experiments. Bound proteins were eluted from beads with a low-pH buffer. Eluted lysates were mixed with 200µl of UA (*see Materials*) in the filter and centrifuged. Supernatant was discarded and 100 µl IAA (*see Materials*) was added and mixed at 600 rpm in a thermo-mixer for 1 min. and samples were incubated without mixing for 20 mins. Then, samples were centrifuged twice at 13000 rpm for 10 min. Subsequently, filters were washed two times 100 µl UA, and again two times with 100 µl ABC (*see Materials*) buffer. Following the addition of 40 µl trypsin, samples were incubated at 37°C for O/N. After that filter units were transferred into new collection tubes, and centrifuged at 13000 rpm for 10 min. Finally, peptides were eluted using 0.5 M NaCl and desalted. Before to LC-MS/MS analysis, peptides dried in vacuum centrifuge and reconstituted in 5% formic acid (FA).

After preparation of samples with in-gel digestion, or in solution digestion method (FASP), peptides were loaded to a reversed phase nano-LC-MS/MS analysis consisting of an Agilent 1200 series HPLC system connected to an LTQ-Orbitrap mass-spectrometer (Thermo Fischer Scientific).

Raw spectrometric data from the SILAC experiments were analyzed by using MaxQuant software package (version 1.0.13.12). MS/MS spectra were searched against IPI human database (version 3.52) using Mascot (Version 2.2.04).

### 2.2.9 *In vivo* studies

#### 2.2.9.1 Morpholino injections of Zebrafish embryos

For knockdown of Ccdc124 function in zebrafish embryos a specific morpholino was designed to block translation of Ccdc124 by complementary binding to Ccdc124 transcripts three nucleotides upstream of the AUG site. Ccdc124 and control

morpholinos were diluted at 2.5 ng/µl in 1x Danieau solution supplemented with 0.05% phenol red (Sigma). A total of 4 nl of diluted morpholino was injected into 1 cell stage zebrafish embryos and embryos were analyzed at 2 hpf, 5 hpf, and 3 dpf. Western blot quantification using a zebrafish sequence-specific anti Ccdc124 antibody in 3 dpf larvae revealed a 35 % decrease of Ccdc124 protein in morphants when compared to uninjected or control morpholino-injected embryos. For early embryo analysis and quantification of DNA content, embryos were incubated with the vital stain BODIPY 505/515 (Molecular Probes) and subjected to confocal microscopy imaging. Embryos were co-labeled with DAPI to visualize nuclear DNA contents. Confocal images were thresholded and binarized and the number of positive pixels was counted as a measure of DNA content per cell.

# CHAPTER 3. RESULTS

## 3.1 Molecular characterization of Ccdc124 as a protein

*CCDC124* was previously found in our group as an expressed eukaryotic conserved gene when putative down-stream *cis*-acting transcriptional regulatory elements of the $Na^+/I^-$ Symporter (NIS) gene were studied (unpublished results). In those past studies, in an attempt to find novel transcriptional regulatory sites of NIS, we had started computational analyses to identify conserved non-coding regions of NIS gene (Hani Alotaibi, Serap Erkek, Pelin Telkoparan, and Uygar H. Tazebay, unpublished results). Different putative conserved regions were identified in human, rat and mouse genomes by using VISTA bioinformatics tools [67]. These regions were then analyzed by luciferase assays, and the most 3′ fragment displayed a very high transcriptional activity (Hani Alotaibi and Uygar H. Tazebay, unpublished). It was then realized that this did not contain a 3′ regulatory element of the NIS gene, but rather it was a region that control the expression of a novel gene called *CCDC124*.

In the present thesis work, we carried-out functional analysis of *CCDC124* which encodes an mRNA that is transcribed from chromosome 19p13.11, consisting of five exons, of which exon 1 is non-coding. Ccdc124 protein sequence was aligned with other species via BLAST analysis it was indicated that the protein encoded from this genetic locus shares, 70% identity/89.1% similarity with its orthologue NP_956859 in the vertebrate model *Danio rerio* (zebrafish), or 50.4% identity/72.6% similarity with Y73E7A.1 in the invertebrate *Caenorhabditis elegans*. *CCDC124* has also other orthologs in lower eukaryotes, such as the filamentous fungus *Aspergillus nidulans* (AN0879.2; 35.1% identity/58.2% similarity), or the fission yeast *Schizosaccharomyces pombe* (SPBC29A10.12; 33% identity/57.8% similarity), while it is not found in the budding yeast *Saccharomyces cerevisiae*.

Protein sequences of Ccdc124 from different species were compared by Clustal W2 alignment program (Fig. 3.1).

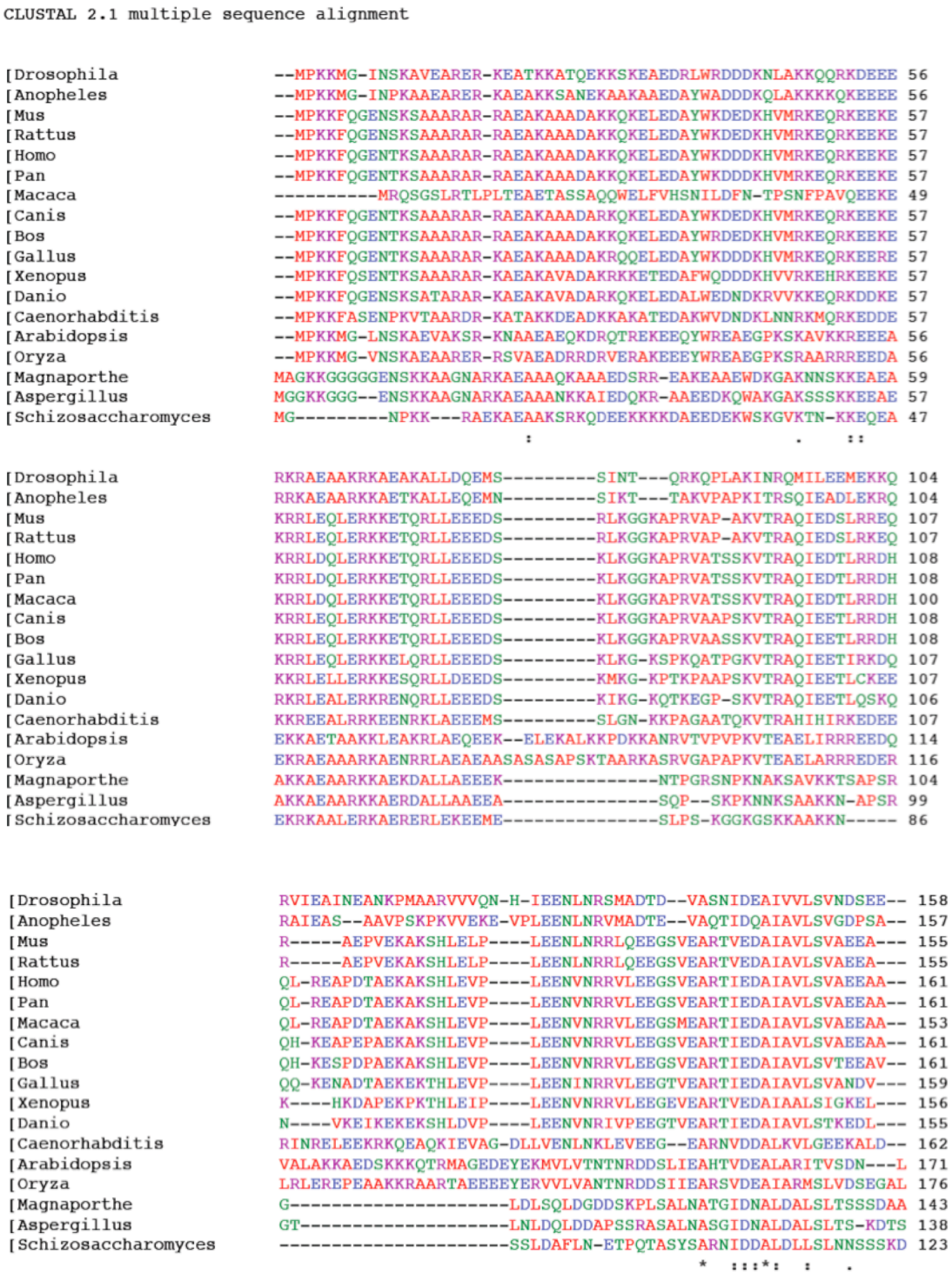
CLUSTAL 2.1 multiple sequence alignment
[Drosophila --MPKKMG-INSKAVEARER-KEATKKATQEKKSKEAEDRLWRDDDKNLAKKQQRKDEEE 56
[Anopheles --MPKKMG-INPKAAEARER-KAEAKKSANEKAAKAAEDAYWADDDKQLAKKKKQKEEEE 56
[Mus --MPKKFQGENSKSAAARAR-RAEAKAAADAKKQKELEDAYWKDEDKHVMRKEQRKEEKE 57
[Rattus --MPKKFQGENSKSAAARAR-RAEAKAAADAKKQKELEDAYWKDEDKHVMRKEQRKEEKE 57
[Homo --MPKKFQGENTKSAAARAR-RAEAKAAADAKKQKELEDAYWKDDDKHVMRKEQRKEEKE 57
[Pan --MPKKFQGENTKSAAARAR-RAEAKAAADAKKQKELEDAYWKDDDKHVMRKEQRKEEKE 57
[Macaca ----------MRQSGSLRTLPLTEAETASSAQQWELFVHSNILDFN-TPSNFPAVQEEKE 49
[Canis --MPKKFQGENTKSAAARAR-RAEAKAAADARKQKELEDAYWKDEDKHVMRKEQRKEEKE 57
[Bos --MPKKFQGENTKSAAARAR-RAEAKAAADAKKQKELEDAYWRDEDKHVMRKEQRKEEKE 57
[Gallus --MPKKFQGENTKSAAARAR-KAEAKAAADAKRQQELEDAYWKDDDKHVMRKEERE 57
[Xenopus --MPKKFQSENTKSAAARAR-KAEAKAVADAKRKKETEDAFWQDDDKHVVRKEHRKEEKE 57
[Danio --MPKKFQGENSKSATARAR-KAEAKAVADARKQKELEDALWEDNDKRVVKKEQRKDDKE 57
[Caenorhabditis --MPKKFASENPKVTAARDR-KATAKKDEADKKAKATEDAKWVDNDKLNNRKMQRKEDDE 57
[Arabidopsis --MPKKMG-LNSKAEVAKSR-KNAAEAEQKDRQTREKEEQYWREAEGPKSKAVKKREEEA 56
[Oryza --MPKKMG-VNSKAEAARER-RSVAEADRRDRVERAKEEEYWREAEGPKSRAARRREEDA 56
[Magnaporthe MAGKKGGGGGENSKKAAGNARKAEAAAQKAAAEDSRR-EAKEAAEWDKGAKNNSKKEAEA 59
[Aspergillus MGGKKGGG--ENSKKAAGNARKAEAAANKKAIEDQKR-AAEEDKQWAKGAKSSSKKEEAE 57
[Schizosaccharomyces MG---------NPKK---RAEKAEAAKSRKQDEEKKKKDAEEDEKWSKGVKTN-KKEQEA 47
: . ::
[Drosophila RKRAEAAKRKAEAKALLDQEMS---------SINT---QRKQPLAKINRQMILEEMEKKQ 104
[Anopheles RRKAEAARKKAETKALLEQEMN---------SIKT---TAKVPAPKITRSQIEADLEKRQ 104
[Mus KRRLEQLERKKETQRLLEEEDS---------RLKGGKAPRVAP-AKVTRAQIEDSLRREQ 107
[Rattus KRRLEQLERKKETQRLLEEEDS---------RLKGGKAPRVAP-AKVTRAQIEDSLRKEQ 107
[Homo KRRLDQLERKKETQRLLEEEDS---------KLKGGKAPRVATSSKVTRAQIEDTLRRDH 108
[Pan KRRLDQLERKKETQRLLEEEDS---------KLKGGKAPRVATSSKVTRAQIEDTLRRDH 108
[Macaca KRRLDQLERKKETQRLLEEEDS---------KLKGGKAPRVATSSKVTRAQIEDTLRRDH 100
[Canis KRRLEQLERKKETQRLLEEEDS---------KLKGGKAPRVAAPSKVTRAQIEETLRRDH 108
[Bos KRRLEQLERKKETQRLLEEEDS---------KLKGGKAPRVAASSKVTRAQIEETLRRDH 108
[Gallus KRRLEQLERKKELQRLLEEEDS---------KLKG-KSPKQATPGKVTRAQIEETIRKDQ 107
[Xenopus KKRLELLERKKESQRLLDEEDS---------KMKG-KPTKPAAPSKVTRAQIEETLCKEE 107
[Danio RKRLEALERKRENQRLLEEEDS---------KIKG-KQTKEGP-SKVTRAQIEETLQSKQ 106
[Caenorhabditis KKREEALRRKEENRKLAEEEMS---------SLGN-KKPAGAATQKVTRAHIHIRKEDEE 107
[Arabidopsis EKKAETAAKKLEAKRLAEQEEK--ELEKALKKPDKKANRVTVPVPKVTEAELIRRREEDQ 114
[Oryza EKRAEAAARKAENRRLAEAEAASASASAPSKTAARKASRVGAPAPKVTEAELARRREDER 116
[Magnaporthe AKKAEAARKKAEKDALLAEEEK---------------NTPGRSNPKNAKSAVKKTSAPSR 104
[Aspergillus AKKAEAARKKAERDALLAAEEA---------------SQP--SKPKNNKSAAKKN-APSR 99
[Schizosaccharomyces EKRKAALERKAERERLEKEEME---------------SLPS-KGGKGSKKAAKKN----- 86
[Drosophila RVIEAINEANKPMAARVVVQN-H-IEENLNRSMADTD--VASNIDEAIVVLSVNDSEE-- 158
[Anopheles RAIEAS--AAVPSKPKVVEKE-VPLEENLNRVMADTE--VAQTIDQAIAVLSVGDPSA-- 157
[Mus R-----AEPVEKAKSHLELP----LEENLNRRLQEEGSVEARTVEDAIAVLSVAEEA--- 155
[Rattus R-----AEPVEKAKSHLELP----LEENLNRRLQEEGSVEARTVEDAIAVLSVAEEA--- 155
[Homo QL-REAPDTAEKAKSHLEVP----LEENVNRRVLEEGSVEARTIEDAIAVLSVAEEAA-- 161
[Pan QL-REAPDTAEKAKSHLEVP----LEENVNRRVLEEGSVEARTIEDAIAVLSVAEEAA-- 161
[Macaca QL-REAPDTAEKAKSHLEVP----LEENVNRRVLEEGSMEARTIEDAIAVLSVAEEAA-- 153
[Canis QH-KEAPEPAEKAKSHLEVP----LEENVNRRVLEEGSVEARTIEDAIAVLSVAEEAA-- 161
[Bos QH-KESPDPAEKAKSHLEVP----LEENVNRRVLEEGSVEARTIEDAIAVLSVTEEAV-- 161
[Gallus QQ-KENADTAEKEKTHLEVP----LEENINRRVLEEGTVEARTIEDAIAVLSVANDV--- 159
[Xenopus K----HKDAPEKPKTHLEIP----LEENVNRRVLEEGEVEARTVEDAIAALSIGKEL--- 156
[Danio N----VKEIKEKEKSHLDVP----LEENVNRIVPEEGTVEARTIEDAIAVLSTKEDL--- 155
[Caenorhabditis RINRELEEKRKQEAQKIEVAG-DLLVENLNKLEVEEG--EARNVDDALKVLGEEKALD-- 162
[Arabidopsis VALAKKAEDSKKKQTRMAGEDEYEKMVLVTNTNRDDSLIEAHTVDEALARITVSDN---L 171
[Oryza LRLEREPEAAKKRAARTAEEEEYERVVLVANTNRDDSIIEARSVDEAIARMSLVDSEGAL 176
[Magnaporthe G----------LDLSQLDGDDSKPLSALNATGIDNALDALSLTSSSDAA 143
[Aspergillus GT----------LNLDQLDDAPSSRASALNASGIDNALDALSLTS-KDTS 138
[Schizosaccharomyces ----------SSLDAFLN-ETPQTASYSARNIDDALDLLSLNNSSSKD 123
* :::*: : .

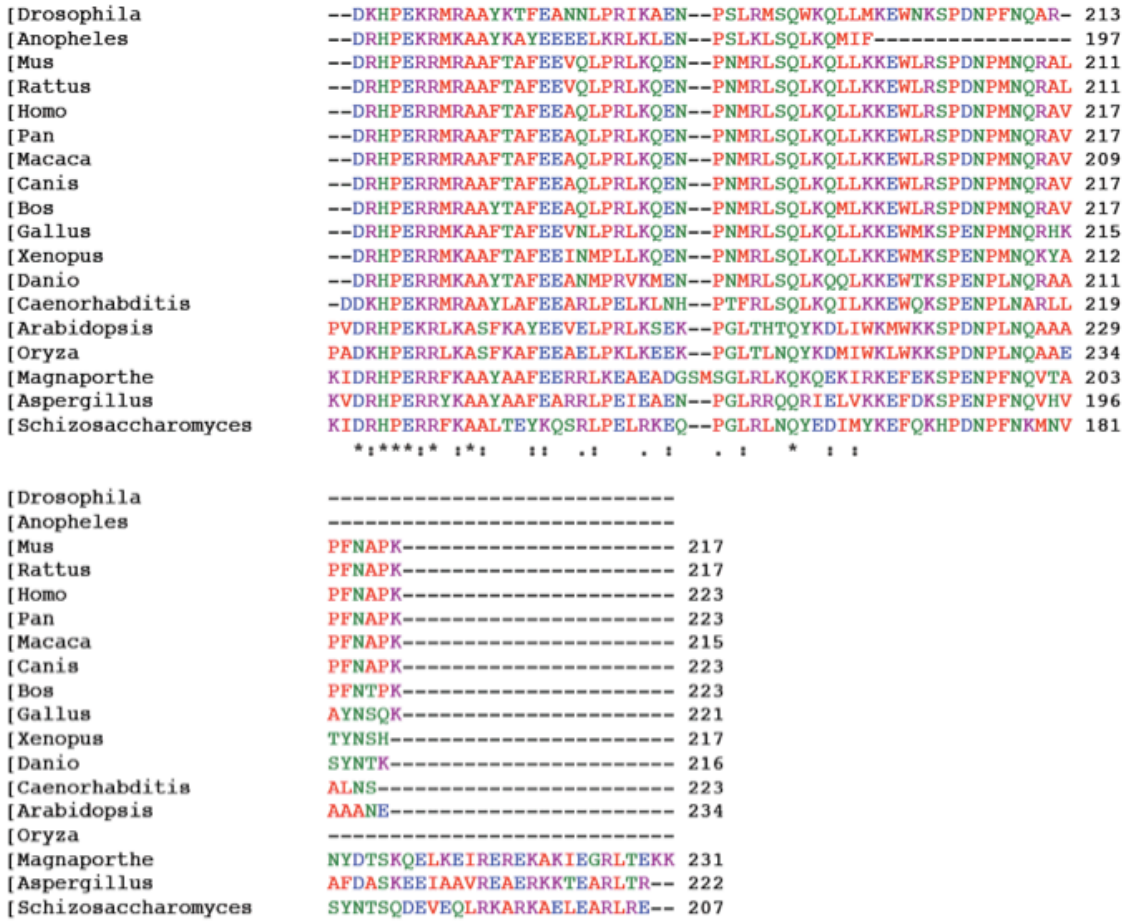


**Figure 3.1** Protein sequence alignment of known and predicted amino-acid sequences of Ccdc124 orthologs from different species (*see the text*). The alignment was performed by using ClustalW (2.1 version) alignment program (http://www.ebi.ac.uk/clustalw/). Asterisks (*) indicate positions of fully conserved residues; column (: shows conservation within a strong group of amino acids; and dots (.) indicate conservation within weaker groups of amino acids. Residue coloring is according to standard physiochemical criteria (red: small hydrophobic; blue: acidic; magenta: basic; green: hydroxyl, amine and basic).

This analysis showed that Ccdc124 is highly conserved especially through residues 25-80 and 160-210 among all investigating eukaryotic species including lower eukaryotic species, except the budding yeast *Saccharomyces cerevisiae*. This strong evolutionary conservation suggests a very basic biological function for Ccdc124.

Subsequently, we constructed phylogenetic trees from alignments shown in Fig. 3.1 using neighbor joining (Fig.3.2). Amino acid sequences derived from the full-length cDNA sequences encoding Ccdc124 from 17 species were indicated in the alignment presented in Fig. 3.1. The following sequences were used to construct alignments:

(NP_001129675.1) Ccdc124 [Homo sapiens], (XP_001173732.1) Ccdc124 isoform 2 [Pantroglodytes], (XP_001115097.1) Ccdc124-like [Macaca mulatta],(XP_003432943.1) Ccdc124-isoform 1, (NP_001033612.1) Ccdc124 [Bos aurus], (NP_081240.1) Ccdc124 [Mus musculus], (NP_001099541.1) Ccdc124 [Rattus norvegicus], (XP_424681.1) Ccdc124 [Gallus gallus], (NP_956859.1) Ccdc124 [Danio rerio], (NP_650777.1) CG6013 [Drosophila melanogaster], (XP_312989.3) AGAP004110-PA [Anopheles gambiae str. PEST], (NP_001040712.2) Protein Y73E7A.1, isoform a [Caenorhabditis elegans], (NP_596057.1) HMG-box variant [Schizosaccharomyces pombe 972h-],(XP_363558.1) hypothetical protein MGG_01484 [Magnaporthe oryzae 70-15],(XP_962308.1) hypothetical protein NCU07666 [Neurospora crassa OR74A], (NP_563993.1) uncharacterized protein [Arabidopsis thaliana] (NP_001053553.1) Os04g0561600 [Oryza sativa Japonica Group]. As expected, Ccdc124 is conserved from Human to lower eukaryotes. Vertebrate Ccdc124s were clustered together reflecting taxonomic relationship among these organisms. Similarly invertebrate, plant and lower eukaryote members formed separate but related clusters (Fig.3.2).

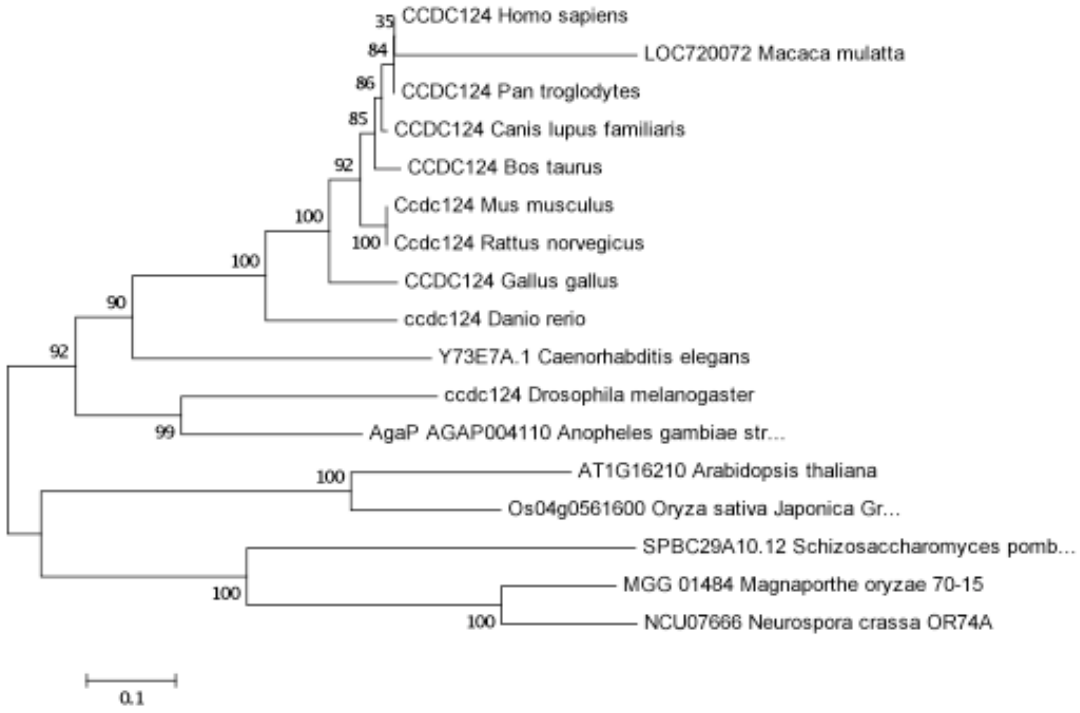


**Figure 3.2** Phylogenetic trees of Ccdc124.The tree was generated using the program MEGA version 4. The tree was calculated using Neighbour Joining method. Numbers at the branches indicate bootstrap values. The bar shows number of substitutions per mutation site.

*CCDC124* gene encodes a 223 amino acids protein and have two conserved coiled coil domains (CCD) in the N-terminus of the protein between residues 18-82 via ELM (http://elm.eu.org) search. An analysis of coiled-coil domains using COILS (www.ch.embnet.org/software/COILS_form.html) bioinformatics platforms indicated that the protein has two independent coiled motifs located at the N-terminus between residues 18-82 (Fig. 3.3), and therefore it is considered as a CCD containing protein.

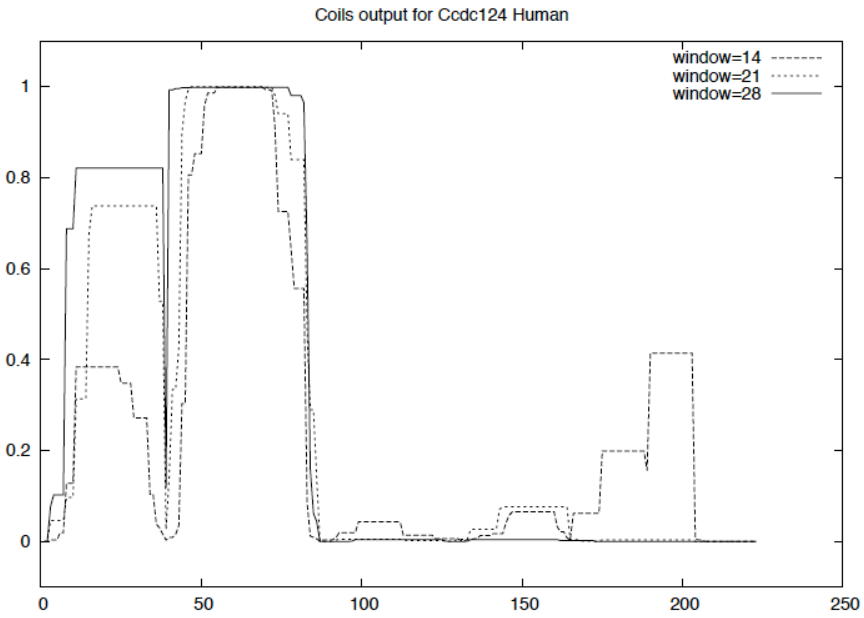


**Figure 3.3** Schematic representation of the coiled-coil prediction of Ccdc124 obtained by the COILS (www.ch.embnet.org/software/COILS_form.html) bioinformatics analysis platform. Ccdc124 contains two main coiled-coil domains at its N-terminal part.

CCD is an interaction domain and it typically consists of two α-helices that are twisted around each other to form a supercoil. Most coiled coil proteins are in their left-handed forms. Sequences of left-handed parallel coiled coils are characterized by heptad repeats [68]. The first and fourth of the residues of heptads are formed by apolar (leucine, valine, isoleucine) residues and these residues stabilize helix by hydrophobic interactions. The residues fifth and seventh are usually charged (glutamate or lysine) to form ionic inter-helical interactions. The other three residues are hydrophilic, and they form helical surfaces [68]. As indicated in Fig. 3.3, our bioinformatics analysis has revealed that human Ccdc124 fulfills these sequence requirements of CCD-containing (CCDC) proteins (see Fig. 3.3).

CCDC proteins have many roles in different biological functions, such as signal transduction, molecular recognition, establishment of mechanical stability to cells, and it is also involved in kinesin-linked movement processes [69]. Previous biochemical studies and mass-spectrometry analyses on purified centrosomes have shown that proteins with CCD motifs are abundant in Pericentriolar matrix (PCM) [30, 70]. Close to 150 different proteins were identified in the PCM at different cellular stages, about 60% of which contain predicted CCD type oligomerization

motifs [30]. This gave us initial hints about a possible centrosome localization of Ccdc124, a hypothesis that we followed closely in coming sections, below.

### 3.2 Expression profiling of *CCDC124* in mammalian tissues and cell lines

Previous work in our laboratory involving Northern blot analysis of *CCDC124* gene revealed that this gene is ubiquitously expressed in all human tissues, and relatively high levels of expression were detected in brain, liver, spleen, skeletal muscle, testis, and ovaries (Serap Erkek, M.Sc. thesis, 2008 and [71] ). In these analyses, a transcript of ~1061 nucleotides was detectable in all human organs tested, in agreement with the predicted size of *CCDC124* mRNA in the NCBI databases (http://genome.ucsc.edu), except the placenta where we observed a second shorter mRNA species (~950) indicative of a transcript variant [71].

We established the expression profile of *CCDC124* by RT-PCR in various cell lines of different tissue origins. In this study, we have not observed a significant expresssion variation among those cell lines compared to *GAPDH* (Fig. 3.4). This study also indicated that *CCDC124* was ubiquitously expressed in all cell lines tested.

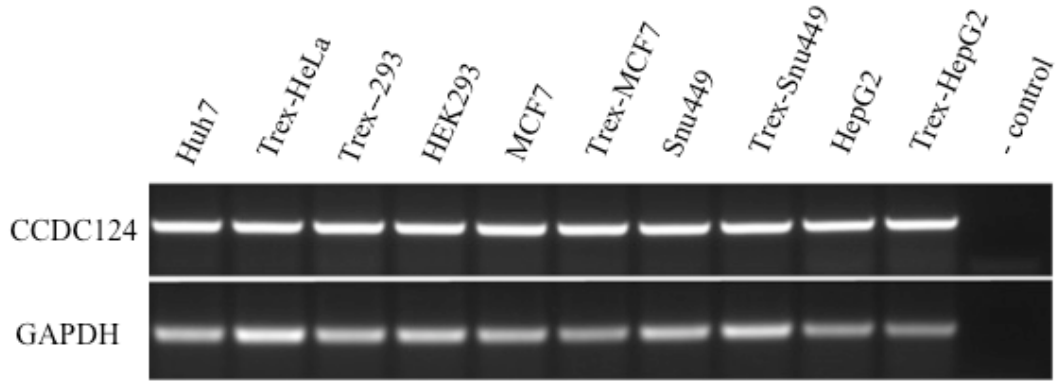


**Figure 3.4** Expression analysis of *CCDC124* in different human cell lines. cDNA from cell lines were amplified with *CCDC124* RT primers. PCR products were loaded agarose gel and analyzed by electrophoresis. Human embryonic kidney (HEK293), Human cervical cancer cell line (HeLa), Human osteosarcoma U2OS cell line, Huh7, MCF7N, HepG2, Snu449 cell lines were used in this study. Cell lines having Trex in their names are similar to those explained above, except that they contain a constitutively expressed bacterial tetracycline repressor (TetR) gene. (-) control, indicates the negative control reaction sample without the RT enzyme.

To characterized *CCDC124*, we first decided to characterize the recognition specificity of Ccdc124 in Western blots by different specific antibodies that are

available to us. This is because there are three rabbit polyclonal antibodies that recognize different epitopes in Ccdc124: two commercially available ones (Bethyl labs. A301-834, and A301-835), and one self-generated antibody through Cambridge Biological Research (CRB) laboratory. Note that Ccdc124 is a 223 residue protein, and Bethyl-A301-834 recognize an internal epitope located between residues 100 to 150 of Ccdc124. Therefore, we will refer to this antibody in this thesis as the "anti-mid-Ccdc124" antibody. Bethyl-A301-835 recognize a C-terminus epitope (residues 173-223), thus it is referred as "anti-C-ter-Ccdc124" antibody in the text. The third reagent, the antibody that was produced by our laboratory on order to CRB, recognize the very N-terminus 24 amino acids of Ccdc124, and therefore it is referred as the "anti-N-ter-Ccdc124" ab (Serap Erkek, M.Sc. thesis, 2008; [71]).

We have carried out Western blots either by using lysates from untransfected HEK293 cells, or lysates from CMV-promoter expressed Ccdc124, from N-terminus Flag-epitope tagged Ccdc124, from C-terminus Flag-epitope tagged Ccdc124, C-terminus HA-tagged Ccdc124, N-terminus GFP-tagged Ccdc124, and as a control empty vector transfected cells (Fig. 3.5 A-D). We first incubated the blot membrane with the N-ter-Ccdc124 specific antibody, and clearly validated that this Ab recognized the 32 kDa Ccdc124 band, as the band intensity was increased in CMV-Ccdc124 transfected cell lysates (Fig. 3.5 B). As expected, the N-terminus flag-tagged Ccdc124 had an increased size (~35 kDa) due to flag-epitope insertion (Fig. 3.5 B). Again, expectedly, this antibody detected GFP-Ccdc124 as a band of ~55 kDa (Fig. 3.5 B). Also, HA-tagged Ccdc124 was correctly detected as a ~34 kDa protein (Fig. 3.5 B). In addition to those, we noticed that the N-ter-Ccdc124-specific antibody also detected an unspecific band of around 70 kDa (upper band). We did not pay further attention to this unspecific band in coming experiments, because the intensity of this band did not increase when cells were transfected with CMV-Ccdc124 vectors (Fig. 3.5B)

Interestingly, flag-tag insertion to Ccdc124 also had some unexpected consequences such as destabilization of the protein: in this blot we have not detected a size increase in Ccdc124 when flag-tag was inserted to C-terminus, and the N-terminus flag-tag containing protein was very much destabilized. (Fig. 3.5 B). When a similar blot membrane was incubated with mid-Ccdc124 ab, we observed similar bands, but we also noticed an extra band of ~26 kDa (indicated with asterisk) in cells transfected

with CMV-Ccdc124, N-terminus flag-tagged, or C-ter HA-tagged Ccdc124 plasmid constructs (Fig. 3.5 C). The same 26 kDa band was also detected by C-ter-Ccdc124 recognizing ab (Fig. 3.5 A) in CMV-Ccdc124 or N-ter Flag-Ccdc124 transfected cells

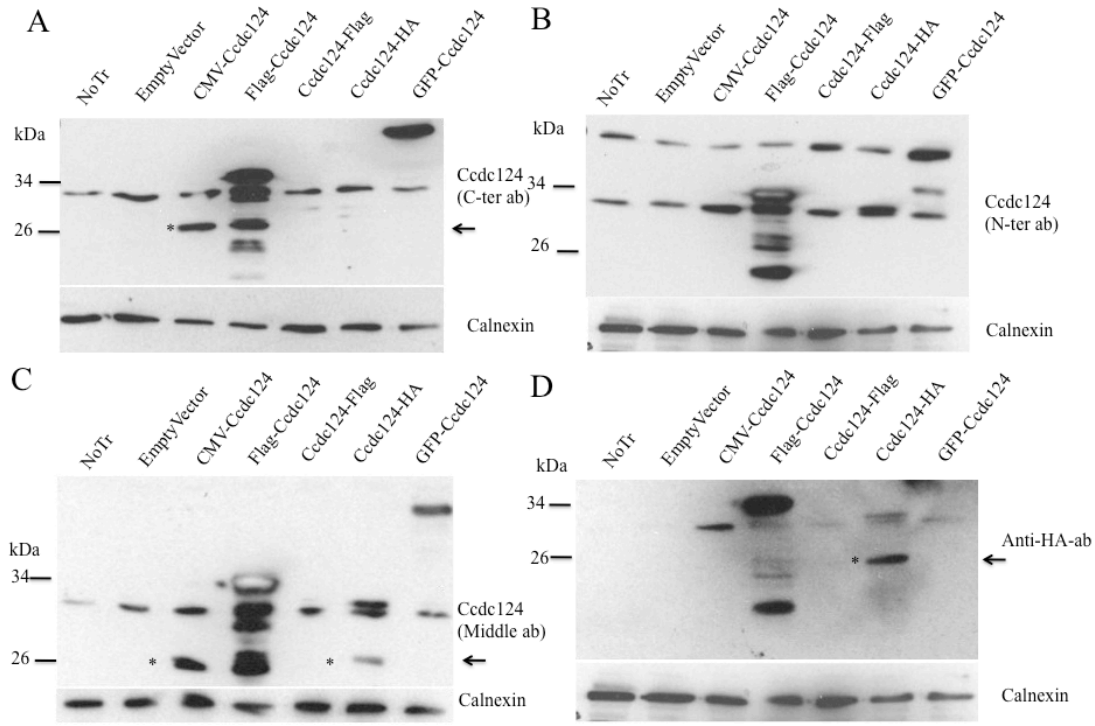


**Figure 3.5** Characterization of Ccdc124 protein in immunoblots by using three different antibodies recognizing different epitopes. HEK293 cells were transfected with Empty Vector, CMV-Ccdc124, N-ter/C-ter-Flag tagged-Ccdc124, C-Ter-HA-Ccdc124 and N-ter-GFP tagged-Ccdc124 plasmid constructs. Proteins extracted from transfected HEK293 cells and 40µg of proteins were loaded into %12 SDS gel and stained with **A)** anti-Cter-Ccdc124 antibody, **B)** anti-Nter-Ccdc124 antibody, **C)** anti-Mid-Ccdc124 antibody, **D)** N-ter-Ccdc124 antibody incubated membrane was stripped then incubated with anti-HA antibody. Asterisks (*) indicate an alternative smaller band that was undetectable with the N-ter-Ccdc124 specific Ab. Calnexin expressions were indicated as gel-loading controls.

But interestingly not in C-ter HA-epitope carrying lysates (Fig. 3.5 C). We wondered whether the non-recognition of the 26 kDa band in C-ter HA-tagged Ccdc124 could be due to a possible masking of the C-ter epitope by HA, and therefore we incubated the blot membrane shown in Fig. 3.5 B this time with an HA-tag specific Ab (Fig. 3.5 D), which revealed the 26 kDa band once again. This indicated that the C-ter epitope in C-ter HA-tagged Ccdc124 protein was masked possibly by steric hindrance between epitopes. Because this 26 kDa protein was recognized both by anti-mid-

Ccdc124 Ab, by anti-C-ter-Ccdc124 Ab, and by anti-HA antibody in cells having suitable constructs, we were sure that it was a part of Ccdc124 and not a non-specific protein detected by those Abs.

We wondered the origin of this 26 kDa band, and hypothesized that this smaller Ccdc124 could be generated by the usage of a possible alternative start codon in the protein. When a bioinformatics analysis was carried out on ATG codons of Ccdc124, we detected codon of the Met-47 residue as such an alternative putative start site. Subsequently, when we mutated this ATG codon to CTG (Leu), this 26 kDa Ccdc124 have now disappeared, clearly indicating that it was resulting from this second alternative start (ATG) codon (Fig. 3.6). After we established the possibility of an alternative start codon in Ccdc124, it was shown that the ATG that we found truly provides an alternative Kozak sequence, forming a second ribosome recognition site in *CCDC124* [72].

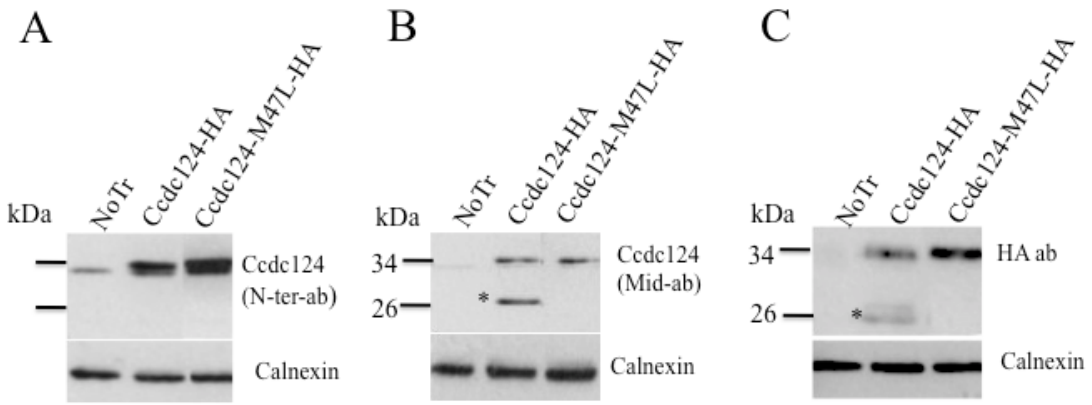


**Figure 3.6.** Identification of an alternative translation start site in Ccdc124 ORF. An internal methionine residue (Met-47) in Ccdc124 ORF was mutated to Leu amino acids in a Ccdc124-HA vector construct. Ccdc124-M47L-HA, and Ccdc124-HA (wt) plasmids were transfected into HEK293 cells. Whole-cell lysates were immunoblotted using anti-N-ter-Ccdc124 **(A),** anti-Mid-Ccdc124 **(B),** anti-HA **(C)** antibodies. Asterisks (*) indicate the alternative smaller protein generated from the Ccdc124 ORF.

We then addressed the instability problem of Flag-tagged Ccdc124 (see Fig. 3.5 A-D), by further analyzing these Flag-tagged versions of Ccdc124 in Western blots using an anti-Flag Ab (Fig. 3.7). We observed that when Flag-tag is inserted to C-terminus of the protein, the size of Ccdc124 did not increase to previously detected

~35 kDa level, but the intensity of the ~32 kDa band increased (Fig. 3.7). Whereas, when the flag-tag was inserted to N-terminus, size of Flag-Ccdc124 was detected as ~35 kDa (Fig. 3.7). This suggested the possibility that when flag-epitope was inserted

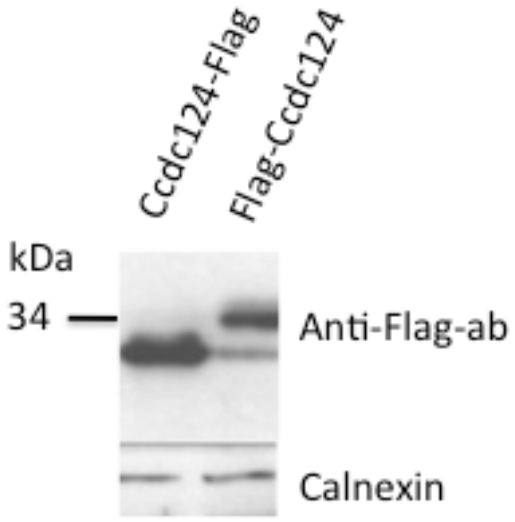


**Figure 3.7** Position of flag-tag insertion affects the stability of Ccdc124. C-ter or N-ter-Flag tagged Ccdc124 plasmids were transfected into HEK293 cells. Whole cell lysates were extracted, and analyzed by immunoblots using anti-Flag antibody. Calnexin expression was displayed as loading control.

to C-terminus, the protein was cleaved either from the N-terminus or from an internal position. In collaboration with the laboratory of Johannes L. Bos at the Utrecht University Medical Center (the Netherlands), we thus decided to carry-out a mass-spectrometry peptide analysis on major bands obtained in experiments with N- and C-ter flag-tagged versions of Ccdc124, in order to fully characterize this observation. For this work, we first established stable HEK293 cell lines that either carried Flag-Ccdc124, Ccdc124-Flag, or empty vector as negative control (Fig. 3.8; empty vector not shown). N-ter and C-ter Flag tagged-Ccdc124 vectors were transfected into HEK293 cells and were left in antibiotic selection for 15 days.

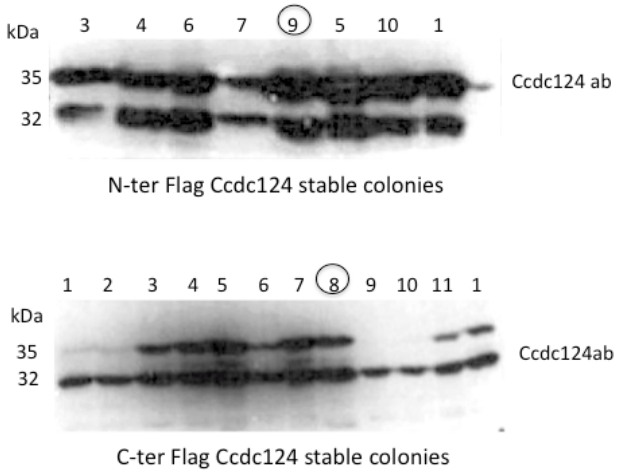


**Figure 3.8.** Analysis of Ccdc124 expression in stable colonies. N-ter or C-ter-Flag-tagged Ccdc124 vectors were stably transfected to HEK293 cell line, and colonies were selected in geneticin containing selection medium. Encircled colonies bearing Flag-Ccdc124 (colony 9), and Ccdc124-Flag (colony 8) vectors

We then selected colonies with high expression levels of Flag-Ccdc124 (colony 9) or Ccdc124-Flag (colony 8) constructs, and flag-tagged Ccdc124 proteins were immuno-precipitated by using sephadex beads covered with anti-flag-Abs (see Materials and Methods). We then run these purified proteins in nuPAGE commercial SDS gel (Invitrogen), followed by cutting relevant bands from the gel, and subjected these bands to mass-spectrometry analysis (Fig. 3.9 A-B). This analysis have indicated that the Ccdc124-Flag protein band labeled as the "band 3" in Fig. 3.9 had lost an N-terminal peptide, and thus it was converted to a protein of 30 kDa. A similar change in size was not observed in N-ter Flag-tag inserted Ccdc124, indicating that the N-ter proteolytic cleavage in C-ter Flag-tagged Ccdc124 was due to the positioning of the flag-tag. Briefly, when Flag-tag was inserted to C-ter of Ccdc124, the stability of N-ter of Ccdc124 was compromised, leading to a proteolytic cleavage of the protein (Fig. 3.9).

A

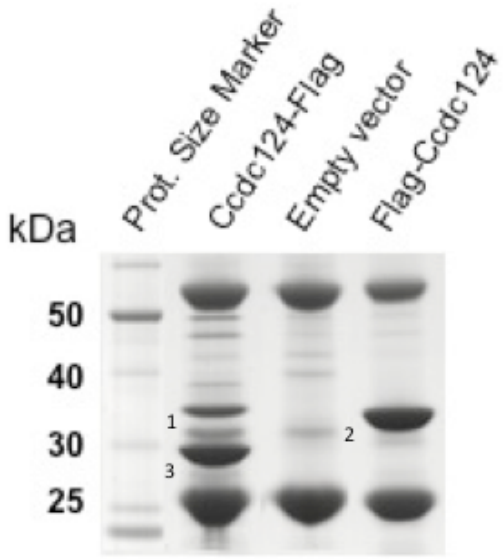


B

FLAG-Ccdc124 **(Band 2)**

sequence MPKKFQGENTKSAAARARRAEAKAAADAKKQKELEDAYWKDDDKHVMRKEQRKEEKEKRRLDQLE

sequence RKKETQRLLEEEDSKLKGGKAPRVATSSKVTRAQIEDTLRRDHQLREAPDTAEKAKSHLEVPLEE

sequence NVNRRVLEEGSVEARTIEDAIAVLSVAEEAADRHPERRMRAAFTAFEEAQLPRLKQENPNMRLSQ

sequence LKQLLKKEWLRSPDNPMNQRAVPFNAPK

Ccdc124-FLAG Higher band **(Band 1)**

sequence MPKKFQGENTKSAAARARRAEAKAAADAKKQKELEDAYWKDDDKHVMRKEQRKEEKEKRRLDQLE

sequence RKKETQRLLEEEDSKLKGGKAPRVATSSKVTRAQIEDTLRRDHQLREAPDTAEKAKSHLEVPLEE

sequence NVNRRVLEEGSVEARTIEDAIAVLSVAEEAADRHPERRMRAAFTAFEEAQLPRLKQENPNMRLSQ

sequence LKQLLKKEWLRSPDNPMNQRAVPFNAPK

Ccdc124-FLAG Lower Band **(Band 3)**

sequence MPKKFQGENTKSAAARARRAEAKAAADAKKQKELEDAYWKDDDKHVMRKEQRKEEKEKRRLDQLE

sequence RKKETQRLLEEEDSKLKGGKAPRVATSSKVTRAQIEDTLRRDHQLREAPDTAEKAKSHLEVPLEE

sequence NVNRRVLEEGSVEARTIEDAIAVLSVAEEAADRHPERRMRAAFTAFEEAQLPRLKQENPNMRLSQ

sequence LKQLLKKEWLRSPDNPMNQRAVPFNAPK

**Figure 3.9.** Mass-spectrometric peptide analysis of N-ter and C-ter Flag epitop tagged Ccdc124 proteins. **A)** Gel photo: Flag-tagged proteins were immunoprecipitated by anti-flag antibodies and they were separated by SDS-PAGE. Bands around 30-35 kDa that were differentially expressed in flag-tagged Ccdc124 expressing cells (numbered as 1, 2, and 3) as compared to empty vector controls were cut from the gel, and subjected to mass-spectrometry analysis**. B)** Peptides obtained in those molecular analysis were indicated as red in sequences presented below. Band 3 was missing the very N-terminus peptide (QKEL…) as compared to bands 1 and 2.

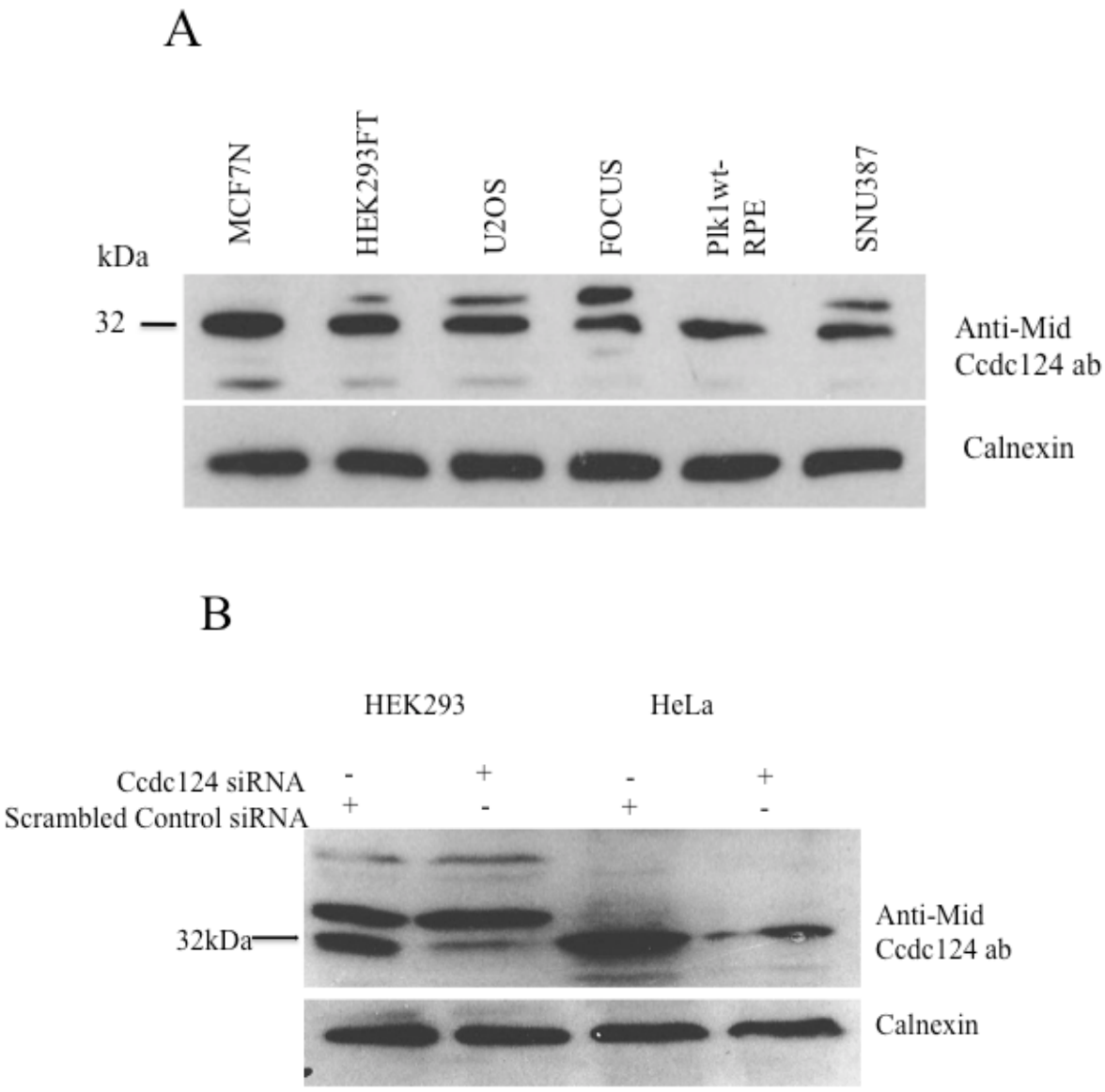


**Figure 3.10**. Expression analysis of Ccdc124 in different cell lines by Western blotting method. **A**) Proteins extracted from indicated cell lines and 40μg of proteins were loaded into %12 SDS gel and blotted using anti-Ccdc124 antibodies. **B**) HEK293 or HeLa cells were transfected with Ccdc124 specific siRNAs (+) or control (scrambled) siRNAs, and similar immunoblots were carried-out to identify the Ccdc124 band. When two bands were detected in a cell line, the lower band turned out to be the specific Ccdc124 band. Calnexin was monitored as loading control.

Endogenous expression level of Ccdc124 was also checked in different cell lines protein extracts by western blotting method. In order to detect Ccdc124, a commercially purchased antibody, which recognizes between residues 100-150 of

Ccdc124 was used. This antibody gave the expected 32 kDa band belonging to Ccdc124. We also proved the Ab specificity of this 32 kDa band after transfecting selected cell lines (HeLa and HEK293) by *CCDC124* specific siRNAs and monitoring the protein band that was lost (Fig. 3.10). We did not observe any difference at the expression levels of *CCDC124* among the tested cell lines.

### 3.3 Subcellular Localization of Ccdc124

In order to understand the biological function of Ccdc124, we assessed the subcellular localization of endogenous Ccdc124 in HeLa (human cervix cancer origin) cells in culture. We fixed HeLa cells with %100 cold methanol and blocked them firstly with %2 BSA, then we incubated fixed cells with anti-N-ter, anti-mid, and anti-C-ter specific Ccdc124 antibodies, followed by anti-Alexa 488 rabbit secondary antibody to determine localization of the protein. Stainings of the HeLa cells with Ccdc124-specific antibodies revealed a dot-like staining pattern, independent of the Ccdc124 antibody selected (Fig. 3.11A, and Fig. 3.12). However, we have detected Ccdc124-HA or N-ter-GFP-labeled-Ccdc124 as diffused cytoplasmic proteins, whereas C-ter-GFP-tagged Ccdc124 had a dot like subcellular localizational appearance (Fig 3.11 D) reminiscent of stainings with anti-mid-Ccdc124 and anti-C-ter-Ccdc124 antibodies (see below, compare Fig. 3.11B with C and D), even though there were some cytoplasmic backgrounds as well. One explanation of these discrepancies could rely on the strong promoters (CMV) of vectors expressing tagged-versions of Ccdc124, which was resulting in high background signals hiding precise localization of complexes including Ccdc124.

A

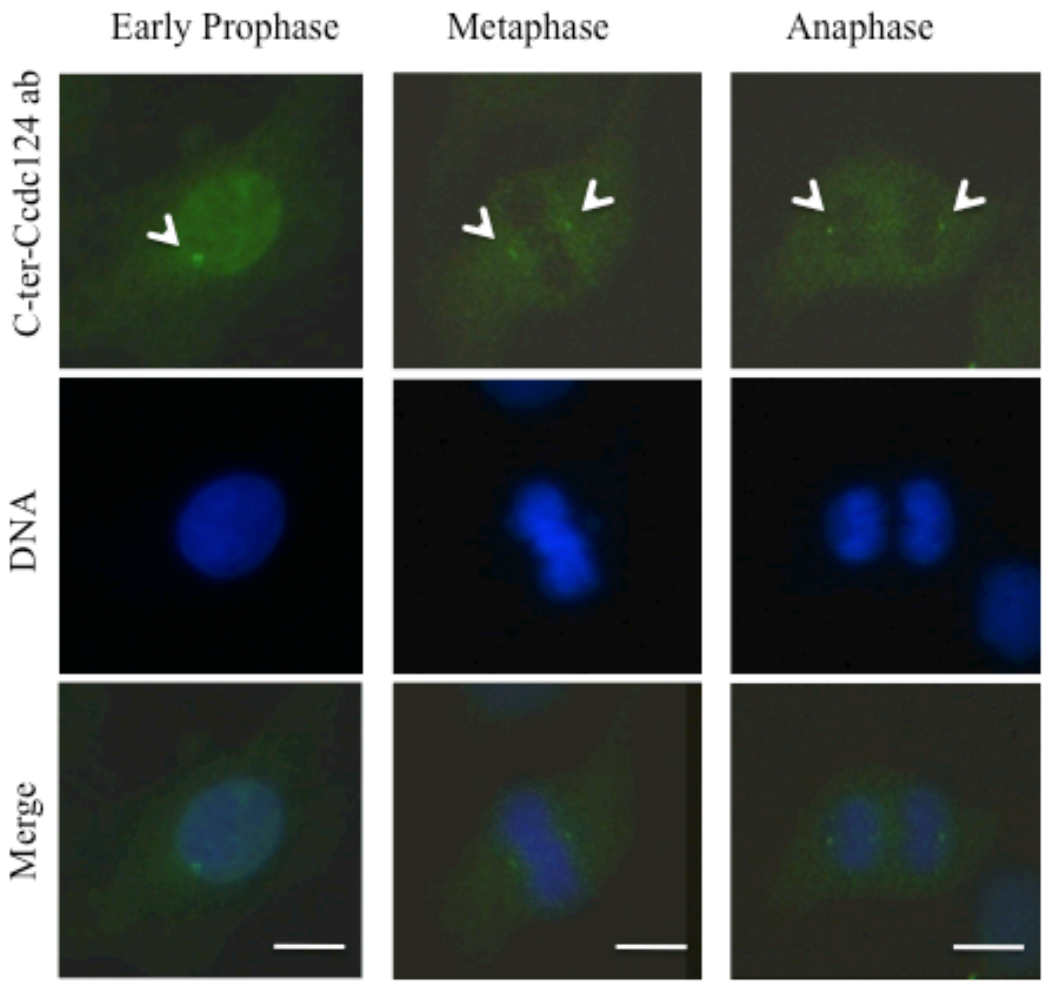
Early Prophase
Metaphase
Anaphase
C-ter-Ccdc124 ab
DNA
Merge

B

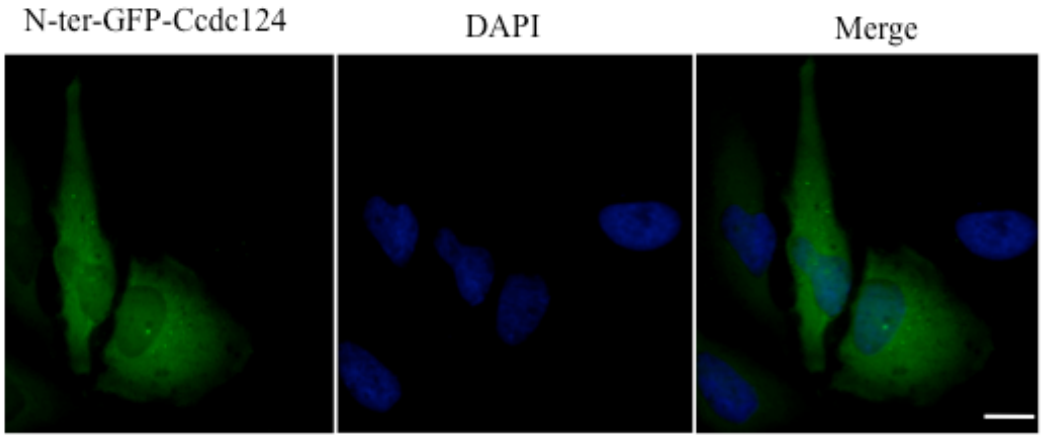
N-ter-GFP-Ccdc124
DAPI
Merge

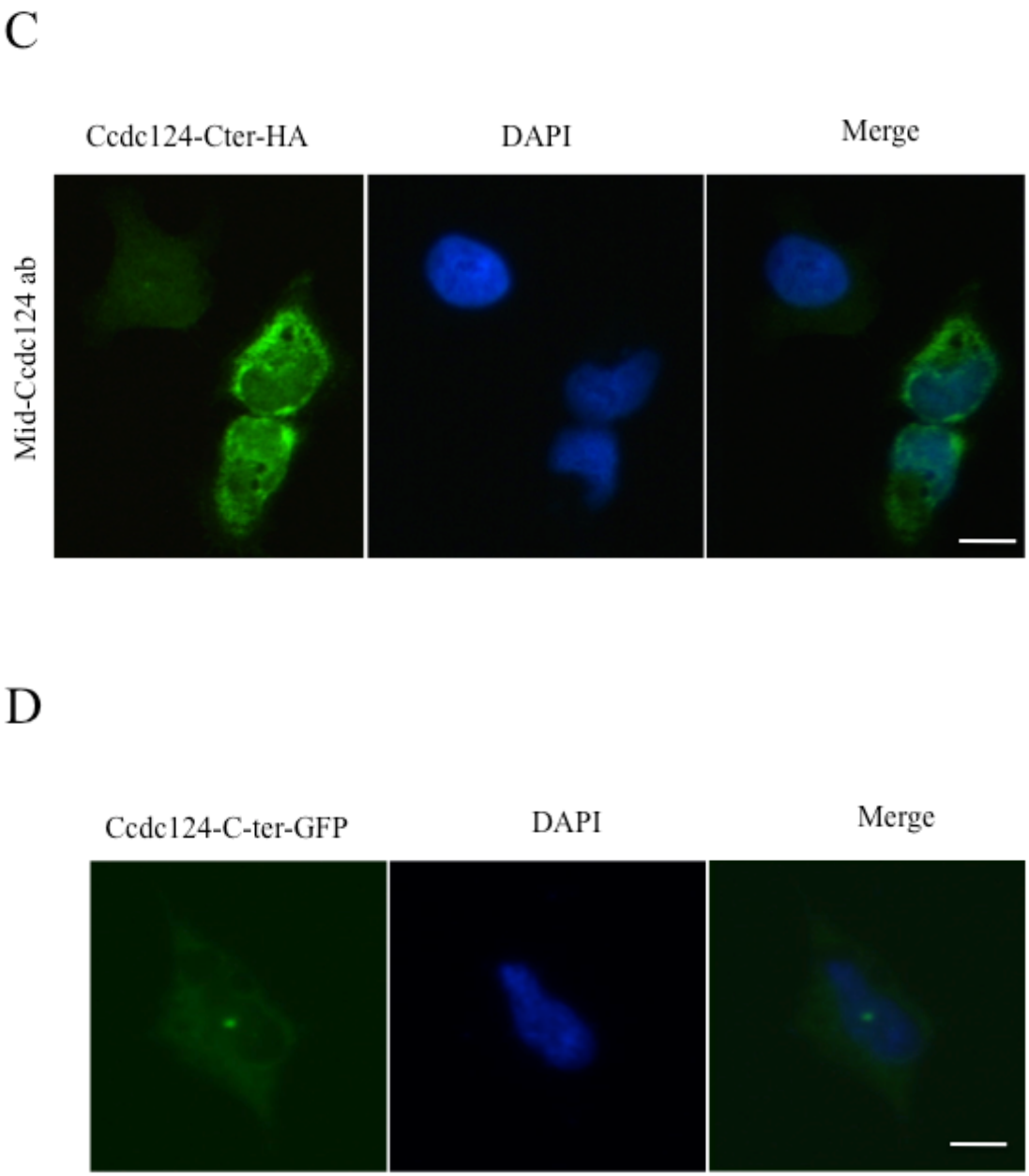


**Figure 3.11** Cell stainings of endogenous or overexpressed Ccdc124. **(A)** HeLa cells were stained by using anti-C-ter Ccdc124 antibody, and a dot-like (puncta) subcellular localization pattern of Ccdc124 was observed. HeLa cells were transfected with N-ter-GFP-Ccdc124 **(B)**, C-ter-HA Ccdc124 **(C)**, or C-ter-GFP-Ccdc124 vector constructs, and transfected cells were either stained with mid-Ccdc124 ab **(C)**, or the GFP-signal is used to assess subcellular localization of Ccdc124 **(B and D)**.

Stainings of the HeLa cells with anti-C-ter and anti-mid Ccdc124 antibodies reveal a dot-like pattern, which made us think that Ccdc124 could be localized in the centrosome (Fig.3.11-B). Furthermore, it was previously shown that coiled-coil domain containing proteins are abundant in centrosomes [30]. To analyse whether Ccdc124 was localized to centrosome or not, we syncronized cells at G2/M stage of the cell cycle by by sequential double thymidine and nocodazole treatments (*see Materials and Methods*) and followed cell cycle stage-dependent subcellular localization of endogenous Ccdc124 by immunofluorescence assays using mid-region, or C-terminal epitope (residues 173 to 223)-specific antibodies together with the centrosome marker protein, γ-tubulin (Fig. 3.12). These experiments indicated centrosome colocalization of Ccdc124 with γ-tubulin at interphase, metaphase, and anaphase stages, albeit it was relatively diffused to the pericentrosomal region at anaphase (please see Fig. 3.13 for growth synchronized cells).

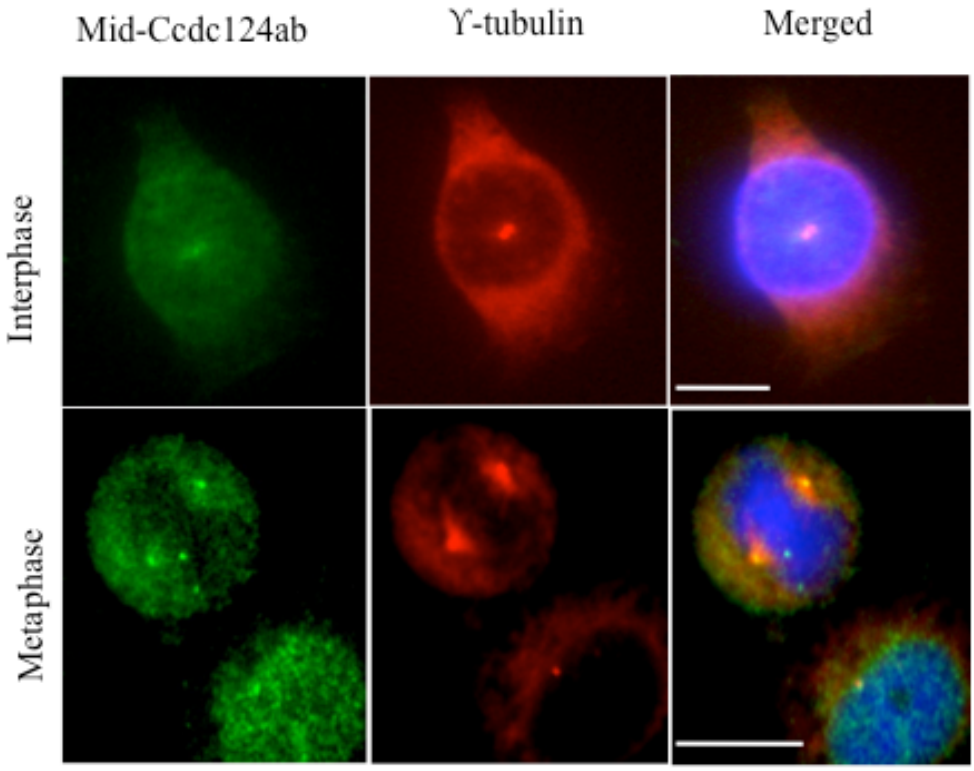


**Figure 3.12** Endogenous Ccdc124 is localized at the centrosome in asynchronous growing cells. HeLa cells was fixed with % methanol, then costained with anti-mid Ccdc124 and anti-γ-tubulin antibodies. During different stages of the cell cycle Ccdc124 is clearly localized at the centrosome together with centrosome marker γ-tubulin protein. Bars represent 10 μm.

A

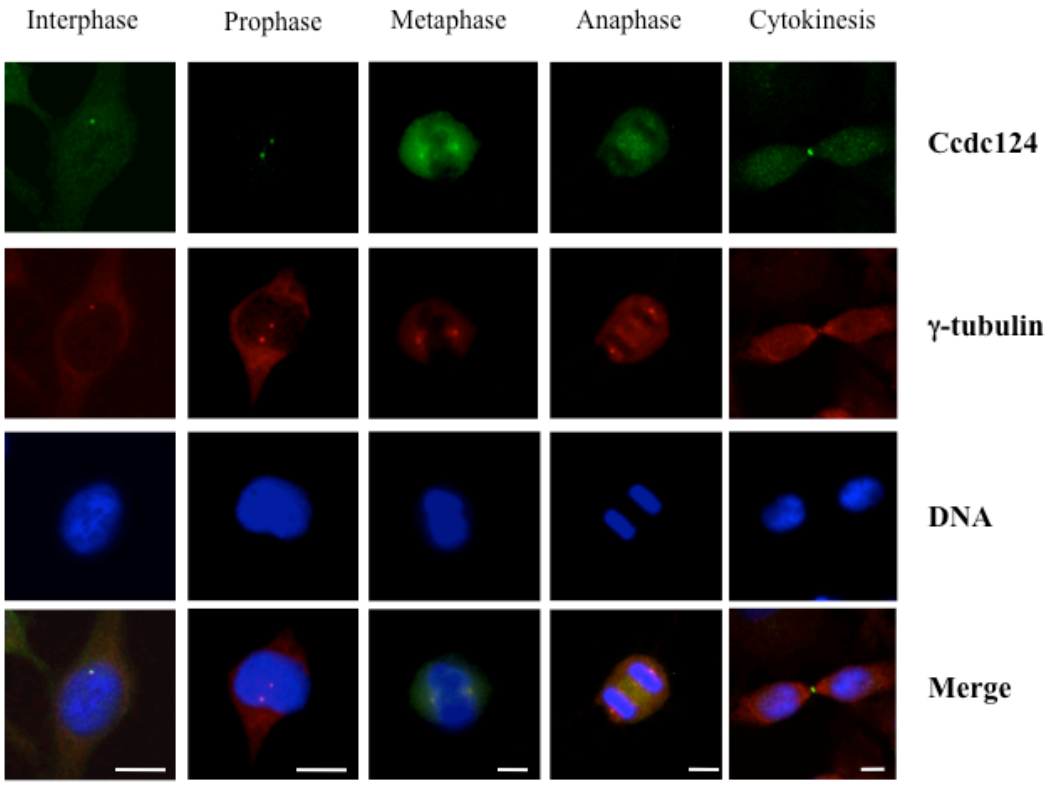
Interphase
Prophase
Metaphase
Anaphase
Cytokinesis
Ccdc124
γ-tubulin
DNA
Merge

B

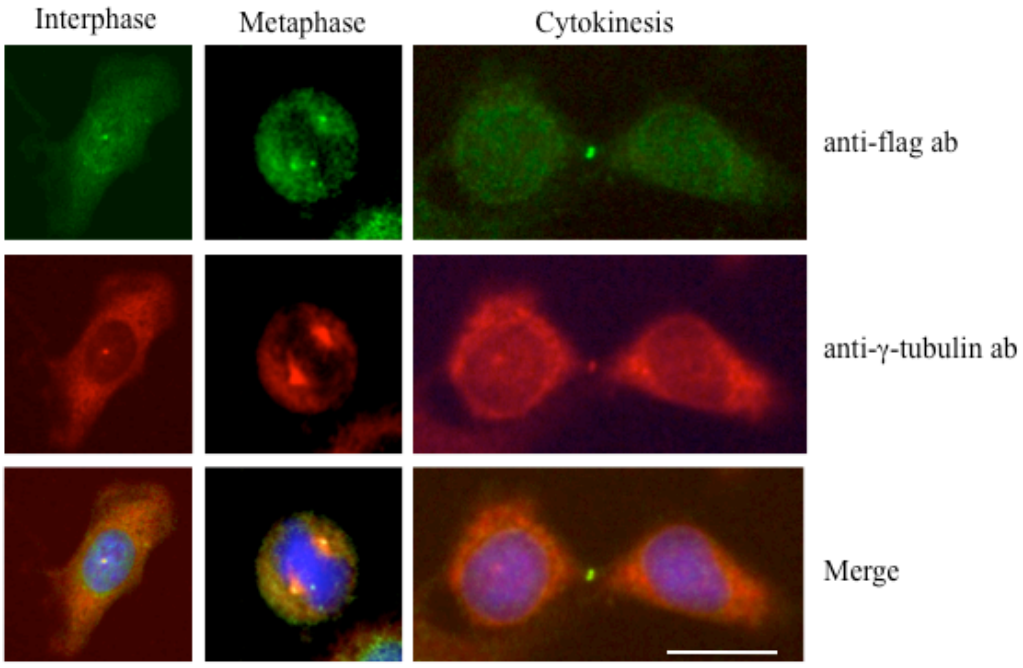
Interphase
Metaphase
Cytokinesis
anti-flag ab
anti-γ-tubulin ab
Merge

C

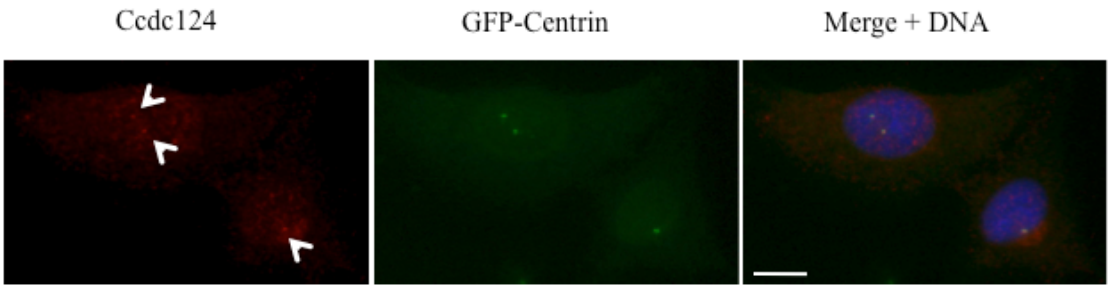
Ccdc124
GFP-Centrin
Merge + DNA

D

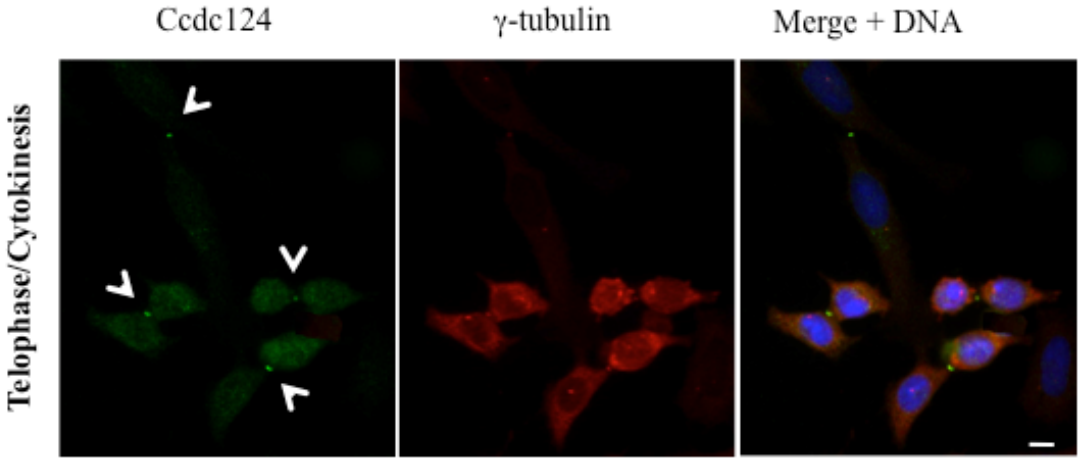
Ccdc124
γ-tubulin
Merge + DNA
Telophase/Cytokinesis

E

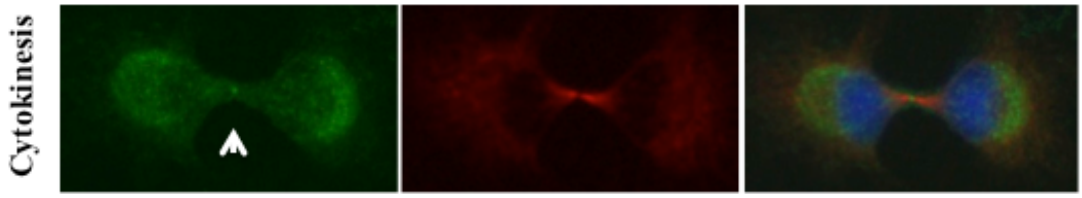
Cytokinesis

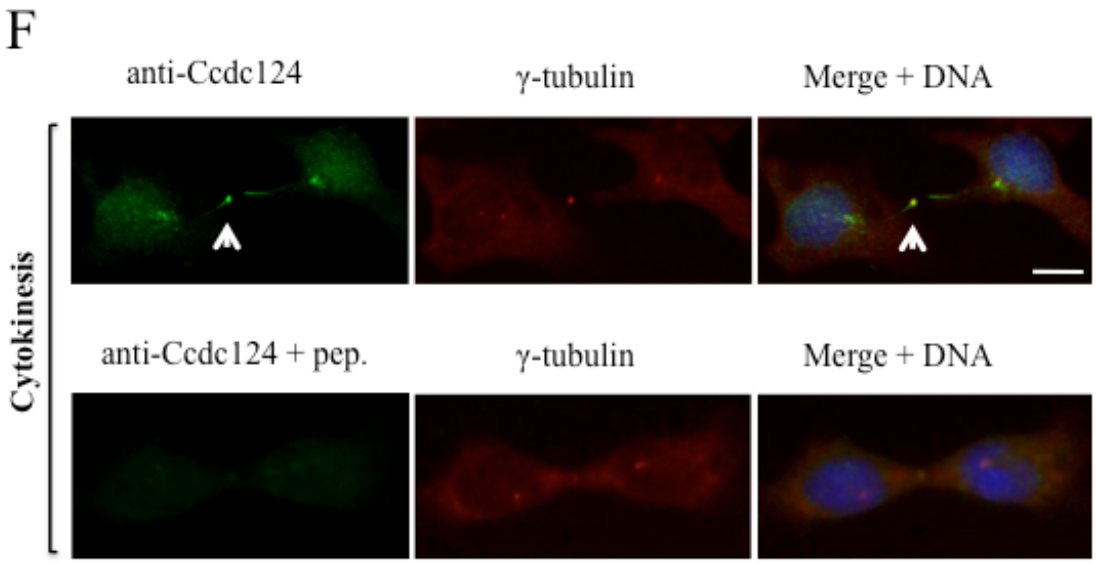


**Figure 3.13**. Endogenous Ccdc124 is present at the centrosome and it concentrates at the center of the midbody in cytokinesis. **(A)** HeLa cells were arrested at G2/M phase by sequential double thymidine and nocodazole treatments, then the drug was washed-off, cells were analyzed by Immunofluorescence at time points with intervals of 15 minutes, and they were classified according to phases of mitosis, and cytokinesis. Samples of cells were then costained with anti-Ccdc124 and anti-γ-tubulin antibodies, and in interphase and prophase, Ccdc124 was observed as puncta in cells, and it is located in the MTOC area. In metaphase and anaphase cells, Ccdc124 appeared at the spindle poles. Ccdc124 was present at the cleavage furrow and at the spindle poles in late anaphase, and concentrated in the midbody during cytokinesis. **(B)** HeLa cells were transfected with the N-ter flag-Ccdc124 vector construct and 48 hours later samples of cells were subjected to immunofluorescence costainings using anti-flag and anti-γ-tubulin Abs together. Representative micrographs of cells at different stages of cell cycle are given. **(C)** Ccdc124 was also colocalized with GFP-centrin on centrosomes in RPE1 cells. **(D-E)** At telophase and cytokinesis Ccdc124 is observed as puncta typically associated with the midbody positioned at the middle of intercellular bridge separating daughter cells, as detected with α-tubulin staining. **(F)** Peptide competition assays were done by pre-incubating anti-N-ter-Ccdc124 antibody with the corresponding epitope peptide in 200-fold molar excess amounts. Signals generated by Ccdc124 localized at the midbody (shown with arrowhead) were lost in immunoflurescence assays where peptide pre-treated antibodies were used. Bars represent 10 μm.

Centrosome localization of endogenous Ccdc124 was further confirmed in cells containing another centrosomal marker, GFP-Centrin (Fig. 3.13-C) , [73]. Centrin is localized in centrioles and it is required for centriole duplication and segregation.

Very interestingly, we found that at telophase and in cytokinesis Ccdc124 dissociates from centrosomes and relocalizes first to the midzone, subsequently accumulating at the midbody at cytokinesis, as assessed by its colocalization with the midzone-specific γ-tubulin (Figure 3.13-A, or B for the colocalization of flag-Ccdc124 with γ-tubulin), or by its positioning at the midbody marked by the empty mid-space in α-tubulin stainings (Figure 3.13-E). Immunofluorescence signals generated by Ccdc124 localized at the midbody (shown with arrow-head) were lost in when peptide pre-treated antibodies were used in peptide competition assays. In these studies we used anti-N-ter-Ccdc124 antibodies pre-incubated with the corresponding epitope peptide (200-fold molar excess amounts). This result indicated that Ccdc124 signals coming from the midbody were specific. Polo-like-kinase-1 (Plk1) is involved in regulation of cytokinesis by translocating to the midbody, and therby contributing to its assembly [39, 34]. We decided to use Plk1 as a second midzone/midbody marker, and we assessed once again the midbody localization of Ccdc124 in two separate cell lines, the stable GFP-Plk1 expressing Retinal Pigment Epithelia-1 (RPE1-Plk1(WT), a gift from Prasad Jallepalli at Memorial Sloan kettering Institute, NY, USA) and HeLa (Figure 3.14A and B). In these analysis, we detected that at the midbody Plk1 in fact surrounds the puncta where Ccdc124 is localized, rather than being fully superimposed with it (Figure 3.14, inset).

These results indicated that Ccdc124 is a component of centrosomes at interphase, and mitosis, and moreover it translocates to the midbody during the last stages of cell division and separation of post-mitotic sister cells; a stage termed as cytokinetic abscission.

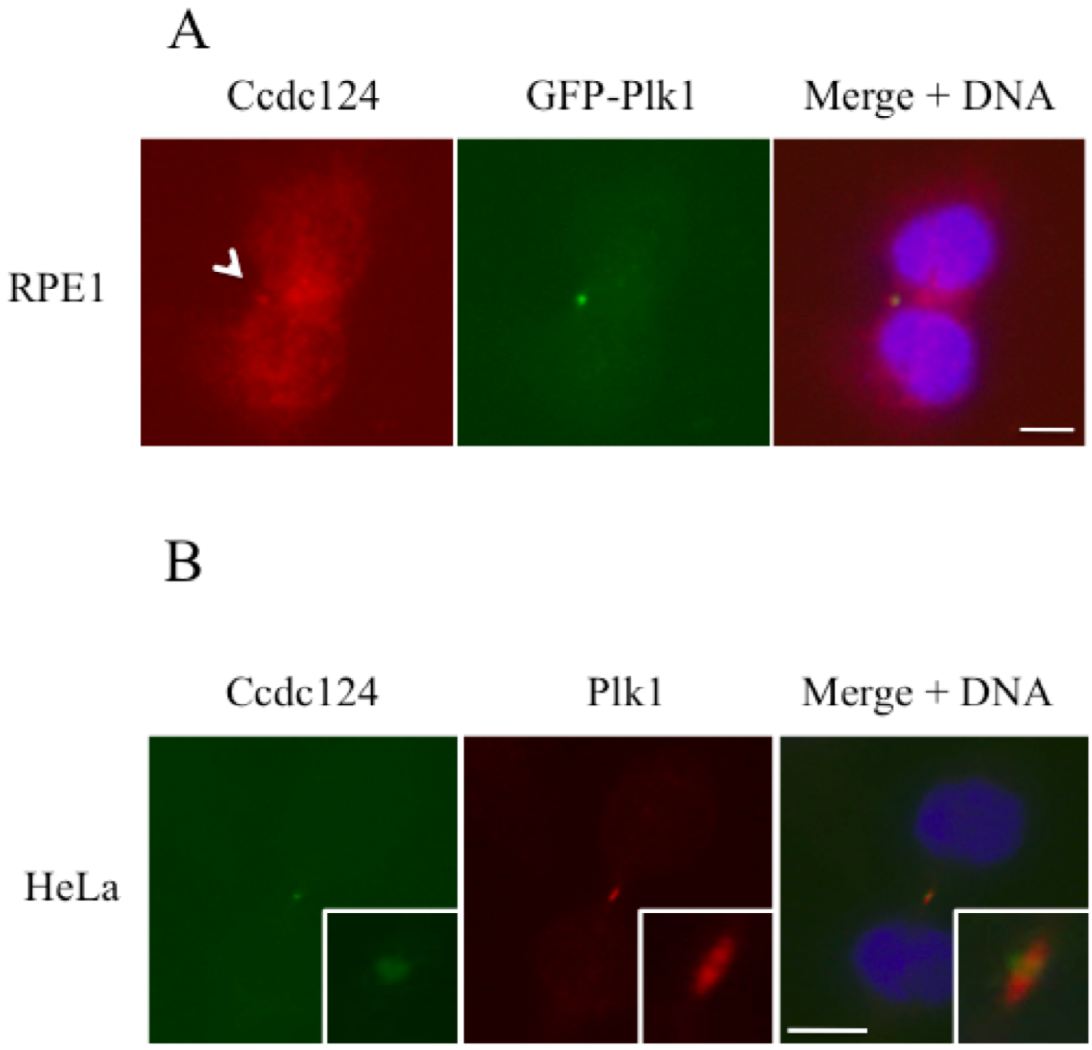


**Figure 3.14** Ccdc124 colocalized with Plk1 on midbody in HeLa and RPE1 cells at cytokinesis. Cell divisions were synchronized as described in the legend of Figure 2, above. **(A)** Subcellular localization of Ccdc124 was detected with anti-Ccdc124 antibodies recognizing the mid-region of protein in RPE1 cells stably expressing GFP-Plk1, indicating a colocalization of Ccdc124 and Plk1 at the midbody during cytokinetic abscission. **(B)** Representative immunofluorescence microscopy images of HeLa cells costained with anti-Ccdc124 (mid-region specific) and anti-Plk1 antibodies illustrating midbody colocalization of both proteins. Inset; 25x digital magnification of the midbody region. Bars represent 10 μm

### 3.4 Ccdc124 knockdown in human cell lines and in Zebrafish embryos

Subcellular localization of Ccdc124 dynamically changes during mitosis. Endogenous Ccdc124 is present at the centrosome in interphase, prophase and metaphase (Fig. 3.13). Subsequently, it concentrates at the midzone and at the pericentriolar space in late-anaphase, and localized in the midbody during cytokinesis (Fig. 3.13 and 3.14). Essential roles of centrosomes on cytokinesis were described in previous studies [74, 26, 75].

Additionally, a number of midbody localized proteins were previously shown to be involved in cytokinetic abscission [34]. Therefore, we investigated whether down-regulation of Ccdc124 by RNAi methods would cause cyctokinetic failure as well, or not. Thus, in order to investigate a possible function of Ccdc124 in separation of dividing sister cells, we initially knocked-down *CCDC124* in HeLa cells by separately transfecting them with siRNAs specifically targeting this gene, and control scrambled siRNAs. 48 hours after transfection of siRNA, we firstly monitored the knock-down efficiency by immunoblots that we carried-out using lysates obtained from Ccdc124-specific siRNA transfected or scrambled siRNA transfected controls, and observed approximately 75-80% decrease in Ccdc124 levels in cells that received gene specific siRNAs as compared to scrambled siRNA transfected controls (Figure 3.15).

We then analyzed cellular phenotypes, centrosome localizations, and midbody functions in Ccdc124 depleted cells using above mentioned siRNA species. Immunofluorescence microscopy analysis reveled that cytokinetic abscission was remarkably blocked as assessed by the increased percentage of multinucleated cells (Figure 3.15-B) from less than ~3% in scrambled control siRNA transfected cases to ~15% in Ccdc124-specific siRNA received asynchronous cultures 48 hours after Ccdc124 siRNA transfections (Figure 3.15-C). However, in those Ccdc124 depleted cells centrosomes still form, although in aberrant numbers as asessed by immunostainings that mark γ-tubulin complexes (Fig. 3.15 D). It should be noted, however, that Ccdc124 was not completely depleted at the protein level by siRNA mediated knock-downs, and was still present at lower levels in siRNA treated cells (Figure 3.15-C).

A

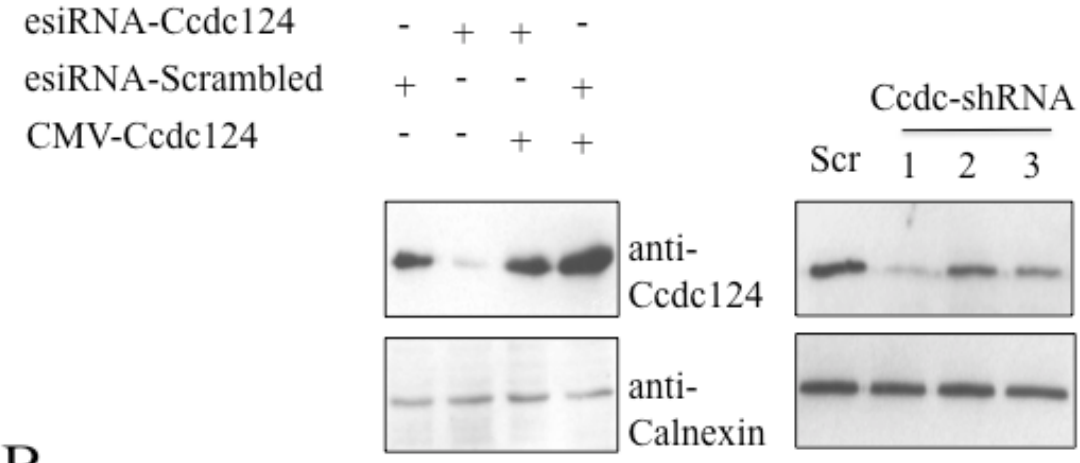
esiRNA-Ccdc124 - + + -
esiRNA-Scrambled + - - +
CMV-Ccdc124 - - + +
Ccdc-shRNA
Scr 1 2 3
anti-Ccdc124
anti-Calnexin

B

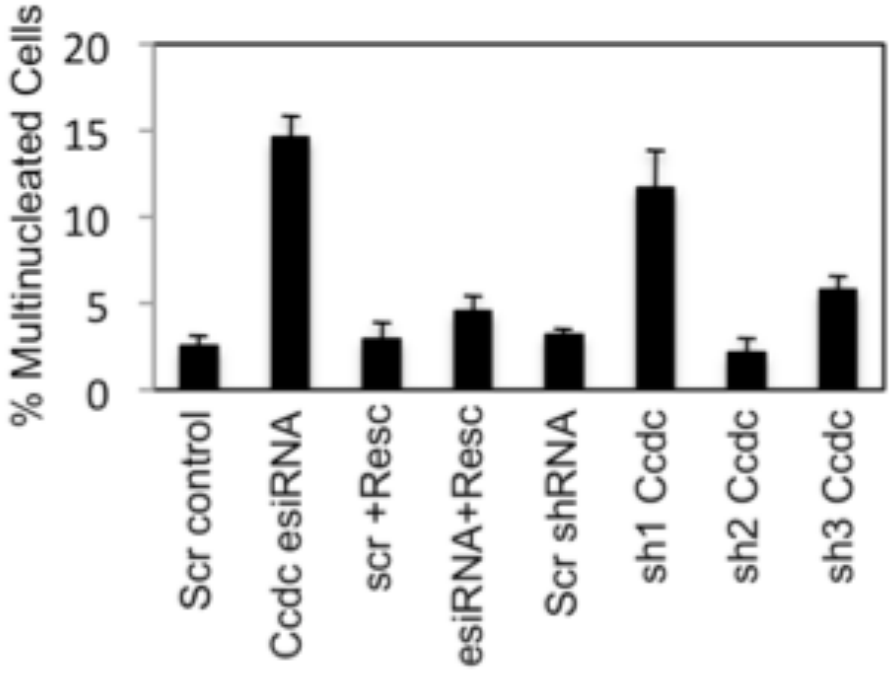
% Multinucleated Cells
20
15
10
5
0
Scr control
Ccdc esiRNA
scr +Resc
esiRNA+Resc
Scr shRNA
sh1 Ccdc
sh2 Ccdc
sh3 Ccdc

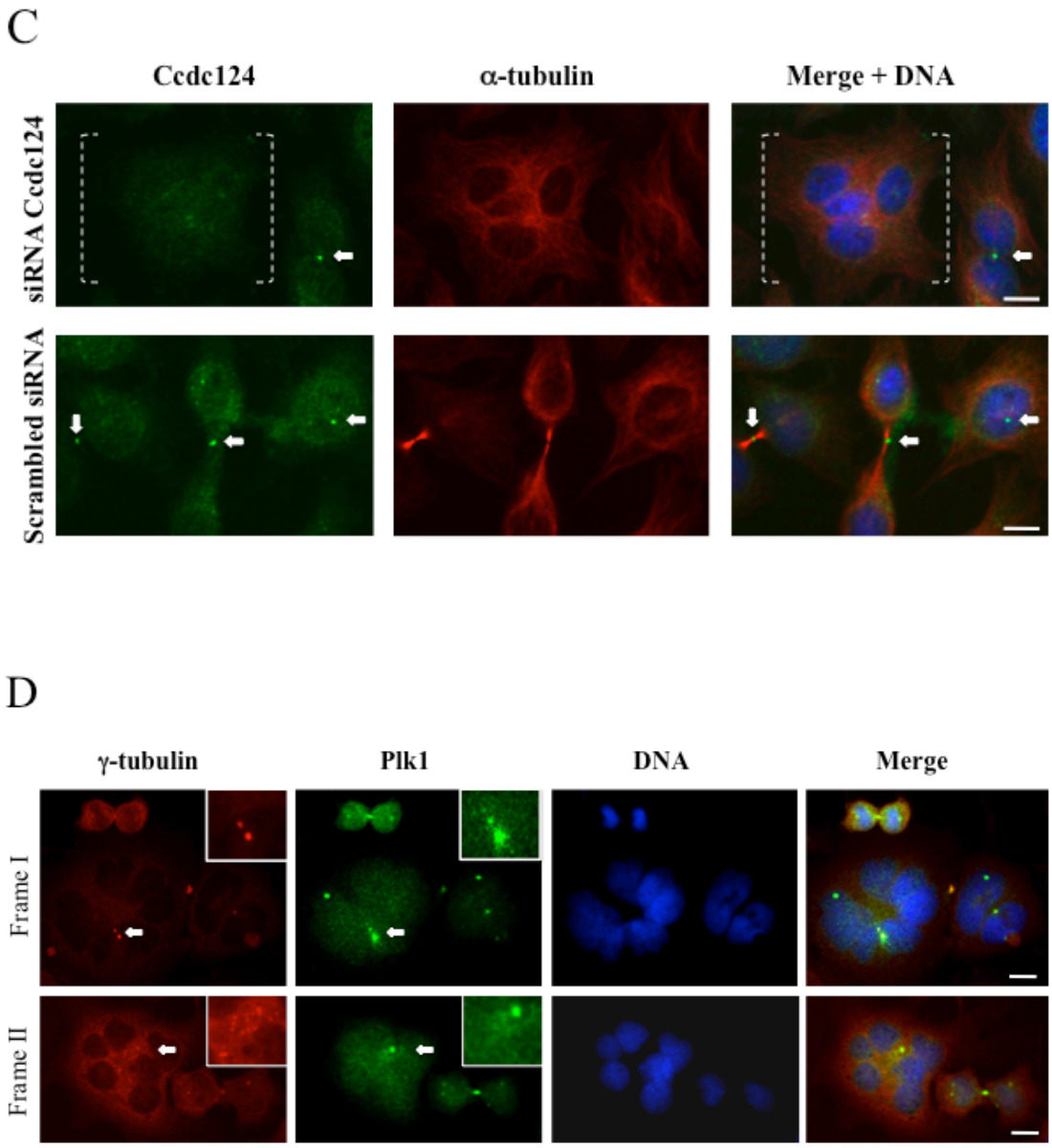


**Figure 3.15** siRNA mediated depletion of Ccdc124 in HeLa cells leads to cytokinesis failure. **A)** Immunoblot of Ccdc124 in scrambled siRNA and Ccdc124 esiRNA or shRNAs (1, 2, 3) transfected HeLa cells at 48 hrs post-transfection. Calnexin expression was monitored as loading control. **B)** Graph of immunofluorescence microscopy data shows the percentage of scrambled (Scrmbl) or Ccdc124 esiRNA transfected cells (n=1814 and n=2029, respectively; counts obtained in at least 3 independent experiments) that proceeded through mitosis but repetitively failed to cleave, leading to multinucleation. **C)** Representative images of Ccdc124 depleted multinuclear cells described in **B)**. α-tubulin is shown in red, green immunofluorescence stainings that indicate centrosome and midbody localizations of Ccdc124 were shown by white arrowheads. Such strong dot-like Ccdc124 stainings were missing in Ccdc124-depleted multinuclear cells. **D)** In Ccdc124 depleted multinuclear cells MTOCs still form as detected by γ-tubulin and Plk1 costainings. Two different sets of representative cells are shown. One normally dividing

cytokinetic cell was also present in each representative picture set as internal control. Bars represent 10 μm.

Thus, we established that Ccdc124 had an important role in cytokinesis of cells growing in culture, as down-regulation of this gene leads to an aberrant accumulation of multinuclear cells. We then decided to test whether the same effect will be observed *in vivo* when the expression of Ccdc124 homologue in zebrafish embryos are down-regulated by using morpholino (MO) mediated knock-down methods (see below). MOs are typically 25 bases antisense oligonucleotides and they have altered nonionic backbone when compared to DNA and RNA [76]. MOs trigger formation of RNA-MO hybrids, and the altered backbone of morpholinos make them resistant to digestion by RNAse-H. Therefore, MO antisense oligonucleotides block *translation* directly by binding complementary mRNA sequences within 5' untranslated region (UTR), usually close to translation start site. Because MO-mRNA hybrids are not degraded (as in siRNA mediated knock-down mechanisms), RT-PCR is not an effective method of analysis to detect MO dependent changes on the expression levels of targeted genes. Typically, in zebrafish MOs are introduced into the yolks of 1-8 cell-staged embryos [77] One of the most important advantages of MO treatments are fast identification of morphological changes (phenotypes) within the first 3 days of zebrafish embryo development. To investigate the function of Ccdc124 in an *in vivo* system, we studied the effect of Ccdc124 depletion in zebrafish embryos by using MO injections. A translation-blocking MO was designed to bind immediately upstream of the translation start codon of Ccdc124, and it was injected into fertilized zebrafish embryos at one-cell stage. Morphants were then compared to control MO injected embryos, and uninjected embryos (Fig. 3.16). We first observed that a high number of morphant embryos exhibited mortality. A total of 41.4 ± 5.3% of Ccdc124 morphant embryos terminated development before 3 dpf, in contrast to 9.28 ± 3.94% and 5.35 ± 1.97% in control morpholino-injected and uninjected embryos, respectively (Figure 3.16-A).

A

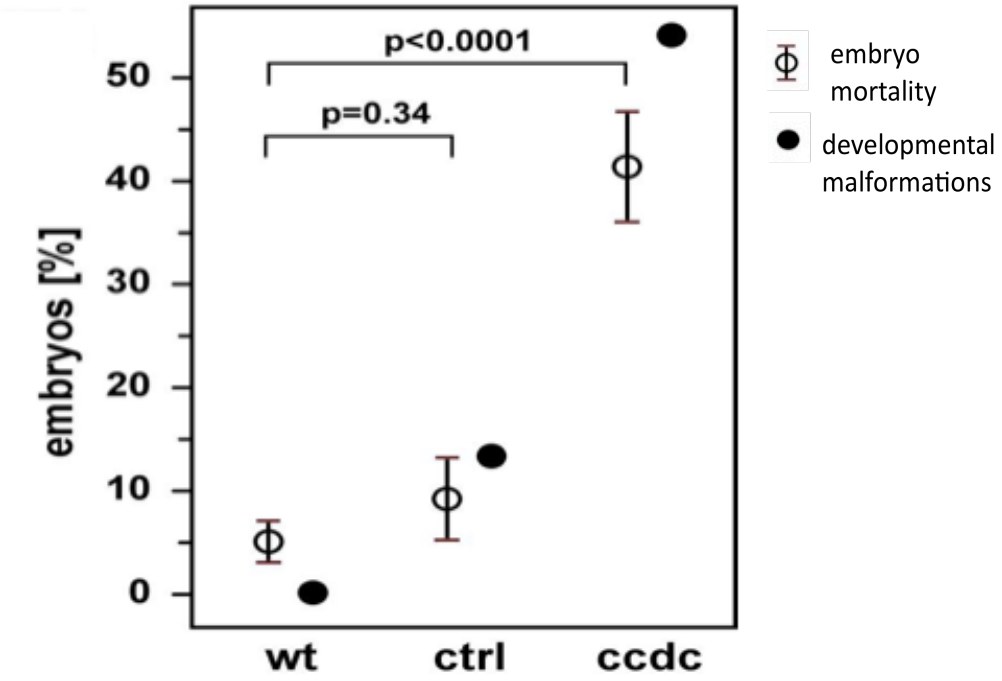
p<0.0001
p=0.34
50
40
30
20
10
0
embryos [%]
wt
ctrl
ccdc
embryo mortality
developmental malformations

B

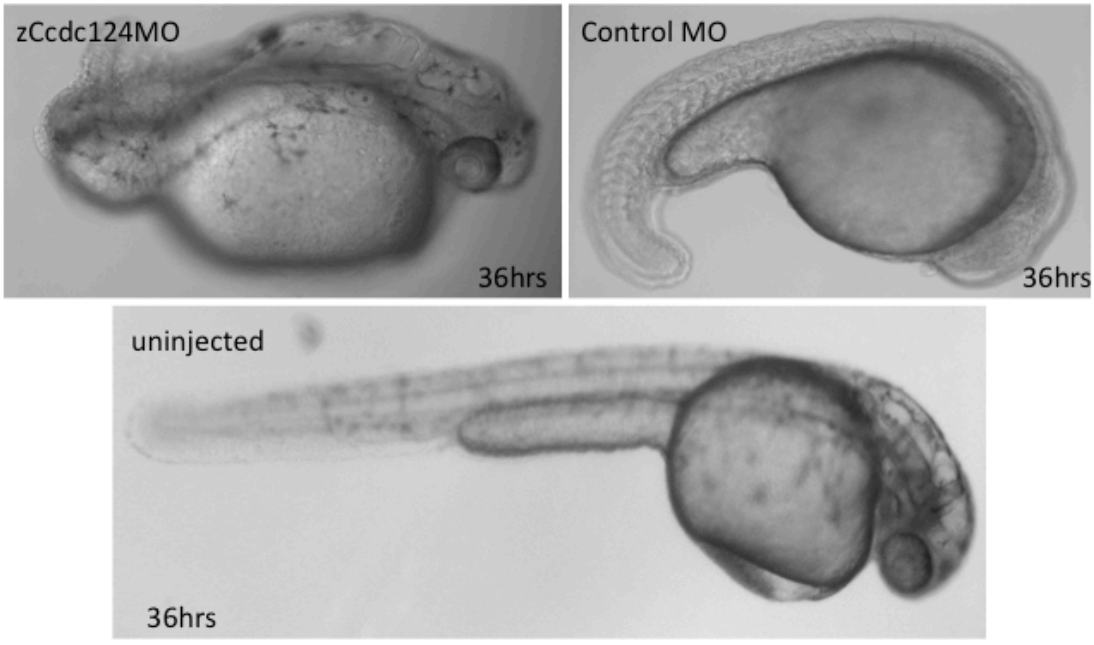
zCcdc124MO
36hrs
Control MO
36hrs
uninjected
36hrs

C

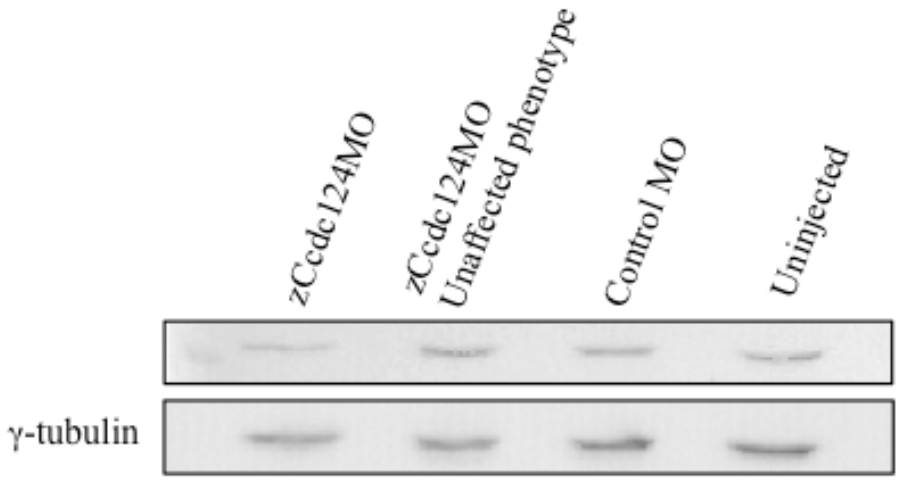
zCcdc124MO
zCcdc124MO Unaffected phenotype
Control MO
Uninjected
γ-tubulin

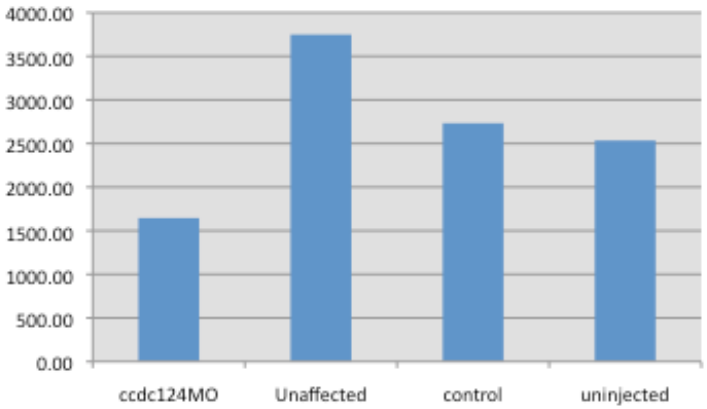
4000.00
3500.00
3000.00
2500.00
2000.00
1500.00
1000.00
500.00
0.00
ccdc124MO
Unaffected
control
uninjected

D

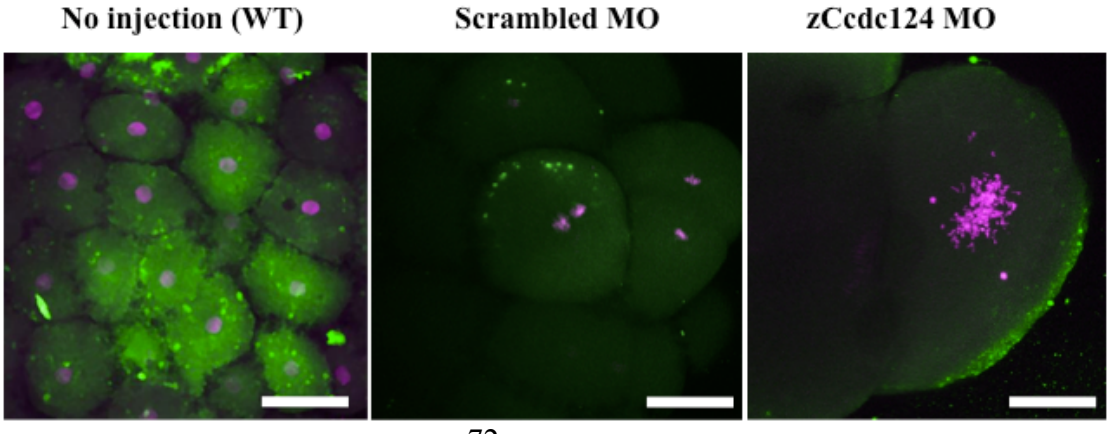
No injection (WT)
Scrambled MO
zCcdc124 MO

**Figure 3.16.** Effects of Ccdc124 knock-down in zebrafish embryos. **(A)** Quantification of embryo mortality (open circles) and developmental malformations (filled circles) for control morpholino-injected (ctrl, 254 embryos, 4 independent experiments), Ccdc124 morphants (ccdc, 661 embryos, 7 experiments) and wild type (wt, 374 embryos, 7 experiments) control embryos. The incidence of embryos displaying irregular cleavage patterns at 2 hpf (filled circles) parallels embryo mortality. **(B)** zCcdc124 depleted embryos show developmental defects characterized by a shortened body and spinal cord malformations. Control morpholino injected embryos have clear developmental retardations, but they do not display drastic morphological aberrations. Developments of uninjected embryos were normal. **(C)** Protein was extracted 36 h after injection, and 80 μg of proteins were immunoblotted for analysis of zCcdc124 and zebrafish γ-tubulin. A densitometric analysis of band intensities corresponding to this blot was also shown. zCcdc124 expression level was reduced in MO injected samples. γ-tubulin was used a loading control and it was not affected by zCcdc124 depletion. **(D)** Wild type (left panel), scrambled MO injected (middle panel), and Ccdc124 morphant (right panel) embryos stained with the nuclear stain DAPI (pink) and BODIPY-505/515 (green) to visualize cell boundaries. Ccdc124 morphants show developmental defects with irregular numbers of unusually large cells containing large amounts of nuclear DNA. Bars represent 100 μm.

The surviving zebrafish larvae displayed severe developmental defects, such as small head, reduced eye, and spinal cord malformation phenotypes. No such phenotypes were observed in wild type and control morpholino-injected embryos, but injection of control morpholino caused a slight growth retardation **(3.16-B),** without major developmental defects. We also checked expression levels of zCcdc124 proteins in MO injected, scrambled control MO injected, and MO-uninjected 36h embryos, and we confirmed that zCcdc124 was down-regulated in morphologically defective morphants, as compared to controls. Interestingly, zCcdc124 expression levels were not affected by Ccdc124-specific MO injections in morphants without major morphological defects (see unaffected phenotypes, Fig. 3.16 B-C). Densitometric quantification of band intensities have indicated an approximately 42% decrease in Ccdc124 levels in morphants, as compared to scrambled MO received embryos (3.16 C).

The failure of Ccdc124 morphants to develop normally, and the high incidence of mortality suggest a crucial function of Ccdc124 during early zebrafish development. We therefore analyzed Ccdc124 morphants for developmental abnormalities at early

stages (2 hpf and 5 hpf) wondering whether they would parallel the results of Ccdc124 knock-downs by specific siRNA transfections to HeLa cells in our *in vitro* experiments. Indeed, a high percentage of early embryos showed an abnormally reduced number of cells at 2 hpf. At this time point wild type littermates developed to the 64-cell stage, but Ccdc124 morphants displayed perturbed cleavage patterns with far less than 64 cells at the same time point. Moreover, a high number of embryos showed unusually large cells and abnormal patterns and localization of nuclear DNA, suggesting that cytokinesis might be affected when Ccdc124 is knocked-down (Figure 3.16-D). Only slight developmental delays were observed in scrambled control-MO received early embryos, but other than this, developmental defects and genomic instabilities were not observed at levels comparable to Ccdc124-morphants (Fig 3.16 B and D). Co-injections have not done together with p53 morpholino injections, therefore this experiment will be provided when Zebrafish injections are repeated in future experiments. Again, unlike WT embryos or scrambled MO received controls, nuclear DNA in morphant embryos was less compact and widely distributed within affected cells lacking clear nuclear organization. Strikingly, the incidence of embryos that underwent abnormal development closely resembled the percentage of dying embryos when compared across morphant and control embryos (Figure 3.16-D).

The disrupted cleavage pattern of early Ccdc124 morphant zebrafish embryos with large cells that contained an abnormally large quantity of DNA strongly suggests that developing blastomeres were able to replicate their DNA but might have failed to undergo proper cytokinesis, which is similar to the results that we observed in our cell culture assay (see above, Figure 3.16-C). This clearly reconfirms the crucial role of Ccdc124 during cell division.

### 3.5 Ccdc124 interaction with RasGEF1B

A yeast-two-hybrid analysis previously carried-out in our laboratory identified RasGEF1B as an interaction partner of Ccdc124. A direct interaction between Ccdc124 and RasGEF1B was also detected by *in vitro* GST-pull down assays [51]. We decided to study and validate this interaction by co-IP experiments. We transfected HEK293 cells together with Flag-Ccdc124 and GFP-RasGEF1B containing expression vectors. Flag-tagged Ccdc124 proteins were immuno-

precipitated by using G-agarose beads covered with anti-flag-Abs (see Materials and Methods) and western blot analysis was done with anti-GFP antibody (to detect RasGEF1B) and Flag antibodies. We observed a very clear interaction between Ccdc124 and RasGEF1B in these assays (Fig. 3.17).

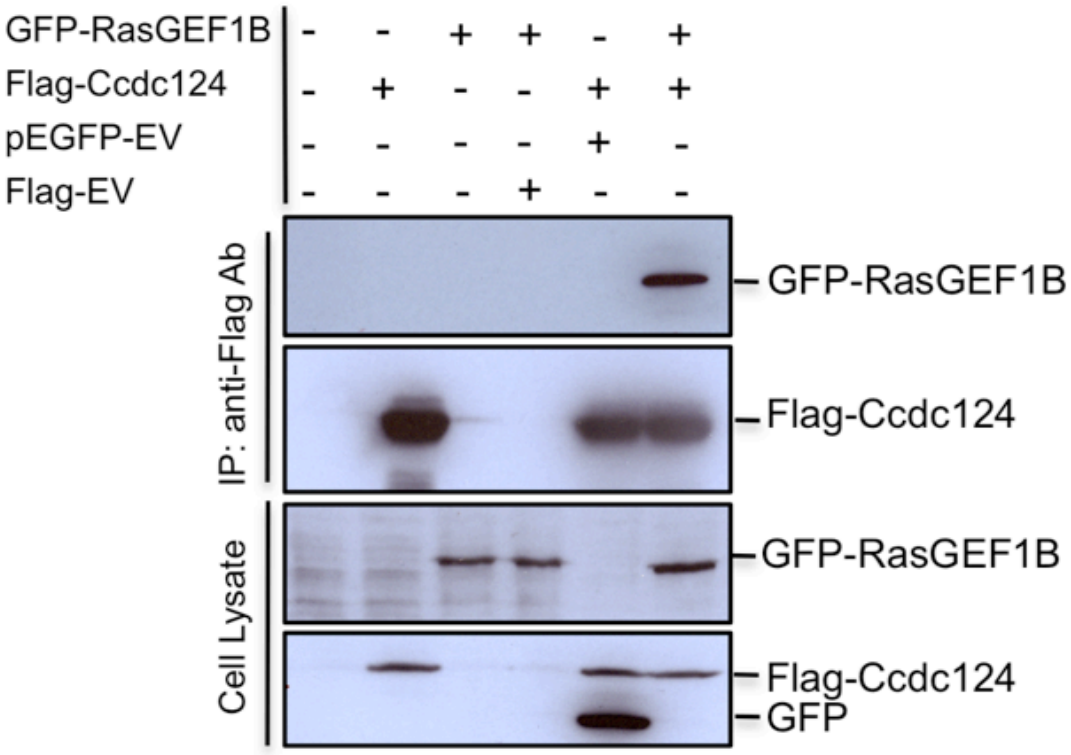


**Figure 3.17** RasGEF1B is an interaction partner of Ccdc124. HEK293 cells were either transfected with Flag-Ccdc124 or GFP-RasGEF1B expression vectors alone, or they were co-transfected with Flag-Ccdc124 and GFP-RasGEF1B together, then immunoprecipitations (IP) were carried-out on cell lysates using protein-G beads with anti-Flag antibodies, and subsequently immunoblots were done using anti-GFP (monitoring GFP-RasGEF1B) or anti-Flag-HRP (to assess Flag-Ccdc124) antibodies. Lysates from HEK293 cells that did not receive any expression vectors (NoTr) were used as controls. Presence of GFP-RasGEF1B in transfected cells was confirmed by immunoblots done using anti-GFP Abs and lysates of cells that received GFP-RasGEF1B expression vectors.

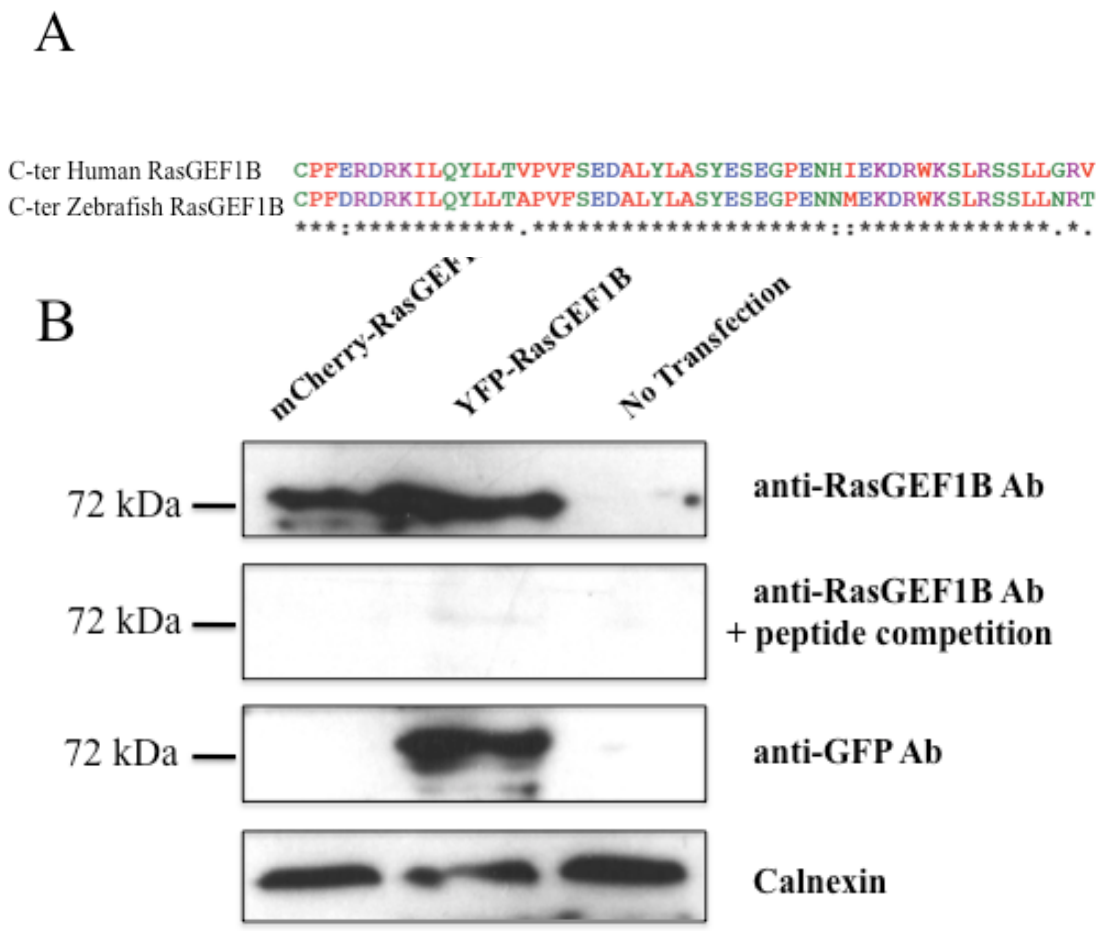


**Figure 3.18** Validation of RasGEF1B antibody. (A) Alignment of C-ter Human and Zebrafish protein sequences. The alignment was performed as mentioned before. (B) HEK293 cells were transfected with mCherry-labeled human RasGEF1B or YFP-labeled humanRasGEF1B expression vectors (mCherry-RasGEF1B and YFP-RasGEF1B, respectively), after 48 hours cells were lysed, proteins were separated by SDS-PAGE, and immunoblot was performed with anti-RasGEF1B antibody alone (1 µg at 1:1000 dilution), and then the membrane was stripped and sequentially reprobed first with the same antibody pre-incubated with 100 ng of competing 20mer peptide epitope [C]- NNMEKDR-W-KSLRSSLLNRT corresponding to C-terminus of ZF-RasGEF1B, and then with anti-GFP antibody recognizing YFP as its epitope in YFP-RasGEF1B. Calnexin expression was monitored as loading control.

We wondered whether interactions between YFP-RasGEF1B and Flag-Ccdc124 as detected in co-IP experiments could indicate a functional interaction between these two proteins. In order to analyze possible cellular functions of endogeneous RasGEF1B protein in human cells lines, and to be used in *in vivo* Zebrafish studies

we generated a rabbit polyclonal antibody recognizing the conserved C-terminal 19 amino acids epitope of both Human the Zebrafish orthologue of RasGEF1B (Fig.3.18-A). Those antibodies were ordered by our team to an antibody production company called Cambridge Reserach Biochemicals (CRB, UK) which generated the antibodies and delivered to our laboratory. We performed immunoblot assay to investigate specificities of these antibodies. For this, we overexpressed RasGEF1B in HEK293 cells by using RFP-RasGEF1B and YFP-RasGEF1B plasmid constructs. 48 hours after transfections, immunoblots were performed with anti-RasGEF1B antibody, and then the membrane was stripped and sequentially reprobed first with the same antibody pre-incubated with 100 ng of competing 20mer peptide, and then with anti-GFP antibody recognizing YFP-RasGEF1B (Fig.3.18-B). We observed that the new antibody specifically recognizes human RasGEF1B protein.

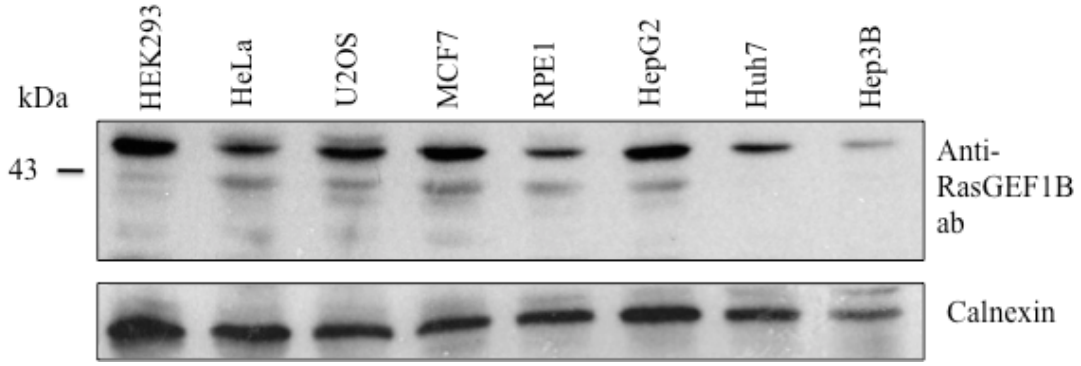


**Figure 3.19.** Representative Western blotting results of endogenous RasGEF1B protein expression in various selected human cell lines. 60 μg protein was loaded on the SDS gel. Calnexin was used as a loading control.

We also analyzed endogenous expression level of RasGEF1B in 8 different human cell lines by western blotting method. RasGEF1B is ubiquitously expressed in all cell lines that we used. However, the most expression of RasGEF1B was observed in HEK293 cell lines and the lowest expression was observed in Hep3B.

By using the new RasGEF1B antibody we wanted to determine whether the subcellular localizations of RasGEF1B and Ccdc124 were comparable throughout the cell cycle. In fact, in a previous study, RasGEF1B was shown to localize in endosomal vesicles when fluorescent protein-fused versions (YFP-RasGEF1B or

mRFP-RasGEF1B) were ectopically expressed in asynchronous CHO cells [78]. We validated localization of RasGEF1B in asynchronous U2OS cell line. We observed similar results as above, as RasGEF1B was co-localized together with the early endosomal marker Rab-5 in U2OS cell line (Fig. 3.20).

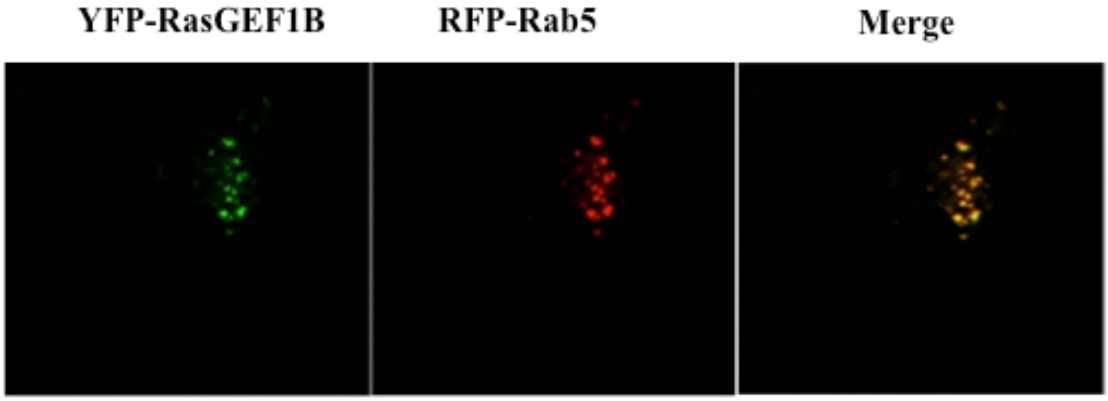


**Figure 3.20** RasGEF1B is colocalized with early endosomal marker protein Rab-5 in U2OS cells. U2OS cells were transfected with both YFP-RasGEF1B and RFP-Rab5 plasmid constructs, and then images were taken by using a time-lapse confocal microscope in collaboration with Johannes L. Bos laboratory at the University Medical Center (UMC), Utrecht, the Netherlands.

However, the subcellular localization of RasGEF1B was not previously addressed in cell cycle-synchronized cells. Identification of an endosomal vesicle factor such as RasGEF1B as an interaction partner of centrosomal and/or midbody localized Ccdc124 is particularly interesting, because critical roles of endosomes in formation of multi-vesicular bodies required for physical separation of cells during cytokinetic abscission are very well established in recent studies [79].

Subsequently we analysed localization of RasGEF1B and we observed that even though in HeLa cells at interphase and prophase it displays characteristics of previously suggested cytoplasmic/early endosome localization [78], in metaphase cells, RasGEF1B was located at a pericentrosomal/centrosomal position, as assessed by its co-localization with γ-tubulin; a subcellular localization identical to that of Ccdc124 (Figure 3.21, compare with Figure 3.13-A). Again similar to Ccdc124, at telophase and during cytokinesis RasGEF1B was detected at the midzone and in the midbody (Figure 3.13), implying a possible role of Ccdc124 in linking RasGEF1B dependent signaling at the midbody to cellular abscission.

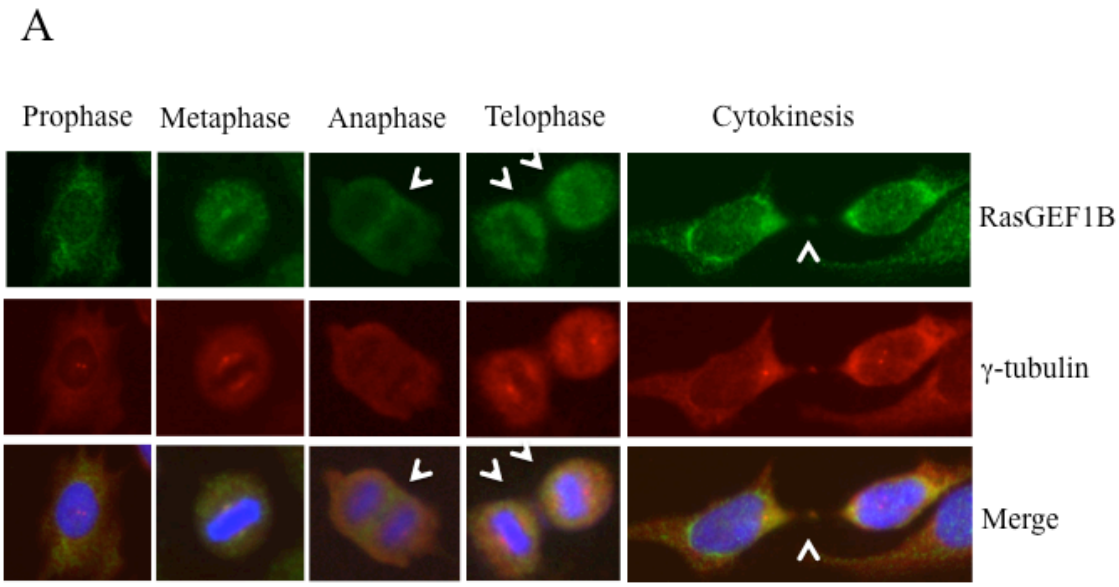
A
Prophase
Metaphase
Anaphase
Telophase
Cytokinesis
RasGEF1B
γ-tubulin
Merge

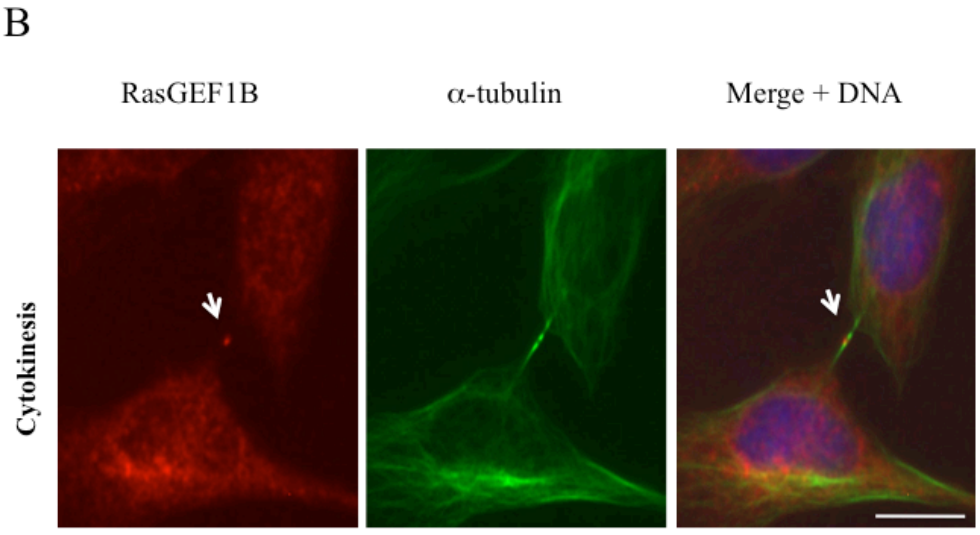
B
RasGEF1B
α-tubulin
Merge + DNA
Cytokinesis

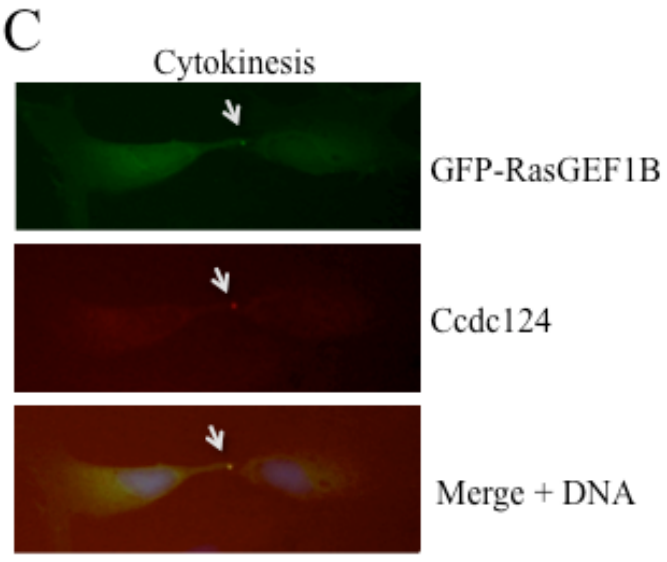
C
Cytokinesis
GFP-RasGEF1B
Ccdc124
Merge + DNA

**Figure 3.21** RasGEF1B is an interaction partner of Ccdc124, and it is localized at peri-centrosomal space and midbody. Subcellular localizations of RasGEF1B proteins in synchronously dividing HeLa cells were detected with specific anti-RasGEF1B antibodies. Cell division was synchronized as described in the legend of Figure 3.13, above. **(A)** Representative immunofluorescence microscopy images of HeLa cells costained with anti-RasGEF1B and anti-γ-tubulin antibodies, the latter illustrating the position of MTOCs and the midbody at cytokinesis. **(B)** HeLa cells costained with anti-RasGEF1B and anti-α-tubulin antibodies. RasGEF1B detected at the midzone and at the midbody were shown by white arrows. **(C)** HeLa cells transiently transfected with GFP-RasGEF1B were fixed and stained using anti-Ccdc124 Abs. Arrowheads indicate midbody positions of GFP-RasGEF1B, Ccdc124, and their colocalizations at the midbody. Bars represent 10 μm.

### 3.6 RasGEF1B knock-down in human cell lines and Zebrafish embryos.

Subcellular localization of RasGEF1B changes dynamically similar Ccdc124 during cell cycle. It is also localized to the midbody during cytokinesis like Ccdc124, so we wondered whether down-regulation of RasGEF1B by RNAi methods would cause any cyctokinetic failure. We tried to down regulate RasGEF1B in HeLa and HEK293 cell lines. However, our target siRNAs did not downregulate the expression of RasGEF1B in both cell lines, we could not investigate the effect of the RasGEF1B ablation on cytokinesis in human cell line.

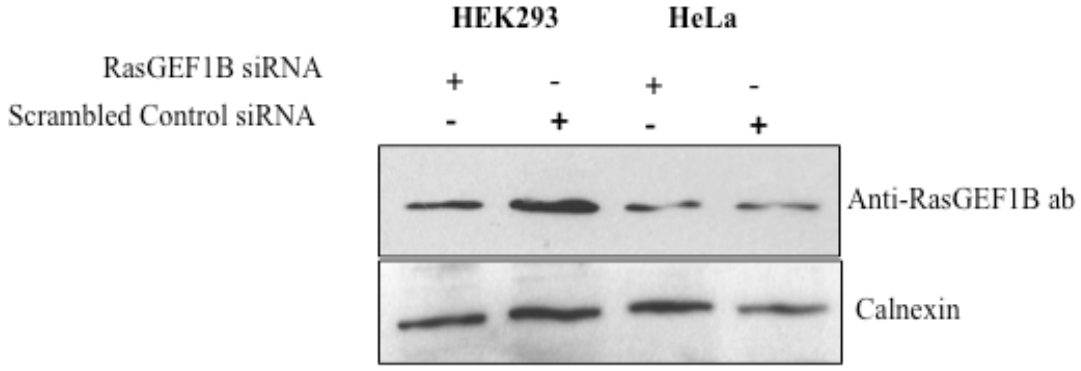


**Figure 3.22.** Transfection of RasGEF1B siRNA into HeLa and HEK293 cells. Cells transfected with target RasGEF1B siRNA or Scrambled control siRNA. 48 after transfection proteins were extracted from the cells, and loaded into SDS-gel. Corresponding PVDF membrane was covered with anti-RasGEF1B antibodies, then visulized by ECL plus detection reagent. Calnexin was used as loading control.

In addition we made efforts to observe the effect of RasGEF1B depletion in *in vivo* Zebrafish system. We designed morpholino oligos against the 5' UTR region of the RasGEF1B gene, and we have started injections in parellel to Ccdc124 studies on zebrafish embryos. We observed similar morphant phenotypes on RasGEF1B MO injected embryos in our preliminary results (data not shown). Our studies on the effect of RasGEF1B ablation in Zebrafish embryo models are ongoing.

**3.7 Functional interactions between RasGEF1B and Rap2 small G proteins.**

Activation of small G proteins is regulated by guanine nucleotide exchange factors (GEFs, please see the Introduction part). Previous functional studies in our laboratory have shown that RasGEF1 family of GEFs specifically activates Rap2 *in vitro* by stimulating guanine nucleotide exchange of this small G protein, while they do not activate other members of the Ras family. We therefore wondered whether Rap2A will also localize in centrosomes and midbody during different stages of cell cycle, and at cytokinetic abscission similar to Ccdc124 and/or RasGEF1B. First, we checked endogenous expression profiles of RAP2A by RT-PCR in various different cell lines. In these studies, we did not observe a significant expression variation among different cell lines (Fig. 3.23). Also, this study showed that RAP2A was ubiquitously expressed in all cell lines that we tested.

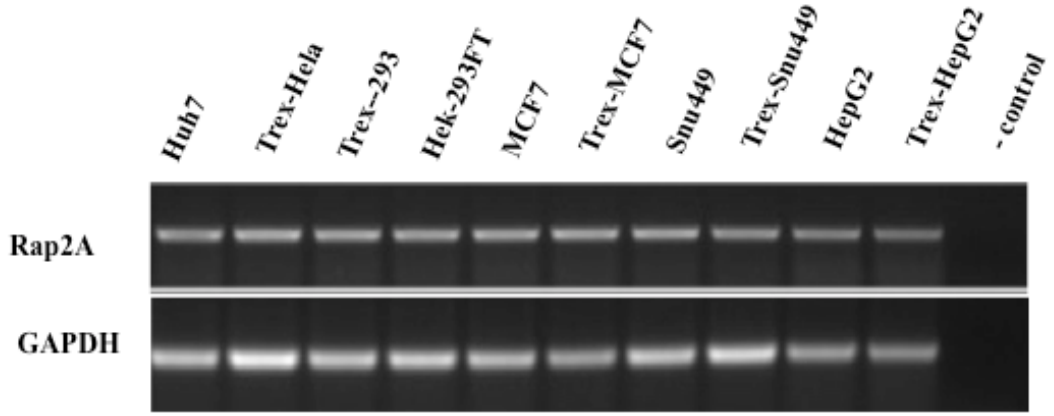


**Figure 3.23** Expression analysis of Rap2A in various human cell lines. cDNA from cell lines were amplified with Rap2A RT primers. PCR products were loaded agarose gel and analyzed by electrophoresis. Human embryonic kidney (HEK293), Human cervical cancer cell line (HeLa), Human osteosarcoma U2-OS cell line, Huh7, MCF7N, HepG2, Snu449, Retinal Pigment Epithelial-1 (RPE-1) cell line, and RPE1-GFP-Centrin, RPE1-GFP-Plk1 cell lines were used in this study. Cell lines having Trex in their names are similar to those explained above, except that they contain a

constitutively expressed bacterial tetracycline repressor (TetR) gene. –Control, indicate the negative control reaction sample without the RT enzyme.

Subsequently, we performed immunofluorescence assays by using anti-Rap2A antibody in HeLa cells and we did not observed Rap2A in centrosomes of asynchronous cells, or at any stage during cell cycle. However, Rap2 localized peri-centrosomal region in metaphase cells, and migrates to the midzone during anaphase/telophase (Figure 3.24-A). This result was in contrast to its homologue Rap1 that is non-responsive to RasGEF1B (Figure 3.24-B), [51]. We also observed that in synchronously dividing cells, 90 mins after they were released from nocodazole, at initial stages of cytokinesis Rap2 associates with microtubules originating at the midzone, and it migrates to the very center of intercellular bridge (boundaries marked with α-tubulin), relocating itself to midbody during cytokinetic abscission (Figure 3.24-C). Expectedly, at midbody the position of Rap2 overlapped both with RasGEF1B and with Ccdc124 in binary comparisons (Figure 3.24-D and 3.24-E).

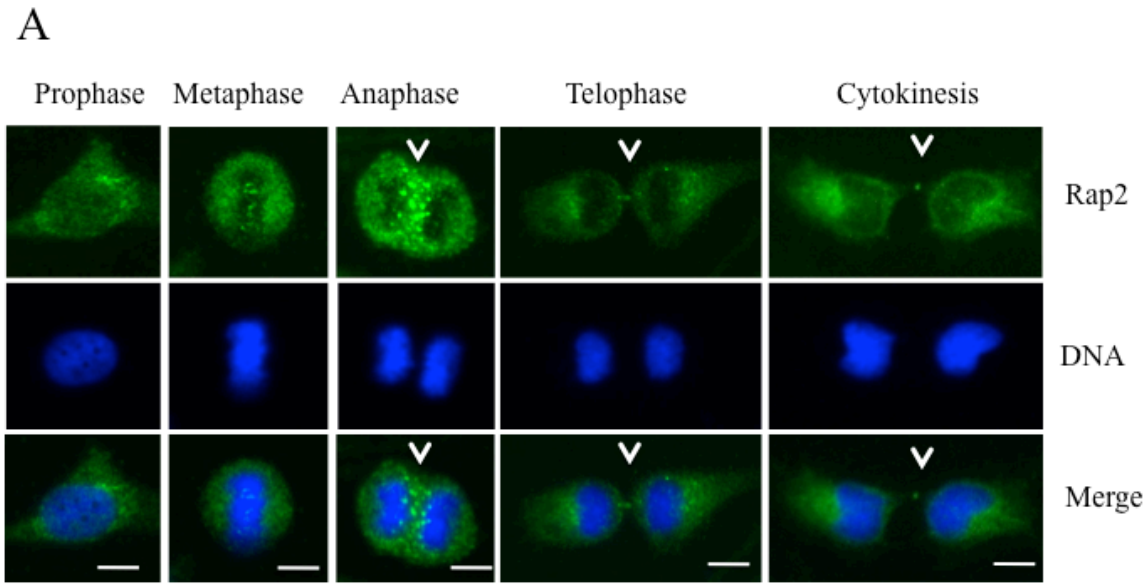

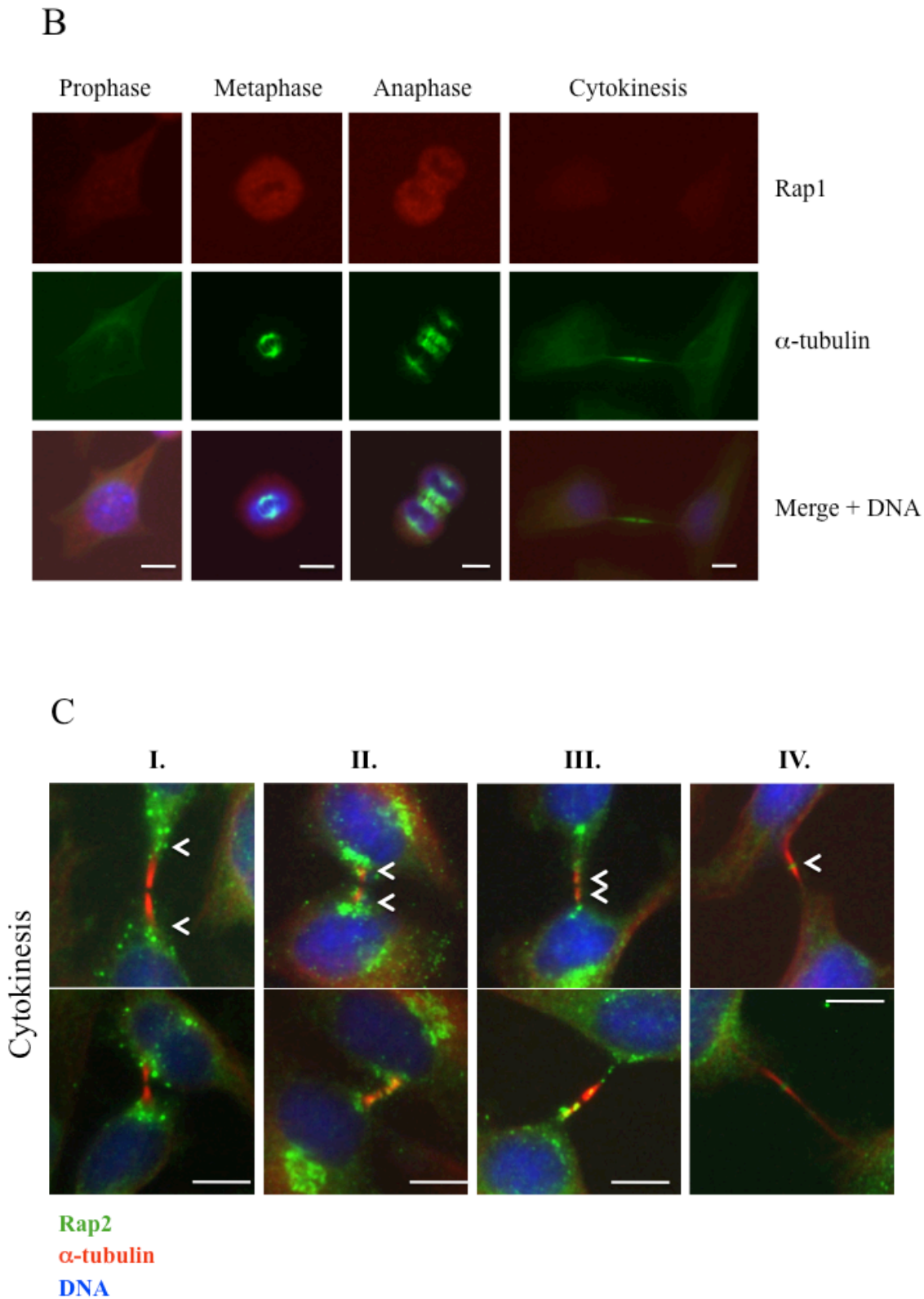
B
Prophase
Metaphase
Anaphase
Cytokinesis
Rap1
α-tubulin
Merge + DNA
C
I.
II.
III.
IV.
Cytokinesis
Rap2
α-tubulin
DNA

D

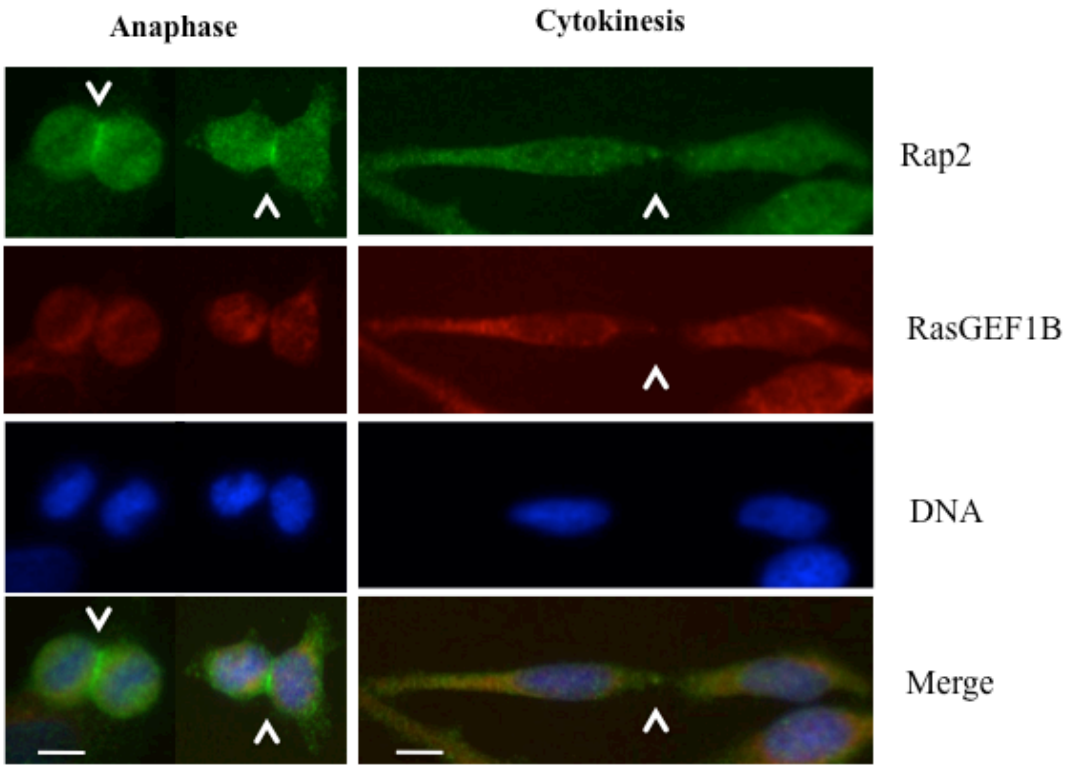
Anaphase
Cytokinesis
Rap2
RasGEF1B
DNA
Merge

E

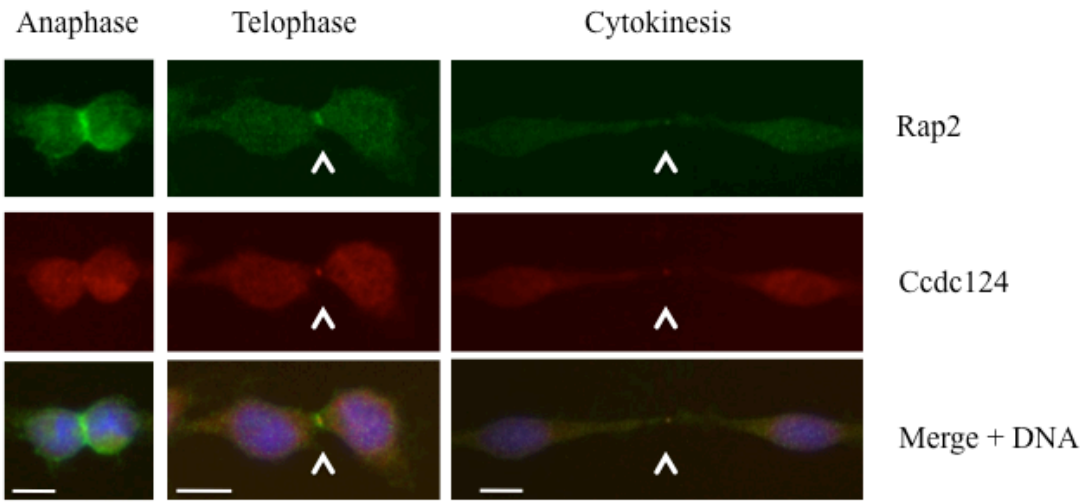
Anaphase
Telophase
Cytokinesis
Rap2
Ccdc124
Merge + DNA

**Figure 3.24** Endogenous Rap2 relocates to the midzone at anaphase, and to the midbody during late-telophase/cytokinetic abscission. **(A)** HeLa cells were arrested atG2/M phase by sequential double thymidine and nocodazole treatments as described in the legend of Figure 2, and they were classified according to phases of mitosis, and cytokinesis. Samples of cells were then stained with anti-Rap2 antibody, and with DAPI to visualize DNA. At anaphase Rap2 was detected at the midzone with staining characteristics reminiscent of endosomes, and at telophase/cytokinesis Rap2 wasobserved as puncta at the middle of the intercellular bridge, a position typically occupied by midbody associated factors. (B) Endogenous Rap1 does not relocate to the midzone/midbody during anaphase to cytokinetic abscission. HeLa cells were arrested at G2/M phase by sequential double thymidine and nocodazole treatments as described in the legend of Figure 2, and they were classified according to phases of mitosis, and cytokinesis. Samples of cells were then costained with anti-Rap1 and anti-α-tubulin antibodies, which were used to monitor intercellular bridge and the space containing midbody complexes. DAPI staining was used to visualize DNA. **(C)** Following synchronization of cells as above, 80 mins. After nocodazole was washed-off samples were taken with four consecutive intervals of 10 minutes (I, II, III, and IV), the last one (IV) corresponding to ~120 minutes after the drug was removed, and dynamic positioning of Rap2 at the intercellular bridge in respect to α-tubulin was monitored. A time-dependent relocalization of Rap2 from peripheral flanking regions to the midbody was detected.
Intercellular bridge localizations of Rap2 were concluded with observations from a sample of ~50 cells in which over 75% showed similar positioning patterns. Two representative pictures were displayed. **(D)** At anaphase, Rap2 was clearly localized at the midzone, and RasGEF1B was flanking Rap2, while during cytokinetic abscission both proteins were colocalized at the puncta characterizing the midbody.
(E). Rap2 and Ccdc124 colocalize to the midzone/midbody at telophase, and to the midbody during late-telophase/cytokinetic abscission. HeLa cells were arrested at G2/M phase by sequential double thymidine and nocodazole treatments as described in the legend of Figure 2, and they were classified according to phases of mitosis, and cytokinesis. Samples of cells were then stained with anti-Rap2 and anti-Ccdc124 Abs, and with DAPI to visualize DNA. At anaphase Rap2 was detected at the midzone, but did not colocalize with Ccdc124. At telophase, however, the two proteins were observed at the midzone/midbody, and they fully overlapped at midbody during cytokinetic abscission. Bars represent 10 μm.

### 3.8. Rap2 effectors in cytokinesis (RBD-RalGDS and YFP-TNIK).

We inquired whether midbody localized Rap2A was functionally active during cytokinesis. In order to assess this, we transfected cells with GFP tagged Rap Binding Domain of RalGDS (GFP-RBD/RalGDS) that acts as an artificial effector of GTP-bound (active) Rap2, and it serves as a subcellular Rap2 activity reporter [80]. 24 hours after transfection of the GFP-tagged RBD, we immuno-stained HeLa cells using Rap2A specific antibodies and Alexa-568-labeled secondary antibodies (red). We detected subcellular localization of both Rap2A and GFP-RBD in diffusely cytoplasm with partial co-localization at interphase (Figure 3.25-A).

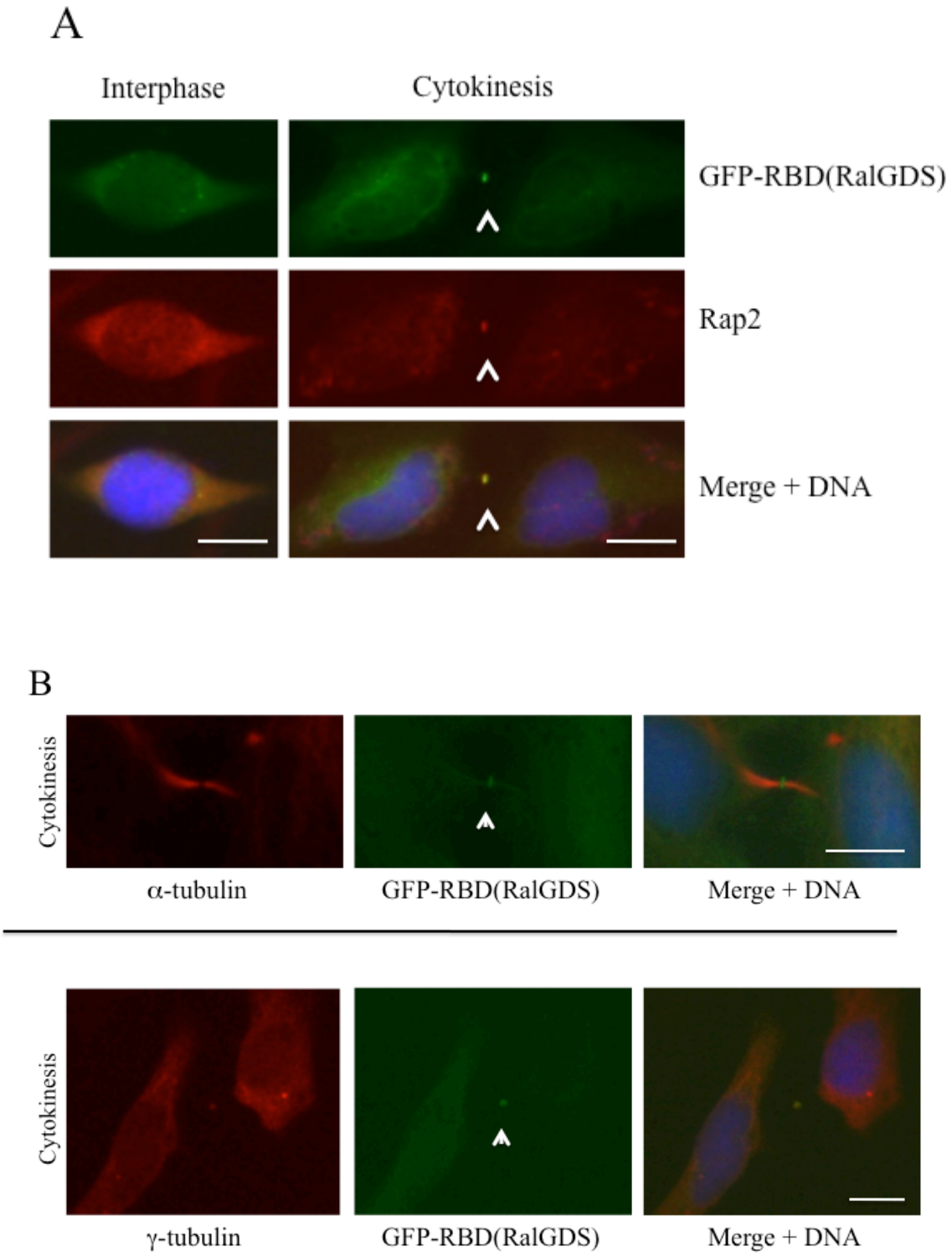


**Figure 3.25** Active form of Rap2 (Rap2˙GTP) is localized at the midbody **(A)** HeLa cells were transfected with the vector containing GFP-labeled Rap Binding Domain of RalGDS [GFP-RBD (RalGDS)] which interacts only with the GTP-bound active form of Rap2, and cells were monitored at interphase and at cytokinetic abscission following immunostainings involving anti-Rap2 monoclonal Abs and Alexa568-red labeled anti-mouse secondary Abs. Colocalization of GFP-RBD (RalGDS) with Rap2 indicated that at the midbody Rap2 is in its active (Rap2.GTP) form (B) GFP-RBD

(RalGDS) transfected HeLa cells immuno-stained with anti-RasGEF1B and anti-α-tubulin and anti-α-tubulin antibodies. GFP-RBD (RalGDS) detected at the midbody was shown by white arrow heads. Bars represent 10 μm.

However, during cytokinetic abscission, GFP-RBD (RalGDS) very clearly colocalized with Rap2 at the midbody, indicating that Rap2 protein identified at the spindle midzone/midbody is in its GTP-bound active form (Figures 3.25-A), and that it may potentially act on its specific effectors at this location. Additionally, we have also shown midbody localization of GFP-RBD (RalGDS) by immunostaining cells together with α-tubulin or γ– tubulin antibodies (Figure 3.25-B).

The dominant negative (Rap2-S17N) and constitutively active mutant (Rap2-G12V) forms of Rap2 also localized to midbody, suggesting that Rap2 protein activity was not essential for its own localization to midzone/midbody (Figure 3.26-A).

However, midbody localization of GFP-labeled RBD (RalGDS) depended on the presence of an active Rap2, as in cells co-transfected with dominant negative version of Rap2 (Rap2-S17N) the reporter protein GFP-RBD (RalGDS) did not relocate with the same efficiency to the midbody during cytokinesis as compared to cells transfected with wild-type Rap2 (Figure 3.26-). No aberrations in cytokinetic processes in cells expressing neither dominant negative (S17N) nor constitutively activated mutant (G12V) Rap2 proteins were observed.

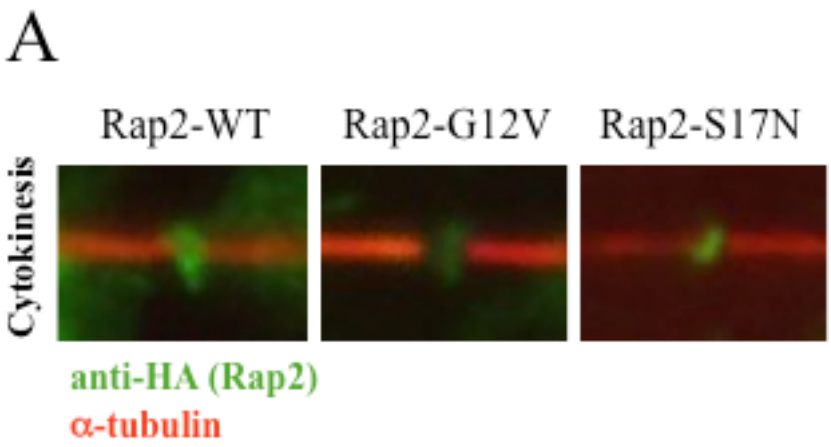

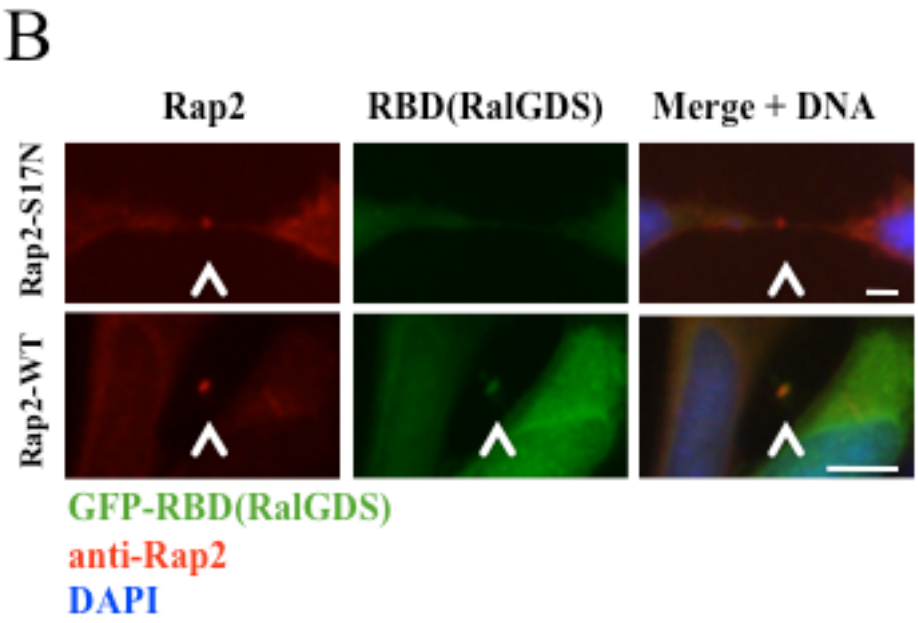


**Figure 3.26** Midbody localization of Rap2 is independent of its signal transduction activity. **(A)** HeLa cells were transfected either with WT Rap2 tagged containing HA epitope (Rap2-WT), with HA-Rap2 having an activating mutation (Rap2-G12V), or with the dominant negative form of HA-tagged Rap2 (Rap2-S17N) and midbody localizations of Rap2 proteins were monitored by using monoclonal HA-antibodies followed by Alexa488-labeled (green) secondary anti-mouse IgG Abs. Samples were co-stained with α-tubulin (polyclonal) antibodies followed by Alexa568-red labeled anti-rabbit IgG secondary antibody treatments. At least 50 cells were monitored after each transfections, with ~95% of cells displaying similar HA-Rap2 localizations. Localization of Rap2 to the midbody was independent of its cellular G protein activity. **(B)** HeLa cells were cotransfected with GFP-RBD (RalGDS) either together with HA-Rap2-WT, or with HA-Rap2-S17N (inactive dominant negative form) and positioning of GFP-RBD (RalGDS) were assessed by monitoring GFP-signal observed at the midbody. Localization of the GFP-RBD (RalGDS) depended on the presence of active Rap2 in cells. As in (A), at least 50 cells were monitored in each experiment, and representative pictures display Rap2 and GFP-RBD (RalGDS) localizations observed at least ~90% of cells cotransfected with indicated vectors. Bars represent 10 μm.

In addition, we tested whether a known effector of Rap2, **Traf2- and Nck-interacting kinase (TNIK)** [65], accumulated at the cytokinetic abscission site. When we monitored subcellular localization of a YFP labeled version of TNIK after transfection of HeLa cells with vectors carrying this recombinant Rap2 effector protein, we identified YFP-TNIK at midbody during cytokinesis (Figure 3.27-A). Interestingly, in experiments where we have transfected HeLa cells with YFP-TNIK expression vector alone, we observed that nearly 41.6% of transfected cells remained joint to each other at time points corresponding to immediate post-cytokinetic stages, as compared to ~4.9% joint cells observed among population of cells transfected with

GFP-RBD-RalGDS, or to ~7.9% joint cells found in the population of cells transfected with Rap2-WT alone (Figure 3.27, B and C), with a clear YFP-TNIK accumulation at the borders of these joint (unseparated) cells.

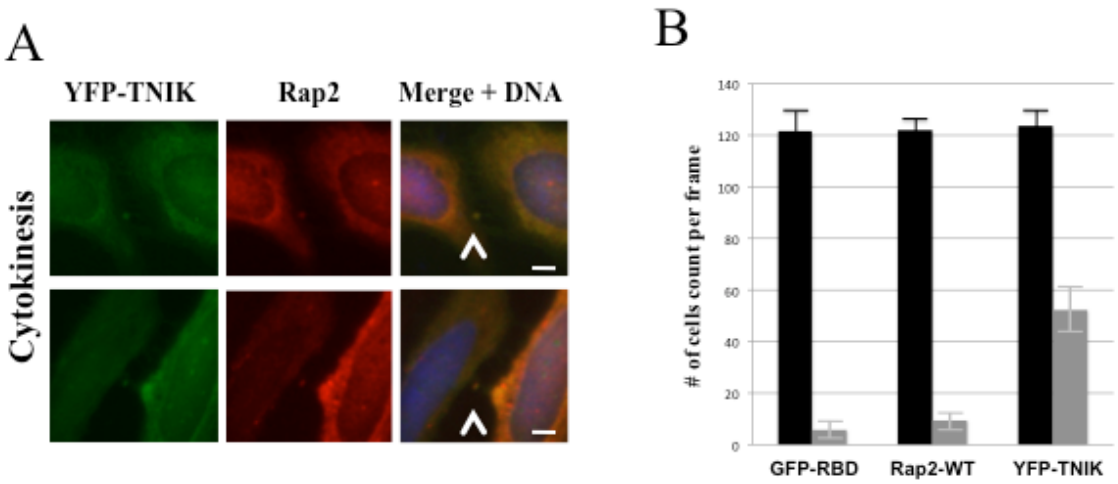


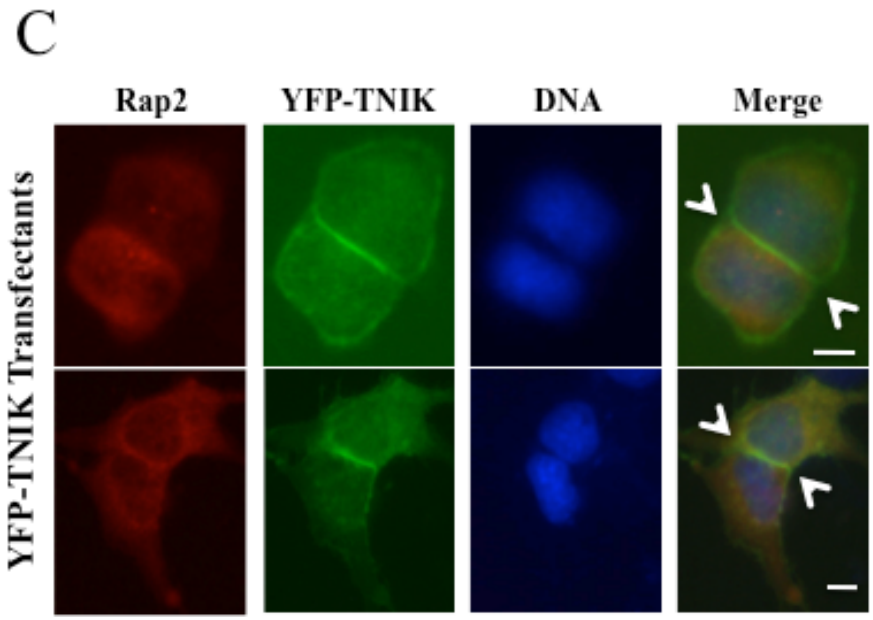

**Figure. 3.27** Rap2 effector TNIK relocates to midbody during cytokinesis, and it triggers accumulation of joint post-cytokinetic sister cells when overexpressed. **(A)** HeLa cells were transfected YFP-labeled Rap2 effector protein TNIK (YFP-TNIK), they were synchronized as described at the legend for Figure 2, samples were then fixed for immunofluorescence and subcellular localizations of YFP-TNIK and Rap2 were established. The small G protein Rap2 and its effector YFP-TNIK colocalizes at the midbody in cells at cytokinesis. **(B)** Graph presenting results of HeLa cell transfections with vectors expressing GFP-RBD (RalGDS), wild-type Rap2, or YFP-TNIK. Black bars, average numbers of cells count per frames at 200x magnification; grey bars, average numbers of joint cells (as in panel B) count at each frame. GFP-RBD transfectants: average cell counts/frame 121.6 ± 6.62, average number of joint cells/frame: 6.0 ± 0.63 (approx. 4.9%); Rap2-WT transfectants: average cell counts/frame 122.1 ± 3.48, average number of joint cells/frame: 9.6 ± 3.38 (approx. 7.9%); YFP-TNIK transfectants: average cell counts/frame 123.5 ± 3.15, average number of joint cells/frame: 52.5 ± 4.61 (approx. 41.6%). Arbitrarily, about 120 cells were count per frame, and 7 frames were analyzed per transfections (n=3, data are mean ± s.d). **(C)** HeLa cells that were transfected with YFP-TNIK were synchronized as above, released from nocodazole treatment for 150 min. in order to enrich at the post-cytokinetic stage, and then sub-cellular localizations of YFP-TNIK and Rap2 were established. Two representatives of joint cells marked with YFP-TNIK localization at borders of post-mitotic daughters were shown. Bars represent 10 μm.

The endogenous activation of local Rap2 signaling at midbody did not require pretreatment of cells with secondary messengers such as cAMP, diacylglycerol (DAG), or calcium that were previously shown to stimulate Rap signaling through activation of various GEFs [81, 82]. This indicate that recruitement of RasGEF1B to the midbody could be sufficient for regulation of Rap2 activity, as well as for translocation of Rap2 effectors YFP-TNIK or GFP-RBD-RalGDS to this subcellular location.

### 3.9 Mass-spectrometric analysis of Ccdc124 and RasGEF1B

A large number of peptides from a variety of complex mixtures can be sequenced and characterized by mass spectrometry approaches. We performed mass spectrometry analysis using liquid chromatography-mass spectrometry (LC-MS/MS) to assess possible additional interacting partners of Ccdc124 and RasGEF1B proteins. This would help us to better characterize cellular complexes in which these proteins were involved. For this purpose we first generated stable HEK293 N-ter/C-ter-flag tagged Ccdc124, HEK293-Empty-Flag cell lines (see *section 3.2*) and HEK293-YFP-RasGEF1B, HEK293-YFP cell lines to be used in affinity purification of Ccdc124 or RasGEF1B.

Initially, stable C-ter/N-ter-Flag-Ccdc124 and EV-HEK293 cells were pulled down using Flag-Ab covered sephadex beads (see *Materials and Methods*). Then, proteins were eluted from beads and elutions were fractionated by SDS-gel (Fig.3.28). Subsequently, we sliced-out bands corresponding to both the N-ter/C-ter-Flag-Ccdc124, as well as bands obtained in Ccdc124 pull-downs as compared to samples coming from EV-transfected controls (14 different bands, as indicated in Fig. 3.27). We then performed trypsin digestion on all those gel slices. Following the trypsin digestion, we purified peptides and analyzed them by using a high resolution and high accuracy LC-MS/MS platform (see Materials and Methods). Table 3.1 includes a list of proteins pulled down together with Ccdc124 proteins that were flag-tagged at both ends. Proteins indicated by bold letters in Table 3.1 were at least 1.5-fold higher in Ccdc124 pulled-down samples, as compared to control EV pull-downs. Moreover, this analysis validated once again that Ccdc124 encodes an approximately 32 kDa protein, as we previously explained (see Figure 3.9 above). We have also observed that the C-ter-flag leads to a proteolytic cleavage of the Ccdc124 protein unlike the N-ter-positioning of the flag-tag in Ccdc124, as we had observed and presented previously in Results section 3.2 (see Fig. 3.9).

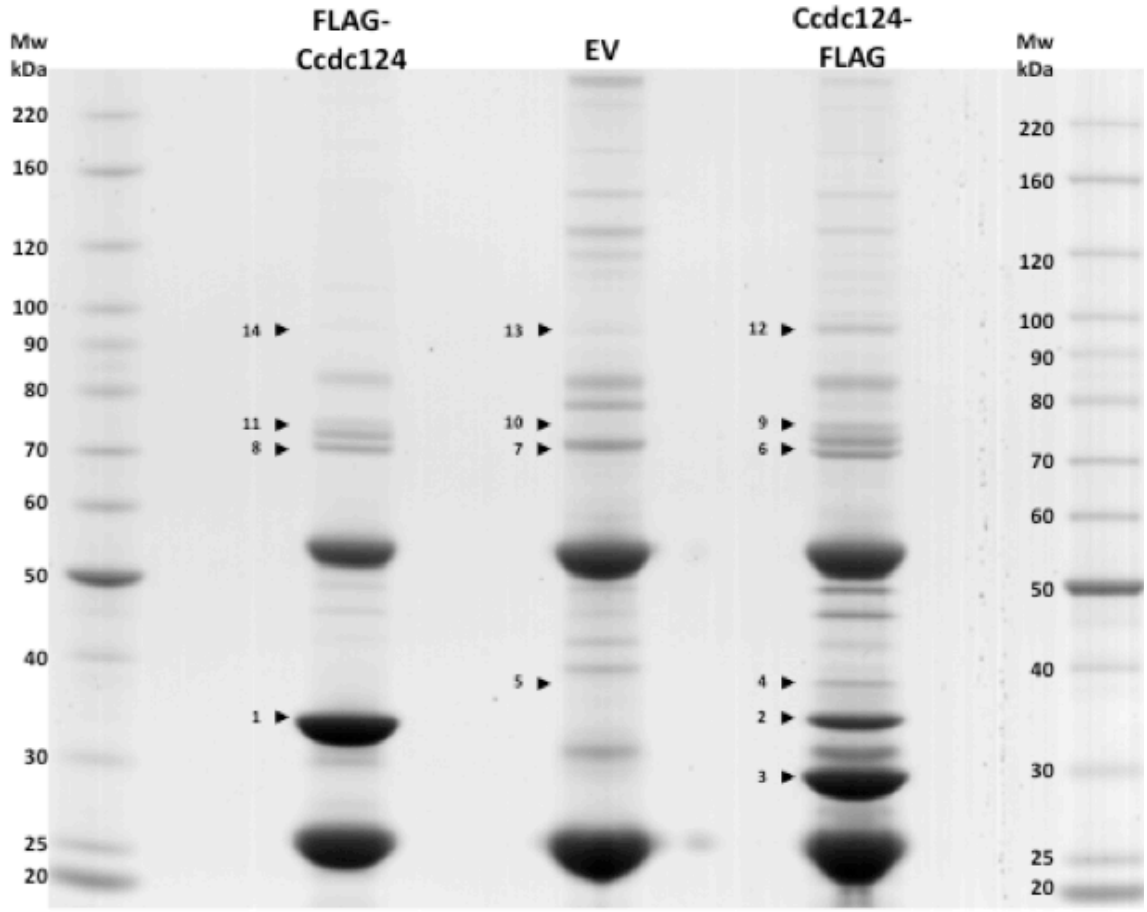


**Figure 3.28.** Gel purification of N-ter/C-ter flag-tagged Ccdc124 and its interaction partners. Numbers indicate purified bands that were subjected to LC-MS/MS analysis.

Table 3.1 List of Ccdc124 putative interacting proteins identified using LC-MS/MS method from gel digestion.

| # | Correspond. band in gel | Identifed Protein | Mol. Weight [kDa] | FLAG Ccdc124 | Ccdc124-FLAG | FLAG-EV | Fold in FLag-CCDC124 | Fold in CCDC124-Flag |
|---|---|---|---|---|---|---|---|---|
| **1** | **1, 2, 3** | **CCDC124** | **25.8** | **187** | **319** | **26** | **7.2** | **12.3** |
| **2** | **6,7,8,9,11** | **HSPA1;Heat shock protein** | **70.1** | **166** | **232** | **91** | **1.8** | **2.5** |
| 3 | | DSP;DSP variant protein;;Desmoplakin | 331.8 | 146 | 243 | 227 | 0.6 | 1.1 |
| **4** | **6,11** | **HSC70;Heat shock protein** | **70.9** | **65** | **77** | **31** | **2.1** | **2.5** |
| **5** | **9,11** | **GRP78;HSPA5;Endoplasmic reticulum lumenal Ca(2+)-binding protein** | **72.4** | **64** | **113** | **45** | **1.4** | **2.5** |
| 6 | | CTNNG;DP3;JUP;Junction plakoglobin | 81.7 | 52 | 75 | 72 | 0.7 | 1.0 |
| **7** | **9,11** | **GRP75;HSPA9;HSPA9B** | **73.7** | **52** | **65** | **21** | **2.5** | **3.1** |
| **8** | **6,11** | **HSP70B';HSPA6;HSP70B;HSPA7** | **71.0** | **42** | **66** | **13** | **3.2** | **5.1** |
| 9 | | EEF2;EF2;Elongation facto | 95.3 | 33 | 85 | 41 | 0.8 | 2.1 |
| 10 | | PSF;SFPQ | 76.1 | 30 | 36 | 30 | 1.0 | 1.2 |
| **11** | **10,14** | **LMN1** | **74.1** | **26** | **21** | **18** | **1.4** | **1.2** |
| 12 | | CDHF4;DSG1 | 113.7 | 24 | 53 | 51 | 0.5 | 1.0 |
| 13 | | HRMT1L5 | 72.7 | 22 | 52 | 46 | 0.5 | 1.1 |
| **14** | **8,** | **Histone H4** | **11.4** | **22** | **8** | **1** | **22.0** | **8.0** |
| 15 | | KPRP;Keratinocyte proline-rich protein | 64.1 | 19 | 29 | 21 | 0.9 | 1.4 |
| **16** | **12,13,14** | **NCL;Nucleolin** | **76.6** | **18** | **24** | **16** | **1.1** | **1.5** |
| 17 | | CASP14;Caspase-14 | 27.7 | 17 | 25 | 27 | 0.6 | 0.9 |
| 18 | | MSTP030;RPL5(Ribosomal proteinR5) | 34.4 | 16 | 36 | | 0.0 | 0.0 |
| 19 | | suprabasin isoform 1 precursor | 60.5 | 15 | 36 | 22 | 0.7 | 1.6 |
| 20 | | VCP protein;Transitional endoplasmic reticulum ATPase | 89.3 | 13 | 18 | 15 | 0.9 | 1.2 |
| 21 | | POF1B;pemature ovarian failure protein 1 | 68.7 | 13 | 14 | 16 | 0.8 | 0.9 |
| 22 | | RPL6;TXREB1,Neoplasm-related protein C140 | 32.9 | 12 | 60 | 18 | 0.7 | 3.3 |
| **23** | **9,** | **PAB1;Polyadenylate-binding protein 1** | **70.7** | **12** | **27** | **8** | **1.5** | **3.4** |
| 24 | | CDHF1;DSC1;Desmocollin 1b | 100.0 | 12 | 23 | 20 | 0.6 | 1.2 |
| 25 | | PKP1; highly similar to Plakophilin-1 | 82.9 | 12 | 17 | 19 | 0.6 | 0.9 |
| **26** | **6,** | **HME1;SFN (14-3-3 protein sigma;Epithelial cell marker protein 1)** | **27.8** | **12** | **15** | **3** | **4.0** | **5.0** |
| **27** | **9,** | **DBX;DEAD box protein 3** | **73.2** | **12** | **11** | **9** | **1.3** | **1.2** |
| 28 | | DDX21;DEAD box protein 21 | 87.3 | 11 | 38 | 18 | 0.6 | 2.1 |
| 29 | | GAPD;Glyceraldehyde-3-phosphate dehydrogenase | 36.0 | 11 | 19 | 20 | 0.6 | 1.0 |
| **30** | **14,** | **GNL1;HSR1;Homo sapiens guanine nucleotide binding protein-like 1** | **68.7** | **11** | **15** | **2** | **5.5** | **7.5** |
| 31 | | EEF1A;Eukaryotic elongation factor 1 A | 50.1 | 11 | 15 | 14 | 0.8 | 1.1 |
| 32 | | CRFG;GTPBP4;GTP-binding protein NGB | 31.9 | 10 | 36 | 13 | 0.8 | 2.8 |
| 33 | | LGALS7;LGALS7B;p53-induced gene 1 protein | 29.4 | 10 | 14 | 13 | 0.8 | 1.1 |
| 34 | | FABP5;Fatty acid-binding protein 5 | 55.6 | 10 | 12 | 20 | 0.5 | 0.6 |
| 35 | | DCD;PIF;Proteolysis inducing factor | 20.7 | 9 | 13 | 9 | 1.0 | 1.4 |
| 36 | | HSP27;Estrogen-regulated 24 kDa protein | 21.5 | 9 | 9 | 10 | 0.9 | 0.9 |
| **37** | **1,2,8** | **H1F3;HIST1H1D;Histone H1.3** | **14.9** | **9** | **6** | **1** | **9.0** | **6.0** |
| 38 | | HSP90AB1;HSP90B;Heat shock 84 kDa | 11.5 | 9 | 6 | 6 | 1.5 | 1.0 |
| 39 | | ANX2;;CAL1H;Calpactin-1 heavy chain | 24.9 | 8 | 28 | 20 | 0.4 | 1.4 |
| **40** | **2,** | **GNB2L1;Cell proliferation-inducing gene 21 protein;RACK1** | **43.8** | **8** | **24** | **1** | **8.0** | **24.0** |
| 41 | | CALML5;Calmodulin-like protein 5 | 39 | 8 | 19 | 13 | 0.6 | 1.5 |
| **42** | **3,** | **IGK@;IGKC;Anti-RhD monoclonal T125 kappa light chain** | **13.8** | **8** | **18** | **6** | **1.3** | **3.0** |
| 43 | | TGM3;Protein-glutamine gamma-glutamyltransferase E | 11.4 | 8 | 16 | 18 | 0.4 | 0.9 |
| 44 | | LDHA;L-lactate dehydrogenase | 14.7 | 8 | 14 | 7 | 1.1 | 2.0 |
| 45 | | C1orf68;XP32;Skin-specific protein 32 | 20.4 | 8 | 9 | 7 | 1.1 | 1.3 |
| 46 | | FKSG9;;GSDMA;Gasdermin-A | 7.6 | 8 | 9 | 12 | 0.7 | 0.8 |
| **47** | **6,** | **ACTN4;Alpha-actinin-4** | **10** | **7** | **13** | **5** | **1.4** | **2.6** |
| 48 | | ADA2B;TADA2B;ADA2-like protein beta | 1.7 | 7 | 9 | 7 | 1.0 | 1.3 |

For the quantitative analysis of Ccdc124 or RasGEF1B interaction partners by MS, we performed stable isotope labeling by amino acids (SILAC) metabolic labeling methods [83]. It involves growing of two cell populations (control and target sample) in the presence of light amino acids and heavy amino acids separately. After five cell doublings, SILAC labels amino acids in proteomes of cells through normal metabolic ways. SILAC method distinguishes two proteomes by molecular weight of light and heavy amino acids, facilitating the removal of false positives, and therefore it provides a reliable quantitative proteomics analysis [84].

Following the above mentioned methodologies, HEK293-Flag-Ccdc124 cells, HEK293-YFP-RasGEF1B cells and HEK293-EV containing cells (CMV-Flag, or YFP) were grown in appropriate (light and heavy) SILAC media. In forward experiments, heavy amino acids (Lys8, Arg10) labeled specifically HEK293-Flag-Ccdc124, HEK293-YFP-RasGEF1B cells, and light amino acids (Lys0, Arg0) labeled HEK-EV cells. In reverse experiments, cells were labeled oppositely. Then, the cells were lysed, immunoprecipitated using flag antibody-bound beads, and mixed in a 1:1 ratio. Subsequently, proteins were subjected to trypsin digestions, and analyzed by LC-MS/MS. The heavy amino acids labeled peptides are not chemically different from the light amino acids labeled peptides, but their masses change in relation with the type of amino acids (heavy or light) used in SILAC treatments. A higher peak intensity coming from heavy amino acids labeled cells indicates that protein was more abundant than light amino acids labeled proteins. In this way, we calculated ratio of interacting proteins abundance by comparisons of forward and reverse experiments, and we quantified those data by using MaxQuant software package (Appendix I). Figure 3.29-A shows putative sub-cellular localizations of Ccdc124 interacting partners, and similarly Figure 3.29-B shows putative sub-cellular localizations of detected RasGEF1B interacting partners. Nearly half of the proteins that were found to interact with target factors (Ccdc124 or RasGEF1B) were either heat shock proteins or ribosome components that tend to bind to massively over-expressed proteins in mass-spectrometry analysis (Appendix II).

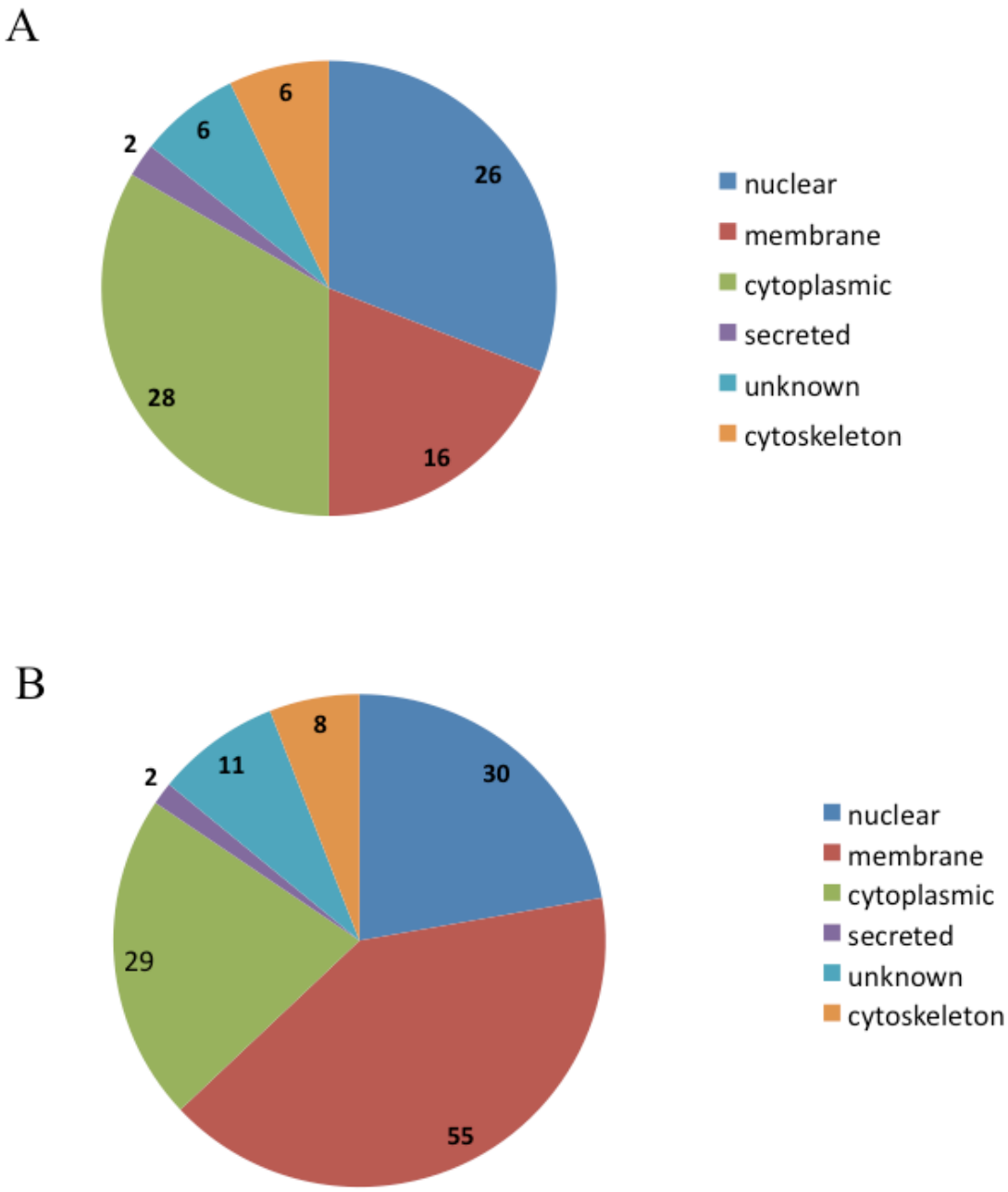


**Figure 3.29** Putative Localizations of Mass-Spectrometry Identified Ccdc124 and RasGEF1B Interaction Partners. **(A)** Sub-cellular distribution of putative Ccdc124 interaction partners**. (B)** Sub-cellular distribution of putative RasGEF1B interaction partner.

This analysis indicated a common set of 11 different proteins interacting both with Ccdc124 and RasGEF1B (Fig. 3.30 and Table 3.2). This list includes proteins with very interesting possible molecular functions, such as multidrug resistance, cellular proliferation, nucleosome assembly, or mRNA poly-A site binding (Table 3.2). Among those, GNB2L1 which is also known as RACK1 particularly stands out as it is shown in multiple studies that (similar to RasGEF1B and Ccdc124) this protein localizes to the centrosomes, kinetochores, the midbody, and nuclear envelopes during the cell cycle in *Caenorhabditis elegans*, and its knockdown caused cytokinesis failures in the early *C. elegans* embryo [33, 85].

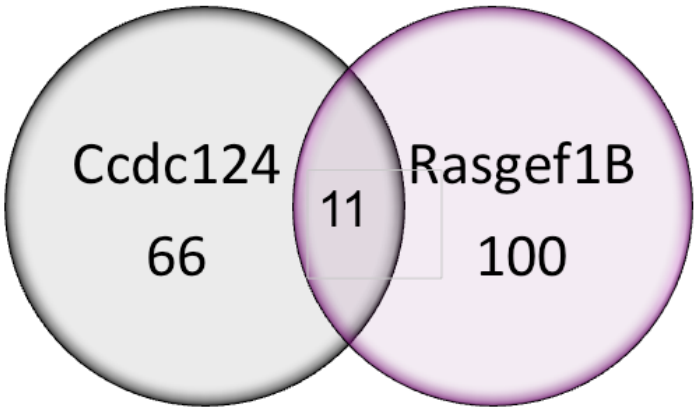


**Figure 3.30** Numbers of proteins interacting with Ccdc124 and RasGEF1B

| Identified proteins | MW(kDa) | Protein Descriptions |
|---|---|---|
| Multidrug resistance-associated protein MGr1-Ag | 33.313 | Colon carcinoma laminin-binding protein |
| HSPA5 protein | 72.421 | Endoplasmic reticulum lumenal protein grp78 |
| GNB2L1, RACK1 | 35.076 | Guanine nucleotide-binding protein subunit beta-2 |
| GCN1-like protein 1 | 26.599 | Eukaryotic translation initiation factor 6 |
| GRP75 | 72.421 | 75kDa glucose-regulated Heat shock70kDa protein |
| PAB1 | 70.67 | Polyadenylate-binding protein 1 |
| NAP-1-related protein | 45.374 | Nucleosome assembly protein 1-like 1 |
| DNAJC9 | 29.909 | DnaJ homolog subfamily C member |
| FASN protein | 273.42 | Fatty acid synthase |
| 14-3-3 protein | 29.174 | 14-3-3 protein epsilon |
| U2 small nuclear ribonucleoprotein A' | 28.415 | Small nuclear ribonucleoprotein polypeptide A' |

**Table 3.2** Common set of interaction partners of Ccdc124 and RasGEF1B as detected by LC-MS/MS analysis.

Therefore, as a priority we decided to focus on interactions with RasGEF1B/Ccdc124 and RACK1 in validating our MS data.

In this analysis, we first performed expression analysis for RACK1 in different cell lines by using immunoblotting methods. This analysis has revealed that RACK1 is ubiquitously expressed in all cell lines that we had in our collection in the laboratory.

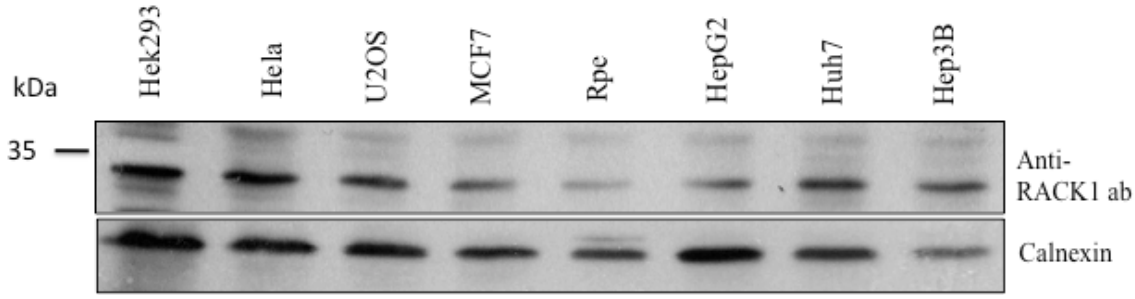


**Figure 3.31** Representative Western blotting results of endogenous RACK1 protein expression in various selected human cell lines. 40 μg protein was loaded on the SDS gel. Calnexin was used as a loading control.

Subsequently, we decided to monitor the subcellular localization of RACK1, in order to assess whether it could have also a common subcellular localization with RasGEF1B and Ccdc124. When asynchronous HeLa cells were co-stained with anti-γ-tubulin and anti-RACK1 antibodies, the metaphase centrosome and midbody associations of RACK1 were clearly observed (Fig. 3.32).

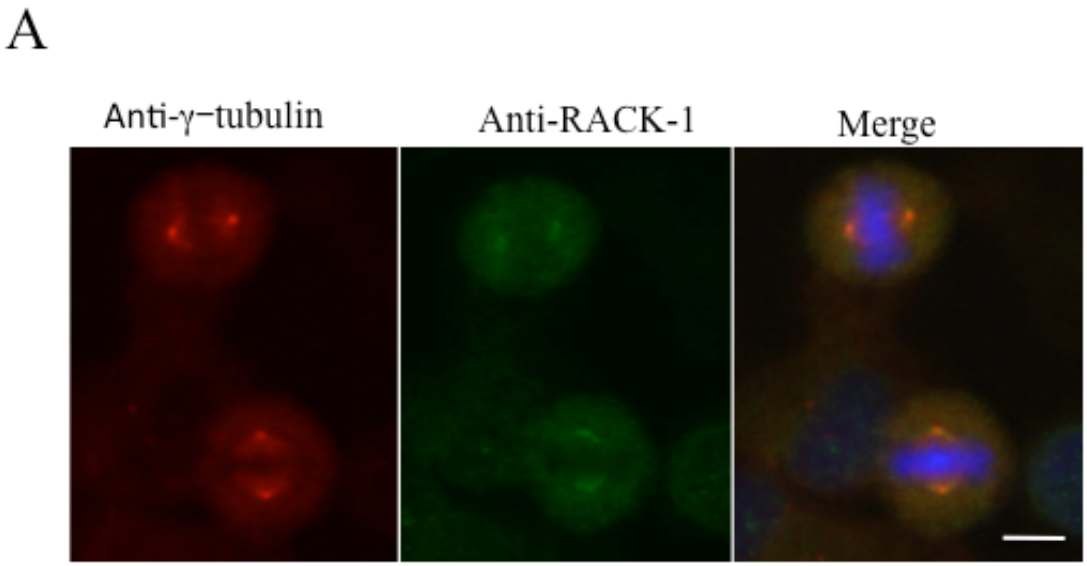

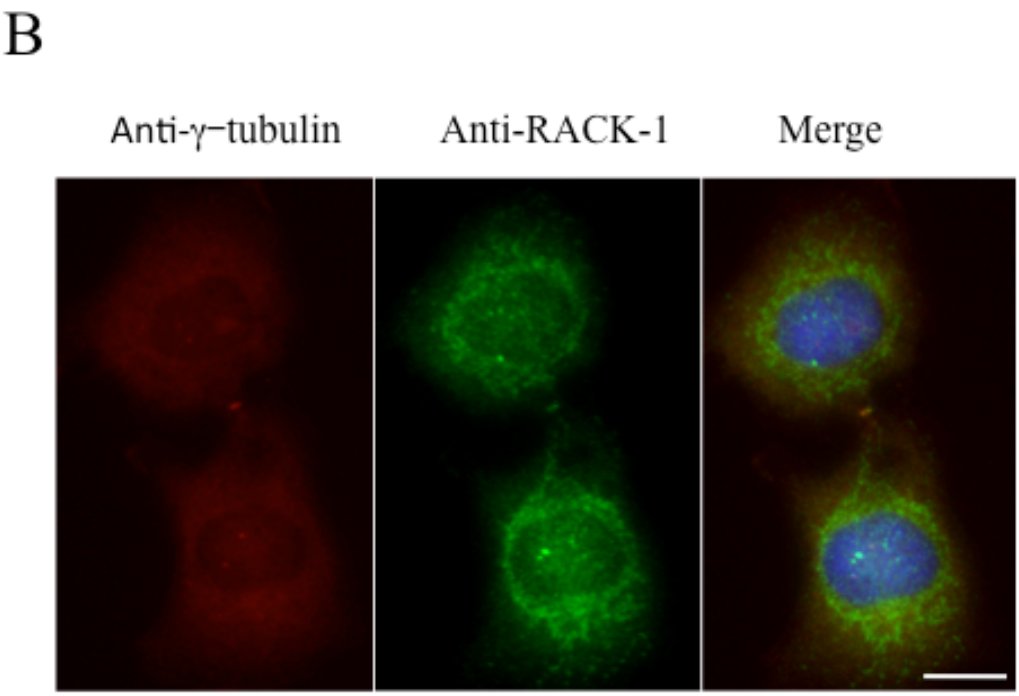


**Figure 3.32** The subcellular localization of endogenous RACK1. HeLa cells were immunostained using anti-RACK1 antibody (Green) and centrosome-midbody marker anti-γ-tubulin (Red) antibody **(A)** RACK1 localizes to centrosome together with anti-γ-tubulin during metaphase and **(B)** to the midbody during late-telophase/cytokinetic abscission.

This result indicate that RACK1 and Ccdc124/RasGEF1B share common subcellular localizations, which suggests that MS detected interacting partners could be specific partners of these proteins, and they could be involved in similar cellular activities.

### 3.10 Phosphorylation based post-translational regulation of Ccdc124

There were several evidences indicating that Ccdc124 could be a phospho-protein. First, in our MS analysis (see above) the Ser-141 residue of Ccdc124 was found to be a phosphosite (see Appendix III). Second, bioinformatic analysis of Ccdc124 using ELM tools (http://elm.eu.org/) indicates Ser-92 and Thr-103 residues phosphorylated according to UniProtKB/Swiss Prot entry database, based on the experimental evidence provided by the study "Global proteomic profiling of phosphopeptides using electron transfer dissociation tandem mass spectrometry" (Serap Erkek M.Sc. thesis, Bilkent University 2009), [86]. Furthermore, phosphorylation sites were

predicted via NetPhos [87] which suggested 5 serines, 7 threonines, and one tyrosine residue in Ccdc124 protein to constitute target sequnces of various kinases, such as Casein Kinase-I (CK-I), Casein Kinase-II (CK-II), and Plk-I. Several components of MTOC were previously shown to translocate to midbody (or shuffle between midbody and centrosomes) by phosphorylation depending modifications of those proteins. Among those, CLIP-170 was shown to be sequentially phosphorylated first by CK-II and then by Plk-1, which targets the protein to kinetochores [88]. Also, the midbody forming centrosomal factor Cep55 were shown to be a protein phosphorylated by Plk-1, and dephosphorylation of Cep55 was essential for its translocation to the midbody [39].

We therefore decided to assess whether Ccdc124 is a phospho-protein, and which sites in Ccdc124 could be functional phospho-sites. For this, we initially mutated all possible CK-I, CK-II, and Plk-1 sites in Ccdc124 either to phospho-inactivating residue Ala or to phospho-mimicking residues, Asp (D) and Glu (E). We then studied stabilities of these mutant proteins by Western blot analysis (Fig. 3.33-A).

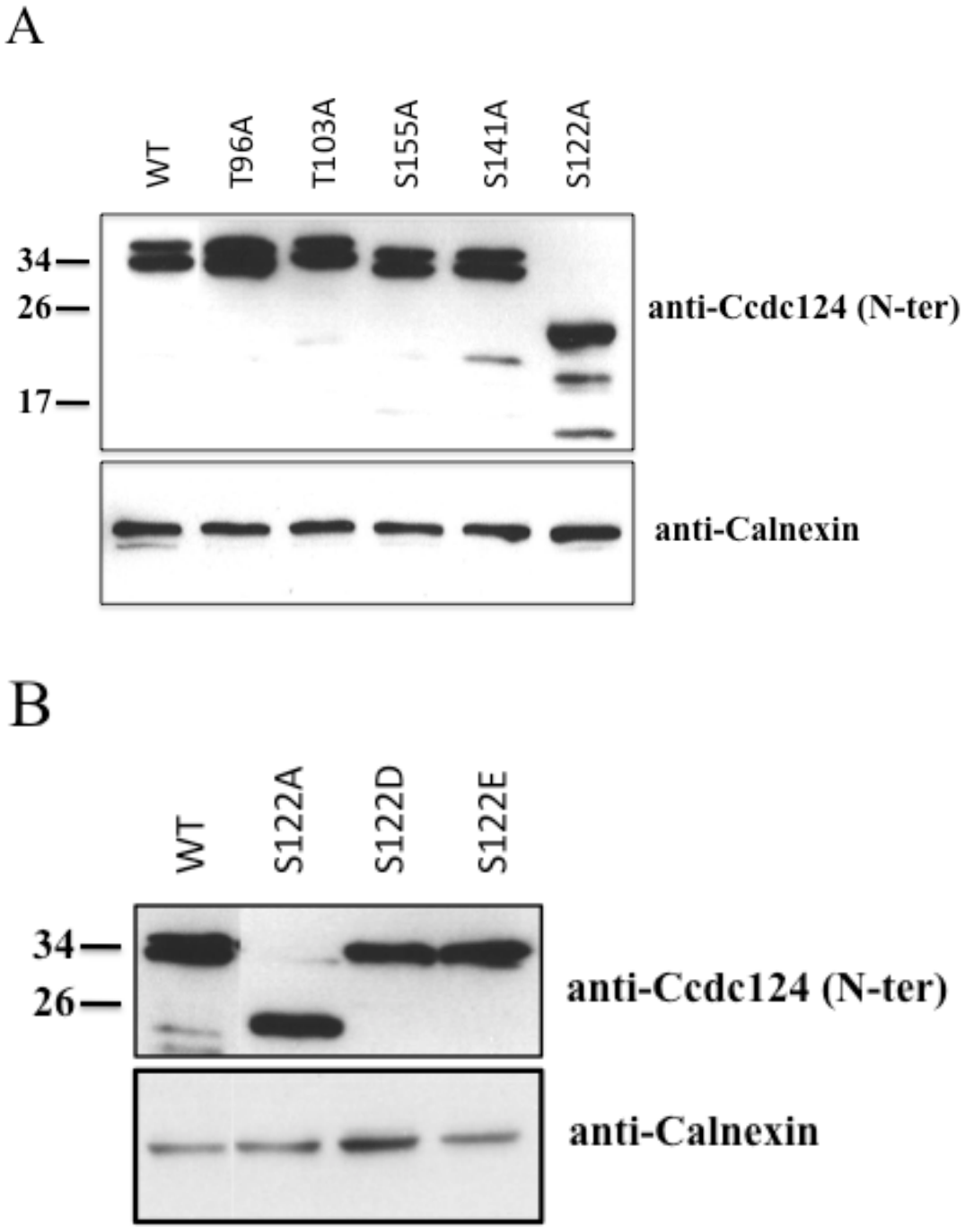


**Figure 3.33** Mutating the putative consensus CK2 phosphorylation site Ser122 residue of Ccdc124 to Ala leads to a compromised stability. (A-B) HEK293 cells were transfected either with HA-tagged wild-type Ccdc124 expression vector, or with similar vectors carrying indicated mutations on Figures, and stabilities of mutants proteins were monitored by immunoblots using anti-Ccdc124 antibodies recognizing the N-terminus of the protein. Only one CK2 phosphorylation consensus site (Ser122) turned out to be essential for the stability of Ccdc124 protein as S122A mutants were cleaved at their C-terminus, whereas phospho-mimicking mutations

S121D, and S121E were normal in terms of Ccdc124 stability (B). Calnexin expressions were monitored as loading control.

This analysis indicated that most putative phosphosites are dispensible for the stability of Ccdc124. However, conversion of the residue Ser-122 to Ala (S122A) leads to a destabilized Ccdc124, which is observed as degraded peptides on blots (Fig. 3.33-A). Both of the phospho-mimicking S122D or S122E mutations reconstituted stable Ccdc124 proteins (Fig. 3.33-B), indicating that it is not the loss of Ala-122 that leads to stability problems, but very likely, it is the lack of S122 phosphorylation that leads to a compromised stability in Ccdc124 (Fig. 3.33 A-B).

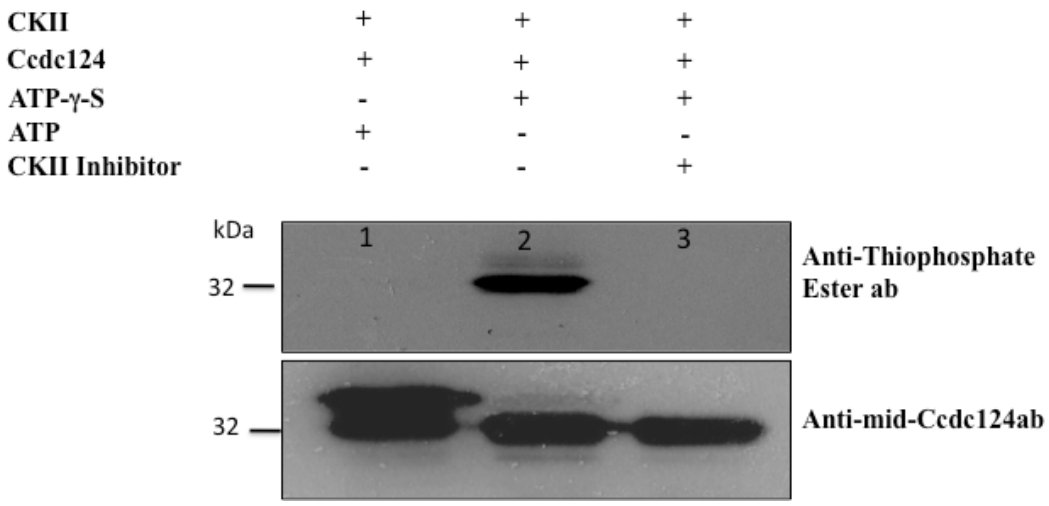


**Figure 3.34** CKII kinase phosphorylates specifically Ccdc124 *in vitro*. *In vitro* kinase assay of recombinant Ccdc124 by CKII kinase. The kinase assay was performed for 30 min. at 30°C using in the presence of equal amounts of Ccdc124 (1.5μg) protein and CKII (10 units) kinase. CKII kinase assay was performed in the presence of ATP-γ-S (100μM), PNMB (**lane 2**), in the presence of normal ATP (100μM), PNMB (**line 1**) and in the presence of ATP-γ-S (100μM), PNMB, CKII (10 μM) inhibitor TBBt (**line 3**). Samples were then run on an SDS-gel. Lanes 1 and 2 represent control experiments where proteins incubated normal ATP and PNBM (alkylate only ATP-γ-S) or ATP-γ-S, PNMB and CKII inhibitor. Lane 2 shows phosphorylation experiments of Ccdc124 by CKII.

Bioinformatics analysis of Ccdc124 protein indicated that Ser-122 residue is found in a possible CK-II target peptide consensus sequence (119-KAK**S**HLE-125). Therefore, in an *in vitro* experimental methodology, we studied phosphorylation of Ccdc124 by the CK-II enzyme. In this assay, we incubated bacteria purified full size Ccdc124 protein with pure CK-II enzyme in the presence of either ATP or ATP-γ-S, with or without a CK-II inhibitor, TBBt. CKII thiophosphorylated Ccdc124 by using ATP-γ-S. Then thiophosphorylated site of Ccdc124 was alkylated with PNBM and tagged Ccdc124 was detected by Thiophosphate Ester specific antibody (Fig. 3.34). This preliminary *in vitro* analysis indicated that Ccdc124 could be one of the targets of CK-II. Biological implications of a possible interaction between Ccdc124 and CK-II remains to be established in future studies.

# CHAPTER 4. DISCUSSION

We were initially interested in finding the cellular function of Ccdc124, as the gene that encodes this protein was conserved from yeast-to-man (Fig. 3.1). Previous studies in our laboratory have indicate that Ccdc124 was an expressed gene in human cells in culture, and also in zebra fish vertebrate model, as well as in a lower eukaryote fungus, *Aspergillus nidulans* (Pelin Telkoparan, Hani Alotaibi, Elif Yaman, and Uygar H. Tazebay, unpublished results). We hypothesized that the conservation of an expressed gene in all eukaryotes might indicate a basic and essential function in eukaryote cell biology. We have started our studies by the molecular characterization of Ccdc124 at the protein level. In respect to this, we ordered polyclonal antibodies against the N-terminal 24 amino acids peptide of Ccdc124, and also we commercially obtained anti-Ccdc124 antibodies recognizing the mid- and C-terminal regions of Ccdc124 (see *Material and Methods*). By using these reagents, we first established that Ccdc124 encodes a protein of ~32 kDa (Fig. 3.5). We also generated flag-epitope tagged forms of Ccdc124 with the purpose of using it in cell biology analysis, by inserting the epitope both at the N- and at the C-termini of the protein. As a result, we have observed that insertion of the flag-epitope to the C-terminus of the protein leads to an N-terminus cleavage in Ccdc124 (Fig. 3.7). We have further analyzed these two flag-epitope tagged versions of Ccdc124 by mass-spectrometry (LC-MS/MS) analysis in collaboration with Prof. Dr. Johannes L. Bos group at the Utrecht University Medical Center, the Netherlands. These analyses have further proven that the flag-tag at the C-terminus affects the stability of Ccdc124 (Fig. 3.9). Even though we have not analyzed the stability pattern of endogenous Ccdc124, it is likely that the protein could be subjected to a post-translational regulation involving proteolytic cleavage(s).

Subsequently, we have used anti-Ccdc124 or anti-flag antibodies in order to assess the sub-cellular localization of the Ccdc124 protein. In these cell immunofluoresce assays, we have established that this coiled-coil domain (CCD) protein is localized at single or double dot-like (puncta) structures in asynchronous growing cells (Fig. 3.11). In the literature, previous biochemical studies and mass-spectrometry analyses

on purified centrosomes have shown that proteins with CCD motifs are abundant in PCM [30], [70]. More than 150 different proteins were identified in the PCM at different cellular stages, and about 60% of these were shown to contain predicted CCD type oligomerization motifs [8]. With the hypothesis that Ccdc124 could be a novel PCM/centrosome factor, we asked whether this protein colocalizes with PCM markers such as centrin (results not shown) or γ-tubulin (Fig. 3.12). Thus, by using molecular and cell biology methods, we identified Ccdc124 as a novel component of the centrosome, as in synchronized cells at interphase and in mitotic cells up to the late-anaphase/telophase stage it clearly colocalized with two different centrosome markers, such as γ-tubulin and centrin (Fig. 3.12, and results not presented). Despite multiple high throughput proteomics analyses targeting centrosome composition in the past, Ccdc124 was not in the list of PCM proteins prior to our work, indicating that combined genetic, cell biology and biochemical approaches are still necessary to identify all the components of PCM which has a remarkably dynamic composition [19], [89].

Conservation of Ccdc124 in lower eukaryotic species without centrosomes, such as *A. nidulans*, or *S. pombe* was not surprising, as also some major centrosome proteins (for instance, γ-tubulin) were common between this organelle and fungal spindle pole bodies [32].

Our further studies presented in this work indicate that in synchronized cells at late-anaphase/telophase stages of the cell cycle, Ccdc124 changes its subcellular localization: it dissociates from centrosomes, and first relocalizes to the midzone at late-anaphase, and then it accumulates at the midbody puncta at telophase and during cytokinetic abscission (Fig. 3.13). At the present, we do not know what stimulates the displacement of Ccdc124 from the centrosome, or its association to the midzone/midbody. In fact, Cep55, a relatively well studied CCD containing centrosome protein that relocates to the midbody and controls cytokinetic abscission, was shown to be a substrate of Plk1 [39]. Phosphorylation of Cep55 by Plk1 on its Ser436 residue is required for its interaction with centralspindlin and ESCRT complex proteins, leading to the recruitment of CHMP4B to the midbody [39], [34].

CHMP4B then organizes series of ring-like structures at the abscission site, and brings the two membranes of the intercellular bridge into close proximity for the final cutting event [90], [42]. Even though in the current thesis work we have not fully addressed post-translational modifications of Ccdc124, we have carried-out a number of preliminary studies, and there are several reasons why we think that its functions/stability could be regulated by phosphorylation dependent mechanisms. First, Ccdc124 is identified as a phosphoprotein in our phosphopeptide analysis by mass-spectrometry methods, and Ser141 residue of Ccdc124 (which is a consensus Plk1 phosphorylation site) was detected as a phosphorylated residue (Pelin Telkoparan, Lars A.T. Meijer, and Uygar H. Tazebay, unpublished results). Second, as shown in Fig. 3.33, when we mutated predicted Ser, Thr, or Tyr phosphorylation sites to Ala residues in Ccdc124 by *in vitro* mutagenesis, the Ser121 residue conforming to a Casein Kinase-II phosphorylation consensus site turned out to be essential for the stability of Ccdc124 protein, even though phospho-mimicking mutations S121D, and S121E were normal in terms of protein stability (Fig. 3.33), indicative of possible phosphorylation dependent regulatory mechanisms operating on Ccdc124. Furthermore, a preliminary *in vitro* kinase assay indicate that Ccdc124 could potentially be a substrate of CK-II, as an inhibitor of CK-II (TBBt, see *Material and Methods*) inhibits phosphorylation of Ccdc124 under these conditions (Fig. 3.34).

By RNAi techniques, we have depleted Ccdc124 in a variety of human cells in culture, and assessed its results on cell biology. We found that Ccdc124 knocked-down cells can still make intact centrosomes, but they undergo severe cytokinesis failure inducing aneuploidy and generating genomic instability in cultured human cells (Fig. 3.15). Also in the zebrafish vertebrate model, when Ccdc124 was knocked-down by specific morpholino oligonucleotides in early stages of embryogenesis, we observed very similar genomic unstabilities resulting in multinuclear cellular patterns, indicative of a blockage in cytokinetic abscission (Fig. 3.16). According to current models of abscission, resolution of the membrane connection between two prospective daughter cells requires a concerted action of ESCRT proteins together with the targeting of three main types of recycling

endosomes to midbody for an appropriate regulation of cytokinetic abscission [18], [90]. In an early work, Gromley *et al*, proposed a role for secretory vesicle fusion in the final stages of cytokinetic abscission, as they have shown that the coiled-coil protein centriolin relocates to midbody where, preceding abscission, it interacts with components of vesicle-targeting exocyst complexes and membrane-fusion inducing SNARE components [40]. However, subsequent studies indicated that even though the secretary pathway could contribute to formation of the intracellular bridge membrane, it is rather recycling endosome-dependent mechanisms that make major contributions to spatiotemporal regulation of cytokinetic abscission [91]. Furthermore, other than Ral family G proteins RalA and RalB, endosome enriched complexes such as Rab35/OCRL and FYVE-CENT/TTC19 that were found on different types of endosomes, were previously shown to enable the completion of the final stages of abscission [92]-[94]. Our data suggested the following possible links between Ccdc124 and recycling endosomes: first, we identified an endosome localized nucleotide exchange factor RasGEF1B [77] as an interaction partner of the coiled-coil protein Ccdc124 (Fig. 3.21). Second, RasGEF1B activated small G protein Rap2 that we detected at the midzone/midbody, was previously reported to colocalize with Rab11-positive endosomes in *Xenopus* early embryos [95]. Importantly, Rab11-positive recycling endosomes containing the effector protein FIP3 (Rap11 Family of Interacting Protein 3) were previously shown to control the reorganization of the cortical actomyosin network during cytokinetic abscission, as they accumulate at the intercellular space between dividing cells and regulate local actin depolymerization by recruiting p50RhoGAP, and thus contributing to further thinning of the bridge [96].

In this thesis work, we focused on the biological significance of the interaction between Ccdc124 and RasGEF1B, rather than studying mechanistic aspects of it. Yet, previous studies from our laboratory on the effect of bacteria purified Ccdc124 on the rate of nucleotide exchange by RasGEF1B on RAP2A in *in vitro* reconstituted assay systems suggested that Ccdc124 does not functionally interfere with RasGEF1B activity (Elif Yaman, Alfred Wittinghofer, Uygar H. Tazebay, unpublished observations). We hypothesized that rather than affecting its GEF

activity, Ccdc124 could recruit RasGEF1B to midzone/midbody where the exchange factor activate its substrate G protein(s). A similar spatiotemporal regulation of Rap1 signaling localized at the plasma membrane by recruitement and translocation of its cAMP responsive GEF, Epac1, through activation of Ezrin-Radixin-Moesin (ERM) complex proteins was previously described [97]. In follow-up studies regarding interaction partners of RasGEF1B and Ccdc124, we have purified complexes involving these two proteins, and analyzed their compositions by LC-MS/MS mass-spectrometry analysis methods (Table 3.1 and Figs. 3.29 and 3.30). These assays have revealed that there are 11 possible common interacting proteins between Ccdc124 and RasGEF1B (Fig. 3.30). Among those factors, we are giving priority in studying possible interactions between RasGEF1B/Ccdc124 and RACK1, as this kinase was previously shown to be involved in cytokinesis in *C. Elegans* [33, 84], and it has a similar sub-cellular localization pattern as Ccdc124 and RasGEF1B (Fig. 3.32).

We have shown that both the activator RasGEF1B and its partner G protein Rap2 have identical spatiotemporal subcellular distributions (Fig. 3.24). This indicated that RasGEF1B could potentially activate GDP/GTP exchange of Rap2 at midbody during late-telophase stage of cell cycle and at cytokinesis. Importantly, we observed the RasGEF1B substrate Rap2, but not its close homologue Rap1, accumulated in vesicular structures proximal to the midzone and at the midbody (Fig. 3.24, see panels metaphase to cytokinesis). Detection of active Rap2 (Rap2·GTP) binding reporter protein GFP-RBD(RalGDS) in midbody further proved local activation of Rap2 at midbody puncta during cytokinesis (Fig. 3.25). This midbody localization of GFP-RBD(RalGDS), was only observed in cells having Rap2-WT, but not its dominant negative form, Rap2-S17N, indicating that midbody localization of Rap2 effectors requires activation of this small G protein (Fig. 3.26).

A schematic representation of sub-cellular localizations of Ccdc124, RasGEF1B, and Rap2 at different stages of cell cycle is shown in Fig. 3.35.

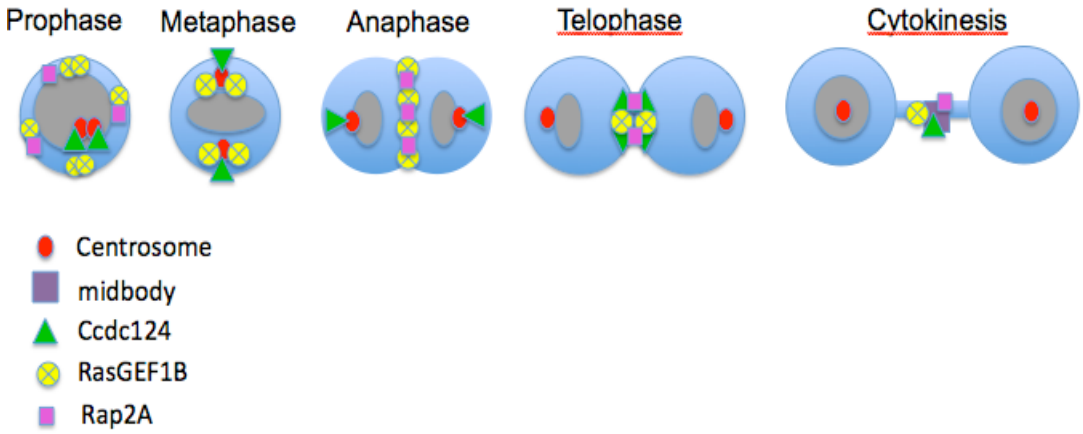


**Figure 3.35** A schematic representation of subcellular localizations of Ccdc124, RasGEF1B, and Rap2 at various stages of the cell cycle.

Recently, it has been shown that Rap2 and its effector TNIK are components of the Lbk1 signaling pathway that control cellular polarity, and when induced by Lkb1, Rap2/TNIK control formation of brush borders by specification of the apical membranes of intestinal epithelial cells [66]. When in our study, HeLa cells were transfected with vectors carrying a YFP-linked version of TNIK, we also observed this effector protein of Rap2 at the midbody during cytokinetic abscission (Fig. 3.27), and interestingly approximately 41.6% of cells transfected with YFP-TNIK remained unseparated in culture conditions at time points corresponding to early post-cytokinetic stages (i.e., 150 mins. After G2/M blocking MT polymerization inhibitor nocodazole was washed-off, Fig. 3.27). Moreover, YFP-TNIK was found to accumulate it these cells all along the membrane separating two postmitotic daughters (Fig. 3.27). This suggested that over-expression and accumulation of the effector YFP-TNIK at the intermembrane between the daughter cells alone could lead to joining of post-mitotic cells, independent of Rap2 signaling. These observations support the notion that localization of Rap2 at the midbody may serve to functionalize local membrane environment for molecular events following cytokinetic abscission, such as establishment of cell-cell junctions, cell-extracellular matrix adhesions, or polarizations of cells after division of daughter cells fully accomplished. Interestingly, neither cellular depletion of endogenous Rap2 by specific shRNA transfections, nor over-expression of the dominant negative form of Rap2 (S17N) has led to cytokinesis defects, as assessed by normal levels of bi- and

multinucleated cells in corresponding cellular assays (Fig. 3.26). Therefore, it seems that rather than playing a direct role in cytokinesis, localization of Rap2 at the midbody might serve to modulate and/or functionalize local membrane environment for molecular events following cytokinetic abscission, such as establishment of cell-cell junctions, cell-extracellular matrix adhesions, or polarizations of cells after division of daughter cells fully accomplished. When we consider results obtained in this thesis altogether, we propose Ccdc124 as a novel factor that links cytokinesis to Rap signaling dependent junction/adhesion or cellular polarization promoting molecular mechanisms, thus bonding different cellular events that must closely follow each other in tissues of live organisms.

# CHAPTER 5. FUTURE PERSPECTIVES

Ccdc124 is conserved in all eukaryotes including lower yeast and fungal species. Also, RasGEF1B and Rap2 orthologues exist in lower eukaryotes [50]. Therefore, functional and mechanistic studies on Ccdc124 could effectively be carried-out in these simple model organisms, which also bring advantages of classical genetics. In simple yeast models (for instance *Schizosaccharomyces pombe*) where genetic crosses could be performed, not only mutants of Ccdc124, RasGEF1B, and Rap2 could be obtained and analyzed, but also revertant strains (or second site repressors) can be selected, and double mutants are easily constructed.

When we analyzed Ccdc124 proteins expressed from the mammalian expression vectors by immunoblots, we observed two bands of ~32kDa and ~26 kDa when we used antibodies recognizing middle or c-terminus epitopes in Ccdc124. The ~26 kDa band was not detectable in blots incubated with an N-ter specific anti-Ccdc124 antibody, indicating that the small form was missing the N-terminus part (Fig. 3.5). In bioinformatics analysis, we found a second methionine residue (Met-47), which could have formed an alternative ATG start codon. We tested this hypothesis by inserting a M47L mutation in CMV-Ccdc124-HA vector construct, and then repeating a similar Western blot analysis (Fig. 3.6). As a result, the ~26 kDa band have disappeared, indicating that the second ATG (codon 47) was an alternative start site for Ccdc124 gene translation. In support of our result, Lee *et al*. [72] have recently found that in the endogenous gene, Met-47 codon provides an alternative Kozak sequence forming an alternative ribosome-binding site. In future work, we aim to analyze possible alternative cellular functions of these two different forms (short and long forms) of Ccdc124.

By using a mass-spectrometry based proteomics system, we initiated studies for identification of complexes in which Ccdc124 and RasGEF1B proteins are involved. In this study we identified about 11 possible common interaction partners including some (for example, RACK1) that have a role in cytokinesis. However, as we were not aware of the localization of Ccdc124 when these mass-spectrometry analyses were done, immunoprecipitated complexes analyzed in this study were not coming from synchronized cells. We now anticipate that in future mass-spectrometry

analysis, Ccdc124 and RasGEF1B immunoprecipitations could be done on synchronized cells at different phases of the cells cycle, including the cytokinesis phase (post-anaphase/telophase). In other words, a better profile of possible interactions could be obtained, if similar analyses were done on purified centrosomes or midbody at appropriate stages of the cell cycle. This will be addressed in future studies.

Mass-spectrometry studies revealed that Ccdc124 is in fact a phosphoprotein, as Ser-141 appeared to be phosphorylated in phospho-peptide analysis. This residue (Ser-141) is localized in a consensus Plk-1 modification site. We mutated this Ser-141 residue to phospho-mimicking Asp, or Glu, or to phospho-mutant Ala residue. These mutations did not cause any stability problems in Ccdc124. On the other hand, by these experiments we could not conclude on the effect of Plk-1 to post-translational modifications of Ccdc124. Follow-up studies should address whether or not Ccdc124 is a substrate of the Plk-1. For this, chemical genetics approaches with engineered cells having analogue sensitive Plk-1 forms (Plk1-AS), as well as typical *in vitro* kinase assays could be done.

Bioinformatics analyses also identified CK-I and CK-II as putative kinases that could post-translationally modify Ccdc124. When possible CK-I and CK-II substrate residues are mutated to phospho-mimicking and phospho-mutant residues, we observed that a particular CK-II substrate residue is important for the stability of Ccdc124 (Fig. 3.33). We further extended these analyses to *in vitro* kinase assays, and found that under these conditions CK-II specifically phosphorylates Ccdc124 (Fig. 3.34). It remains to be established whether or not Ccdc124 is a CK-II substrate under *in vivo* conditions.

We have constructed GFP-tagged versions of Ccdc124, with GFP localized at different domains of Ccdc124 (results not shown). By using these vector constructs, we prepared stable cell lines (U2OS) expressing GFP-tagged versions of Ccdc124. These cell lines will be used in live imaging confocal microscopy for the analysis of subcellular localization dynamics of Ccdc124. These constructs will also be used for interaction mapping between Ccdc124 and its interaction partners (for instance RasGEF1B) in Co-IP experiments.

Zebrafish embryo model is a useful *in vivo* system for functional analysis of Ccdc124 and its interaction partners. In our preliminary knockdown studies by using specific morpholino oligonucleotides, we observed cytokinesis defects with pronounced genomic unstabilities in early embryonic tissues, followed by an important embryonic lethality rate in these Ccdc124 depleted early embryos (Fig. 3.16). Furthermore, in later embryonic stages, Ccdc124 depleted individuals have shown major developmental defects characterized by shortened body forms and spinal cord malformations (Fig. 3.16). In future work, these results should be developed with rigorous molecular analysis including several other experimental controls. For example, phenotype rescue experiments where morpholino and wt-RNA injections are done simultaneously should be included to experimental designs. In order to establish functions of RasGEF1B and Rap2 in Zebrafish embryo development, the same experiments should also be done for these two genes, RasGEF1B and Rap2. Mouse knock-out projects will also be carried out to define the function of Ccdc124 and RasGEF1B in development of mammalian models. For this purpose, we have already purchased from the University of California at Davis-KOMP facility the suitable mouse embryonic stem cells where Ccdc124 was unconditionally deleted. These ES cells will be implemented to mice in collaboration with the Animal Genetics facility located at the BIOGEM-Institute of Salvatore Gaitano, Ariano Irpino, Italy.

Even though we have established the function of Ccdc124 in cytokinesis in mammalian cells, we have not addressed possible roles of Ccdc124 mutations in human diseases. For example, mutations of Cep152 that is another coiled-coil domain containing centrosomal protein, was shown to result in genomic instability, and a rare developmental disorder called Seckel syndrome in humans [98]. Depletion of Ccdc124 also causes genomic instability both in cell line models, and in the *in vivo* Zebrafish model. It is possible that mutations in Ccdc124 could be associated with similar developmental disorders in human. Genomic instability due to cytokinetic defects was also associated with human cancers in past studies [99-100]. Therefore, in future work, human cancer samples should be screened for mutations in

Ccdc124, in order to establish possible correlations between oncogenesis and Ccdc124. Possible epigenetic factors resulting in Ccdc124 expression modifications in human cancers should also be assessed in future studies.

## REFERENCES


1. Schafer, K A. "The Cell Cycle: A Review." *Veterinary pathology* 35, no. 6 (1998): 461-78.
2. Ozlü, N., Monigatti, F., Renard, B.Y., Field, C.M., Steen, H., Mitchison, T.J. and Steen, J.J., 2010, Binding partner switching on microtubules and aurora-B in the mitosis to cytokinesis transition, *Molecular & cellular proteomics : MCP*, 9(2), pp. 336-50
3. van den Heuvel, S., 2005, Cell-cycle regulation, *WormBook : the online review of C. elegans biology*, pp. 1-16
4. Johnson, D G, and C L Walker. "Cyclins and Cell Cycle Checkpoints." *Annual review of pharmacology and toxicology* 39 (1999): doi:10.1146/annurev.pharmtox.39.1.295.
5. Israels, E D, and L G Israels. "The Cell Cycle." *The oncologist* 5, no. 6 (2000): 510-3.
6. Malumbres, M. and Barbacid, M., 2009, Cell cycle, CDKs and cancer: a changing paradigm, *Nature reviews. Cancer*, 9(3), pp. 153-66.
7. Pines, J. & Rieder, C.L., 2001, *Nature Cell Biology*, 3(1), pp. E3-6
8. Werner, M. and Glotzer, M., 2008, Control of cortical contractility during cytokinesis, *Biochemical Society transactions*, 36(Pt 3), pp. 371-7
9. Fededa, J.P. and Gerlich, D.W., 2012, Molecular control of animal cell cytokinesis, *Nature cell biology*, 14(5), pp. 440-7.
10. Green, R.A., Paluch, E. and Oegema, K., 2012, Cytokinesis in animal cells, *Annual review of cell and developmental biology*, 28, pp. 29-58.
11. Jordan, S.N. and Canman, J.C., 2012, Rho GTPases in animal cell cytokinesis: an occupation by the one percent, *Cytoskeleton (Hoboken, N.J.)*, 69(11), pp. 919-30.
12. Barr, F.A. and Gruneberg, U., 2007, Cytokinesis: placing and making the final cut, *Cell*, 131(5), pp. 847-60.
13. Gruneberg, U., Neef, R., Honda, R., Nigg, E.A. and Barr, F.A., 2004, Relocation of Aurora B from centromeres to the central spindle at the

metaphase to anaphase transition requires MKlp2, *The Journal of cell biology*, 166(2), pp. 167-72.

**14.** Goto, H., Yasui, Y., Kawajiri, A., Nigg, E.A., Terada, Y., Tatsuka, M., Nagata, K. and Inagaki, M., 2003, Aurora-B regulates the cleavage furrow-specific vimentin phosphorylation in the cytokinetic process, *The Journal of biological chemistry*, 278(10), pp. 8526-30.

**15.** Kawajiri, A., Yasui, Y., Goto, H., Tatsuka, M., Takahashi, M., Nagata, K. and Inagaki, M., 2003, Functional significance of the specific sites phosphorylated in desmin at cleavage furrow: Aurora-B may phosphorylate and regulate type III intermediate filaments during cytokinesis coordinatedly with Rho-kinase, *Molecular biology of the cell*, 14(4), pp. 1489-500

**16.** Murata-Hori, M., Fumoto, K., Fukuta, Y., Iwasaki, T., Kikuchi, A., Tatsuka, M. and Hosoya, H., 2000, Myosin II regulatory light chain as a novel substrate for AIM-1, an aurora/Ipl1p-related kinase from rat, *Journal of biochemistry*, 128(6), pp. 903-7.

**17.** Neto, H. and Gould, G.W., 2011, The regulation of abscission by multi-protein complexes, *Journal of cell science*, 124(Pt 19), pp. 3199-207.

**18.** Steigemann, P. and Gerlich, D.W., 2009, Cytokinetic abscission: cellular dynamics at the midbody, *Trends in cell biology*, 19(11), pp. 606-16

**19.** Lüders, J. and Stearns, T., 2007, Microtubule-organizing centres: a re-evaluation, *Nature reviews. Molecular cell biology*, 8(2), pp. 161-7.

**20.** Kollman, J.M., Merdes, A., Mourey, L. and Agard, D.A., 2011, Microtubule nucleation by γ-tubulin complexes, *Nature reviews. Molecular cell biology*, 12(11), pp. 709-21.

**21.** Bettencourt-Dias, M. and Glover, D.M., 2007, Centrosome biogenesis and function: centrosomics brings new understanding, *Nature reviews. Molecular cell biology*, 8(6), pp. 451-63.

**22.** Nigg, E.A.and Stearns, T., 2011, The centrosome cycle: Centriole biogenesis, duplication and inherent asymmetries, *Nature cell biology*, 13(10), pp. 1154-60.

**23.** Debec, A., Sullivan, W. and Bettencourt-Dias, M., 2010, Centrioles: active players or passengers during mitosis? *Cellular and molecular life sciences : CMLS*, 67(13), pp. 2173-94.

**24.** Bornens, M., 2012, The centrosome in cells and organisms, *Science (New York, N.Y.)*, 335(6067), pp. 422-6

**25.** Mardin, B.R. and Schiebel, E., 2012, Breaking the ties that bind: new advances in centrosome biology, *The Journal of cell biology*, 197(1), pp. 11-8.

**26.** Hinchcliffe, E.H., Miller, F.J., Cham, M., Khodjakov, A. and Sluder, G., 2001, Requirement of a centrosomal activity for cell cycle progression through G1 into S phase, *Science*, 291(5508), pp. 1547-5.

**27.** Khodjakov, A., Cole, R.W., Oakley, B.R. and Rieder, C.L., 2000, Centrosome-independent mitotic spindle formation in vertebrates, *Current biology : CB*, 10(2), pp. 59-67

**28.** Basto, R., Lau, J., Vinogradova, T., Gardiol, A., Woods, C.G., Khodjakov, A. and Raff, J.W., 2006, Flies without centrioles, *Cell*, 125(7), pp. 1375-86

**29.** Andersen, J.S., Wilkinson, C.J., Mayor, T., Mortensen, P., Nigg, E.A. and Mann, M., 2003, Proteomic characterization of the human centrosome by protein correlation profiling, *Nature*, 426(6966), pp. 570-4

**30.** Jakobsen, L., Vanselow, K., Skogs, M., Toyoda, Y., Lundberg, E., Poser, I., Falkenby, L.G., Bennetzen, M., Westendorf, J., Nigg, E.A., Uhlen, M., Hyman, A.A. and Andersen, J.S., 2011, Novel asymmetrically localizing components of human centrosomes identified by complementary proteomics methods, *The EMBO journal*, 30(8), pp. 1520-35.

**31.** Oakley, C.E. and Oakley, B.R., 1989, Identification of gamma-tubulin, a new member of the tubulin superfamily encoded by mipA gene of Aspergillus nidulans, *Nature*, 338(6217), pp. 662-4.

**32.** Oakley, B.R., Oakley, C.E., Yoon, Y. and Jung, M.K., 1990, Gamma-tubulin is a component of the spindle pole body that is essential for microtubule function in Aspergillus nidulans, *Cell*, 61(7), pp. 1289-301.

**33.** Skop, A.R., Liu, H., Yates, J., Meyer, B.J. and Heald, R., 2004, Dissection of the mammalian midbody proteome reveals conserved cytokinesis mechanisms, *Science (New York, N.Y.)*, 305(5680), pp. 61-6

**34.** Hu, C.K., Coughlin, M. and Mitchison, T.J., 2012, Midbody assembly and its regulation during cytokinesis, *Molecular biology of the cell*, 23(6), pp. 1024-34.

**35.** Boman, A.L., Kuai, J., Zhu, X., Chen, J., Kuriyama, R. and Kahn, R.A., 1999, Arf proteins bind to mitotic kinesin-like protein 1 (MKLP1) in a GTP-dependent fashion, *Cell motility and the cytoskeleton*, 44(2), pp. 119-3.

**36.** Yüce, O., Piekny, A. and Glotzer, M., 2005, An ECT2-centralspindlin complex regulates the localization and function of RhoA, *The Journal of cell biology*, 170(4), pp. 571-82.

**37.** Tang, B.L., 2012, Membrane Trafficking Components in Cytokinesis, *Cellular physiology and biochemistry : international journal of experimental cellular physiology, biochemistry, and pharmacology*, 30(5), pp. 1097-108.

**38.** Bastos, R.N. and Barr, F.A., 2010, Plk1 negatively regulates Cep55 recruitment to the midbody to ensure orderly abscission, *The Journal of cell biology*, 191(4), pp. 751-60

**39.** Fabbro, M., Zhou, B.B., Takahashi, M., Sarcevic, B., Lal, P., Graham, M.E., Gabrielli, B.G., Robinson, P.J., Nigg, E.A., Ono, Y. and Khanna, K.K., 2005, Cdk1/Erk2- and Plk1-dependent phosphorylation of a centrosome protein, Cep55, is required for its recruitment to midbody and cytokinesis, *Developmental cell*, 9(4), pp. 477-88.

**40.** Gromley, A., Yeaman, C., Rosa, J., Redick, S., Chen, C.T., Mirabelle, S., Guha, M., Sillibourne, J. and Doxsey, S.J., 2005, Centriolin anchoring of exocyst and SNARE complexes at the midbody is required for secretory-vesicle-mediated abscission, *Cell*, 123(1), pp. 75-87.

**41.** Schweitzer, J.K., Burke, E.E., Goodson, H.V. and D'Souza-Schorey, C., 2005, Endocytosis resumes during late mitosis and is required for cytokinesis, *The Journal of biological chemistry*, 280(50), pp. 41628-35.

**42.** Morita, E., Sandrin, V., Chung, H.Y., Morham, S.G., Gygi, S.P., Rodesch, C.K. and Sundquist, W.I., 2007, Human ESCRT and ALIX proteins interact

with proteins of the midbody and function in cytokinesis, *The EMBO journal*, 26(19), pp. 4215-27.

**43.** Reid, E., Connell, J., Edwards, T.L., Duley, S., Brown, S.E. and Sanderson, C.M., 2005, The hereditary spastic paraplegia protein spastin interacts with the ESCRT-III complex-associated endosomal protein CHMP1B, *Human molecular genetics*, 14(1), pp. 19-38

**44.** Connell, J.W., Lindon, C., Luzio, J.P. and Reid, E., 2009, Spastin couples microtubule severing to membrane traffic in completion of cytokinesis and secretion, *Traffic (Copenhagen, Denmark)*, 10(1), pp. 42-56.

**45.** Doxsey, S., 2001, Re-evaluating centrosome function, *Nature reviews. Molecular cell biology*, 2(9), pp. 688-98.

**46.** Doxsey, S.J., 2005, Molecular links between centrosome and midbody, *Molecular cell*, 20(2), pp. 170-2.

**47.** Bos, J.L., Rehmann, H. and Wittinghofer, A., 2007, GEFs and GAPs: critical elements in the control of small G proteins, *Cell*, 129(5), pp. 865-77.

**48.** Buday, L. and Downward, J., 2008, Many faces of Ras activation, *Biochimica et biophysica acta*, 1786(2), pp. 178-87.

**49.** Wennerberg, K., Rossman, K.L. and Der, C.J., 2005, The Ras superfamily at a glance, *Journal of cell science*, 118(Pt 5), pp. 843-6

**50.** van Dam, T.J., Rehmann, H., Bos, J.L. and Snel, B., 2009, Phylogeny of the CDC25 homology domain reveals rapid differentiation of Ras pathways between early animals and fungi, *Cellular signalling*, 21(11), pp. 1579-8

**51.** Yaman, E., Gasper, R., Koerner, C., Wittinghofer, A. and Tazebay, U.H., 2009, RasGEF1A and RasGEF1B are guanine nucleotide exchange factors that discriminate between Rap GTP-binding proteins and mediate Rap2-specific nucleotide exchange, *The FEBS journal*, 276(16), pp. 4607-16

**52.** Bos, J.L., de Rooij, J. and Reedquist, K.A., 2001, Rap1 signalling: adhering to new models, *Nature reviews. Molecular cell biology*, 2(5), pp. 369-77

**53.** Gloerich, M. and Bos, J.L., 2011, Regulating Rap small G-proteins in time and space, *Trends in cell biology*, 21(10), pp. 615-23.

**54.** Schwamborn, J.C. and Püschel, A.W., 2004, The sequential activity of the GTPases RAP1B and Cdc42 determines neuronal polarity, *Nat Neurosci*, 7(9), pp. 923-9

**55.** Shimonaka, M., Katagiri, K., Nakayama, T., Fujita, N., Tsuruo, T., Yoshie, O. and Kinashi, T., 2003, Rap1 translates chemokine signals to integrin activation, cell polarization, and motility across vascular endothelium under flow, *The Journal of cell biology*, 161(2), pp. 417-27

**56.** Caron, E., Self, A.J. and Hall, A., 2000, The GTPase Rap1 controls functional activation of macrophage integrin alphaMbeta2 by LPS and other inflammatory mediators, *Current biology : CB*, 10(16), pp. 974-8.

**57.** Katagiri, K., Hattori, M., Minato, N., Irie, S.k., Takatsu, K. and Kinashi, T., 2000, Rap1 is a potent activation signal for leukocyte function-associated antigen 1 distinct from protein kinase C and phosphatidylinositol-3-OH kinase, *Molecular and cellular biology*, 20(6), pp. 1956-69

**58.** Reedquist, K.A., Ross, E., Koop, E.A., Wolthuis, R.M., Zwartkruis, F.J., van Kooyk, Y., Salmon, M., Buckley, C.D. and Bos, J.L., 2000, The small GTPase, Rap1, mediates CD31-induced integrin adhesion, *The Journal of cell biology*, 148(6), pp. 1151-8.

**59.** Tsukamoto, N., Hattori, M., Yang, H., Bos, J.L. and Minato, N., 1999, Rap1 GTPase-activating protein SPA-1 negatively regulates cell adhesion, *The Journal of biological chemistry*, 274(26), pp. 18463-9.

**60.** Hogan, C., Serpente, N., Cogram, P., Hosking, C.R., Bialucha, C.U., Feller, S.M., Braga, V.M., Birchmeier, W. and Fujita, Y., 2004, Rap1 regulates the formation of E-cadherin-based cell-cell contacts, *Molecular and cellular biology*, 24(15), pp. 6690-700

**61.** Price, L.S., Hajdo-Milasinovic, A., Zhao, J., Zwartkruis, F.J., Collard, J.G. and Bos, J.L., 2004, Rap1 regulates E-cadherin-mediated cell-cell adhesion, *The Journal of biological chemistry*, 279(34), pp. 35127-32

**62.** Altschuler, D.L. and Ribeiro-Neto, F., 1998, Mitogenic and oncogenic properties of the small G protein RAP1B, *Proceedings of the National Academy of Sciences of the United States of America*, 95(13), pp. 7475-9

**63.** Crittenden, J.R., Bergmeier, W., Zhang, Y., Piffath, C.L., Liang, Y., Wagner, D.D., Housman, D.E. and Graybiel, A.M., 2004, CalDAG-GEFI integrates signaling for platelet aggregation and thrombus formation, *Nat Med*, 10(9), pp. 982-6.

**64.** D'Silva, N.J., Jacobson, K.L., Ott, S.M. and Watson, E.L., 1998, Beta-adrenergic-induced cytosolic redistribution of Rap1 in rat parotid acini: role in secretion, *Am J Physiol*, 274(6 Pt 1), pp. C1667-73.

**65.** Taira, K., Umikawa, M., Takei, K., Myagmar, B.E., Shinzato, M., Machida, N., Uezato, H., Nonaka, S. and Kariya, K., 2004, The Traf2- and Nck-interacting kinase as a putative effector of Rap2 to regulate actin cytoskeleton, *The Journal of biological chemistry*, 279(47), pp. 49488-96.

**66.** Gloerich, M., ten Klooster, J.P., Vliem, M.J., Koorman, T., Zwartkruis, F.J., Clevers, H. and Bos, J.L., 2012, RAP2A links intestinal cell polarity to brush border formation, *Nature cell biology*, 14(8), pp. 793-801.

**67.** Alotaibi, H., Yaman, E., Salvatore, D., Di Dato, V., Telkoparan, P., Di Lauro, R. and Tazebay, U.H., 2010, Intronic elements in the Na+/I- symporter gene (NIS) interact with retinoic acid receptors and mediate initiation of transcription, *Nucleic acids research*, 38(10), pp. 3172-85.

**68.** Mason, J.M. and Arndt, K.M., 2004, Coiled coil domains: stability, specificity, and biological implications, *Chembiochem : a European journal of chemical biology*, 5(2), pp. 170-6.

**69.** Burkhard, P., Stetefeld, J. and Strelkov, S.V., 2001, Coiled coils: a highly versatile protein folding motif, *Trends in cell biology*, 11(2), pp. 82-8.

**70.** Sterns, T., and Winey, M., " The Cell Center at 100." *Cell* 91, (1997): 303–309.

**71.** Telkoparan, P., Erkek, S., Yaman, E., Alotaibi, H., Bayik, D., Tazebay, U.H., 2013, Coiled-coil domain containing protein 124 is a novel centrosome and midbody protein that interacts with the Ras-guanine nucleotide exchange factor 1B and is involved in cytokinesis (*in press, PLoS ONE*)

**72.** Lee, S., Liu, B., Lee, S., Huang, S.X., Shen, B. and Qian, S.B., 2012, Global mapping of translation initiation sites in mammalian cells at single-nucleotide

resolution, *Proceedings of the National Academy of Sciences of the United States of America*, 109(37), pp. E2424-32

**73.** Uetake, Y., Loncarek, J., Nordberg, J.J., English, C.N., La Terra, S., Khodjakov, A. and Sluder, G., 2007, Cell cycle progression and de novo centriole assembly after centrosomal removal in untransformed human cells, *The Journal of cell biology*, 176(2), pp. 173-82

**74.** Schuyler, S.C. and Pellman, D., 2001, Search, capture and signal: games microtubules and centrosomes play, *Journal of cell science*, 114(Pt 2), pp. 247-55.

**75.** Khodjakov, A. and Rieder, C.L., 2001, Centrosomes enhance the fidelity of cytokinesis in vertebrates and are required for cell cycle progression, *The Journal of cell biology*, 153(1), pp. 237-42.

**76.** Bill, B.R., Petzold, A.M., Clark, K.J., Schimmenti, L.A. and Ekker, S.C., 2009, A primer for morpholino use in zebrafish, *Zebrafish*, 6(1), pp. 69-77

**77.** Heasman, J., 2002, Morpholino oligos: making sense of antisense? *Developmental biology*, 243(2), pp. 209-14.

**78.** Andrade, W.A., Silva, A.M., Alves, V.S., Salgado, A.P., Melo, M.B., Andrade, H.M., Dall'Orto, F.V., Garcia, S.A., Silveira, T.N. and Gazzinelli, R.T., 2010, Early endosome localization and activity of RasGEF1B, a toll-like receptor-inducible Ras guanine-nucleotide exchange factor, *Genes and immunity*, 11(6), pp. 447-57.

**79.** Carlton, J.G., Caballe, A., Agromayor, M., Kloc, M. and Martin-Serrano, J., 2012, ESCRT-III governs the Aurora B-mediated abscission checkpoint through CHMP4C, *Science (New York, N.Y.)*, 336(6078), pp. 220-5.

**80.** Bivona, T.G., Wiener, H.H., Ahearn, I.M., Silletti, J., Chiu, V.K. and Philips, M.R., 2004, Rap1 up-regulation and activation on plasma membrane regulates T cell adhesion, *The Journal of cell biology*, 164(3), pp. 461-7.

**81.** de Rooij, J., Zwartkruis, F.J., Verheijen, M.H., Cool, R.H., Nijman, S.M., Wittinghofer, A. and Bos, J.L., 1998, Epac is a Rap1 guanine-nucleotide-exchange factor directly activated by cyclic AMP, *Nature*, 396(6710), pp. 474-7.

**82.** Ghandour, H., Cullere, X., Alvarez, A., Luscinskas, F.W. and Mayadas, T.N., 2007, Essential role for Rap1 GTPase and its guanine exchange factor CalDAG-GEFI in LFA-1 but not VLA-4 integrin mediated human T-cell adhesion, *Blood*, 110(10), pp. 3682-90.

**83.** Ong, S.E. and Mann, M., 2006, A practical recipe for stable isotope labeling by amino acids in cell culture (SILAC), *Nature protocols*, 1(6), pp. 2650-6

**84.** Mann, M., 2006, Functional and quantitative proteomics using SILAC, *Nature reviews. Molecular cell biology*, 7(12), pp. 952-8.

**85.** Ai, E., Poole, D.S. and Skop, A.R., 2009, RACK-1 directs dynactin-dependent RAB-11 endosomal recycling during mitosis in Caenorhabditis elegans, *Molecular biology of the cell*, 20(6), pp. 1629-38

**86.** Molina, H., Horn, D.M., Tang, N., Mathivanan, S. and Pandey, A., 2007, Global proteomic profiling of phosphopeptides using electron transfer dissociation tandem mass spectrometry, *Proceedings of the National Academy of Sciences of the United States of America*, 104(7), pp. 2199-20.

**87.** Blom, N., Gammeltoft, S. and Brunak, S., 1999, Sequence and structure-based prediction of eukaryotic protein phosphorylation sites, *Journal of molecular biology*, 294(5), pp. 1351-62.

**88.** Li, H., Liu, X.S., Yang, X., Wang, Y., Wang, Y., Turner, J.R. and Liu, X., 2010, Phosphorylation of CLIP-170 by Plk1 and CK2 promotes timely formation of kinetochore-microtubule attachments, *The EMBO journal*, 29(17), pp. 2953-65.

**89.** Piel, M., Nordberg, J., Euteneuer, U. and Bornens, M., 2001, Centrosome-dependent exit of cytokinesis in animal cells, *Science*, 291(5508), pp. 1550-3.

**90.** Elia, N., Sougrat, R., Spurlin, T.A., Hurley, J.H. and Lippincott-Schwartz, J., 2011, Dynamics of endosomal sorting complex required for transport (ESCRT) machinery during cytokinesis and its role in abscission, *Proceedings of the National Academy of Sciences of the United States of America*, 108(12), pp. 4846-51.

**91.** Schiel, J.A., Childs, C. and Prekeris, R., 2013, Endocytic transport and cytokinesis: from regulation of the cytoskeleton to midbody inheritance, *Trends in cell biology* .

**92.** Cascone, I., Selimoglu, R., Ozdemir, C., Del Nery, E., Yeaman, C., White, M. and Camonis, J., 2008, Distinct roles of RalA and RalB in the progression of cytokinesis are supported by distinct RalGEFs, *The EMBO journal*, 27(18), pp. 2375-87

**93.** Dambournet, D., Machicoane, M., Chesneau, L., Sachse, M., Rocancourt, M., El Marjou, A., Formstecher, E., Salomon, R., Goud, B. and Echard, A., 2011, Rab35 GTPase and OCRL phosphatase remodel lipids and F-actin for successful cytokinesis, *Nature cell biology*, 13(8), pp. 981-8.

**94.** Sagona, A.P., Nezis, I.P., Pedersen, N.M., Liestøl, K., Poulton, J., Rusten, T.E., Skotheim, R.I., Raiborg, C. and Stenmark, H., 2010, PtdIns(3)P controls cytokinesis through KIF13A-mediated recruitment of FYVE-CENT to the midbody, *Nature cell biology*, 12(4), pp. 362-71.

**95.** Choi, S.C., Kim, G.H., Lee, S.J., Park, E., Yeo, C.Y. and Han, J.K., 2008, Regulation of activin/nodal signaling by Rap2-directed receptor trafficking, *Developmental cell*, 15(1), pp. 49-61.

**96.** Schiel, J.A., Simon, G.C., Zaharris, C., Weisz, J., Castle, D., Wu, C.C. and Prekeris, R., 2012, FIP3-endosome-dependent formation of the secondary ingression mediates ESCRT-III recruitment during cytokinesis, *Nature cell biology*, 14(10), pp. 1068-7.

**97.** Gloerich, M., Ponsioen, B., Vliem, M.J., Zhang, Z., Zhao, J., Kooistra, M.R., Price, L.S., Ritsma, L., Zwartkruis, F.J., Rehmann, H., Jalink, K. & Bos, J.L., 2010, Spatial regulation of cyclic AMP-Epac1 signaling in cell adhesion by ERM proteins, *Molecular and cellular biology*, 30(22), pp. 5421-31.

**98.** Kalay, E., Yigit, G., Aslan, Y., Brown, K.E., Pohl, E., Bicknell, L.S., Kayserili, H., Li, Y., Tüysüz, B., Nürnberg, G., Kiess, W., Koegl, M., Baessmann, I., Buruk, K., Toraman, B., Kayipmaz, S., Kul, S., Ikbal, M., Turner, D.J., Taylor, M.S., Aerts, J., Scott, C., Milstein, K., Dollfus, H., Wieczorek, D., Brunner, H.G., Hurles, M., Jackson, A.P., Rauch, A., Nürnberg, P., Karagüzel, A. & Wollnik, B., 2011, CEP152 is a genome maintenance protein disrupted in Seckel syndrome, *Nature genetics*, 43(1), pp. 23-6

**99.** Sagona, A.P. and Stenmark, H., 2010, Cytokinesis and cancer, *FEBS letters*, 584(12), pp. 2652-61

**100.** Godinho, S.A., Kwon, M. & Pellman, D., 2009, Centrosomes and cancer: how cancer cells divide with too many centrosomes, *Cancer metastasis reviews*, 28(1-2), pp. 85-98

## LIST OF APPENDICES

# APPENDIX I

## CCDC124 LC-MS/MS DATA

A- filter-aided sample preparation (FASP) methods

B- samples with in-gel digestion

| | Protein Names | Gene Names | Protein Descriptions | Ratio H/L Stable Forward | Ratio H/L Normalized Stable Forward | Ratio L/H Stable Reverse | Ratio L/H Normalized Stable Reverse | Ratio H/L Trans Forward | Ratio H/L Normalized Trans Forward | Ratio L/H Trans Reverse | Ratio L/H Normalized Trans Reverse |
|---|---|---|---|---|---|---|---|---|---|---|---|
| | | | | Previously identified proteins are shown in this color | | | | | | | |
| 138 | Antigen MLAA-34;Calcium-binding protein 39-like;Mo25-like prote | CAB39L;hCG_30046;RP11-103J1 | Calcium-binding protein 39-like | 37.06 | 64.20 | n.d. | n.d. | 6.90 | 11.48 | n.d. | n.d. |
| 139 | 60S acidic ribosomal protein P1;RPLP1 protein;Acidic ribosomal p | RPLP1;RRP1 | 60S acidic ribosomal protein P | 35.96 | 62.47 | 95.52 | 115.83 | n.d. | n.d. | 42.88 | 37.76 |
| 140 | 60S ribosomal protein L35;Similar to 60S ribosomal protein L35 | RPL35;LOC154880;tcag7.829 | 60S ribosomal protein L35;Sim | 35.30 | 63.45 | n.d. | n.d. | n.d. | n.d. | n.d. | n.d. |
| 141 | 60S acidic ribosomal protein P0;60S ribosomal protein L10E;cDN | RPLP0 | 60S acidic ribosomal protein P | 33.13 | 57.91 | 118.71 | 130.15 | 11.82 | 20.05 | 56.47 | 50.51 |
| 142 | Ribosomal protein L36a;60S ribosomal protein L36a-like;cDNA, Fl | RP1-164F3.1-004;RPL36A;RPL3 | Protein;Ribosomal protein L36 | 31.28 | 40.12 | 62.52 | 46.30 | n.d. | n.d. | n.d. | n.d. |
| 143 | 40S ribosomal protein S25 | RPS25 | 40S ribosomal protein S25;14 | 29.08 | 50.50 | 63.06 | 63.90 | 8.09 | 10.42 | 15.87 | 13.25 |
| 144 | 60S ribosomal protein L22;EBER-associated protein;Epstein-Barr | RPL22;RPL22L2 | 60S ribosomal protein L22;11 | 28.94 | 34.49 | 81.36 | 86.55 | 7.53 | 10.71 | 33.42 | 28.27 |
| 145 | 60S ribosomal protein L24;60S ribosomal protein L30;Putative uni | RPL24;hCG_2023003 | 19 kDa protein;60S ribosomal | 28.67 | 50.06 | 27.58 | 31.32 | 8.22 | 13.10 | 18.80 | 15.75 |
| 146 | 60S ribosomal protein L31;cDNA, FLJ92036, highly similar to Hom | RPL31;hCG_27618 | 60S ribosomal protein L31;Put | 27.96 | 48.40 | 200.66 | 210.00 | n.d. | n.d. | 23.01 | 18.93 |
| 147 | Putative uncharacterized protein RPL23A;Ribosomal protein L23a | hCG_1988529;RPL23A | Ribosomal protein L23a, isofor | 25.48 | 44.52 | 25.36 | 22.91 | 3.79 | 6.43 | n.d. | n.d. |
| 148 | 60S ribosomal protein L12;Ribosomal protein L12 variant | RPL12 | Isoform 1 of 60S ribosomal pro | 24.84 | 29.55 | 104.01 | 109.16 | 7.02 | 7.04 | 13.07 | 10.37 |
| 149 | 40S ribosomal protein S19;cDNA, FLJ92047, Homo sapiens ribos | RPS19;hCG_1995572 | 40S ribosomal protein S19 | 23.90 | 41.69 | 80.53 | 83.64 | 4.81 | 5.02 | 22.44 | 17.81 |
| 150 | 60S ribosomal protein L14;CAG-ISL 7;cDNA FLJ76611, highly sim | RPL14 | Ribosomal protein L14 variant; | 23.53 | 29.62 | 54.79 | 50.02 | 6.77 | 6.90 | 12.70 | 10.34 |
| 151 | 60S ribosomal protein L18a;cDNA, FLJ92035, highly similar to Ho | RPL18A | 60S ribosomal protein L18a;21 | 22.96 | 30.28 | 85.18 | 84.93 | 6.74 | 8.82 | 4.06 | 3.22 |
| 152 | 60S ribosomal protein L11;CLL-associated antigen KW-12;Cell gr | RPL11;hCG_1739238;RP11-223J | Isoform 1 of 60S ribosomal pro | 22.88 | 39.87 | 60.89 | 57.67 | 13.90 | 23.48 | 20.24 | 17.65 |
| 153 | 60S ribosomal protein L3;HIV-1 TAR RNA-binding protein B;Ribos | OK/SW-cl.32;RPL3;hCG_201519 | 60S ribosomal protein L3;ribos | 22.20 | 38.72 | 20.54 | 21.36 | 3.18 | 4.26 | 2.76 | 2.22 |
| 154 | 40S ribosomal protein S12 | RPS12 | 40S ribosomal protein S12 | 22.10 | 38.65 | 41.85 | 42.76 | n.d. | n.d. | n.d. | n.d. |
| 155 | 60S ribosomal protein L18;Ribosomal protein L18 | RPL18 | 60S ribosomal protein L18;Rib | 21.56 | 21.46 | 21.45 | 25.62 | 7.56 | 12.79 | 19.08 | 15.15 |
| 156 | 60S ribosomal protein L6;Neoplasm-related protein C140;Tax-resp | RPL6;TXREB1 | 60S ribosomal protein L6;60S | 20.69 | 31.98 | 33.05 | 28.62 | 6.87 | 8.23 | 12.64 | 10.81 |
| 157 | 60S ribosomal protein L17;60S ribosomal protein L23;PD-1;cDNA | RPL17 | 60S ribosomal protein L17;21 | 20.67 | 36.12 | 34.17 | 34.91 | n.d. | n.d. | 7.92 | 6.67 |
| 158 | 60S ribosomal protein L27a;Ribosomal protein L27a | RPL27A;L27a | 60S ribosomal protein L27a | 19.75 | 16.67 | 68.60 | 72.04 | 7.48 | 7.92 | n.d. | n.d. |
| 159 | 60S ribosomal protein L7;Putative uncharacterized protein RPL7;S | RPL7;WUGSC:H_RG054D04.1 | Putative uncharacterized prote | 19.64 | 20.49 | 35.27 | 41.67 | 9.02 | 15.42 | 6.81 | 5.67 |
| 160 | 60S ribosomal protein L13;Breast basic conserved protein 1;Ribos | BBC1;OK/SW-cl.46;RPL13;hCG_ | 60S ribosomal protein L13;24 | 19.48 | 15.09 | 54.02 | 51.68 | 5.32 | 5.86 | 34.75 | 27.58 |
| 161 | 37 kDa laminin receptor precursor;37/67 kDa laminin receptor;40S | LAMBR;LAMR1;RPSA;LAMR1P1 | 33 kDa protein;40S ribosomal | 19.39 | 17.55 | 53.59 | 56.06 | 5.22 | 6.98 | 13.31 | 10.56 |
| 162 | 60S ribosomal protein L15;Ribosomal protein L15 | EC45;RPL15;TCBAP0781;hCG_1 | 60S ribosomal protein L15;21 | 19.33 | 20.59 | 11.30 | 11.38 | n.d. | n.d. | 12.79 | 10.15 |
| 163 | 60S ribosomal protein L38 | RPL38 | 60S ribosomal protein L38;8 kD | 18.95 | 33.08 | 113.46 | 81.46 | 10.20 | 17.03 | 14.20 | 9.64 |
| 164 | 60S ribosomal protein L8;cDNA FLJ53750, highly similar to 60S ri | RPL8 | 32 kDa protein;60S ribosomal | 18.45 | 17.93 | 48.56 | 58.62 | 6.76 | 8.95 | n.d. | n.d. |
| 165 | 60S ribosomal protein L21;cDNA, FLJ92056, Homo sapiens ribos | RPL21;hCG_2020044;RP11-428C | 60S ribosomal protein L21;Sim | 18.42 | 17.32 | 15.31 | 13.88 | n.d. | n.d. | n.d. | n.d. |
| 166 | Putative uncharacterized protein RPL26;60S ribosomal protein L2 | RPL26;RPL26L1;RPL26P1 | Putative uncharacterized prote | 18.38 | 17.54 | 51.12 | 46.98 | 5.95 | 6.01 | 8.74 | 6.99 |
| 167 | 60S ribosomal protein L10a;CSA-19;Neural precursor cell express | NEDD6;RPL10A;hCG_1787790 | 60S ribosomal protein L10a;Ri | 18.26 | 22.39 | 50.91 | 60.59 | 6.11 | 10.27 | 22.76 | 18.38 |
| 168 | B(2)GCN homolog;B4 integrin interactor;CAB;Eukaryotic translatio | EIF3A;EIF6;ITGB4BP;OK/SW-cl.2 | Eukaryotic translation initiation | 17.84 | 16.75 | 65.92 | 78.78 | 4.86 | 6.51 | 9.13 | 7.24 |
| 169 | 60S ribosomal protein L1;60S ribosomal protein L4;cDNA FLJ568 | RPL1;RPL4 | 60S ribosomal protein L4;cDNA | 17.67 | 19.34 | 38.82 | 33.87 | 8.71 | 14.83 | 26.20 | 22.06 |
| 170 | 60S acidic ribosomal protein P2;Renal carcinoma antigen NY-REN | D11S2243E;RPLP2;RPP2;hCG_1 | 60S acidic ribosomal protein P | 17.49 | 27.64 | 35.66 | 37.32 | 12.30 | 20.93 | 29.67 | 24.80 |
| 171 | Cell cycle protein p38-2G4 homolog;ErbB3-binding protein 1;Prolif | EBP1;PA2G4 | Proliferation-associated protein | 17.34 | 24.86 | 15.84 | 17.78 | 1.37 | 2.14 | 10.12 | 8.03 |
| 172 | 40S ribosomal protein S18;Ke-3;Ribosomal protein S18;Ribosoma | D6S218E;RPS18;DADB-159G18. | 40S ribosomal protein S18;18 | 16.58 | 15.69 | 59.38 | 68.78 | 6.01 | 5.76 | 19.30 | 16.68 |
| 173 | cDNA FLJ58953, highly similar to 40S ribosomal protein S20;40S | RPS20 | ribosomal protein S20 isoform | 16.33 | 18.85 | 58.55 | 67.01 | 5.40 | 7.16 | n.d. | n.d. |

| 2 | Protein Names | Gene Names | Protein Descriptions | Ratio H/L Stable Forward | Ratio H/L Normalized Stable Forward | Ratio L/H Stable Reverse | Ratio L/H Normalized Stable Reverse | Ratio H/L Transformed Forward | Ratio H/L Normalized Transformed Forward | Ratio L/H Transformed Reverse | Ratio L/H Normalized Transformed Reverse |
|---|---|---|---|---|---|---|---|---|---|---|---|
| 173 | cDNA FLJ58953, highly similar to 40S ribosomal protein S20;40S | RPS20 | ribosomal protein S20 isoform | 16.33 | 18.85 | 58.55 | 67.01 | 5.40 | 7.16 | n.d. | n.d. |
| 174 | 40S ribosomal protein S3;Ribosomal protein S3 variant;Ribosoma | OK/SW-cl.26;RPS3 | 40S ribosomal protein S3;Ribo | 16.25 | 16.55 | 40.68 | 36.84 | 5.69 | 6.68 | 17.20 | 14.45 |
| 175 | 40S ribosomal protein S3a;v-fos transformation effector protein;cD | FTE1;MFTL;RPS3A | 40S ribosomal protein S3a;30 | 16.21 | 24.87 | 12.02 | 9.10 | 4.98 | 6.71 | 10.57 | 8.39 |
| 176 | 60S ribosomal protein L9;cDNA, FLJ92535, Homo sapiens ribosor | OK/SW-cl.103;RPL9;RPL9P7;RPI | 60S ribosomal protein L9;19 kD | 16.17 | 27.93 | 35.03 | 35.60 | 5.96 | 10.12 | 30.20 | 25.66 |
| 177 | 60S ribosomal protein L17;60S ribosomal protein L23;Similar to rit | RPL23 | 60S ribosomal protein L23;15 k | 16.13 | 28.50 | 33.50 | 38.00 | 13.39 | 22.71 | 33.21 | 28.64 |
| 178 | 60S ribosomal protein L30 | RPL30 | Putative uncharacterized prote | 15.78 | 20.12 | 76.12 | 79.21 | 5.00 | 7.96 | 20.51 | 16.72 |
| 179 | 40S ribosomal protein S9;Ribosomal protein S9;Ribosomal protein | RPS9;hCG_2009111;XXbac-BCX | 40S ribosomal protein S9;Simil | 15.65 | 20.18 | 15.79 | 17.87 | 7.87 | 10.01 | 14.16 | 11.24 |
| 180 | Nucleolin;Protein C23;cDNA FLJ10452 fis, clone NT2RP1000986, | NCL;hCG_33980 | Nucleolin;cDNA FLJ45706 fis, | 15.31 | 23.20 | 48.00 | 54.78 | 4.90 | 7.71 | 21.24 | 18.45 |
| 181 | Carboxypeptidase, vitellogenic-like;Probable serine carboxypeptid | CPVL;PSEC0124;UNQ197/PRO2 | Probable serine carboxypeptid | 14.91 | 15.00 | 10.19 | 9.83 | n.d. | n.d. | n.d. | n.d. |
| 182 | 60S ribosomal protein L7a;PLA-X polypeptide;Surfeit locus protein | RPL7A;SURF3;SURF-3;hCG_203 | 60S ribosomal protein L7a;30 k | 14.78 | 22.01 | 49.77 | 44.78 | 6.83 | 9.06 | 20.13 | 15.48 |
| 183 | 40S ribosomal protein S15;RIG protein | RIG;RPS15 | 40S ribosomal protein S15 | 14.66 | 22.23 | n.d. | n.d. | n.d. | n.d. | n.d. | n.d. |
| 184 | Putative uncharacterized protein RPS27;Ribosomal protein S27;4 | RP11-422P24.3-002;RPS27;MPS | 9 kDa protein;Putative unchara | 14.50 | 25.66 | 16.81 | 19.58 | n.d. | n.d. | 6.29 | 5.39 |
| 185 | 40S ribosomal protein S6;Phosphoprotein NP33;cDNA FLJ78049, | OK/SW-cl.2;RPS6;hCG_1741512 | 40S ribosomal protein S6;Ribo | 14.29 | 18.23 | 53.89 | 53.32 | 5.35 | 7.31 | 12.55 | 9.98 |
| 186 | 40S ribosomal protein S14 | PRO2640;RPS14 | 40S ribosomal protein S14 | 14.27 | 13.57 | 50.12 | 52.36 | 4.64 | 4.61 | 50.77 | 40.30 |
| 187 | Cell proliferation-inducing gene 21 protein;Guanine nucleotide-bin | GNB2L1;HLC7;PIG21 | Guanine nucleotide-binding pro | 14.25 | 17.39 | 29.88 | 26.54 | 5.70 | 7.56 | 10.14 | 8.05 |
| 188 | 60S ribosomal protein L27 | RPL27 | 60S ribosomal protein L27;60S | 14.05 | 12.57 | 52.21 | 48.01 | 8.61 | 11.03 | 19.14 | 16.35 |
| 189 | 60S ribosomal protein L36;Ribosomal protein L36 | RPL36 | 60S ribosomal protein L36 | 13.90 | 14.29 | 14.80 | 13.40 | 2.39 | 2.43 | 7.94 | 6.30 |
| 190 | PAI1 RNA-binding protein 1;Plasminogen activator inhibitor 1 RNA | CGI-55;PAIRBP1;SERBP1;RP11- | Isoform 3 of Plasminogen activ | 13.57 | 23.67 | 26.63 | 20.55 | 4.65 | 6.14 | 46.73 | 36.50 |
| 191 | 40S ribosomal protein S13 | RPS13 | 40S ribosomal protein S13 | 13.21 | 14.56 | 10.25 | 11.80 | 6.68 | 6.58 | n.d. | n.d. |
| 192 | Coiled-coil domain-containing protein 124 | CCDC124 | Coiled-coil domain-containing | 13.05 | 19.16 | 23.24 | 18.97 | 8.13 | 10.19 | 11.16 | 8.94 |
| 193 | 40S ribosomal protein S4, X isoform;SCR10;Single copy abundan | CCG2;RPS4;RPS4X;SCAR;hCG_ | 40S ribosomal protein S4, X is | 13.02 | 20.60 | 18.70 | 18.80 | n.d. | n.d. | n.d. | n.d. |
| 194 | 40S ribosomal protein S16;cDNA FLJ56786, moderately similar to | RPS16 | 40S ribosomal protein S16;cDI | 12.94 | 22.63 | 92.41 | 96.66 | 6.99 | 7.08 | 22.91 | 17.90 |
| 195 | 40S ribosomal protein S5;40S ribosomal protein S5, N-terminally | RPS5 | 40S ribosomal protein S5 | 12.77 | 15.28 | 23.52 | 21.55 | 5.66 | 9.61 | 26.59 | 21.10 |
| 196 | 3-ketoacyl-CoA thiolase;Acetyl-CoA acyltransferase;Beta-ketothiol | HADHB;MSTP029 | Trifunctional enzyme subunit b | 12.57 | 18.91 | 21.29 | 21.17 | n.d. | n.d. | n.d. | n.d. |
| 197 | 60S ribosomal protein L37a;Putative uncharacterized protein RPL | RPL37A;hCG_16380 | 60S ribosomal protein L37a;Ri | 11.70 | 20.23 | 20.29 | 22.80 | n.d. | n.d. | n.d. | n.d. |
| 198 | GTP-binding protein HSR1;Guanine nucleotide-binding protein-like | GNL1;HSR1;DADB-87H23.2-002; | Isoform 1 of Guanine nucleotid | 11.04 | 17.77 | 10.76 | 9.50 | n.d. | n.d. | n.d. | n.d. |
| 199 | 40S ribosomal protein S24 | RPS24;hCG_22610;RP11-6P10.1 | ribosomal protein S24 isoform | 10.86 | 19.83 | n.d. | n.d. | n.d. | n.d. | n.d. | n.d. |
| 200 | 40S ribosomal protein S8;Ribosomal protein S8;Similar to ribosom | OK/SW-cl.83;RPS8;hCG_203185 | 40S ribosomal protein S8;Ribo | 10.49 | 12.38 | 23.62 | 21.43 | n.d. | n.d. | n.d. | n.d. |
| 201 | 78 kDa gastrin-binding protein;Long chain 3-hydroxyacyl-CoA deh | HADH;HADHA | Trifunctional enzyme subunit a | 9.64 | 12.81 | 19.04 | 17.23 | 3.62 | 3.99 | 12.46 | 9.89 |
| 202 | 60S ribosomal protein L5;cDNA, FLJ95579, Homo sapiens ribosor | MSTP030;RPL5;hCG_2028912 | 60S ribosomal protein L5 | 9.57 | 13.76 | 23.82 | 26.28 | 5.08 | 5.58 | n.d. | n.d. |
| 203 | 40S ribosomal protein S10;Ribosomal protein S10 variant;Ribosor | RPS10;RP11-375E1__A.4-005;RI | 40S ribosomal protein S10;Rib | 9.52 | 15.73 | 71.57 | 63.13 | 4.37 | 4.87 | 8.48 | 6.73 |
| 204 | Interleukin enhancer-binding factor 2;Nuclear factor of activated T | ILF2;NF45;PRO3063 | Interleukin enhancer-binding fa | 9.33 | 17.14 | 32.36 | 35.20 | 1.56 | 2.68 | 3.81 | 3.09 |
| 205 | PABPC4 protein;Poly(A) binding protein, cytoplasmic 4 (Inducible | PABPC4;hCG_2031827;RP11-69 | poly A binding protein, cytoplas | 8.57 | 14.59 | 7.38 | 7.18 | n.d. | n.d. | n.d. | n.d. |
| 206 | CCAAT-binding transcription factor I subunit A;DNA-binding protei | NSEP1;YB1;YBX1 | Protein;Nuclease-sensitive ele | 8.56 | 15.56 | 30.89 | 33.09 | n.d. | n.d. | n.d. | n.d. |
| 207 | Putative uncharacterized protein RPL32;60S ribosomal protein L3 | RPL32;PP9932;hCG_18290 | Putative uncharacterized prote | 8.10 | 14.71 | 45.59 | 53.89 | 5.81 | 5.76 | 7.44 | 6.34 |
| 208 | DnaJ homolog subfamily C member 9;DnaJ protein SB73;cDNA F | DNAJC9;hCG_2024613 | DnaJ homolog subfamily C me | 7.94 | 14.51 | 12.59 | 12.08 | n.d. | n.d. | n.d. | n.d. |

| | | | | | | | | | | | |
|---|---|---|---|---|---|---|---|---|---|---|---|
| 206 | CCAAT-binding transcription factor I subunit A;DNA-binding protei | NSEP1;YB1;YBX1 | Protein;Nuclease-sensitive ele | 8.56 | 15.56 | 30.89 | 33.09 | n.d. | n.d. | n.d. | n.d |
| 207 | Putative uncharacterized protein RPL32;60S ribosomal protein L3 | RPL32;PP9932;hCG_18290 | Putative uncharacterized prote | 8.10 | 14.71 | 45.59 | 53.89 | 5.81 | 5.76 | 7.44 | 6.34 |
| 208 | DnaJ homolog subfamily C member 9;DnaJ protein SB73;cDNA F | DNAJC9;hCG_2024613 | DnaJ homolog subfamily C me | 7.94 | 14.51 | 12.59 | 12.08 | n.d. | n.d. | n.d. | n.d |
| 209 | Caprin-1;Cell cycle-associated protein 1;Cytoplasmic activation- a | CAPRIN1;GPIAP1;GPIP137;M11 | Isoform 1 of Caprin-1;Isoform 2 | 7.89 | 14.30 | 12.83 | 13.52 | n.d. | n.d. | n.d. | n.d |
| 210 | Nucleolar phosphoprotein B23;Nucleolar protein NO38;Nucleophc | NPM;NPM1 | Isoform 1 of Nucleophosmin;Is | 7.47 | 13.89 | 27.00 | 25.75 | 5.03 | 7.02 | n.d. | n.d |
| 211 | 78 kDa glucose-regulated protein;Endoplasmic reticulum lumenal | GRP78;HSPA5 | HSPA5 protein | 7.47 | 13.16 | 18.02 | 16.86 | 4.26 | 5.88 | 16.12 | 13.31 |
| 212 | Coding region determinant-binding protein;IGF-II mRNA-binding p | CRDBP;IGF2BP1;VICKZ1;ZBP1 | Insulin-like growth factor 2 mR | 7.33 | 13.24 | 12.23 | 12.94 | n.d. | n.d. | n.d. | n.d |
| 213 | DEAH box protein 30;Putative ATP-dependent RNA helicase DHX | DDX30;DHX30;KIAA0890 | Isoform 2 of Putative ATP-depe | 7.06 | 13.34 | 15.50 | 12.96 | n.d. | n.d. | n.d. | n.d |
| 214 | Ribosomal protein S21;Ribosomal protein S21, isoform CRA_e;40 | hCG_41768;RP5-908M14.8-003;F | Ribosomal protein S21, isoform | 6.85 | 9.95 | 12.95 | 10.78 | n.d. | n.d. | n.d. | n.d |
| 215 | Polyadenylate-binding protein 1;cDNA FLJ57246, highly similar to | PAB1;PABP1;PABPC1;PABPC2 | Isoform 1 of Polyadenylate-bin | 6.68 | 11.11 | 21.22 | 21.57 | 4.85 | 5.70 | 6.60 | 5.24 |
| 216 | ATP-dependent RNA helicase A;DEAH box protein 9;Nuclear DNA | DDX9;DHX9;LKP;NDH2 | ATP-dependent RNA helicase A | 6.35 | 11.66 | 11.27 | 9.98 | n.d. | n.d. | 4.96 | 3.94 |
| 217 | Heat shock-related 70 kDa protein 2 | HSPA2 | Heat shock-related 70 kDa pro | 5.71 | 9.44 | 10.53 | 10.25 | n.d. | n.d. | n.d. | n.d |
| 218 | ATP-dependent DNA helicase VIII;GAP SH3 domain-binding prote | G3BP;G3BP1;DKFZp313K0921;D | Ras GTPase-activating protein | 5.68 | 10.75 | 6.56 | 6.46 | n.d. | n.d. | n.d. | n.d |
| 219 | Histone H1.3;Histone H1c;Histone H1.4;Histone H1b;Liver histone | H1F3;HIST1H1D;H1F4;HIST1H1 | Histone H1.3;Histone H1.4;His | 5.27 | 9.29 | 35.62 | 36.45 | 3.77 | 6.43 | n.d. | n.d |
| 220 | 40S ribosomal protein S11 | RPS11 | 40S ribosomal protein S11 | 5.24 | 5.15 | 61.65 | 53.63 | n.d. | n.d. | 27.02 | 21.44 |
| 221 | Ribosomal protein L10;60S ribosomal protein L10;Laminin recept | RPL10;XX-FW83563B9.1-011;DX | Ribosomal protein L10 (Fragm | 5.13 | 9.04 | 3.69 | 3.71 | n.d. | n.d. | 9.76 | 8.08 |
| 222 | cDNA FLJ56474, highly similar to Histone deacetylase 6;HDAC6 p | HDAC6;JM21;KIAA0901;hCG_19 | cDNA FLJ56474, highly similar | 5.07 | 5.58 | 10.45 | 9.42 | 1.19 | 1.24 | n.d. | n.d |
| 223 | 75 kDa glucose-regulated protein;Heat shock 70 kDa protein 9;Mc | GRP75;HSPA9;HSPA9B | Stress-70 protein, mitochondri | 4.97 | 7.64 | 10.94 | 10.92 | 3.57 | 4.24 | 10.85 | 8.86 |
| 224 | cDNA FLJ36192 fis, clone TESTI2027450, highly similar to Eukary | hCG_1784554;EIF3F;EIF3S5 | HCG1784554, isoform CRA_a; | 4.95 | 9.72 | 10.90 | 11.54 | n.d. | n.d. | n.d. | n.d |
| 225 | Histone H2A.x;Histone H2A type 1-A;Histone H2A/r;Histone H2A t | H2AFX;H2AX;H2AFR;HIST1H2A | Histone H2A.x;Histone H2A typ | 4.74 | 6.36 | n.d. | n.d. | n.d. | n.d. | n.d. | n.d |
| 226 | Zinc finger protein 622;Zinc finger-like protein 9 | ZNF622;ZPR9 | Zinc finger protein 622 | 4.71 | 7.03 | 26.60 | 30.14 | n.d. | n.d. | n.d. | n.d |
| 227 | 40S ribosomal protein S26;Ribosomal protein S26;Ribosomal prot | RPS26;RP11-151A6.3-001;hCG_ | 40S ribosomal protein S26;Rib | 4.47 | 7.90 | 19.63 | 21.47 | n.d. | n.d. | 21.37 | 17.39 |
| 228 | Double-stranded RNA-binding protein Staufen homolog 1;cDNA F | STAU;STAU1;RP3-470L14.2-007; | Isoform Long of Double-strand | 4.38 | 8.79 | 5.74 | 5.65 | n.d. | n.d. | n.d. | n.d |
| 229 | La autoantigen;La ribonucleoprotein;Lupus La protein;Sjoegren sy | SSB;hCG_2005701 | Lupus La protein;SS-B/La prot | 4.31 | 8.14 | 8.70 | 7.30 | n.d. | n.d. | n.d. | n.d |
| 230 | Chronic renal failure gene protein;GTP-binding protein NGB;Nucle | CRFG;GTPBP4;NOG1;RP11-38M | Nucleolar GTP-binding protein | 4.15 | 7.78 | n.d. | n.d. | n.d. | n.d. | n.d. | n.d |
| 231 | 60S ribosomal protein L19;Ribosomal protein L19 | RPL19 | 60S ribosomal protein L19;23 k | 3.91 | 4.71 | 29.08 | 28.60 | n.d. | n.d. | n.d. | n.d |
| 232 | Eukaryotic translation initiation factor 3 subunit M;Fetal lung protei | EIF3M;GA17;HFLB5;PCID1;PNAS | Eukaryotic translation initiation | 3.77 | 7.17 | 7.45 | 7.45 | n.d. | n.d. | n.d. | n.d |
| 233 | p180/ribosome receptor;180 kDa ribosome receptor homolog;ES/ | RRBP1;KIAA1398;RP11-462D18. | p180/ribosome receptor;Isoforr | 3.76 | 7.23 | n.d. | n.d. | n.d. | n.d. | n.d. | n.d |
| 234 | Elongation factor 2;cDNA FLJ60696, highly similar to Elongation fa | EEF2;EF2 | Elongation factor 2;cDNA FLJ5 | 3.72 | 6.45 | 4.98 | 4.63 | n.d. | n.d. | n.d. | n.d |
| 235 | 40S ribosomal protein S17;Putative uncharacterized protein ENSF | RPS17 | 40S ribosomal protein S17;16 k | 3.57 | 6.31 | 15.58 | 14.20 | n.d. | n.d. | n.d. | n.d |
| 236 | Double-stranded RNA-binding protein 76;Interleukin enhancer-bin | DRBF;ILF3;MPHOSPH4;NF90 | interleukin enhancer binding fa | 3.49 | 6.74 | 4.77 | 5.04 | n.d. | n.d. | n.d. | n.d |
| 237 | ATP-dependent RNA helicase DDX1;DEAD box protein 1;DEAD b | DDX1;hCG_15914 | ATP-dependent RNA helicase D | 3.30 | 6.16 | 8.94 | 9.52 | n.d. | n.d. | n.d. | n.d |
| 238 | Neoplastic transformation inhibitor protein;Nuclear antigen H731-li | H731;PDCD4;RP11-348N5.4-004 | Programmed cell death protein | 3.28 | 4.78 | n.d. | n.d. | n.d. | n.d. | n.d. | n.d |
| 239 | Heterogeneous nuclear ribonucleoproteins C1/C2;cDNA FLJ7515 | HNRNPC;HNRPC;HNRNPCL1;HI | Isoform C2 of Heterogeneous r | 3.23 | 6.04 | 6.73 | 5.10 | n.d. | n.d. | n.d. | n.d |
| 240 | | | 17 kDa protein | 3.11 | 5.75 | n.d. | n.d. | n.d. | n.d. | n.d. | n.d |
| 241 | Histone H1x | H1FX | Histone H1x | 3.08 | 5.36 | 6.65 | 6.38 | n.d. | n.d. | n.d. | n.d |

| | | | | | | | | | | | |
|---|---|---|---|---|---|---|---|---|---|---|---|
| 243 | DEAD box protein 21;Gu-alpha;Nucleolar RNA helicase 2;Nucleol | DDX21;OK/SW-cl.65 | Isoform 1 of Nucleolar RNA he | 2.96 | 5.54 | n.d. | n.d. | n.d. | n.d. | n.d. | n. |
| 244 | eIF-3 p48;Eukaryotic translation initiation factor 3 subunit 6;Eukar | EIF3E;EIF3S6;INT6;hCG_200879 | Eukaryotic translation initiation | 2.91 | 5.23 | n.d. | n.d. | n.d. | n.d. | n.d. | n. |
| 245 | Ribosome maturation protein SBDS;Shwachman-Bodian-Diamon | CGI-97;SBDS | Ribosome maturation protein S | 2.46 | 4.63 | n.d. | n.d. | n.d. | n.d. | n.d. | n. |
| 246 | 40S ribosomal protein S2;40S ribosomal protein S4;Protein LLRe | RPS2;RPS4;LOC392781;tcag7.9 | 40S ribosomal protein S2;31 k | 2.34 | 4.16 | 25.26 | 29.88 | 4.07 | 6.97 | 3.85 | 3.1 |
| 247 | Deoxyuridine 5'-triphosphate nucleotidohydrolase, mitochondrial;d | DUT | Isoform 1 of Deoxyuridine 5'-tri | 2.33 | 4.40 | 6.29 | 5.97 | n.d. | n.d. | n.d. | n. |
| 248 | La ribonucleoprotein domain family member 1;La-related protein 1 | KIAA0731;LARP;LARP1 | Isoform 1 of La-related protein | 2.30 | 4.20 | 4.28 | 4.56 | n.d. | n.d. | n.d. | n. |
| 249 | ATP-binding cassette 50;ATP-binding cassette sub-family F memb | ABC50;ABCF1;DADB-129D20.7-( | Isoform 1 of ATP-binding casse | 2.16 | 3.96 | n.d. | n.d. | n.d. | n.d. | n.d. | n. |
| 250 | CCT-theta;Renal carcinoma antigen NY-REN-15;T-complex protei | C21orf112;CCT8;CCTQ;KIAA000 | T-complex protein 1 subunit the | 2.10 | 4.09 | 2.95 | 2.76 | n.d. | n.d. | n.d. | n. |
| 251 | CCT-beta;T-complex protein 1 subunit beta;cDNA FLJ75037, high | 99D8.1;CCT2;CCTB;hCG_24460 | T-complex protein 1 subunit be | 2.08 | 3.92 | n.d. | n.d. | n.d. | n.d. | n.d. | n. |
| 252 | CCT-gamma;hTRiC5;T-complex protein 1 subunit gamma;cDNA F | CCT3;CCTG;TRIC5;RP11-443G1 | T-complex protein 1 subunit ga | 2.01 | 3.84 | 4.02 | 3.39 | n.d. | n.d. | n.d. | n. |
| 253 | ATP-dependent RNA helicase p54;DEAD box protein 6;Oncogene | DDX6;HLR2;RCK | Probable ATP-dependent RNA | 1.96 | 3.79 | 3.35 | 2.88 | n.d. | n.d. | n.d. | n. |
| 254 | Acute morphine dependence-related protein 2;CCT-zeta-1;HTR3; | CCT6;CCT6A;CCTZ | T-complex protein 1 subunit ze | 1.91 | 3.59 | 4.17 | 4.40 | n.d. | n.d. | n.d. | n. |
| 255 | CCT-delta;Stimulator of TAR RNA-binding;T-complex protein 1 sul | CCT4;CCTD;SRB | T-complex protein 1 subunit de | 1.90 | 3.56 | 2.43 | 2.26 | n.d. | n.d. | n.d. | n. |
| 256 | Eukaryotic translation initiation factor 3, subunit E interacting prote | AL022311.1-001;EIF3EIP;EIF3L;E | Eukaryotic translation initiation | 1.87 | 3.51 | n.d. | n.d. | n.d. | n.d. | n.d. | n. |
| 257 | ATP-dependent RNA helicase DDX3X;DEAD box protein 3, X-chro | DBX;DDX3;DDX3X;hCG_19318;F | ATP-dependent RNA helicase | 1.75 | 3.30 | n.d. | n.d. | n.d. | n.d. | n.d. | n. |
| 258 | Heterogeneous nuclear ribonucleoprotein K;Transformation up-re | HNRNPK;HNRPK;hCG_1985922; | Isoform 2 of Heterogeneous nu | 1.71 | 3.20 | 3.96 | 4.08 | n.d. | n.d. | n.d. | n. |
| 259 | [Acyl-carrier-protein] S-acetyltransferase;[Acyl-carrier-protein] S-m | FAS;FASN | Fatty acid synthase | 1.71 | 3.16 | 3.46 | 3.36 | n.d. | n.d. | n.d. | n. |
| 260 | Medium tumor antigen-associated 61 kDa protein;PP2A subunit A | PPP2R1A;hCG_19686 | Serine/threonine-protein phosp | 1.67 | 3.20 | 5.39 | 5.62 | n.d. | n.d. | n.d. | n. |
| 261 | Phenylalanine--tRNA ligase beta chain;Phenylalanyl-tRNA synthet | FARSB;FARSLB;FRSB;HSPC173 | Phenylalanyl-tRNA synthetase | 1.46 | 2.74 | 4.34 | 4.57 | n.d. | n.d. | n.d. | n. |
| 262 | NAP-1-related protein;Nucleosome assembly protein 1-like 1;cDN | NAP1L1;NRP;hCG_2015037 | Nucleosome assembly protein | 1.42 | 2.70 | 2.33 | 2.47 | n.d. | n.d. | n.d. | n. |
| 263 | Adapter protein CMS;Cas ligand with multiple SH3 domains;CD2- | CD2AP | CD2-associated protein | 1.28 | 2.39 | n.d. | n.d. | n.d. | n.d. | n.d. | n. |
| 264 | SDHA protein | | SDHA protein | 1.23 | 2.39 | 4.66 | 4.07 | n.d. | n.d. | n.d. | n. |
| 265 | 14-3-3 protein epsilon;cDNA, FLJ79100, highly similar to 14-3-3 p | YWHAE | 14-3-3 protein epsilon;22 kDa | 1.22 | 2.35 | 2.47 | 2.35 | n.d. | n.d. | n.d. | n. |
| 266 | La ribonucleoprotein domain family member 4B;La ribonucleoprob | KIAA0217;LARP4B;LARP5;hCG_ | La-related protein 4B;Putative | 1.22 | 1.81 | n.d. | n.d. | n.d. | n.d. | n.d. | n. |
| 267 | Heat shock 70 kDa protein 4-like protein;Heat shock 70kDa protei | hCG_37382;HSPA4L;APG1;OSP | Heat shock 70kDa protein 4-lik | 1.18 | 2.06 | 2.67 | 2.47 | n.d. | n.d. | n.d. | n. |
| 268 | UPF0027 protein C22orf28;cDNA FLJ58027;cDNA FLJ57752;cDN | C22orf28;HSPC117 | UPF0027 protein C22orf28;cD | 1.15 | 2.06 | n.d. | n.d. | n.d. | n.d. | n.d. | n. |
| 269 | Programmed cell death protein 2-like | PDCD2L | Programmed cell death protein | 1.11 | 2.13 | 6.84 | 5.18 | n.d. | n.d. | n.d. | n. |
| 270 | 17-beta-hydroxysteroid dehydrogenase 10;3-hydroxy-2-methylbut | ERAB;HADH2;HSD17B10;MRPP | Isoform 1 of 3-hydroxyacyl-Co | 1.06 | 1.95 | 2.99 | 2.65 | n.d. | n.d. | n.d. | n. |
| 271 | Replication protein C;Serine/threonine-protein phosphatase 2A ca | PPP2CA;hCG_16586;PPP2CB | Serine/threonine-protein phosp | 1.04 | 2.00 | 2.88 | 2.50 | n.d. | n.d. | n.d. | n. |
| 272 | CapZ alpha-2;F-actin-capping protein subunit alpha-2;Capping pro | CAPZA2;hCG_37884;tcag7.31 | F-actin-capping protein subunit | 1.03 | 1.49 | 2.79 | 2.45 | n.d. | n.d. | n.d. | n. |
| 273 | Apoptosis-linked gene 2 protein;Probable calcium-binding protein | ALG2;PDCD6;hCG_1985580 | Programmed cell death protein | 1.01 | 1.94 | 0.90 | 0.85 | n.d. | n.d. | n.d. | n. |
| 274 | Heat shock 70 kDa protein 4;Heat shock 70-related protein APG-2 | APG2;HSPA4;HS24/p52;HS24/P5 | Heat shock 70 kDa protein 4 | 0.99 | 1.75 | 2.12 | 2.19 | 0.94 | 1.19 | 3.03 | 2.4 |
| 275 | U2 small nuclear ribonucleoprotein A';Small nuclear ribonucleopro | SNRPA1 | U2 small nuclear ribonucleopro | 0.98 | 1.79 | 1.58 | 1.36 | n.d. | n.d. | n.d. | n. |
| 276 | ATP synthase subunit beta, mitochondrial;ATP synthase subunit b | ATP5B;ATPMB;ATPSB | ATP synthase subunit beta, mi | 0.94 | 1.76 | n.d. | n.d. | n.d. | n.d. | n.d. | n. |
| 277 | Heat shock 70 kDa protein 8;Heat shock cognate 71 kDa protein;( | HSC70;HSP73;HSPA10;HSPA8 | Isoform 1 of Heat shock cogna | 0.86 | 1.49 | 1.60 | 1.65 | 0.79 | 1.16 | 1.73 | 1.4 |
| 278 | Actin, cytoplasmic 2;Actin, cytoplasmic 2, N-terminally processed; | ACTB;ACTG;ACTG1 | Actin, cytoplasmic 2;cDNA FLJ | 0.85 | 1.47 | 2.53 | 2.33 | 4.38 | 6.96 | 4.29 | 3.5 |

| | Protein Names | Gene Names | Protein Descriptions | Sequence Coverage [%] | Mol. Weight [kDa] | Sequence Length | Number of identified peptides: 1-5 / 6-10 / 11-20 / 21-40 / 41-- | | | | | | | | | | | | | | | | Experiment FLAG Ccdc124 | Experiment Ccdc124-FLAG | Experiment FLAG-EV |
|---|---|---|---|---|---|---|---|---|---|---|---|---|---|---|---|---|---|---|---|---|---|---|---|---|---|
| | | | | | | | Band 1 | Band 2 | Band 3 | Band 4 | Band 5 | Band 6 | Band 7 | Band 8 | Band 9 | Band 10 | Band 11 | Band 12 | Band 13 | Band 14 | | | | | |
| 3 | Coiled-coil domain-containing protein 1: | CCDC124 | Coiled-coil domain-containing | 65 | 25.8 | 223 | 170 | 79 | 164 | 50 | 10 | 9 | 5 | 5 | 9 | 5 | 7 | 8 | 6 | 5 | | | | 187 | 319 | 26 |
| 4 | Heat shock 70 kDa protein 1/2;Heat sho | HSPA1;HSPA1A;HSPA1B;DAAP- | Heat shock 70 kDa protein 1; | 40.4 | 70.1 | 641 | 1 | | 2 | 5 | 12 | 146 | 59 | 104 | 51 | 12 | 47 | 26 | 8 | 14 | | | | 166 | 232 | 91 |
| 5 | 250/210 kDa paraneoplastic pemphigus | DSP;DSP variant protein | Isoform DPI of Desmoplakin; | 25.5 | 331.8 | 2871 | 1 | | 12 | 21 | 59 | 105 | 68 | 43 | 82 | 81 | 47 | 23 | 19 | 55 | | | | 146 | 243 | 227 |
| 6 | Heat shock 70 kDa protein 8;Heat shoc | HSC70;HSP73;HSPA10;HSPA8 | Isoform 1 of Heat shock cogn | 40.1 | 70.9 | 646 | 2 | 1 | 1 | 3 | 2 | 35 | 10 | 25 | 28 | 17 | 35 | 9 | 2 | 3 | | | | 65 | 77 | 31 |
| 7 | 78 kDa glucose-regulated protein;Endo | GRP78;HSPA5 | HSPA5 protein | 44.4 | 72.4 | 655 | | | | 2 | 5 | 9 | 5 | 11 | 81 | 33 | 49 | 21 | 2 | 4 | | | | 64 | 113 | 45 |
| 8 | Catenin gamma;Desmoplakin III;Desmc | CTNNG;DP3;JUP | Junction plakoglobin | 32.9 | 81.7 | 745 | | | 6 | 10 | 20 | 24 | 21 | 22 | 26 | 25 | 18 | 9 | 6 | 12 | | | | 52 | 75 | 72 |
| 9 | 75 kDa glucose-regulated protein;Heat | GRP75;HSPA9;HSPA9B | Stress-70 protein, mitochondr | 39.8 | 73.7 | 679 | | | | 1 | | 1 | | 2 | 50 | 21 | 48 | 13 | | 2 | | | | 52 | 65 | 21 |
| 10 | Heat shock 70 kDa protein 6;Heat shoc | HSP70B';HSPA6;HSP70B;HSPA7 | Heat shock 70 kDa protein 6; | 15.7 | 71.0 | 643 | 1 | 1 | 1 | 3 | 3 | 32 | 5 | 17 | 21 | 4 | 22 | 8 | 1 | 2 | | | | 42 | 66 | 13 |
| 11 | Elongation factor 2;cDNA FLJ60696, hig | EEF2;EF2 | Elongation factor 2;cDNA FLJ | 27.6 | 95.3 | 858 | | | 1 | 6 | 7 | 6 | 3 | 5 | 7 | 3 | 4 | 65 | 28 | 24 | | | | 33 | 85 | 41 |
| 12 | 100 kDa DNA-pairing protein;DNA-bind | PSF;SFPQ | Isoform Long of Splicing factc | 19.2 | 76.1 | 707 | | | | | | | | 1 | 1 | 2 | 4 | 35 | 28 | 25 | | | | 30 | 36 | 30 |
| 13 | 70 kDa lamin;Lamin-A/C;Renal carcinor | LMN1;LMNA;RP11-54H19.1-004; | Isoform A of Lamin-A/C;Proge | 21.2 | 74.1 | 664 | | | | 3 | 3 | 10 | 2 | 5 | 7 | 12 | 10 | 1 | 1 | 11 | | | | 26 | 21 | 18 |
| 14 | Cadherin family member 4;Desmoglein- | CDHF4;DSG1 | Desmoglein-1 | 22.9 | 113.7 | 1049 | | | 2 | 6 | 11 | 21 | 23 | 10 | 20 | 12 | 9 | 4 | 5 | 5 | | | | 24 | 53 | 51 |
| 15 | 72 kDa ICln-binding protein;Histone-arg | HRMT1L5;IBP72;JBP1;PRMT5;S | Protein arginine N-methyltran | 22.9 | 72.7 | 637 | | | | 6 | 6 | 27 | 23 | 16 | 13 | 11 | 6 | 6 | 6 | | | | | 22 | 52 | 46 |
| 16 | Histone H4 | H4/A;H4/B;H4/C;H4/D;H4/E;H4/G | Histone H4 | 50.5 | 11.4 | 103 | | | | | 1 | 6 | | 12 | 2 | | 7 | | | 3 | | | | 22 | 8 | 1 |
| 17 | Keratinocyte proline-rich protein | C1orf45;KPRP | Keratinocyte proline-rich prote | 16.4 | 64.1 | 579 | 1 | | 4 | 3 | 7 | 8 | 5 | 7 | 12 | 6 | 2 | 2 | 3 | 9 | | | | 19 | 29 | 21 |
| 18 | Nucleolin;Protein C23;cDNA FLJ10452 | NCL;hCG_33980 | Nucleolin;cDNA FLJ45706 fis | 16.3 | 76.6 | 710 | | | | | | 2 | 1 | 1 | 5 | 3 | 4 | 17 | 12 | 13 | | | | 18 | 24 | 16 |
| 19 | Caspase-14;Caspase-14 subunit p10;C | CASP14;hCG_38589 | Caspase-14 | 26.5 | 27.7 | 242 | | | 3 | 3 | 13 | 13 | 9 | 1 | 3 | 2 | 3 | 3 | 3 | 13 | | | | 17 | 25 | 27 |
| 20 | 60S ribosomal protein L5;cDNA, FLJ95 | MSTP030;RPL5;hCG_2028912 | 60S ribosomal protein L5 | 41.4 | 34.4 | 297 | 16 | 26 | 4 | 6 | | | | | | | | | | | | | | 16 | 36 | |
| 21 | | | suprabasin isoform 1 precurs | 38.5 | 60.5 | 590 | | | | | 6 | 27 | 12 | 5 | 8 | 4 | 3 | 1 | | 7 | | | | 15 | 36 | 22 |
| 22 | 15S Mg(2+)-ATPase p97 subunit;Transi | VCP;DKFZp434K0126 | Transitional endoplasmic retic | 20.3 | 89.3 | 806 | | | | | 1 | 4 | | | | | 1 | 14 | 14 | 12 | | | | 13 | 18 | 15 |
| 23 | Premature ovarian failure protein 1B;Pr | POF1B;hCG_18178 | Isoform 1 of Protein POF1B;Is | 19.2 | 68.7 | 595 | | | 1 | 2 | 6 | 10 | 7 | 1 | 1 | 2 | 2 | | 1 | 10 | | | | 13 | 14 | 16 |
| 24 | 60S ribosomal protein L6;Neoplasm-rel | RPL6;TXREB1 | 60S ribosomal protein L6;60S | 34.6 | 32.9 | 289 | | 1 | 4 | 39 | 10 | 6 | 1 | 3 | 5 | 4 | 6 | 5 | 3 | 3 | | | | 12 | 60 | 18 |
| 25 | Polyadenylate-binding protein 1;cDNA F | PAB1;PABP1;PABPC1;PABPC2;F | Isoform 1 of Polyadenylate-bi | 28.9 | 70.7 | 636 | | | | | | | | 5 | 25 | 8 | 6 | 2 | | 1 | | | | 12 | 27 | 8 |
| 26 | Cadherin family member 1;Desmocollin | CDHF1;DSC1;hCG_25474 | Isoform 1A of Desmocollin-1;I | 10 | 100.0 | 894 | 1 | | | 2 | 5 | 8 | 7 | 3 | 11 | 6 | 5 | 2 | 2 | 3 | | | | 12 | 23 | 20 |
| 27 | Band 6 protein;Plakophilin-1;cDNA FLJ | PKP1 | Isoform 2 of Plakophilin-1;Isol | 11.8 | 82.9 | 747 | | | 1 | 3 | 6 | 3 | 3 | 7 | 9 | 8 | 3 | 1 | 2 | 2 | | | | 12 | 17 | 19 |
| 28 | 14-3-3 protein sigma;Epithelial cell mar | HME1;SFN | Isoform 1 of 14-3-3 protein sig | 35.1 | 27.8 | 248 | | | 1 | 2 | 2 | 12 | | 3 | | 1 | 1 | | | 8 | | | | 12 | 15 | 3 |
| 29 | ATP-dependent RNA helicase DDX3X;D | DBX;DDX3;DDX3X;hCG_19318;F | ATP-dependent RNA helicase | 15.3 | 73.2 | 662 | | | | | | | | | 11 | 9 | 9 | | | 3 | | | | 12 | 11 | 9 |
| 30 | DEAD box protein 21;Gu-alpha;Nucleol | DDX21;OK/SW-cl.65 | Isoform 1 of Nucleolar RNA h | 23.1 | 87.3 | 783 | | | | | | | | | | | | 36 | 18 | 11 | | | | 11 | 38 | 18 |
| 31 | Glyceraldehyde-3-phosphate dehydrog | GAPD;CDABP0047;GAPDH;OK/S | Glyceraldehyde 3-phosphate | 19.7 | 36.0 | 335 | | | | 9 | 10 | 5 | 4 | 3 | 4 | 3 | 2 | 1 | 3 | 6 | | | | 11 | 19 | 20 |
| 32 | GTP-binding protein HSR1;Guanine nu | GNL1;HSR1 | Isoform 1 of Guanine nucleoti | 14.2 | 68.7 | 607 | | | | | | 1 | 1 | 1 | 14 | 1 | 10 | | | | | | | 11 | 15 | 2 |
| 33 | Elongation factor 1-alpha 1;Elongation f | EEF1A;EEF1A1;EF1A;LENG7;EE | Elongation factor 1-alpha 1;P | 10.8 | 50.1 | 462 | 1 | 1 | | 3 | 5 | 6 | 3 | 5 | 5 | 5 | 3 | | 1 | 2 | | | | 11 | 15 | 14 |
| 34 | Chronic renal failure gene protein;GTP- | CRFG;GTPBP4;NOG1 | Nucleolar GTP-binding protei | 31.9 | 74.0 | 634 | | | | | | | | 1 | 28 | 12 | 9 | 8 | 1 | | | | | 10 | 36 | 13 |
| 35 | Galectin-7;HKL-14;p53-induced gene 1 | LGALS7;LGALS7B;PIG1 | Galectin-7 | 29.4 | 15.1 | 136 | | | 1 | 3 | 4 | 7 | 4 | 1 | 3 | 4 | 3 | | 1 | 6 | | | | 10 | 14 | 13 |

| 2 | Protein Names | Gene Names | Protein Descriptions | Sequence Coverage [%] | Mol. Weight [kDa] | Sequence Length | Band 1 | Band 2 | Band 3 | Band 4 | Band 5 | Band 6 | Band 7 | Band 8 | Band 9 | Band 10 | Band 11 | Band 12 | Band 13 | Band 14 | Experiment FLAG Cdc42 | Experiment Cdc42-FLAG | Experiment FLAG-EV |
|---|---|---|---|---|---|---|---|---|---|---|---|---|---|---|---|---|---|---|---|---|---|---|---|
| 36 | Epidermal-type fatty acid-binding protei | FABP5 | Fatty acid-binding protein, epi | 55.6 | 15.2 | 135 | | | 2 | 3 | 6 | 6 | 6 | | 1 | 4 | 2 | | 4 | 8 | 10 | 12 | 20 |
| 37 | Dermcidin isoform 2;DCD-1;Dermcidin;I | DCD;AIDD;DSEP;hCG_1820620; | Dermcidin isoform 2;Dermcidi | 20.7 | 12.4 | 121 | 2 | 1 | 2 | 2 | 2 | 2 | 3 | 1 | 4 | 2 | 2 | 2 | 2 | 4 | 9 | 13 | 9 |
| 38 | 28 kDa heat shock protein;Estrogen-reg | HSP27;HSP28;HSPB1 | Heat shock protein beta-1;cD | 21.5 | 22.8 | 205 | | | | 1 | 5 | 6 | 3 | 3 | 2 | 2 | 1 | | | 5 | 9 | 9 | 10 |
| 39 | Histone H1.3;Histone H1c;Histone H1.4 | H1F3;HIST1H1D;H1F4;HIST1H1I | Histone H1.3;Histone H1.4;Hi | 14.9 | 22.4 | 221 | 5 | 4 | 1 | 1 | 1 | | | 4 | | | | | | | 9 | 6 | 1 |
| 40 | Heat shock 84 kDa;Heat shock protein I | HSP90AB1;HSP90B;HSPC2;HSF | Heat shock protein HSP 90-b | 11.5 | 83.3 | 724 | 1 | | | | 2 | 4 | 1 | 1 | 1 | 1 | 1 | 1 | 2 | 6 | 9 | 6 | 6 |
| 41 | Annexin A2;Annexin II;Annexin-2;Calpa | ANX2;ANX2L4;ANXA2;CAL1H;LF | Isoform 2 of Annexin A2;Isofo | 24.9 | 40.4 | 357 | | | 1 | 8 | 11 | 11 | 4 | 2 | 6 | 3 | 3 | 2 | 2 | 3 | 8 | 28 | 20 |
| 42 | Cell proliferation-inducing gene 21 prote | GNB2L1;HLC7;PIG21 | Guanine nucleotide-binding p | 43.8 | 35.1 | 317 | 8 | 16 | 4 | 1 | 1 | 3 | | | | | | | | | 8 | 24 | 1 |
| 43 | Calmodulin-like protein 5;Calmodulin-lik | CALML5;CLSP | Calmodulin-like protein 5 | 39 | 15.9 | 146 | | 1 | 1 | 3 | 3 | 8 | 5 | 1 | 3 | 3 | 3 | 3 | 2 | 4 | 8 | 19 | 13 |
| 44 | Putative uncharacterized protein;Putativ | IGK@;IGKC | Putative uncharacterized prot | 13.8 | 26.2 | 239 | 3 | 2 | 8 | 3 | 2 | 1 | 1 | 1 | 2 | 2 | 2 | 2 | 1 | 2 | 8 | 18 | 6 |
| 45 | Protein-glutamine gamma-glutamyltrans | TGM3 | Protein-glutamine gamma-glu | 11.4 | 76.6 | 693 | | | | 1 | 5 | 7 | 9 | 2 | 7 | 4 | 2 | 1 | | 4 | 8 | 16 | 18 |
| 46 | L-lactate dehydrogenase;Cell proliferati | LDHA;PIG19;hCG_96677 | lactate dehydrogenase A isof | 14.7 | 39.8 | 361 | 4 | 3 | 2 | 2 | 4 | 5 | 1 | | 1 | 1 | 1 | 1 | 1 | 3 | 8 | 14 | 7 |
| 47 | Skin-specific protein 32 | C1orf68;XP32 | Skin-specific protein 32 | 20.4 | 26.2 | 250 | 1 | | 2 | 1 | 3 | 1 | 1 | 4 | 4 | 1 | 2 | 1 | 2 | 1 | 8 | 9 | 7 |
| 48 | Gasdermin-1;Gasdermin-A | FKSG9;GSDM;GSDM1;GSDMA | Gasdermin-A | 7.6 | 49.4 | 445 | 1 | | | 2 | 5 | 4 | 3 | 3 | 3 | 2 | 2 | | 2 | 2 | 8 | 9 | 12 |
| 49 | Alpha-actinin-4;F-actin cross-linking pro | ACTN4 | Alpha-actinin-4;Actinin alpha4 | 10 | 104.9 | 911 | | | | 1 | 2 | 10 | 2 | 1 | 1 | | 1 | 1 | 1 | 5 | 7 | 13 | 5 |
| 50 | ADA2-like protein beta;Transcriptional a | ADA2B;TADA2B | Isoform 1 of Transcriptional a | 1.7 | 48.5 | 420 | 2 | | 2 | 2 | 2 | 2 | 2 | 2 | 2 | 2 | 2 | 1 | 1 | 1 | 7 | 9 | 7 |
| 51 | Leupin;Peptidase inhibitor 11;Serpin B4 | PI11;SCCA2;SERPINB4;SCCA;S | Serpin B4;Isoform 1 of Serpin | 9.2 | 44.9 | 390 | | | | 1 | 4 | 4 | 3 | | 1 | 2 | 2 | 3 | 1 | 5 | 7 | 9 | 10 |
| 52 | Cytokeratin-6B;Keratin, type II cytoskele | K6B;KRT6B;KRTL1 | Keratin, type II cytoskeletal 6 | 47.2 | 60.1 | 564 | 1 | | 2 | 2 | 2 | | | | 2 | 2 | 4 | 2 | 2 | 2 | 7 | 8 | 6 |
| 53 | NF-kappa-B-repressing factor;Protein IT | ITBA4;NKRF;NRF | NF-kappa-B-repressing factor | 11 | 77.7 | 690 | | | | | | | | | | | 1 | 7 | 4 | 6 | 7 | 7 | 4 |
| 54 | Heat shock protein 75 kDa, mitochondri | HSP75;TRAP1 | Heat shock protein 75 kDa, m | 6.2 | 80.1 | 704 | | | | 1 | 1 | 1 | 1 | 1 | 4 | 4 | 5 | 1 | 1 | 1 | 7 | 7 | 7 |
| 55 | Cytochrome c-releasing factor 21;Gamr | C7orf24;CRF21;GGCT | Isoform 1 of Gamma-glutamy | 22.9 | 21.0 | 188 | | | | | 5 | 6 | 4 | 1 | 1 | 1 | 1 | | | 5 | 7 | 7 | 10 |
| 56 | cDNA FLJ38698 fis, clone KIDNE2002C | DAAP-21F2.8-002;DADB-333F21 | cDNA FLJ54408, highly simila | 38.4 | 63.9 | 586 | | | | | 1 | 2 | 2 | 4 | 2 | 1 | 2 | 1 | 1 | 1 | 7 | 5 | 5 |
| 57 | PABPC4 protein;Poly(A) binding protein | PABPC4;hCG_2031827;RP11-69 | poly A binding protein, cytopla | 22.9 | 72.4 | 660 | | | | | | | | 2 | 13 | 6 | 4 | 1 | | | 6 | 14 | 6 |
| 58 | 14-3-3 protein zeta/delta;Protein kinase | YWHAZ | 14-3-3 protein zeta/delta | 31.4 | 27.7 | 245 | | 1 | 6 | 1 | 2 | 5 | 1 | 1 | | 2 | | | 1 | 5 | 6 | 13 | 6 |
| 59 | Arginase-1;Liver-type arginase;Type I a | ARG1 | Isoform 2 of Arginase-1;Isofor | 11.8 | 35.7 | 330 | 1 | | 1 | 1 | 5 | 4 | 5 | 1 | 4 | 5 | 2 | 2 | 2 | 2 | 6 | 12 | 17 |
| 60 | cDNA FLJ75516, highly similar to Xenop | UBC;DKFZp434K0435;hCG_199 | ubiquitin C;39 kDa protein;UB | 32.8 | 77.0 | 685 | 2 | 1 | 1 | 2 | 2 | 3 | 2 | 2 | 3 | 2 | 1 | 1 | 1 | 1 | 6 | 11 | 7 |
| 61 | 450 kDa epidermal antigen;Epiplakin;Pl | EPIPL;EPPK1;DKFZp434G0719 | epiplakin 1 | 4.3 | 555.6 | 5090 | | | | 2 | 1 | 7 | 2 | 1 | 1 | 1 | 1 | | | 4 | 6 | 10 | 4 |
| 62 | Cathepsin D;Cathepsin D heavy chain;( | CPSD;CTSD | Cathepsin D;Putative uncharz | 13.6 | 44.6 | 412 | | | | 2 | 6 | 5 | 5 | 1 | 3 | 3 | | | | 5 | 6 | 10 | 14 |
| 63 | 2-phospho-D-glycerate hydro-lyase;Alpl | ENO1;ENO1L1;MBPB1;MPB1 | Isoform alpha-enolase of Alph | 16.8 | 47.2 | 434 | | | | 1 | 5 | 8 | 4 | 1 | | 4 | | 1 | 1 | 5 | 6 | 10 | 14 |
| 64 | 60S ribosomal protein L7a;PLA-X polyp | RPL7A;SURF3;SURF-3;hCG_203 | 60S ribosomal protein L7a;30 | 20.7 | 30.0 | 266 | 6 | 1 | 4 | 3 | 1 | 1 | | | | | | | | | 6 | 9 | 1 |
| 65 | Metastasis-associated 1-like 1;Metastas | MTA1L1;MTA2;PID;DKFZp686F2 | Metastasis-associated protein | 7 | 75.0 | 668 | | | | 1 | 2 | 2 | 2 | 2 | 4 | 4 | 3 | 2 | 1 | 1 | 6 | 9 | 9 |
| 66 | Pentatricopeptide repeat-containing pro | PTCD3;TRG15 | Isoform 1 of Pentatricopeptide | 13.8 | 78.5 | 689 | | | | | | | | | 9 | 11 | 6 | | | | 6 | 9 | 11 |
| 67 | Glycogen phosphorylase, liver form;Phc | PYGL | Glycogen phosphorylase, live | 7.4 | 97.1 | 847 | | | | | | | | | | | | 8 | 8 | 6 | 6 | 8 | 8 |
| 68 | Cytosolic thyroid hormone-binding prote | OIP3;PK2;PK3;PKM;PKM2 | 66 kDa protein;Isoform M1 of | 12.4 | 65.9 | 605 | 1 | | 1 | 2 | 5 | 5 | 5 | | | | | | | 5 | 6 | 8 | 10 |

# APPENDIX II

RASGEF1B LC-MS/MS DATA

| 1 | Protein Names | Gene Names | Protein Descripti | Ratio H/L Forwa | Ratio H/L Normalized For 1 | Ratio L/H Rever | Ratio L/H Normalized Rev 1 | Ratio H/L Forwa | Ratio H/L Normalized For 2 | Ratio L/H Rever | Ratio L/H Normalized Rev 2 |
|---|---|---|---|---|---|---|---|---|---|---|---|
| 361 | Adenine nucleotide translocator 2;ADP,ATP carrier protein 2;ADP,ATP carrier pro | ANT2;SLC25A5 | ADP/ATP translo | 18.43 | 18.72 | 11.61 | 6.23 | 16.15 | 11.63 | 34.18 | 19.68 |
| 362 | Citrate transport protein;Solute carrier family 25 member 1;Tricarboxylate carrier | SLC20A3;SLC25A1;hCG_17246 | Tricarboxylate tra | 16.97 | 15.08 | 17.32 | 9.30 | 16.99 | 105.53 | 37.64 | 21.08 |
| 363 | Tubulin beta-2 chain;Tubulin beta-2C chain;Class IVb beta tubulin;Tubulin, beta 2 | TUBB2C;TUBB4;TUBB5 | Tubulin beta-2C c | 11.92 | 10.59 | 12.87 | 7.12 | 12.49 | 6.89 | 27.05 | 18.74 |
| 364 | Phosphate carrier protein, mitochondrial;Phosphate transport protein;Solute carri | OK/SW-cl.48;PHC;SLC25A3 | Isoform A of Phos | 11.73 | 10.42 | 21.02 | 11.64 | 15.53 | 8.23 | 57.81 | 36.51 |
| 365 | Mitochondrial 2-oxoglutarate/malate carrier protein;Solute carrier family 25 memb | SLC20A4;SLC25A11;hCG_32694 | Mitochondrial 2-o | 9.85 | 8.75 | n.d. | n.d. | 15.52 | 36.48 | 15.15 | 10.79 |
| 366 | cDNA FLJ50617, highly similar to Tubulin beta-7 chain;cDNA, FLJ79164, highly s | DAAP-285E11.4-003;DADB-118P | Tubulin, beta;cDN | 9.68 | 9.95 | 5.03 | 2.74 | 13.62 | 5.54 | 15.00 | 9.47 |
| 367 | GPI gamma-4;Ras-GEF domain-containing family member 1B;cDNA FLJ76660, I | GPIG4;RASGEF1B | Isoform 1 of Ras-I | 9.38 | 8.34 | 3.12 | 2.13 | 9.99 | 6.96 | 24.46 | 18.70 |
| 368 | U2 small nuclear ribonucleoprotein A';Small nuclear ribonucleoprotein polypeptid | SNRPA1 | U2 small nuclear | 8.94 | 8.70 | n.d. | n.d. | 8.17 | 4.69 | 15.93 | 11.34 |
| 369 | Elongation factor 1-alpha 1;Elongation factor Tu;Eukaryotic elongation factor 1 A- | EEF1A;EEF1A1;EF1A;LENG7;EE | Elongation factor | 7.79 | 9.27 | 8.81 | 4.88 | 7.91 | 48.14 | 12.19 | 6.83 |
| 370 | ATPase family AAA domain-containing protein 3A;cDNA FLJ31537 fis, clone NT2 | ATAD3A;RP5-832C2.1-002;ATAD | Isoform 2 of ATPa | 7.73 | 6.02 | n.d. | n.d. | 8.29 | 5.34 | 16.26 | 11.58 |
| 371 | Mitochondrial import inner membrane translocase subunit TIM50;Translocase of | PRO1512;TIM50;TIMM50 | Isoform 2 of Mitoc | 7.19 | 6.39 | n.d. | n.d. | 9.46 | 11.27 | 12.11 | 8.62 |
| 372 | Calcium pump 2;Calcium-transporting ATPase sarcoplasmic reticulum type, slow | ATP2A2;ATP2B | Isoform SERCA2I | 7.14 | 7.34 | n.d. | n.d. | 8.44 | 27.90 | 10.63 | 7.57 |
| 373 | HCV F-transactivated protein 2;Up-regulated during skeletal muscle growth prote | HCVFTP2;PD04912;USMG5 | Up-regulated duri | 7.02 | 7.21 | n.d. | n.d. | 8.90 | 18.26 | n.d. | n.d. |
| 374 | 160 kDa phosphotyrosine protein;Insulin receptor substrate 4;Phosphoprotein of | IRS4 | Insulin receptor s | 6.89 | 6.12 | 4.08 | 2.26 | 7.78 | 5.11 | 11.82 | 8.41 |
| 375 | Synaptic glycoprotein SC2;Trans-2,3-enoyl-CoA reductase;cDNA FLJ10554 fis, c | GPSN2;SC2;TECR | Isoform 1 of Trans | 5.94 | 5.28 | n.d. | n.d. | 16.29 | 8.68 | 12.05 | 9.93 |
| 376 | ATP synthase subunit alpha, mitochondrial;ATP synthase subunit alpha;cDNA FL | ATP5A;ATP5A1;ATP5AL2;ATPM | ATP synthase sub | 5.93 | 5.27 | n.d. | n.d. | 8.52 | 4.75 | 8.88 | 4.97 |
| 377 | 26S protease regulatory subunit 7;26S proteasome AAA-ATPase subunit RPT1;F | MSS1;PSMC2 | 26S protease regu | 5.88 | 6.99 | n.d. | n.d. | 6.88 | 29.40 | n.d. | n.d. |
| 378 | DNA-dependent protein kinase catalytic subunit;DNPK1;p460;cDNA FLJ57825, h | HYRC;HYRC1;PRKDC | Isoform 1 of DNA- | 5.81 | 5.46 | 4.95 | 2.70 | 7.71 | 13.31 | 11.86 | 8.45 |
| 379 | Heat shock 84 kDa;Heat shock protein HSP 90-beta;cDNA FLJ77842;cDNA FLJ5 | HSP90AB1;HSP90B;HSPC2;HSF | Heat shock protei | 4.30 | 3.82 | n.d. | n.d. | 5.26 | 39.72 | 5.65 | 3.16 |
| 380 | 60S ribosomal protein L27 | RPL27 | 60S ribosomal pro | 3.99 | 4.11 | n.d. | n.d. | n.d. | n.d. | n.d. | n.d. |
| 381 | 26S protease regulatory subunit 8;26S proteasome AAA-ATPase subunit RPT6;p | PSMC5;SUG1;hCG_41818 | 26S protease regu | 3.83 | 4.56 | n.d. | n.d. | n.d. | n.d. | n.d. | n.d. |
| 382 | Putative uncharacterized protein SSR1;cDNA, FLJ93042, highly similar to Homo | SSR1;PSEC0262;TRAPA | Putative uncharac | 3.66 | 4.35 | n.d. | n.d. | 10.92 | 82.40 | n.d. | n.d. |
| 383 | Complex I-MLRQ;NADH dehydrogenase [ubiquinone] 1 alpha subcomplex subur | NDUFA4 | NADH dehydroge | 3.35 | 3.99 | n.d. | n.d. | n.d. | n.d. | n.d. | n.d. |
| 384 | EP70-P-iso;SM-11044-binding protein;Transmembrane 9 superfamily member 3; | SMBP;TM9SF3;UNQ245/PRO282 | Transmembrane 9 | 3.23 | 3.32 | n.d. | n.d. | 12.14 | 6.08 | n.d. | n.d. |
| 385 | 60S ribosomal protein L18;Ribosomal protein L18 | RPL18 | 60S ribosomal pro | 2.91 | 3.00 | n.d. | n.d. | n.d. | n.d. | n.d. | n.d. |
| 386 | cDNA FLJ75516, highly similar to Xenopus tropicalis ubiquitin C, mRNA;Ubiquitin | UBC;DKFZp434K0435;hCG_1998 | ubiquitin C;39 kD | 2.88 | 2.77 | 7.60 | 4.08 | n.d. | n.d. | 7.59 | 4.25 |
| 387 | Putative uncharacterized protein ENSP00000346598;37 kDa laminin receptor pre | LAMBR;LAMR1;RPSA;LAMR1P1 | 33 kDa protein;Pu | 2.42 | 2.49 | n.d. | n.d. | 2.09 | 1.24 | n.d. | n.d. |
| 388 | Elongation factor 2;cDNA FLJ60696, highly similar to Elongation factor 2;cDNA F | EEF2;EF2 | Elongation factor | 2.05 | 2.11 | n.d. | n.d. | n.d. | n.d. | n.d. | n.d. |
| 389 | Heat shock 70 kDa protein 8;Heat shock cognate 71 kDa protein;cDNA FLJ7784( | HSC70;HSP73;HSPA10;HSPA8 | Isoform 1 of Heat | 2.05 | 2.02 | 4.27 | 2.37 | 6.11 | 9.72 | 5.79 | 3.39 |
| 390 | 60S ribosomal protein L13;Breast basic conserved protein 1;Ribosomal protein L | BBC1;OK/SW-cl.46;RPL13;hCG_ | 60S ribosomal pro | 1.99 | 1.77 | n.d. | n.d. | 2.44 | 1.44 | n.d. | n.d. |
| 391 | 60S acidic ribosomal protein P0;60S ribosomal protein L10E;cDNA FLJ75549, hi | RPLP0 | 60S acidic ribosor | 1.98 | 2.35 | n.d. | n.d. | 3.29 | 24.80 | n.d. | n.d. |
| 392 | 40S ribosomal protein S18;Ke-3;Ribosomal protein S18;Ribosomal protein S18, I | D6S218E;RPS18;DADB-159G18. | 40S ribosomal pro | 1.82 | 1.61 | n.d. | n.d. | n.d. | n.d. | n.d. | n.d. |

| 1 | Protein Names | Gene Names | Protein Descripti | Ratio H/L Forwa | Ratio H/L Normalized For 1 | Ratio L/H Rever | Ratio L/H Normalized Rev 1 | Ratio H/L Forwa | Ratio H/L Normalized For 2 | Ratio L/H Rever | Ratio L/H Normalized Rev 2 |
|---|---|---|---|---|---|---|---|---|---|---|---|
| 392 | 40S ribosomal protein S18;Ke-3;Ribosomal protein S18;Ribosomal protein S18, | D6S218E;RPS18;DADB-159G18. | 40S ribosomal pr | 1.82 | 1.61 | n.d. | n.d. | n.d. | n.d. | n.d. | n.d. |
| 393 | Cell cycle progression restoration gene 3 protein;DnaJ homolog subfamily A mem | CPR3;DNAJA2;HIRIP4 | DnaJ homolog su | 1.81 | 2.15 | n.d. | n.d. | 4.44 | 33.49 | n.d. | n.d. |
| 394 | RPS16 protein;cDNA FLJ56786, moderately similar to 40S ribosomal protein S16 | RPS16 | RPS16 protein;cD | 1.78 | 1.83 | n.d. | n.d. | 2.96 | 6.46 | n.d. | n.d. |
| 395 | [Acyl-carrier-protein] S-acetyltransferase;[Acyl-carrier-protein] S-malonyltransfera | FAS;FASN | Fatty acid synthas | 1.55 | 1.59 | n.d. | n.d. | 1.48 | 1.53 | n.d. | n.d. |
| 396 | Mitochondrial aspartate-glutamate carrier protein;Solute carrier family 25, membe | hCG_40633;SLC25A13;ARALAR2 | solute carrier fam | 1.50 | 1.23 | n.d. | n.d. | 7.29 | 8.05 | n.d. | n.d. |
| 397 | 60S ribosomal protein L12;Ribosomal protein L12 variant | RPL12 | Isoform 1 of 60S r | 1.49 | 1.53 | n.d. | n.d. | n.d. | n.d. | n.d. | n.d. |
| 398 | 60S ribosomal protein L7a;PLA-X polypeptide;Surfeit locus protein 3;cDNA FLJ7 | RPL7A;SURF3;SURF-3;hCG_203 | 60S ribosomal pr | 1.46 | 1.74 | n.d. | n.d. | n.d. | n.d. | n.d. | n.d. |
| 399 | 75 kDa glucose-regulated protein;Heat shock 70 kDa protein 9;Mortalin;Peptide-b | GRP75;HSPA9;HSPA9B | Stress-70 protein, | 1.44 | 1.42 | n.d. | n.d. | 2.29 | 4.40 | n.d. | n.d. |
| 400 | Cell proliferation-inducing gene 4/52 protein;Mitochondrial inner membrane prote | HMP;IMMT;PIG4;PIG52 | Isoform 1 of Mitoc | 1.40 | 1.44 | n.d. | n.d. | 5.27 | 39.75 | 17.88 | 11.36 |
| 401 | Glycosylation-inhibiting factor;L-dopachrome isomerase;L-dopachrome tautomera | GLIF;MIF;MMIF | Macrophage migr | 1.35 | 1.20 | 1.69 | 0.94 | 0.65 | 0.45 | 1.42 | 1.01 |
| 402 | Heat shock 70 kDa protein 1/2;Heat shock 70 kDa protein 1A/1B;cDNA FLJ7512 | HSPA1;HSPA1A;HSPA1B;DAAP- | Heat shock 70 kD | 1.30 | 1.35 | 2.07 | 1.15 | 4.30 | 5.43 | 4.02 | 2.54 |
| 403 | 78 kDa glucose-regulated protein;Endoplasmic reticulum lumenal Ca(2+)-binding | GRP78;HSPA5 | HSPA5 protein | 1.21 | 1.91 | n.d. | n.d. | 2.97 | 2.99 | 3.59 | 2.26 |
| 404 | Natural killer cell-enhancing factor A;Peroxiredoxin-1;Proliferation-associated ger | PAGA;PAGB;PRDX1;TDPX2 | Peroxiredoxin-1;1 | 1.13 | 1.34 | 5.37 | 2.93 | 1.58 | 11.94 | 3.59 | 2.01 |
| 405 | Histone H4 | H4/A;H4/B;H4/C;H4/D;H4/E;H4/G | Histone H4 | 0.48 | 0.43 | 4.57 | 2.53 | n.d. | n.d. | n.d. | n.d. |
| 406 | Histone H1.3;Histone H1c;Histone H1.4;Histone H1b;Liver histone H1e;Histone 1 | H1F3;HIST1H1D;H1F4;HIST1H1E | Histone H1.3;Hist | 0.45 | 0.54 | n.d. | n.d. | n.d. | n.d. | 3.15 | 1.76 |
| 407 | 60S acidic ribosomal protein P2;Renal carcinoma antigen NY-REN-44;cDNA, FL | D11S2243E;RPLP2;RPP2;hCG_1 | 60S acidic ribosor | 0.44 | 0.61 | n.d. | n.d. | 2.91 | 21.95 | n.d. | n.d. |
| 408 | 60 kDa chaperonin;60 kDa heat shock protein, mitochondrial;Chaperonin 60;Hea | HSP60;HSPD1 | 60 kDa heat shoc | 0.28 | 0.29 | n.d. | n.d. | 6.84 | 51.61 | 3.98 | 2.51 |
| 409 | Coiled-coil domain-containing protein 124 | CCDC124 | Coiled-coil domai | 0.18 | 0.37 | 3.25 | 1.32 | 0.25 | 0.29 | 3.41 | 2.19 |
| 410 | 250/210 kDa paraneoplastic pemphigus antigen;Desmoplakin;cDNA FLJ53584, H | DSP;DSP variant protein | Isoform DPI of De | 0.05 | 0.05 | 29.78 | 15.99 | n.d. | n.d. | 11.78 | 8.39 |
| 411 | Cytokeratin-6B;Keratin, type II cytoskeletal 6B;Keratin-6B;Type-II keratin Kb10 | K6B;KRT6B;KRTL1 | Keratin, type II cy | 0.03 | 0.03 | 41.07 | 27.13 | 0.07 | 0.16 | 25.64 | 17.58 |
| 412 | Beta-xin;Cardiomyopathy-associated protein 3;Xeplin;Xin actin-binding repeat-co | CMYA3;XIRP2 | xin actin-binding r | 0.01 | 0.01 | 13.02 | 6.99 | n.d. | n.d. | 49.54 | 27.75 |

# APPENDIX III

## PHOSPHO-PEPTIDE ANALYSIS OF CCDC124

| | 16 | 17 | 18 | 19 | 20 | 23 | 24 | 25 | 26 | 30 | 31 | 32 | 33 |
|---|---|---|---|---|---|---|---|---|---|---|---|---|---|
| 1 | | | | Previously identified proteins are shown in this color | | | | | | | | | |
| 2 | Protein Descriptions | Ratio H/L Stable Forward | Ratio H/L Normalized Stable Forward | Ratio L/H Stable Reverse | Ratio L/H Normalized Stable Reverse | Ratio H/L Trans. Forward | Ratio H/L Normalized Trans. Forward | Ratio L/H Trans. Reverse | Ratio L/H Normalized Trans. Reverse | Uniprot | Sequence Motifs | Phospho Motifs | Proteins |
| 189 | 60S ribosomal protein L36 | 13.90 | 14.29 | 14.80 | 13.40 | 2.39 | 2.43 | 7.94 | 6.30 | Q9Y3U8;Q9BYF3 | | | 1 |
| 190 | Isoform 3 of Plasminogen activator inhibito | 13.57 | 23.67 | 26.63 | 20.55 | 4.65 | 6.14 | 46.73 | 36.50 | Q8NC51-3; | Ken box | | 4 |
| 191 | 40S ribosomal protein S13 | 13.21 | 14.56 | 10.25 | 11.80 | 6.68 | 6.58 | n.d. | n.d. | P62277 | | | 1 |
| 192 | Coiled-coil domain-containing protein 124 | 13.05 | 19.16 | 23.24 | 18.97 | 8.13 | 10.19 | 11.16 | 8.94 | Q96CT7 | | PLK1 | 1 |
| 193 | 40S ribosomal protein S4, X isoform;40S r | 13.02 | 20.60 | 18.70 | 18.80 | n.d. | n.d. | n.d. | n.d. | P62701;B2R491;Q | | HV1;Q96IR1 | 4 |
| 194 | 40S ribosomal protein S16;cDNA FLJ5678 | 12.94 | 22.63 | 92.41 | 96.66 | 6.99 | 7.08 | 22.91 | 17.90 | P62249;B4DP32;Q6IPX4 | | | 3 |
| 195 | 40S ribosomal protein S5 | 12.77 | 15.28 | 23.52 | 21.55 | 5.66 | 9.61 | 26.59 | 21.10 | P46782;Q53G25 | | | 1 |
| 196 | Trifunctional enzyme subunit beta, mitochc | 12.57 | 18.91 | 21.29 | 21.17 | n.d. | n.d. | n.d. | n.d. | P55084;B4DDC9;B4DY96;B4E2W | | | 6 |
| 197 | 60S ribosomal protein L37a;Ribosomal pro | 11.70 | 20.23 | 20.29 | 22.80 | n.d. | n.d. | n.d. | n.d. | P61513;C9J4Z3;Q6P4F4 | | | 4 |

# APPENDIX IV

PUBLICATIONS

**Coiled-coil domain containing protein 124 is a novel centrosome and midbody protein that interacts with the Ras-guanine nucleotide exchange factor 1B and is involved in cytokinesis.**

**Short title: Ccdc124 is involved in cytokinesis**

Pelin Telkoparan[1], Serap Erkek[1§], Elif Yaman[1], Hani Alotaibi[1], Defne Bayık[1], and Uygar H. Tazebay[1,2*]

[1]Department of Molecular Biology and Genetics, Faculty of Science, Bilkent University, Bilkent 06800 Ankara, Turkey.

[2]Department of Molecular Biology and Genetics, Gebze Institute of Technology, Gebze 41400 Kocaeli, Turkey.

***Address correspondence to Uygar H. Tazebay**

Department of Molecular Biology and Genetics,

Gebze Institute of Technology, Gebze 41400 Kocaeli, Turkey

Tel: +90-262-6052522

Fax: +90-262-6052505

Email: tazebay@gyte.edu.tr

[§]Present address: Friedrich Miescher Institute for Biomedical Research, Maulbeerstrasse 66, P.O. Box 2543, 4002 Basel, Switzerland.

**Abstract**

Cytokinetic abscission is the cellular process leading to physical separation of two postmitotic sister cells by severing the intercellular bridge. The most noticeable structural component of the intercellular bridge is a transient organelle termed as midbody, localized at a central region marking the site of abscission. Despite its major role in completion of cytokinesis, our understanding of spatiotemporal regulation of midbody assembly is limited. Here, we report the first characterization of coiled-coil domain-containing protein-124 (Ccdc124), a eukaryotic protein conserved from fungi-to-man, which we identified as a novel centrosomal and midbody protein. Knockdown of Ccdc124 in human HeLa cells leads to accumulation of enlarged and multinucleated cells; however, centrosome maturation was not affected. We found that Ccdc124 interacts with the Ras-guanine nucleotide exchange factor 1B (RasGEF1B), establishing a functional link between cytokinesis and activation of localized Rap2 signaling at the midbody. Our data indicate that Ccdc124 is a novel factor operating both for proper progression of late cytokinetic stages in eukaryotes, and for establishment of Rap2 signaling dependent cellular functions proximal to the abscission site.

**Keywords:** Ccdc124 / Centrosome / Midbody / Cytokinesis / RasGEF1B / Rap2 signaling

## Introduction

Centrosomes are microtubule-organizing centers (MTOCs) that play a key role in determining the geometry of microtubule arrays in animal cells. They control and influence cell shape, polarity, motility, spindle formation, as well as chromosome segregation and cell division [1]. Each centrosome comprises a pair of centrioles that are surrounded by an amorphous and dynamic proteinaceous matrix referred to as the pericentriolar material (PCM), which is considered to be the site where microtubule nucleation initiates [2]. Associated with the multifunctional role of this primary MTOC in the cell, the total amount of PCM organized around centrioles (corresponding to centrosome size) and the composition of PCM vary considerably throughout the cell cycle [2]-[4].

Microtubule-nucleating capacities of centrosomes are increased by recruitment of key PCM proteins such as γ-tubulin and gamma-tubulin complex proteins (GCP) forming the γ-tubulin ring complexes (γ-tuRC), which orchestrate cell division-related MTOC activities leading to the formation of spindle asters and correct positioning of the two spindle poles. These cellular activities are required for genetically stable cells as it facilitates proper segregation of the duplicated chromosomes, ultimately resulting in diploid daughter cells [4]-[7].

Recently, a number of efforts aimed to establish both the precise composition of PCM at different stages of cell cycle, and the nature of dynamic networks of molecular interactions that lead to spatiotemporal regulation of PCM assembly. Jakobsen *et al*. [8] have obtained an extensive coverage of human centrosome proteome by using a mass

spectrometry-based proteomics approach combined with an antibody based subcellular screen of candidate proteins [8]. In this study, the authors identified 126 known and 40 novel candidate centrosome proteins, of which 22 were validated as novel centrosome components, and 5 turned out to associate preferentially either with mother or daughter centrioles. These analyses also indicated that the majority (60%) of centrosomal proteins contain coiled-coil domain (CCD) type oligomerization motifs [8], [9], as their predominant structural features, which seem to be important for proper centrosome assembly.

Previous studies have indicated the presence of microtubule nucleation-related proteins that are shared between the centrosome and the midbody, which is the central region of the intercellular bridge that is rich in anti-parallel microtubule bundles emanating from the central spindle [10]. These include for instance γ-tubulin, as the midbody is also a secondary MTOC associated with the contractile ring forming at the site of cleavage furrow ingression [1], [11]. Again, another protein with a CCD motif, Cep55, is centrosomal in interphase cells but dissociates from the centrosome during entry into mitosis [12]-[14]. Precisely at cytokinetic abscission Cep55 is localized to the midbody where it plays an essential role in recruitment of the endosomal sorting complex required for transport (ESCRT) components such as Alix and tumor susceptibility gene 101 (tsg101, an ESCRT-I member), as well as endobrevin (v-SNARE) [15]-[17]. This is then followed by the recruitment of ESCRT-III components via interactions with Alix and Tsg101, resulting in the translocation of CHMP4B to the midbody [18]. According to current models, polymerization of CHMP4B subunits forms series of cortical rings extending away from the midbody, either as continuous helical contractile filaments

[18], [19] or to give rise to a second immediately distal CHMP4B pool [20]. This then deforms the intercellular bridge membrane neck into a narrow constriction, and subsequently induces the abscission event.

Recent studies have also identified a number of factors other than Cep55 that similarly localize to centrosomes early in mitosis but then move to the midbody at cytokinesis where they execute essential functions in fission of the daughter cells [10], [16]. Among those proteins, Polo-like-kinase-1 (Plk1) plays critical roles in centrosome maturation and microtubule organization [7], [21], [22]. At the midzone Plk1 also phosphorylates Cep55 on Ser-436, thereby modulating its interaction with Mklp1, a kinesin-like component of centralspindlin. This provides a temporal control of abscission, by inhibiting functions of Cep55 in the midbody at stages earlier than late-anaphase [23].

During our earlier studies on specificities of Ras-guanine nucleotide exchange factor-1 (RasGEF1) family members [24], we obtained preliminary evidences regarding possible interactions between RasGEF1B and a previously uncharacterized protein known as the coiled-coil domain-containing protein 124 (Ccdc124). Here, we report the first characterization of this conserved human protein, Ccdc124, and show that it is a novel component of the centrosome during interphase and at the G2/M transition. During cell division, Ccdc124 relocates to the midbody at telophase and acts as an essential molecular component in cytokinesis. Ccdc124 interacts with RasGEF1B at the midbody where this GEF could activate the small G protein Rap2 [24] at pre-abscission stages. Our data propose a mechanistic link between cytokinesis and Rap signaling that is mainly linked to the formation of cell-cell junctions, regulation of cell-extracellular matrix adhesion, and establishment of cell polarity [25], i.e., molecular processes that

must follow cell division while tissues are formed.

## Results

### *Molecular characterization of Ccdc124*

The coiled-coil domain (CCD) is a motif that is found in most centrosome proteins [8]. Intrigued by its strict conservation in all eukaryotic genomes from fungi-to-man, we hypothesized that *CCDC124*, a human gene of unknown function encoding a putative CCD containing novel protein, could in fact be involved in centrosome biology. We carried-out a comparative sequence analysis on *CCDC124* which encodes a cDNA that is transcribed from chromosome 19p13.11, consisting of five exons, of which exon 1 is non-coding. BLAST analysis indicated that the protein encoded from this genetic locus shares, for instance, 70% identity/89.1% similarity with its orthologue NP_956859 in the vertebrate model *Danio rerio* (zebrafish), or 50.4% identity/72.6% similarity with Y73E7A.1 in the invertebrate *Caenorhabditis elegans*. *CCDC124* has also orthologues in lower eukaryotes such as the filamentous fungus *Aspergillus nidulans* (AN0879.2; 35.1% identity/58.2% similarity), or the fission yeast *Schizosaccharomyces pombe* (SPBC29A10.12; 33% identity/57.8% similarity), while it is not found in the budding yeast *Saccharomyces cerevisiae*.

Northern blot analysis have revealed that *CCDC124* is ubiquitously expressed in all tested human tissues, and relatively high levels of expression were detected in the brain, placenta, liver, spleen, and prostate (Fig. 1A). In these analyses, a transcript of ~1061 nucleotides was detectable in tested organs, in agreement with the predicted size of *CCDC124* mRNA in the NCBI databases (http://genome.ucsc.edu), except in the

placenta where we observed a second shorter mRNA species indicative of a transcript variant (Fig. 1A). *CCDC124* cDNA would encode a protein of 223 amino acids with two putative coiled-coil domains between residues 18-82 in the N-terminal half of the protein as detected by the ELM (http://elm.eu.org) and COILS (www.ch.embnet.org/software/COILS_form.html) bioinformatics analysis platforms (Fig. S1). No significant homology to other proteins or domains were found.

We generated a rabbit polyclonal antibody recognizing the peptide corresponding to the N-terminal 24 amino acids of Ccdc124 and characterized its specificity towards Ccdc124 in immunoblots including peptide competition assays (Fig. 1B). We identified Ccdc124 as a ~32 kDa protein in immunoblots using different protein lysates obtained from Ccdc124 expression vector (CMV-Ccdc124) transfected or untransfected human HEK-293 cells (Figs. 1B-C). Furthermore, when the Ccdc124 ORF was tagged with an N-terminal flag-epitope in plasmid vectors, the antibody also detected the flag-Ccdc124 at the expected size (~35 kDa; Fig. 1C). When these bands were gel extracted and subjected to peptide analyses by mass-spectrometry, the band of ~35 kDa were identified as the full-size flag-Ccdc124, suggesting that without the flag epitope *CCDC124* would encode a protein of ~32 kDa (Pelin Telkoparan, Lars A.T. Meijer, and Uygar H. Tazebay, unpublished results). Surprisingly, anti-flag antibodies failed to detect a similar robust band of ~35 kDa when the epitope was inserted at the C-terminus, but instead they revealed a band of ~32 kDa in lysates of cells transfected with vectors expressing Ccdc124-flag (Fig. 1C). This indicated possible proteolytic cleavage of the protein at its N-terminus when flag-epitope is inserted to the C-terminus of Ccdc124. We have not further characterized the proteolytic cleavage of this protein at the molecular level, and

we used the more stable N-terminus flag-tagged Ccdc124 expressing vector (flag-Ccdc124) in the rest of our studies.

***Ccdc124 is a novel centrosome protein relocated to midbody at telophase***

In order to obtain insight into the biological function of Ccdc124, we assessed the subcellular localization of endogenous Ccdc124 by using generated or commercial anti-Ccdc124 antibodies in cellular immunofluorescence assays. When asynchronusly growing HeLa cells were subjected to a preliminary immunofluorescence analysis by using an anti-mid-Ccdc124 antibody recognizing the central part of the protein (between residues 100-150), subcellular dot-like structures reminiscent of centrosomal staining patterns were detected (results not shown, but please see Fig. 2, below). We then synchronized the cells at G2/M stage of the cell cycle by the MT polymerization inhibitor nocodazole following double-thymidine treatments (Fig. S2, see *Methods*), and followed cell cycle stage-dependent subcellular localization of endogenous Ccdc124 by immunofluorescence assays using Ccdc124 N-terminal epitope (residues 1 to 24), mid-region, or C-terminal epitope (residues 173 to 223)-specific antibodies. Independent of the Ccdc124 antibody used, these studies further indicated centrosome colocalization of Ccdc124 with γ-tubulin at interphase, prophase, metaphase, and anaphase stages, albeit it was relatively diffused to the pericentrosomal region at anaphase (Fig. 2A). Similar results were obtained when subcellular localization of an N-terminus flag-tagged version of Ccdc124 was monitored by immunofluorescence stainings using anti-flag antibodies on cells transfected with the corresponding vector construct (Fig. 2B). Moreover, endogenous centrosome immunostainings with anti-Ccdc124 Abs were very significantly reduced in response to Ccdc124 depletion by esiRNAs targeting its

expression (see below, Fig. 4B), further supporting the notion that Ccdc124 is a novel centrosome protein. Centrosome localization of endogenous Ccdc124 was also observed in Retinal Pigment Epithelial cells (RPE1) containing another centrosomal marker, GFP-Centrin [26] (results not shown). Interestingly, at telophase and in cytokinesis Ccdc124 dissociates from centrosomes and relocalizes to the midzone, subsequently accumulating at the midbody at cytokinesis as assessed by its colocalization with the midzone-specific γ-tubulin (Fig. 2A-B, and Fig. 3A, C), or by its positioning at the midbody marked by the empty mid-space in α-tubulin stainings (Fig. 3B). Immunofluorescence studies with peptide competition assays further indicated that the Ccdc124 signal detected at the midbody was specific, as anti-N-ter-Ccdc124 antibodies pre-treated with the epitope peptide failed to recognize Ccdc124 at the midbody (Fig. 3C).

***Knock-down of CCDC124 by siRNAs leads to defects in cytokinesis***

A number of midbody localized proteins were previously shown to be involved in cytokinetic abscission [13], [16], [27]. In order to test a possible role of Ccdc124 during the separation of dividing sister cells, we initially knocked-down *CCDC124* in HeLa cells by separately transfecting them either with esiRNAs or with shRNA vectors specifically targeting this gene. We first monitored knock-down efficiencies by immunoblots that we carried-out using lysates obtained from Ccdc124-specific esiRNA or shRNA vector transfected cells as compared to scrambled esiRNA/shRNA vector transfected controls. We observed approximately 75-80% decrease in Ccdc124 levels in cells that received gene specific esiRNAs as compared to scrambled transfected controls (Fig. 4A). Again, depending on shRNA target sequence, close to 30-65% decrease were detected in Ccdc124 levels in cells

separately transfected with three different sequences of shRNAs (Sh1, Sh2, and Sh3), as compared to scrambled controls. In these assays, Ccdc-Sh1 was identified as the vector containing the most potent Ccdc124-targeting shRNA sequence (Fig. 4A) We then analyzed cellular morphologies, centrosome localizations, and midbody functions of asynchronous growing cells that received either Ccdc124 specific esiRNAs, or shRNA vectors targeting the same gene. In Ccdc124-depleted cells interphase centrosomes still formed, as assessed by immunostainings that mark γ-tubulin complexes (Fig. 4B). This indicated that the absence of Ccdc124 does not impair centrosome formation. However, in Ccdc124-depleted cells cytokinesis was remarkably blocked as assessed by the significantly increased percentage of bi- and multinucleated cells (Fig. 4C-D) from 2.5 ± 0.3 % in scrambled control esiRNA transfected cases to 14.6 ± 1.5 % in Ccdc124-specific esiRNA received asynchronous cultures (Fig. 4C). The percentage of multinucleated cells in Ccdc124-depleted cultures were decreased significantly and nearly restored to normal levels (4.5 ± 0.8 %) when Ccdc124 was reintroduced in a strong expression vector (Fig. 4A, C). This indicated that the cytokinesis defect observed with the esiRNA against Ccdc124 was specific. Further supporting this observation, the ratio of multinucleated cells also raised from 3.1 ± 0.2 % in scrambled shRNA vector received cells to 11.6 ± 2.7 % in cells transfected with Ccdc-Sh1 (Fig. 4B), indicating that defects in cytokinesis was specific to endogenous Ccdc124 depletion in HeLa cells rather than an off-target effect of RNAi.

***Identification and characterization of interaction partners of Ccdc124***

In order to identify possible interaction partners of Ccdc124, a human liver cDNA library was screened in a yeast two-hybrid assay system as described in *Materials and Methods*. Colonies with interacting partners were selected, and the corresponding prey fragments were sequenced at their 5' and 3' junctions. All 15 positive colonies contained overlapping cDNA sequences belonging to only one gene, RasGEF1B, suggesting that this guanine nucleotide exchange factor (GEF) is a strong candidate as an interaction partner of Ccdc124. RasGEF1B was first identified in zebrafish as a protein expressed in neural cells during late embryogenesis and early larval stages [28]. Furthermore, by using *in vitro* assay systems [24] we previously characterized RasGEF1B as an exchange factor exclusively activating the small G protein Rap2. RasGEF1B was also identified in murine macrophages as a toll-like receptor inducible protein with a subcellular localization in early endosomal vesicles [29].

Following the yeast two-hybrid assays, we were able to confirm the interaction between Ccdc124 and RasGEF1B, first by *in vitro* GST pull-down methods (Fig. 5A), and then by analyzing their association in mammalian HEK-293 cells transfected with flag-Ccdc124 and GFP-RasGEF1B containing expression vectors (Fig. 5B). Coimmunoprecipitation of GFP-RasGEF1B and flag-Ccdc124 in transfected cells could indicate a functional interaction between these two proteins. In parallel to functional studies to establish cellular roles of Ccdc124 and RasGEF1B, we sought to determine whether the subcellular localizations of these two proteins were comparable throughout the cell cycle. In fact, in a previous study, RasGEF1B was shown to localize in endosomal vesicles when fluorescent protein-

fused versions (YFP-RasGEF1B or mRFP-RasGEF1B) were ectopically expressed in asynchronous CHO cells [29]. However, the subcellular localization of RasGEF1B was not previously addressed in cell cycle-synchronized cells. Identification of an endosomal vesicle factor such as RasGEF1B as an interaction partner of centrosomal and/or midbody localized Ccdc124 is particularly interesting, as critical roles of endosomes in physical separation of cells during cytokinetic abscission are well established in recent studies (for a review, see [30]). Subsequently, we generated a rabbit polyclonal antibody recognizing the C-terminal 19 amino acids epitope of the Zebrafish orthologue of RasGEF1B, and by immunoblotting analysis we first established that it also recognizes the human RasGEF1B protein (Fig. S3). Then, by using this antibody, we observed that even though in HeLa cells at interphase and prophase it displays characteristics of previously suggested cytoplasmic/early endosome localization [29], in metaphase cells RasGEF1B was located at a pericentrosomal/centrosomal position, as assessed by its co-localization with γ-tubulin, a subcellular localization similar to that Ccdc124 at metaphase cells (Fig. 6A, compare with Fig. 2).

Again similar to Ccdc124, at telophase and during cytokinesis RasGEF1B was detected at the midzone and in the midbody, and the RasGEF1B immunostaining at the midzone/midbody was sensitive to shRNAs (Fig. S4) targeting the expression of this GEF (Fig. 6B-C), indicating that the immunofluorescence signal was specific to the midbody localized RasGEF1B. Furthermore, during late stages of cytokinesis GFP-tagged RasGEF1B localized to the midbody as described for the endogenous protein (Fig. 6D). Noticeably, in these cell assays GFP-RasGEF1B clearly

colocalized with Ccdc124 at the midbody puncta, suggesting that in late-cytokinesis the midbody forms a site of interaction for the two proteins. These results imply a possible role of Ccdc124 in linking cytokinesis to previously uncharacterized RasGEF1B dependent signaling at the midbody. As a note, we observed that bacteria purified Ccdc124 does not functionally interfere with the guanine nucleotide exchange activity of RasGEF1B in *in vitro* reconstituted assay systems (see below, Elif Yaman, Alfred Wittinghofer, and Uygar H. Tazebay, unpublished results), suggesting that Ccdc124 could affect spatial regulation of RasGEF1B, rather than modulating its GEF activity.

***RasGEF1B stimulates guanine nucleotide exchange of Rap2 in mammalian cells in culture***

Activation cycle of small G proteins is regulated by guanine nucleotide exchange factors (GEFs), which induce dissociation of bound GDP and its replacement by the more abundant GTP, and the resulting conformational change allows the binding of effector proteins and thereby stimulation of downstream signaling. Previous functional studies by Yaman *et al*. [24] indicated that under *in vitro* conditions RasGEF1B specifically activates Rap2 by stimulating guanine nucleotide exchange only of this small G protein, whereas it does not activate even its close family member, Rap1, or other members of Ras family. We decided to take these *in vitro* studies to one level up, and confirm the stimulatory effect of RasGEF1B on Rap2 GDP/GTP nucleotide exchange by knocking-down this GEF in HEK-293 cells, followed by assessing GTP-bound active Rap2 (Rap2·GTP) status in these cells. For this, we used a Rap-activity assay method based on immunoprecipitation of active

Rap proteins by the Rap-binding domain of RalGDS (RBD-RalGDS), as previously described [31]. When RasGEF1B is knocked-down to nearly 55% in HEK-293 cells by specific down-regulatory shRNA-containing vectors (Fig. S4), significantly less Rap2·GTP were present in cells, even though total Rap2 amounts were not affected (Fig. 7). This indicated a functional link between RasGEF1B and Rap2 GTP-binding protein activation in this cell system. These results were consistent with our previous *in vitro* studies that established Rap2 as the sole RasGEF1B activated Ras-family GTP-binding protein [24].

***Active Rap2 GTP-binding protein is relocated to the midbody at cytokinesis***

We then decided to assess if RasGEF1B substrate G protein Rap2 was also located in centrosomes and midbody during different stages of cell cycle. Our data indicated that at the midbody the position of Rap2 overlapped both with RasGEF1B and with Ccdc124 in binary comparisons (Fig. 8A, B). Depletion of endogenous Rap2 in HeLa cells by transfecting them with Rap2-specific shRNA vectors have led to the loss of endogenous Rap2 at the midbody (Fig. 8C, D). However, depletion of Rap2 did not result in a significant increase in percentages of multinucleated cells above scrambled controls (Fig. 8C, D). This result could suggest that although Rap2 is located at the midbody, its molecular function(s) at this organelle is(are) not essential for proper completion of cytokinesis. Subsequent immunofluorescence assays using anti-Rap2 antibodies on dividing HeLa cells indicated that Rap2 migrates to the midzone during anaphase/telophase (Fig. 9A, B), which is in contrast to its homologue Rap1 that is non-responsive to RasGEF1B [24] (Fig. S5). We also observed that in synchronously dividing cells 90 mins after they were released from

nocodasole, at initial stages of cytokinesis Rap2 associates with microtubules originating at the midzone, and it migrates to the very center of intercellular bridge (boundaries marked with α-tubulin, Fig. 9B), relocating itself to midbody during cytokinetic abscission (Fig. 9A, B).

We then inquired whether Rap2 located at the midbody was functionally active during cytokinetic abscission, by transfecting HeLa cells with a GFP-labeled recombinant version of the Rap Binding Domain (RBD) of RalGDS referred as GFP-RBD(RalGDS). This GFP-labeled effector protein interacts with Rap2 specifically in the GTP-bound active state of the G protein, and thus serves as a subcellular Rap2 activity reporter [32]. When the signal coming from the GFP-RBD(RalGDS) that interacts with Rap2·GTP was followed at the subcellular level, at the interphase both endogenous Rap2 and GFP-RBD(RalGDS) were detected to localize diffusely at the cytoplasm with only a partial overlap (Fig. 10A, interphase). However, during cytokinetic abscission, GFP-RBD(RalGDS) very clearly colocalized with Rap2 at the midbody, indicating that Rap2 protein identified at the spindle midzone/midbody is in its GTP-bound active form (Fig. 10A, cytokinesis), and that it may potentially act on its specific effectors at this location. Midbody localization of GFP-labeled RBD(RalGDS) strictly depended on the presence of an active Rap2, as in cells co-transfected with dominant negative version of Rap2 (Rap2-S17N) the reporter protein GFP-RBD(RalGDS) did not relocate with the same efficiency to the midbody during cytokinesis as compared to cells transfected with wild-type Rap2 (Fig. 10B). The endogenous activation of local Rap2 signaling at midbody did not require pretreatment of cells with secondary messengers such as cAMP, diacylglycerol

(DAG), or calcium that were previously shown to stimulate Rap signaling through activation of various GEFs [33], [34]. This indicate that the recruitement of RasGEF1B to the midbody could be sufficient for regulation of Rap2 activity, as well as for translocation of Rap2 effectors to this subcellular location.

**Conclusion and Discussion**

Previous biochemical studies and mass-spectrometry analyses on purified centrosomes have shown that proteins with CCD (coiled-coil domain) motifs are abundant in PCM [8], [35]. Close to 150 different proteins were identified in the PCM at different cellular stages, about 60% of which contain predicted CCD type oligomerization motifs [8]. In this work, by using molecular and cell biology methods we identified Ccdc124 as a novel component of the centrosome, as in cells at interphase and in mitotic cells up to the late-anaphase/telophase stage it clearly colocalized with two different centrosome markers, such as γ-tubulin and centrin (Fig. 2, and unpublished data). Despite multiple high throughput proteomics analyses targeting centrosome composition in the past, Ccdc124 was not in the list of PCM proteins prior to this study, indicating that combined genetic, cell biology and biochemical approaches are still necessary to identify all the components of PCM which has a remarkably dynamic composition [1], [36]. Conservation of Ccdc124 in lower eukaryotic species without centrosomes, such as *A. nidulans*, or *S. pombe* was not surprising, as also some major centrosome proteins (for instance, γ-tubulin) were common between this organelle and fungal spindle pole bodies [37]. The absence of an orthologue of Ccdc protein in *S. cerevisiae*, however, might indicate that Ccdc124 is not essential for fungi with budding-type of cell division.

Our data revealed that at late-anaphase/telophase stages of cell cycle Ccdc124 changes its subcellular localization: it dissociates from centrosomes, and first relocalizes to the midzone at late-anaphase, and then it accumulates at the midbody puncta at telophase and during cytokinetic abscission (Fig. 2-4). Currently, we do not know what triggers the displacement of Ccdc124 from the centrosome, or its association to the midzone/midbody. In fact, Cep55, a relatively well studied coiled-coil containing centrosome protein that relocates to the midbody and controls cytokinetic abscission, was shown to be a substrate of Plk1 [13]. Phosphorylation of Cep55 by Plk1 on its Ser436 residue is required for its interaction with centralspindlin and ESCRT complex proteins, leading to the recruitment of CHMP4B to the midbody [13], [16]. This is then followed by the assembly of this ESCRT-III component into a series of ring-like structures organizing the abscission site, mainly by bringing the two membranes of the intercellular bridge into close proximity for the scission [20], [38]. Even though in the current study we have not addressed post-translational modifications of Ccdc124, there are several reasons why we anticipate that its functions/stability could be regulated by phosphorylation dependent mechanisms. First, Ccdc124 is identified as a phosphoprotein in our preliminary phosphopeptide analysis by mass-spectrometry methods, and Ser141 residue of Ccdc124 (which is a consensus Plk1 phosphorylation site) was detected as a phosphorylated residue (Pelin Telkoparan, Lars A.T. Meijer, and Uygar H. Tazebay, unpublished results). Second, when we mutated predicted Ser, Thr, or Tyr phosphorylation sites to Ala residues in Ccdc124 by *in vitro* mutagenesis, the Ser121 residue conforming to a Casein Kinase-II phosphorylation consensus site turned out to be essential for the stability of Ccdc124 protein, even though phospho-mimicking

mutations S121D, and S121E were normal in terms of protein stability (Fig. S6A, B), indicative of possible phosphorylation dependent regulatory mechanisms operating on Ccdc124.

We found that Ccdc124 depleted cells can still form MTOC, but they undergo cytokinesis failure inducing aneuploidy and generating genomic instability in cultured human cells (Fig. 4). According to current models of cytokinetic abscission, resolution of the membrane connection between two prospective daughter cells requires a concerted action of ESCRT proteins together with the targeting of three main types of recycling endosomes to midbody for an appropriate regulation of cytokinetic abscission (see below) [39], [40]. In an early work, Gromley *et al*, proposed a role for secretory vesicle fusion in the final stages of cytokinetic abscission, as they have shown that the coiled-coil protein centriolin relocates to midbody where, preceding abscission, it interacts with components of vesicle-targeting exocyst complexes and membrane-fusion inducing SNARE components [11]. However, subsequent studies indicated that even though the secretary pathway could contribute to formation of the intracellular bridge membrane, it is rather recycling endosome-dependent mechanisms that make major contributions to spatiotemporal regulation of cytokinetic abscission [40]. Furthermore, other than two Ral family G proteins RalA and RalB, endosome enriched complexes such as Rab35/OCRL and FYVE-CENT/TTC19 that were found on different types of endosomes, were previously shown to enable the completion of the final stages of abscission [41]-[43]. Our data suggested possible links between Ccdc124 and recycling endosomes. First, we identified an endosome localized nucleotide

exchange factor RasGEF1B [29] as an interaction partner of the coiled-coil protein Ccdc124 (Fig. 5-6). Second, RasGEF1B activated small G protein Rap2 that we detected at the midzone/midbody, was previously reported to colocalize with Rab11-positive endosomes in *Xenopus* early embryos [44]. Importantly, Rab11-positive recycling endosomes containing the effector protein FIP3 (Rap11 Family of Interacting Protein 3) were previously shown to control the reorganization of the cortical actomyosin network during cytokinetic abscission, as they accumulate at the intercellular space between dividing cells and regulate local actin depolymerization by recruiting p50RhoGAP, and thus contributing to further thinning of the bridge [45].

In this study, we primarily focused on the biological significance of the interaction between Ccdc124 and RasGEF1B, rather than studying mechanistic aspects of it. Yet, our studies on the effect of bacteria purified Ccdc124 on the rate of nucleotide exchange by RasGEF1B on Rap2A in *in vitro* reconstituted assay systems suggested that Ccdc124 does not functionally interfere with RasGEF1B activity (Elif Yaman, Alfred Wittinghofer, Uygar H. Tazebay, unpublished observations). We could hypothesize that rather than modulating its GEF activity, Ccdc124 could recruit RasGEF1B to midzone/midbody where the exchange factor activate its substrate G protein(s). A similar spatiotemporal regulation of Rap1 signaling localized at the plasma membrane by recruitement and translocation of its cAMP responsive GEF, Epac1, through activation of Ezrin-Radixin-Moesin (ERM) complex proteins was previously described [46].

We have shown that both the activator RasGEF1B and its partner G protein Rap2

have identical spatiotemporal subcellular distributions (Fig. 8). This indicated that RasGEF1B could potentially activate GDP/GTP exchange of Rap2 at midbody during late-telophase stage of cell cycle and at cytokinesis. Importantly, we observed the RasGEF1B substrate Rap2, but not its close homologue Rap1, accumulated in vesicular structures proximal to the midzone and at the midbody (Fig. 9A, see panels metaphase to cytokinesis, and Fig. S5). Detection of active Rap2 (Rap2·GTP) binding reporter protein GFP-RBD(RalGDS) in midbody further proved local activation of Rap2 at midbody puncta during cytokinesis (Fig. 10). This midbody localization of GFP-RBD(RalGDS), was only observed in cells having Rap2-WT, but not its dominant negative form, Rap2-S17N, indicating that midbody localization of Rap2 effectors requires activation of this small G protein (Fig. 10B). Neither cellular depletion of endogenous Rap2 by specific shRNA transfections, nor over-expression of the dominant negative form of Rap2 (S17N) has led to cytokinesis defects, as assessed by normal levels of bi- and multinucleated cells in corresponding cellular assays (Fig. 8, 10). Therefore, in our opinion rather than playing a direct role in cytokinesis, localization of Rap2 at the midbody might serve to modulate and/or functionalize local membrane environment for molecular events following cytokinetic abscission, such as establishment of cell-cell junctions, cell-extracellular matrix adhesions, or polarizations of cells after division of daughter cells fully accomplished. When we consider results obtained in this study altogether, we propose Ccdc124 as a novel factor that links cytokinesis to Rap signaling dependent junction/adhesion or cellular polarization promoting molecular mechanisms, thus bonding different cellular events that must closely follow each other in tissues of live organisms.

## Methods

### *Ethics Statement*

All cell lines of human origin used in this study were obtained legally either from commercial sources, or they were previously published. Material transfer agreements were duly signed between appropriate offices/persons-in-charge at donating and receiving institutions.

### *Cell culture and reagents*

Hek-293 and HeLa cells were maintained in DMEM and Retinal Pigment Epithelial-1 (RPE1) cells were grown in DMEM/F12 (1:1) supplemented with 10% FBS and kept at 37 °C in a humidified 5% CO2 atmosphere. Cell lines used in this work were either from commercial sources, or described in previous publications. RPE1 cells [26] were obtained from Nurhan Özlü (Koç University, Istanbul), and RPE1 lines stably expressing GFP-Centrin [26], and GFP-Plk1 [47] were gifts from Greenfield Sluder (U. Mass. Medical School, MA), and Prasad Jallepalli (Memorial Sloan-Kettering, NY), respectively. 50 nM of Mission® esiRNA from Sigma-Aldrich (cat. EHU004061) was used for silencing Ccdc124 in HeLa cells by using Oligofectamine (Invitrogen) as transfection reagent. We have also targeted Ccdc124 expression by using the following three shRNA vector constructs prepared in pTRIPZ plasmids (Open Biosystems-Thermo) closely following the procedures described by Paddison *et al*. [48]. Ccdc124 specific shRNA sequences inserted in pTRIPZ vectors were as follows: shRNA #1: 5'-TGCTGTTGACAGTGAGCGACTCGACCAGCTGGAACGTAA|GTAGTGAAGC

CACAGATGTACTTACGTTCCAGCTGGTCGAGGTGCCTACTGCCTCGGA-3’; shRNA #2: 5’-TGCTGTTGACAGTGAGCGACGAGACCATCAGCTCAGGGA|GTAGTGAAGCCACAGATGTACTCCCTGAGCTGATGGTCTCGGTGCCTACTGCCTCGGA-3; shRNA #3: 5’-TGCTGTTGACAGTGAGCGACCCAAGAAGTTCCAGGGTGA|GTAGTGAAGCCACAGATGTACTCACCCTGGAACTTCTTGGGCTGCCTACTGCCTCGGA-3. pTRIPZ vector containing scrambled shRNA control were purchased (Open Biosystems-Thermo, cat. no. RHS4750). In experiments to rescue cellular effects of Ccdc124 knock-downs by specific esiRNAs, 40 ng of pCDN3.1-CMV-Ccdc124 plasmids were cotransfected with the above indicated amounts of esiRNAs. In order to knock-down RasGEF1B expression, a set of five plasmids containing shRNA sequences specific for human RasGEF1B gene in pLKO1 vectors, and the corresponding scrambled shRNA control plasmid were purchased (Open Biosystems-Thermo) with the catalog number RHS4533 (TRC Lentiviral shRNAs) and following sequences: 1) Oligo ID: TRCN0000072963, 5’-CCGGGCTGACAGATAGACTCAGATTCTCGAGAATCTGAGTCTATCTGTCAGCTTTTTG-3’, renamed as sh-A; 2) Oligo ID: TRCN0000072964, 5’-CCGGCGGAAACATTTCCCTATGATTCTCGAGAATCATAGGGAAATGTTTCCGTTTTTG-3’, renamed as sh-B; 3) Oligo ID: TRCN0000072965, 5’-CCGGCGGTTATTTATGCATCCGTATCTCGAGATACGGATGCATAAATAACCGTTTTTG-3’, renamed as sh-C; 4) Oligo ID: TRCN0000072966, %’-CCGGGCTCTCTACTTGGCTTCTTATCTCGAGATAAGAAGCCAAGTAGAGAGCTTTTTG-3’, renamed as sh-D; 5) Oligo ID: TRCN0000072967, 5’-

CCGGGAAGCACTCATCCAGCACTTACTCGAGTAAGTGCTGGATGAGTGCT TCTTTTTG-3', renamed as sh-E. Similarly, for decreasing Rap2 expression, a set of three plasmids containing shRNA sequences specific for human Rap2 gene in pGIPZ vectors, together with the corresponding scrambled shRNA control vector were purchased (Open Biosystems-Thermo) with the catalog number RHS4531 (TRC Lentiviral shRNAs) and following sequences: 1) Oligo ID: V2LHS_34663, 5'-TGCTGTTGACAGTGAGCGCACTCAGAACAGGTTATGTAAATAGTGAAGC CACAGATGTATTTACATAACCTGTTCTGAGTTTGCCTACTGCCTCGGA-3', renamed as sh-1; 2) Oligo ID: V2LHS_34666, 5'-TGCTGTTGACAGTGAGCGAAGAGATATAGTTCACAGTTAATAGTGAAGC CACAGATGTATTAACTGTGAACTATATCTCTGTGCCTACTGCCTCGGA-3', renamed as sh-2; 3) Oligo ID: V2LHS_34662, 5'-TGCTGTTGACAGTGAGCGCTGACCTTGTGTCACTATTTATTAGTGAAGCC ACAGATGTAATAAATAGTGACACAAGGTCAATGCCTACTGCCTCGGA-3', renamed as sh-3. When indicated, cells were synchronized by a first thymidine block (2,5 mM) for 16 hours, released for 8 hours, and then blocked a second time with thymidine for 16 hours, followed by 200 nM nocodasole treatment/12 hours. Mitotic arrested cells were collected by "mitotic shake-off", and either they were analyzed directly (0 min.), or recultured for 15, 30, 45, 60, 120, 150, and 180 mins. At the beginning of the experiments cell cycle status of samples were established by FACS analysis as described in Fabbro *et al*. [13] and at each time point cells were processed for immunofluorescence.

***Vector Constructions***

pCDNA3.1 was used to generate CMV-promoter controlled Ccdc124 expression vector construct by using EcoRI/BamHI restriction sites and 5'-AAGCTTGAATTCATGCCCAAGAAGTTCCAGGGTGAG-3' (forward) and 5'-GGTACCGGGATCCTCTTGGGGGCATTGAAGGGCAC-3' (reverse) primers. Cloning of RasGEF1B into pEGFP-C1 (Clontech) was done by using 5'-GTCGACGAATTCTTAAACTCTGCCTAAGAGGCTCGACC-3' (forward), and 5'-GTCGACGAATTCTTAAACTCTGCCTAAGAGGCTCGACC-3' (reverse) primers and XhoI/EcoRI sites. Flag-tagged Ccdc124 expressing vectors were constructed by sub-cloning the gene in p3X-Flag-CMV10 or p3X-Flag-CMV14 vectors (Sigma) by using 5'-CTTGAATTCATGCCCAAGAAGTTCCAGGGTGAG-3' (forward) / 5'-GACCGGGATCCTCTTGGGGGCATTGAAGGGCAC-3' (reverse) and 5'-CTTGAATTCATGCCCAAGAAGTTCCAGGGTGAG-3' (forward) / 5'-GGATCCTCTAGAGTCCTTGGGGGCATTGAAG-3' (reverse) primers together with EcoRI/BamHI, and EcoRI/XbaI restriction enzyme sites, respectively. HA-epitope linked versions of Rap2 in Rap2-WT-HA, Rap2-G12V-HA, and Rap2-S17N-HA vectors were kind gifts of Daniel Pak (University of California, Berkeley). GFP-RBD(RalGDS) expression vector was a gift from Johannes L. Bos (University Medical Center Utrecht, the Netherlands).

***Rap Activity Assays***

Rap activity assays were carried-out as described previously by van Triest and Bos [31]. Briefly, HEK-293 cells grown in 6-cm plates were lysed in buffer containing 1% NP-40, 150 mM NaCl, 50 mM Tris-HCl (pH 7.4), 10% glycerol, 2 mM $MgCl_2$,

and protease and phosphatase inhibitors. Lysates were cleared by centrifugation, and active Rap was precipitated with a glutathione S-transferase fusion protein of the Rap-binding domain of RalGDS precoupled to glutathione-Sepharose beads.

***Immunoprecipitation, Immunoblotting and GST-Pull Down Assays***

Cells lysed in 50 µl lysis buffer consisting of 50mM Tris 8.0 Base, 250mM NaCl, proteinase inhibitor cocktail (Roche), and 1% NP40. Protein concentrations were determined by using Bradford assay. 40µg of whole cell extracts were denatured in gel loading buffer [50 mM Tris-HCl pH 6.8, 1% SDS, 0.02% bromophenol blue, 10% Glycerol and 5% 2-mercaptoethanol] at 95°C for 5 min, resolved by SDS-PAGE using a 12% gel, and electrotransferred onto PVDF membranes (Millipore). For RasGEF1B/Ccdc124 coimmunoprecipitation experiments, HEK-293 cells were transfected with flag-Ccdc124 and YFP-Rasgef1B vectors. 48 hours later, cells were lysed in NP-40 lysis buffer, flag-tagged agarose beads (A2220, Sigma-Aldrich) were used to precipitate proteins for two hours, followed by a centrifugation for 30 sec. at 8800 rpm, then beads were washed three times with NP-40 lysis buffer. 50µl sample buffers were added to lysates and incubated at 95°C for 5 min, fractionated by SDS-PAGE for immunoblot analysis and transferred onto PVDF membranes (Millipore). Anti-GFP (G1544, Sigma-Aldrich) and anti-Flag-HRP M2 (A8592, Sigma-Aldrich) were used in Western blot analysis. Blotted proteins were visualized using the ECL detection system (Amersham). For GST pull-down assays, 100µl 50% slurry (~50µl packed) GSH beads were washed 3 times with wash buffer (50mM Tris HCl pH 7.5, 100mM NaCl, 3mM β-Mercaptoethanol). First two vials were immobilized with 200µg purified GST-RasGEF1B protein, second vial was immobilized with 200µg

GST protein, whereas the fourth vial was incubated with buffer only and rotated at 4°C for 1 hour. The first and the third vials incubated with wash buffer only, second and fourth vials incubated with 500µg bacteria purified His-Ccdc124 protein and incubated at 4°C for 1 hour by rotating. Beads were washed 10 times with wash buffer, and samples were eluted with 40µl 4xSDS loading buffer, boiled for 5 min and loaded on an SDS gel. For the control of protein sizes samples from a 10µg/µl stock of each protein were loaded to the same gel. The gel then stained with commassie blue and destained with water.

***Generation of polyclonal antibodies***

3 mg of N-terminus 24mer peptide MPKKFQGENTKSAAARARRAEAK-[C]-amide of human Ccdc124, and [C]-NNMEKDR-W-KSLRSSLLNRT peptide corresponding to partly conserved C-terminus of the zebra fish homologue of RasGEF1B (*Danio rerio* RasGEF domain family member 1Ba, NCBI accession number: NM_199829) were coupled to KLH through their inserted cysteine residues via MBS, and Both peptides were used in rabbit immunizations at the Cambridge Research Biochemicals (Cambridge, United Kingdoms). 10 mg of each peptide affinity column purified (Glycine and TEA eluates) antibodies and pre-immune control sera were then received for use in molecular biology research.

***Immunofluorescence***

HeLa cells on cover slips were fixed by ice cold 100% Methanol for 10 min at -20°C, washed three times with PBS-T; blocked in 2% BSA for 1 hour and incubated 1 hour with primary antibodies, washed again three times with PBS-T and incubated for 1

hour with suitable secondary antibodies. Sources of antibodies: Plk1 a gift from Nurhan Özlü, Koç University, Istanbul; monoclonal (ab17057), or polyclonal (ab109777) Abs were purchased from Abcam; anti-RasGEF1B-C-ter epitope Ab and anti-Ccdc124-N-ter epitope Ab were custom produced by Cambridge Research Biochemicals-UK (see above), Ccdc124 middle-epitope specific (A-301-835A) or C-ter epitope specific (A-301-834A) Abs were from BETHYL Laboratories; anti-γ-tubulin were either from Abcam (ab11316), or from BioLegend (rabbit polyclonal cat.620902); anti-α-tubulin were from Santa Cruz (SC-5286); rabbit anti-flag-Ab was from Sigma (F-7425); rabbit anti-Rap2 polyclonal was purchased from Genetex (GTX108831); mouse anti-Rap2 monoclonal was from BD Biosciences (610215), DNA dye (DAPI) was from Invitrogene (P36931); and Alexa Fluor 488, or 568 labeled anti-rabbit, and anti-mouse secondary antibodies were purchased from Invitrogene.

***Fluorescent microscopy and imaging***

Fluorescent images were done by Zeiss Imager-A1 microscope with a Zeiss Acroplan 40X objective. Images were captured on the Zeiss Axia Cam MRc 5- CCD camera for fixed samples. Microscope control and image processing were done through Axiovision version 4.6 software program (Universal Imaging).

***Northern blot analysis***

Northern blotting was performed on commercially obtained "FirstChoice Northern Human Blot-1 and Blot-2 Membranes" (Ambion) which contained 2 µg poly(A)-RNA from indicated human organs on each lane. Donor information is available at

the suppliers (Ambion) documents; human derived materials have been prepared in the mentioned company from tissues obtained with consent from a fully informed donor, or a member of the donor's family, as certified by the company. DNA probes used in hybridizations were as follows: ApaI-XbaI DNA fragment (381 bp) of *CCDC124* cut-out from Flag-Ccdc124 plasmid vector, GAPDH fragment (408 bp) obtained after PCR amplification of a HeLa cell cDNA library by using forward primer 5'-GGCTGAGAACGGGAAGCTTGTCAT-3' and reverse primer 5'-CAGCCTTCTCCATGGTGGTGAAGA-3' as amplification primers, and β-actin fragment (539 bp) obtained after PCR amplification of the same cDNA library by using forward 5'- GATGACCCAGATCATGTTTG-3' and reverse 5'-CATGGAGGAGCCGCCAGACAGC-3' primers in PCR amplifications in the following conditions: 5 min initial denaturation at 95˚C, 35 cycles of 30 sec denaturation at 95˚C, 30 sec primer annealing at 60˚C and 30 sec extension at 72˚C, and a 5 min final extension at 72˚C. Then, DNA templates corresponding to expected band sizes were isolated from agarose gels, labeled by North-2-South Biotin random prime labeling kit (Pierce). Nucleic acids hybridization and detection were done by North-2-South Chemiluminescent hybridization and detection kit (Pierce). Resulting blots were exposed to autoradiography films (Kodak).

***Identification of CCDC124-interacting proteins by using the yeast two-hybrid (Y2H) screening method***

**Bait cloning and Y2H screening were performed by Hybrigenics, S.A., Paris, France (http://www.hybrigenics.com).** Human CCDC124 **cDNA (encoding 223 a.a protein)** was PCR-amplified and cloned in a LexA C-terminal fusion vector. The

bait construct was checked by sequencing the entire insert, and was subsequently transformed in the L40ΔGAL4 yeast strain [49]. Then, a human liver cDNA library containing ten million independent fragments were transformed into the Y187 yeast strain, which was used for mating. The screen was performed in conditions ensuring a minimum of 50 million interactions tested, in order to cover five times the primary complexity of the yeast-transformed cDNA library. After selection on medium lacking leucine, tryptophane, and histidine, 15 positive clones were picked, and the corresponding prey fragments were sequenced at their 5' and 3' junctions. Sequences were contigued as described previously, and then they were compared to the latest release of the GenBank database using BLASTN [50]. A Predicted Biological Score (PBS) was attributed to assess the reliability of each interaction, as described previously [51].

**Acknowledgements**

The authors would like to thank Mehmet Öztürk for a critical reading of the manuscript. We would like to thank Holger Rehmann and Johannes L. Bos for hosting P.T. in their laboratories for a short stay to learn analysis of Rap signaling, and for providing us GFP-RBD(RalGDS) vector. We are grateful to Greenfield Sluder for GFP-Centrin containing RPE1 cells, to Prasad Jallepalli for providing RPE1 cells with GFP-Plk1(WT), to Daniel Pak for Rap2-WT-HA, Rap2-G12V-HA, and Rap2-S17N-HA expression vectors, and to Nurhan Özlü for anti-Plk1 Abs. This project was funded by the Turkish Scientific and Technological Research Council

(TUBITAK) through grants 109T049, 109T925 to U.H.T, and by the European Science Foundation-Functional Genomics Programme support to P.T.

**Author Contribution**

P.T., D.B, E.Y., S.E., H.A. did cell biology, RNA and protein biochemistry analysis,

P.T., E.Y., D.B., U.H.T. analyzed data,

U.H.T. wrote the manuscript.

**Conflict of Interest**

The authors declare that they have no conflict of interest.

**References**


1. Lüders J, Stearns T (2007) Microtubule-Organizing centres: A re-evaluation. Nat Rev Mol Cell Biol 8:161-7.
2. Conduit PT, Brunk K, Dobbelaere J, Dix CI, Lucas EP, Raff JW (2010) Centrioles regulate centrosome size by controlling the rate of Cnn incorporation into the PCM. Curr Biol 20:2178-86.
3. Debec A, Sullivan W, Bettencourt-Dias M (2010) Centrioles: active players or passengers during mitosis? Cell Mol Life Sci 67:2173-94.
4. Nigg EA, Stearns T (2011) The centrosome cycle: Centriole biogenesis, duplication and inherent asymmetries. Nat Cell Biol 13:1154-60.
5. Haren L, Stearns T, Lüders J (2009) Plk1-dependent recruitment of gamma-tubulin complexes to mitotic centrosomes involves multiple PCM components. PLoS ONE 4:e5976.
6. Schatten H, Sun QY (2010) The role of centrosomes in fertilization, cell division and establishment of asymmetry during embryo development. Semin Cell Dev Biol 21:174-84.
7. Lee K, Rhee K (2011) PLK1 phosphorylation of pericentrin initiates centrosome maturation at the onset of mitosis. J Cell Biol 195:1093-101.
8. Jakobsen L, Vanselow K, Skogs M, Toyoda Y, Lundberg E, Poser I, et al. (2011) Novel asymmetrically localizing components of human centrosomes identified by complementary proteomics methods. EMBO J 30:1520-35.
9. Cohen C, Parry DA (1990) Alpha-helical coiled coils and bundles: how to design an alpha-helical protein. Proteins 7:1-15.

10. Fededa JP, Gerlich DW (2012) Molecular control of animal cell cytokinesis. Nat Cell Biol 14:440-7.
11. Gromley A, Yeaman C, Rosa J, Redick S, Chen CT, Mirabelle S, et al. (2005) Centriolin anchoring of exocyst and SNARE complexes at the midbody is required for secretory-vesicle-mediated abscission. Cell 123:75-87.
12. Skop AR, Liu H, Yates J, Meyer BJ, Heald R (2004) Dissection of the mammalian midbody proteome reveals conserved cytokinesis mechanisms. Science 305:61-6.
13. Fabbro M, Zhou BB, Takahashi M, Sarcevic B, Lal P, Graham ME, et al. (2005) Cdk1/Erk2- and Plk1-dependent phosphorylation of a centrosome protein, Cep55, is required for its recruitment to midbody and cytokinesis. Dev Cell 9:477-88.
14. van der Horst A, Simmons J, Khanna KK (2009) Cep55 stabilization is required for normal execution of cytokinesis. Cell Cycle 8:3742-9.
15. Lee HH, Elia N, Ghirlando R, Lippincott-Schwartz J, Hurley JH (2008) Midbody targeting of the ESCRT machinery by a noncanonical coiled coil in CEP55. Science 322:576-80.
16. Hu CK, Coughlin M, Mitchison TJ (2012) Midbody assembly and its regulation during cytokinesis. Mol Biol Cell 23:1024-34.
17. Carlton JG, Martin-Serrano J (2007) Parallels between cytokinesis and retroviral budding: a role for the ESCRT machinery. Science 316:1908-12.
18. Guizetti J, Schermelleh L, Mantler J, Maar S, Poser I, Leonhardt H, Müller-Reichert T, Gerlich DW (2011) Cortical constriction during abscission involves helices of ESCRT-III-dependent filaments. Science 331:1616-20.

19. Hanson PI, Roth R, Lin Y, Heuser JE (2008) Plasma membrane deformation by circular arrays of ESCRT-III protein filaments. J Cell Biol 180:389-402.
20. Elia N, Sougrat R, Spurlin TA, Hurley JH, Lippincott-Schwartz J (2011) Dynamics of endosomal sorting complex required for transport (ESCRT) machinery during cytokinesis and its role in abscission. Proc. Natl Acad Sci USA 108: 4846-51.
21. Lane HA, Nigg EA (1996) Antibody microinjection reveals an essential role for human polo-like kinase 1 (Plk1) in the functional maturation of mitotic centrosomes. J Cell Biol 135:1701-13.
22. Tong C, Fan HY, Lian L, Li SW, Chen DY, Schatten H, Sun QY (2002) Polo-like kinase-1 is a pivotal regulator of microtubule assembly during mouse oocyte meiotic maturation, fertilization, and early embryonic mitosis. Biol Reprod 67:546-54.
23. Bastos RN, Barr FA (2010) Plk1 negatively regulates Cep55 recruitment to the midbody to ensure orderly abscission. J Cell Biol 191:751-60.
24. Yaman E, Gasper R, Koerner C, Wittinghofer A, Tazebay UH (2009) RasGEF1A and RasGEF1B are guanine nucleotide exchange factors that discriminate between Rap GTP-binding proteins and mediate Rap2-specific nucleotide exchange. FEBS J 276:4607-16.
25. Gloerich M, Bos JL (2011) Regulating Rap small G-proteins in time and space. Trends Cell Biol 21:615-23.
26. Uetake Y, Loncarek J, Nordberg JJ, English CN, La Terra S, Khodjakov A, Sluder G (2007) Cell cycle progression and de novo centriole assembly after centrosomal removal in untransformed human cells. J Cell Biol 176:173-82.

27. Gromley A, Jurczyk A, Sillibourne J, Halilovic E, Mogensen M, Groisman I, et al. (2003) A novel human protein of the maternal centriole is required for the final stages of cytokinesis and entry into S phase. J Cell Biol 161:535-45.
28. Epting D, Vorwerk S, Hageman A, Meyer D (2007) Expression of rasgef1b in zebrafish. Gene Expr Patterns 7:389-95.
29. Andrade WA, Silva AM, Alves VS, Salgado AP, Melo MB, Andrade HM, et al. (2010) Early endosome localization and activity of RasGEF1b, a toll-like receptor-inducible Ras guanine-nucleotide exchange factor. Genes Immun 11:447-57.
30. Schiel JA, Prekeris R (2013) Membrane dynamics during cytokinesis. Curr. Opin. in Cell. Biol 25:92-8.
31. van Triest M, Bos JL (2004) Pull-down assays for guanoside 5'-triphosphate-bound Ras-like guanosine 5'-triphosphatases. Methods Mol Biol 250:97-102.
32. Bivona TG, Wiener HH, Ahearn IM, Silletti J, Chiu VK, Philips MR (2004) Rap1 up-regulation and activation on plasma membrane regulates T cell adhesion. J Cell Biol 164:461-70.
33. de Rooij J, Zwartkruis FJ, Verheijen MH, Cool RH, Nijman SM, Wittinghofer A, Bos JL (1998) Epac is a Rap1 guanine-nucleotide-exchange factor directly activated by cyclic AMP. Nature 396:474-7.
34. Ghandour H, Cullere X, Alvarez A, Luscinskas FW, Mayadas TN (2007) Essential role for Rap1 GTPase and its guanine exchange factor CalDAG-GEFI in LFA-1 but not VLA-4 integrin mediated human T-cell adhesion. Blood 110:3682-90.
35. Stearns T, Winey M (1997) The Cell Center at 100. Cell 91:303-9.

36. Piel M, Nordberg J, Euteneuer U, Bornens M (2001) Centrosome-dependent exit of cytokinesis in animal cells. Science 291:1550-3.

37. Oakley BR, Oakley CE, Yoon Y, Jung MK (1990) Gamma-tubulin is a component of the spindle pole body that is essential for microtubule function in *Aspergillus nidulans*. Cell 61:1289-301.

38. Morita E, Sandrin V, Chung HY, Morham SG, Gygi SP, Rodesch CK, Sundquist WI (2007) Human ESCRT and ALIX proteins interact with proteins of the midbody and function in cytokinesis. EMBO J 26:4215-27.

39. Steigemann P, Gerlich DW (2009) Cytokinetic abscission: cellular dynamics at the midbody. Trends Cell Biol 19:606-16.

40. Schiel JA, Childs C, Prekeris R (2013) Endocytic transport and cytokinesis: from regulation of the cytoskeleton to midbody inheritence Trends Cell Biol (*in press*, http://dx.doi.org/10.1016/j.tcb.2013.02.003).

41. Cascone I, Selimoglu R, Ozdemir C, Del Nery E, Yeaman C, White M, Camonis J (2008) Distinct roles of RalA and RalB in the progression of cytokinesis are supported by distinct RalGEFs. EMBO J 27:2375-87.

42. Dambournet D, Machicoane M, Chesneau L, Sachse M, Rocancourt M, El Marjou A, Formstecher E, Salomon R, Goud B, Echard A (2011) Rab35 GTPase and OCRL phosphatase remodel lipids and F-actin for successful cytokinesis. Nat Cell Biol 13:981-8.

43. Sagona AP, Nezis IP, Pedersen NM, Liestol K, Poulton J, Rousten TE, Skotheim RI, Raiborg C, Stenmark H (2010) PtdIns(3)P controls cytokinesis through KIF13A-mediated recruitment of FYVE-CENT to the midbody. Nat Cell Biol 12:362-71.

44. Choi SC, Kim GH, Lee SJ, Park E, Yeo CY, Han JK (2008) Regulation of activin/nodal signaling by Rap2-directed receptor trafficking. Dev Cell 15:49-61.
45. Schiel JA, Simon GC, Zaharris C, Weisz J, Castle D, Wu CC, et al. (2012) FIP3-endosome-dependent formation of the secondary ingression mediates ESCRT-III recruitment during cytokinesis. Nat Cell Biol 14:1068-78.
46. Gloerich M, Ponsioen B, Vliem MJ, Zhang Z, Zhao J, Kooistra MR, et al. (2010) Spatial regulation of cyclic AMP-Epac1 signaling in cell adhesion by ERM proteins. Mol Cell Biol 30:5421-31.
47. Burkard ME, Randall CL, Larochelle S, Zhang C, Shokat KM, Fisher RP, et al. (2007) Chemical genetics reveals the requirement for Polo-like kinase 1 activity in positioning RhoA and triggering cytokinesis in human cells. Proc. Natl Acad Sci USA 104: 4383-8.
48. Paddison PJ, Cleary M, Silva JM, Chang K, Sheth N, Sachidanandam R, Hannon GJ (2004) Cloning of short hairpin RNAs for gene knock-down in mammalian cells. Nat Methods 1:163-167.
49. Fromont-Racine M, Rain JC, Legrain P (1997) Toward a functional analysis of the yeast genome through exhaustive two-hybrid screens. Nat Genet 16:277-82.
50. Altschul SF, Madden TL, Schäffer AA, Zhang J, Zhang Z, Miller W, et al. (1997) Gapped BLAST and PSI-BLAST: a new generation of protein database search programs. Nucleic Acids Res 25:3389-402.

51. Formstecher E, Aresta S, Collura V, Hamburger A, Meil A, Trehin A, et al. (2005) Protein interaction mapping: a Drosophila case study. Genome Res 15:376-84.

## Figure Legends

**Figure 1. *CCDC124* mRNA is ubiquitously expressed in human tissues, and it encodes a 32 kDa protein. (A)** Hybridization of part of the coding region of *CCDC124* to an adult human multiple tissue Northern blot containing 2μg of polyA-mRNA each lane. A single transcript of ~1061 nucleotides was detectable in all human tissues analyzed, except the placenta with a second smaller transcript variant. The same blot was rehybridized with probes corresponding to two differentially expressed genes, β-actin and GAPDH, to monitor blotting quality. **(B)** Specific detection of ectopically expressed Ccdc124 by anti-Ccdc124 antibodies. HEK-293 cells, either non-transfected, or transfected with CMV-promoter controlled Ccdc124 were lysed, protein lysates were separated by SDS-PAGE, and immunoblot was performed either with anti-Ccdc124 antibodies alone, or same antibodies pre-incubated with 100 ng of competing peptide epitope corresponding to N-terminus 24mer peptide of Ccdc124. **(C)** Expression of Flag-tagged Ccdc124 protein was specifically detected by the anti-Ccdc124 or with anti-Flag antibodies, as indicated. Asterisk (*) indicates C-terminus flag-tag insertion dependent N-terminus cleaved form of Ccdc124. The expression of calnexin was confirmed in all cell lysates as an equal loading control.

**Figure 2. Ccdc124 is present at the centrosome and it concentrates at the midbody in late stages of cytokinesis. (A)** HeLa cells were arrested at G2/M phase by sequential double thymidine and nocodazole treatments, then the drug was washed-off, cells were analyzed by immunofluorescence at time points with intervals of 15 minutes, and they were classified according to phases of mitosis, and

cytokinesis. Samples of cells were then costained with anti-Ccdc124 and anti-γ-tubulin antibodies, and in interphase and prophase, Ccdc124 was observed as puncta in cells, and it is located in the MTOC area. In metaphase and anaphase cells, Ccdc124 appeared at the spindle poles. Ccdc124 was present at the midzone and at the spindle poles in late anaphase, and concentrated in the midbody during cytokinesis. **(B)** HeLa cells were transfected with the N-ter flag-Ccdc124 vector construct as in Fig. 1. 48 hours later samples of cells were subjected to immunofluorescence costainings using anti-flag and anti-γ-tubulin Abs together. Representative micrographs of cells at different stages of cell cycle are given. Bars represent 10 μm.

**Figure 3. Ccdc124 accumulates at the midbody.** HeLa cells were synchronized as described in the legend of Fig. 2, and samples of cells were then stained with anti-Ccdc124 Ab together either with anti-γ-tubulin or with anti-α-tubulin Abs to monitor subcellular positions of centrosomes and the midbody. **(A-B)** At telophase and cytokinesis Ccdc124 is observed as puncta typically associated with the midbody positioned at the middle of intercellular bridge separating daughter cells, as detected in costainings with anti-γ-tubulin and anti-α-tubulin Abs, respectively. **(C)** Peptide competition assays were done by pre-incubating anti-N-ter-Ccdc124 antibody with the corresponding epitope peptide in 200-fold molar excess amounts. Signals generated by Ccdc124 localized at the midbody (shown with arrowhead) were lost in immunofluorescence assays where peptide pre-treated antibodies were used. Bars represent 10 μm.

**Figure 4. Depletion of Ccdc124 in HeLa cells by RNAi leads to cytokinesis**

**failure. (A)** HeLa cells were transfected with either esiRNAs or shRNA vectors (Sh1, Sh2, Sh3) targeting Ccdc124, cell lysates were collected at 48 hrs post-transfection, and immunoblotted with antisera to Ccdc124. Where indicated, Ccdc124 expression vector (CMV-Ccdc124) was cotransfected with gene-specific esiRNAs in order to rescue the cellular effect of Ccdc124 depletion. Scrambled control transfections were indicated (Scr). Calnexin expression was monitored as loading control. **(B)** Immunostainings of endogenous Ccdc124 in cells transfected with Ccdc124-specific esiRNA, or with scrambled control esiRNA were carried out with anti-Ccdc124 Ab. Costainings with γ-tubulin antisera have indicated subcellular positions of MTOCs **(C)** Cells described and analyzed in (A) were scored for bi- and multinucleation (n=5 ± SD). **(D)** Representative micrographs of Ccdc124 depleted multinuclear or control esiRNA treated normal dividing cells described in (C). Bars represent 10 μm.

**Figure 5. RasGEF1B is an interaction partner of Ccdc124. (A)** *In vitro* GST pull-down assay indicating a possible interaction between RasGEF1B and Ccdc124. GST-RasGEF1B protein were immobilized on GSH-beads, followed by incubation with empty PBS buffer control (lane 1), or with bacteria purified His-tagged Ccdc124 (lane 2). As controls, GSH-beads w/o RasGEF1B protein incubated with His-Ccdc124 to monitor the amount of His-Ccdc124 proteins binding to GSH-beads in the absence of a putative interaction partner (lane 3), or GSH-beads immobilized with GST protein and incubated with His-Ccdc124 to monitor interaction capacity of Ccdc124 with GST (lane 4). Lanes 5, 6, 7 are stainings of 100 ng bacteria purified GST-RasGEF1B, His-Ccdc124, and GST proteins, respectively, run in the same gel

to monitor their corresponding sizes. Bands corresponding to His-Ccdc124 were marked with asterisks (*). **(B)** HEK-293 cells were either transfected with Flag-Ccdc124 or GFP-RasGEF1B expression vectors alone or with indicated control plasmids, or alternatively they were co-transfected with Flag-Ccdc124 and GFP-RasGEF1B together, followed by immunoprecipitations (IP) on cell lysates using protein-G beads with anti-Flag antibodies. Subsequently, immunoblots were done on IP or cell lysate samples using anti-GFP (monitoring GFP-RasGEF1B) or anti-Flag-HRP (to assess Flag-Ccdc124) antibodies.

**Figure 6. RasGEF1B and Ccdc124 colocalize at the midbody (A-B)** Subcellular localizations of RasGEF1B proteins in synchronously dividing HeLa cells were detected with specific anti-RasGEF1B antibodies. Cell divisions were synchronized as described in the legend of Figure 2, above. Representative immunofluorescence microscopy images of HeLa cells costained with anti-RasGEF1B, and either anti-γ-tubulin (A) or α-tubulin (B) antibodies illustrating the position of MTOCs and the midbody at cytokinesis. Arrowheads show RasGEF1B detected at the midzone and the midbody. (C) Immunofluorescence signals observed at midbody were significantly decreased when endogenous RasGEF1B were depleted by transfections with specific shRNA vectors (Sh-C or Sh-D, Fig. S4) and representative micrographs were shown. (D) HeLa cells transiently transfected with GFP-RasGEF1B were fixed and stained using anti-Ccdc124 Abs. Arrowheads indicate midbody positions of GFP-RasGEF1B, Ccdc124, and their colocalizations at the midbody. Bars represent 10 μm.

**Figure 7. The guanine nucleotide exchange factor RasGEF1B controls cellular**

**Rap2·GTP status.** HEK-293 cells were transfected either with RasGEF1B specific shRNA expressing vector (Sh-D, Figure S4), scrambled shRNA expressing vector, or empty vector (negative control), 48 hrs later cells were lysed as described at Materials and Methods, they were cleared by centrifugation, and active Rap was precipitated with a glutathione *S*-transferase fusion protein of the Ras-binding domain of RalGDS precoupled to glutathione-Sepharose beads. Rap2 activation assay were carried-out by using anti-Rap2 monoclonal Abs. Results confirmed that shRNA mediated down-regulation of RasGEF1B expression effectively block generation of Rap2·GTP, although total cellular Rap2 was not affected. Calnexin expression was monitored as loading control.

**Figure 8. Rap2 colocalize with Ccdc124 and RasGEF1B at the subcellular level.** Subcellular localizations of endogenous Rap2 and Ccdc124 or RasGEF1B proteins were studied in HeLa cells by immunofluorescence methods. **(A)** At anaphase, Rap2 was clearly localized at the midzone, while Ccdc124 concentration at the same localization was less pronounced. However, at telophase, both proteins were concentrated at the puncta characterizing the midbody, Rap2 rather surrounding Ccdc124. During cytokinetic abscission, a clear colocalization of both Rap2 and Ccdc124 were observed at the midbody. **(B)** Similar to panel (A), Rap2 translocation to the midzone has started during anaphase. Two representative images of anaphase cells were shown in the corresponding panel. Both Rap2 and RasGEF1B proteins colocalized at the midbody during cytokinetic abscission. Arrowheads either indicate subcellular localization of Rap2 at anaphase and telophase, or they indicate the colocalization of Rap2 with RasGEF1B/Ccdc124 at the midbody during cytokinesis.

**(C)** HeLa cells were transfected with shRNA vectors (Sh1, Sh2, Sh3) targeting Rap2, then cell lysates were collected at 48 hrs post-transfection, and immunoblotted with anti-Rap2 Ab. Scrambled control transfection was indicated (Scr). Calnexin expression was monitored as loading control. In parallel experiments, similarly treated cells were immunostained with anti-Rap2 and anti-α-tubulin antibodies, followed by scorings for multinucleation (n=5 ± SD), as reported on the graph above the immunoblot. **(D)** Representative micrographs of midbody stage cells depleted in endogenous Rap2 (C). Bars represent 10 μm.

**Figure 9. Active endogenous Rap2 relocates to midzone at anaphase, and to midbody during cytokinetic abscission. (A)** HeLa cells were arrested at G2/M phase by sequential double thymidine and nocodazole treatments as described in the legend of Figure 2, and they were classified according to phases of mitosis, and cytokinesis. Samples of cells were then stained with anti-Rap2 antibody, and with DAPI to visualize DNA. At anaphase Rap2 was detected at the midzone with staining characteristics reminiscent of endosomes, and at telophase/cytokinesis Rap2 was observed as puncta at the middle of the intercellular bridge, a position typically occupied by midbody associated factors. **(B)** Following synchronization of cells as above, 80 mins. after nocodazole was washed-off samples were taken with four consecutive intervals of 10 minutes (I, II, III, and IV), the last one (IV) corresponding to ~120 minutes after the drug was removed, and dynamic positioning of Rap2 at the intercellular bridge in respect to α-tubulin was monitored. A time-dependent relocalization of Rap2 from peripheral flanking regions to the midbody was detected. Intercellular bridge localizations of Rap2 were concluded with

observations from a sample of ~50 cells in which over 75% showed similar positioning patterns. Two sets of representative micrographs were displayed. Bars represent 10 μm.

**Figure 10. Rap2 effector proteins translocate to the midbody depending on the signal transduction activity of Rap2. (A)** HeLa cells were transfected with the vector containing GFP-labeled Rap Binding Domain of RalGDS [GFP-RBD(RalGDS)] which interacts only with the GTP-bound active form of Rap2, and cells were monitored at interphase and at cytokinetic abscission following immunostainings involving anti-Rap2 monoclonal Abs and Alexa568-red labeled anti-mouse secondary Abs. Colocalization of GFP-RBD(RalGDS) with Rap2 indicated that at the midbody Rap2 is in its active (Rap2·GTP) form. **(B)** HeLa cells were cotransfected with GFP-RBD(RalGDS) either together with HA-Rap2-WT, or with HA-Rap2-S17N (inactive dominant negative form) and their localizations were monitored with anti-HA-epitope Abs. Positioning of GFP-RBD(RalGDS) were assessed by monitoring GFP-signal observed at the midbody. Localization of the GFP-RBD(RalGDS) depended on the presence of active Rap2 in cells. As in (A), at least 50 cells were monitored in each experiment, and representative pictures display Rap2 and GFP-RBD(RalGDS) localizations observed at least ~90% of cells cotransfected with indicated vectors. Bars represent 10 μm.

**Supporting Information Figures**

**Figure S1. Ccdc124 contains two main coiled-coil domains at its N-terminal part.** Schematic representation of the coiled-coil prediction of Ccdc124 is presented.

The graph was obtained by the COILS (www.ch.embnet.org/software/COILS_form.html) bioinformatics analysis platform.

**Figure S2. Double-thymidine and nocodazole treatments synchronized HeLa cells at G2/M phase of cell cycle.** HeLa cells were treated with thymidine and MT polymerization inhibitor drug nocodazole as indicated in *Methods*. $1x10^6$ unsynchronized **(A)** or synchronized **(B)** cells were collected as samples, and resuspended in 0.3 ml of PBS buffer. Cells were fixed by addition of 0.7 ml cold ethanol (70%), left on ice for 1hr, and then washed and resuspended in 0.25 ml of PBS in which it is treated with 0.5mg/ml RNAse-A for 1 hr at 37°C. Cellular DNA is then stained with 10 μg/ml propidium iodide (PI) solution, and cytometric analysis was performed by FACS at 488 nm. Percentages of cells in each sample at various stages of the cell cycle are indicated below each panel **(A-B)**.

**Figure S3. Polyclonal Anti-RasGEF1B antibody raised against zebrafish homologue of RasGEF1B cross-reacts strongly with human RasGEF1B.** HEK-293 cells were transfected with mCherry-labeled human RasGEF1B or YFP-labeled human RasGEF1B expression vectors (mCherry-RasGEF1B and YFP-RasGEF1B, respectively), after 48 hours cells were lysed, proteins were separated by SDS-PAGE, and immunoblot was performed with anti-RasGEF1B antibody alone (1 μg at 1:1000 dilution), and then the membrane was stripped and sequentially reprobed first with the same antibody pre-incubated with 100 ng of competing 20mer peptide epitope [C]-NNMEKDR-W-KSLRSSLLNRT corresponding to C-terminus of ZF-RasGEF1B, and then with anti-GFP antibody recognizing YFP as its epitope in YFP-

RasGEF1B. Calnexin expression was monitored as loading control.

**Figure S4. Screening of RasGEF1B specific shRNA plasmids to monitor their down-regulatory capacities.** HEK-293 cells were transfected with RasGEF1B shRNA plasmids described in Supplementary Materials and Methods. 48 hours after transfections, cells were lysed and proteins were separated by SDS-PAGE. Immunoblot was performed with custom made anti-RasGEF1B antibody. Image-J software program were used to obtain densitometric readings of band intensities corrected by calnexin values, and these were indicated below each band. RasGEF1B specific shRNA expressing vector renamed as sh-D (see *Supplementary Materials and Methods*) was selected to carry-out experiments described in Results. Calnexin expression was monitored as loading control.

**Figure S5. Endogenous Rap1 does not relocate to the midzone/midbody during cytokinetic abscission.** HeLa cells were arrested at G2/M phase by sequential double thymidine and nocodazole treatments as described in the legend of Figure 2, and they were classified according to phases of mitosis, and cytokinesis. Samples of cells were then costained with anti-Rap1 and anti-α-tubulin antibodies, which were used to monitor intercellular bridge and the space containing midbody complexes. DAPI staining was used to visualize DNA. Bars represent 10 μm.

**Figure S6. Mutating the consensus CK2 phosphorylation site Ser122 to Ala leads to compromised stability of Ccdc124. (A-B)** HEK-293 cells were transfected

either with HA-tagged wild-type Ccdc124 expression vector, or with similar vectors carrying indicated mutations on Figures, and stabilities of mutants proteins were monitored by immunoblots using anti-Ccdc124 antibodies recognizing the N-terminus of the protein. Only one CK2 phosphorylation consensus site (Ser122) turned out to be essential for the stability of Ccdc124 protein as S122A mutants were cleaved at their C-terminus, whereas phospho-mimicking mutations S121D, and S121E were normal in terms of Ccdc124 stability (B). Calnexin expressions were monitored as loading control.

**Figure 1**

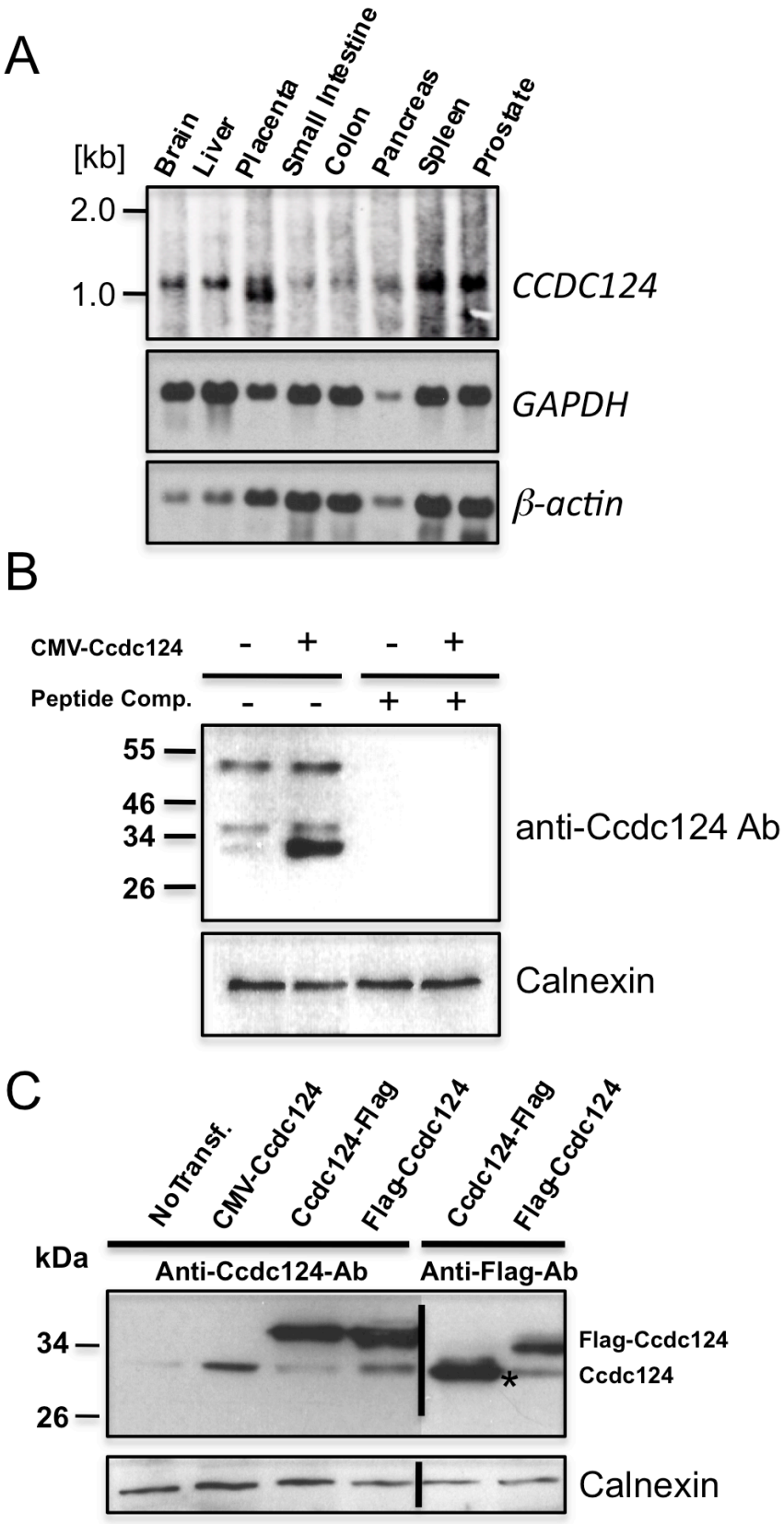
A
Brain
Liver
Placenta
Small Intestine
Colon
Pancreas
Spleen
Prostate
[kb]
2.0
1.0
CCDC124
GAPDH
β-actin
B
CMV-Ccdc124
Peptide Comp.
55
46
34
26
anti-Ccdc124 Ab
Calnexin
C
NoTransf.
CMV-Ccdc124
Ccdc124-Flag
Flag-Ccdc124
Ccdc124-Flag
Flag-Ccdc124
kDa
Anti-Ccdc124-Ab
Anti-Flag-Ab
34
26
Flag-Ccdc124
Ccdc124
Calnexin

**Figure 2**

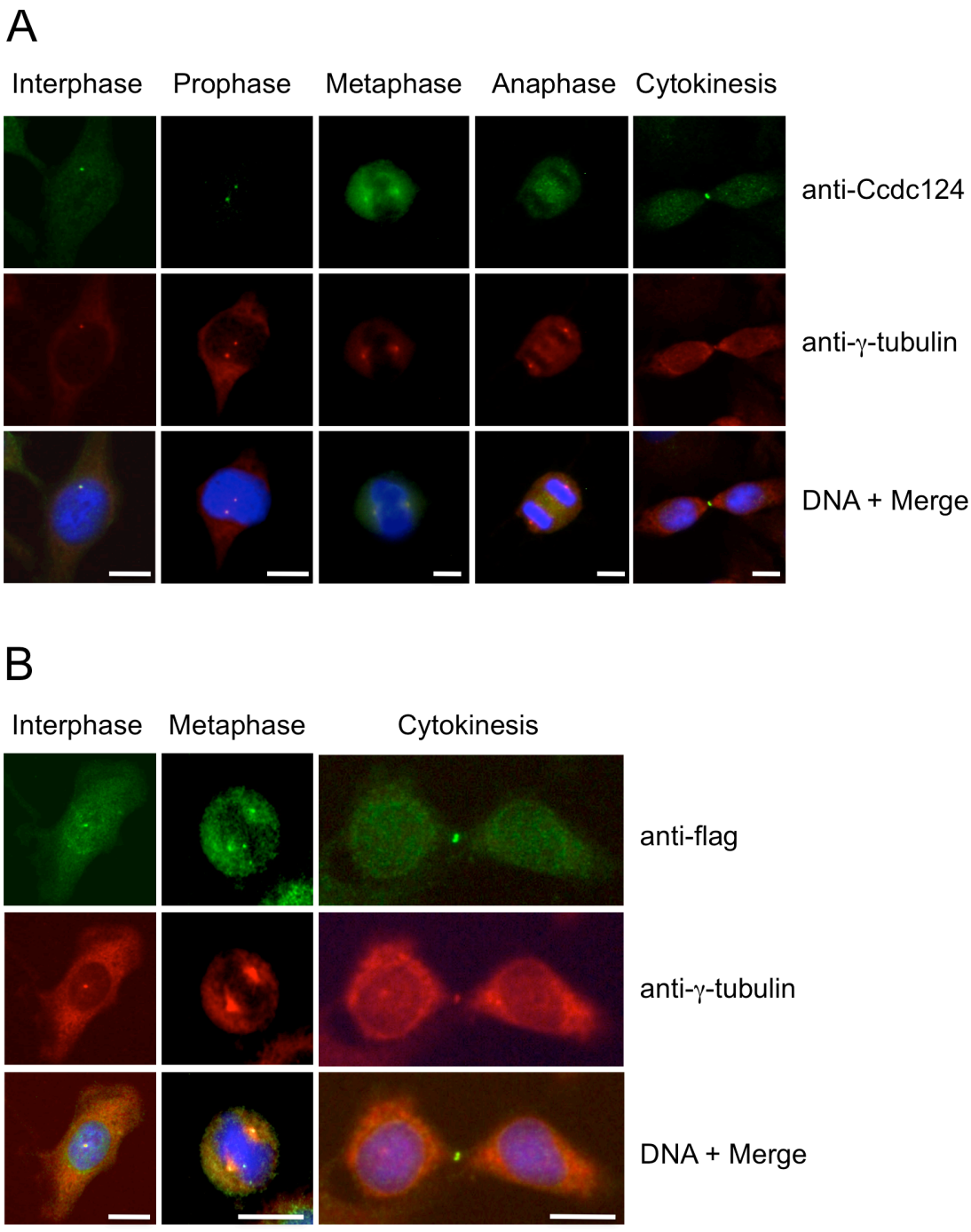
A
Interphase
Prophase
Metaphase
Anaphase
Cytokinesis
anti-Ccdc124
anti-γ-tubulin
DNA + Merge
B
Interphase
Metaphase
Cytokinesis
anti-flag
anti-γ-tubulin
DNA + Merge

**Figure 3**

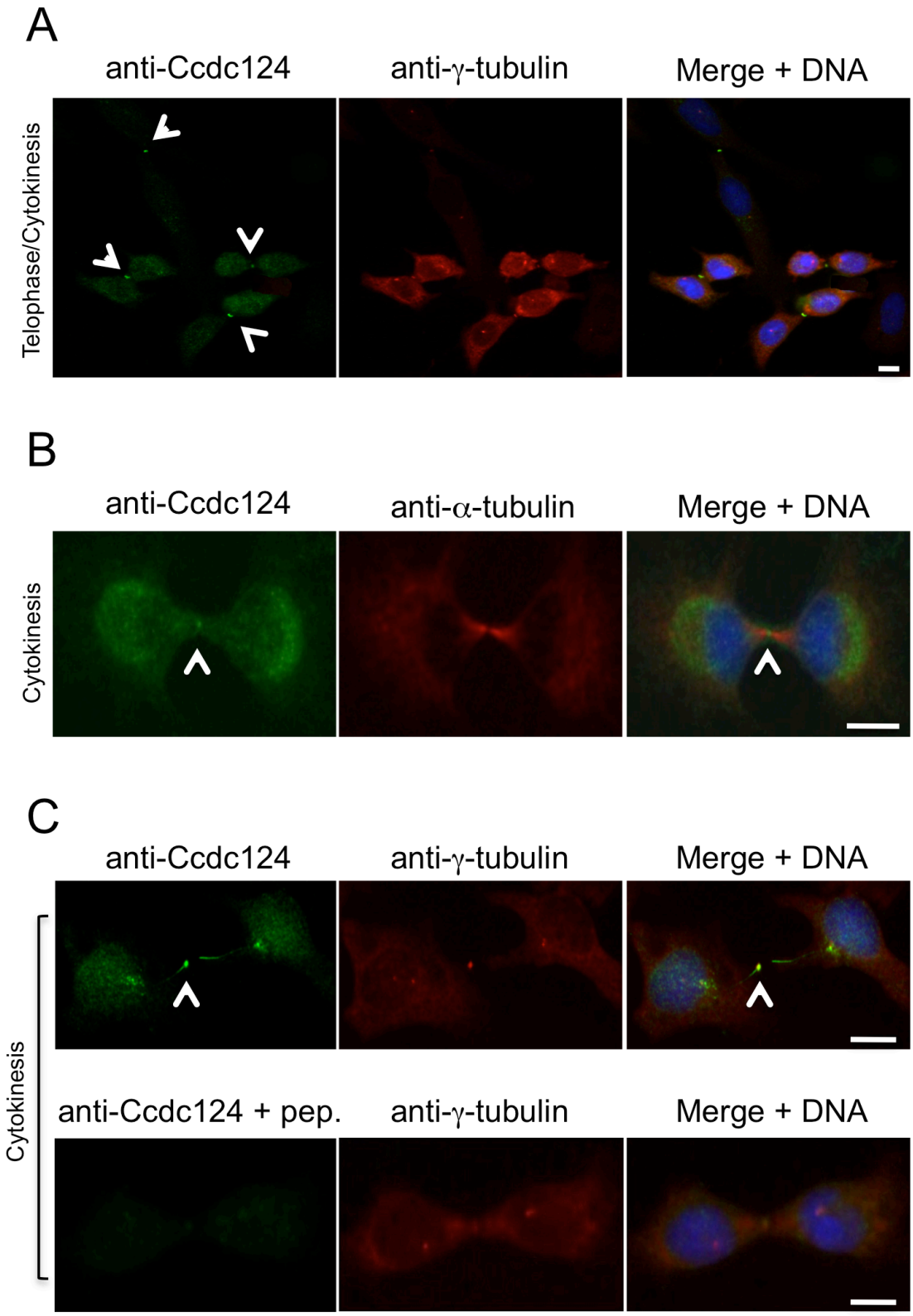
A
anti-Ccdc124
anti-γ-tubulin
Merge + DNA
Telophase/Cytokinesis
B
anti-Ccdc124
anti-α-tubulin
Merge + DNA
Cytokinesis
C
anti-Ccdc124
anti-γ-tubulin
Merge + DNA
anti-Ccdc124 + pep.
anti-γ-tubulin
Merge + DNA
Cytokinesis

# Figure 4

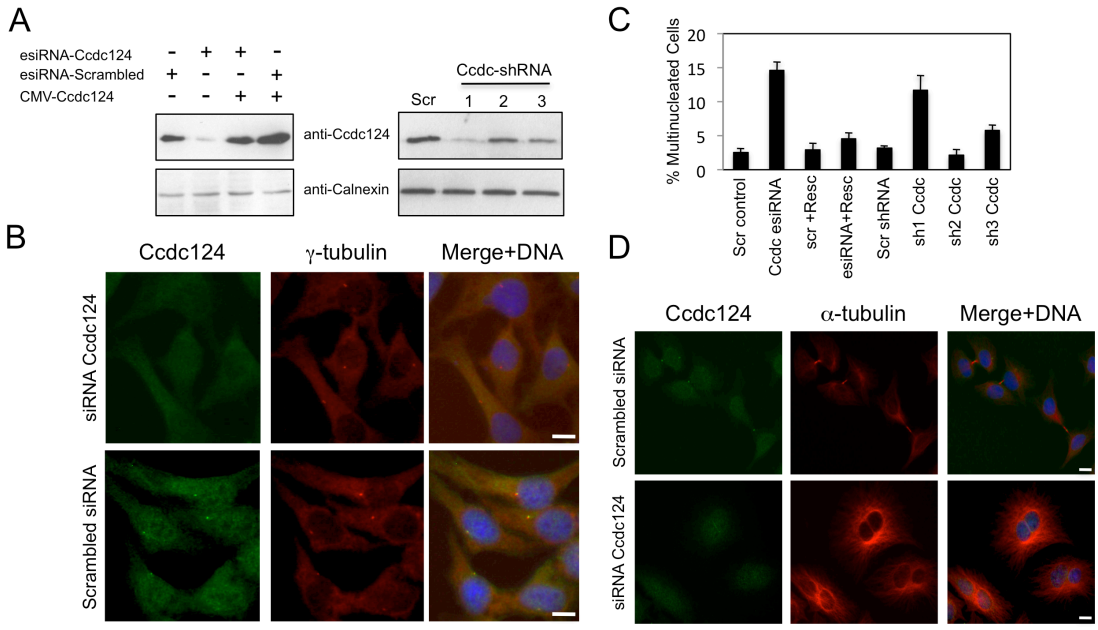
A
esiRNA-Ccdc124
esiRNA-Scrambled
CMV-Ccdc124
Ccdc-shRNA
Scr
1
2
3
anti-Ccdc124
anti-Calnexin
B
Ccdc124
γ-tubulin
Merge+DNA
siRNA Ccdc124
Scrambled siRNA
C
% Multinucleated Cells
20
15
10
5
0
Scr control
Ccdc esiRNA
scr +Resc
esiRNA+Resc
Scr shRNA
sh1 Ccdc
sh2 Ccdc
sh3 Ccdc
D
Ccdc124
α-tubulin
Merge+DNA
Scrambled siRNA
siRNA Ccdc124

**Figure 5**

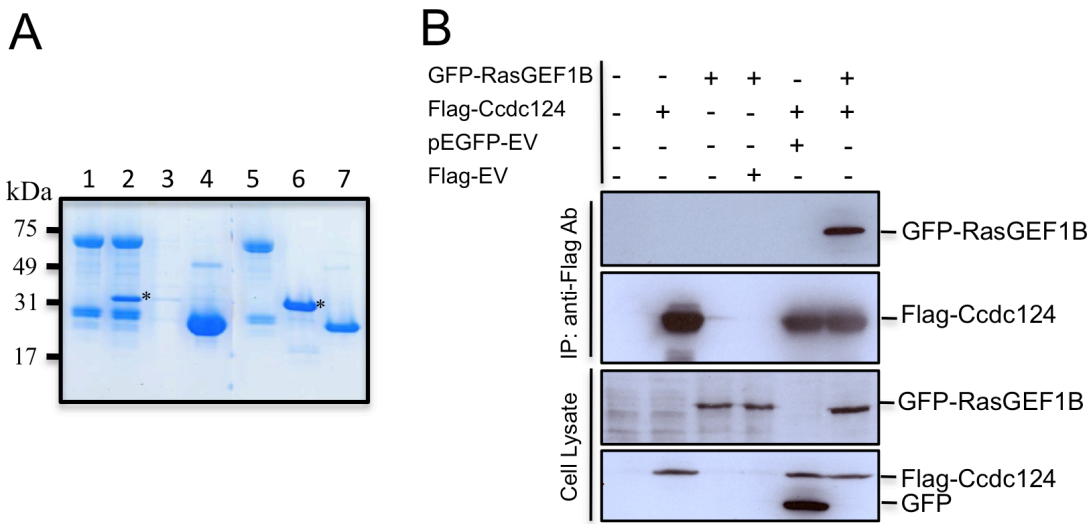
A
kDa
1 2 3 4 5 6 7
75
49
31
17
B
GFP-RasGEF1B
Flag-Ccdc124
pEGFP-EV
Flag-EV
IP: anti-Flag Ab
Cell Lysate
GFP-RasGEF1B
Flag-Ccdc124
GFP-RasGEF1B
Flag-Ccdc124
GFP

## Figure 6

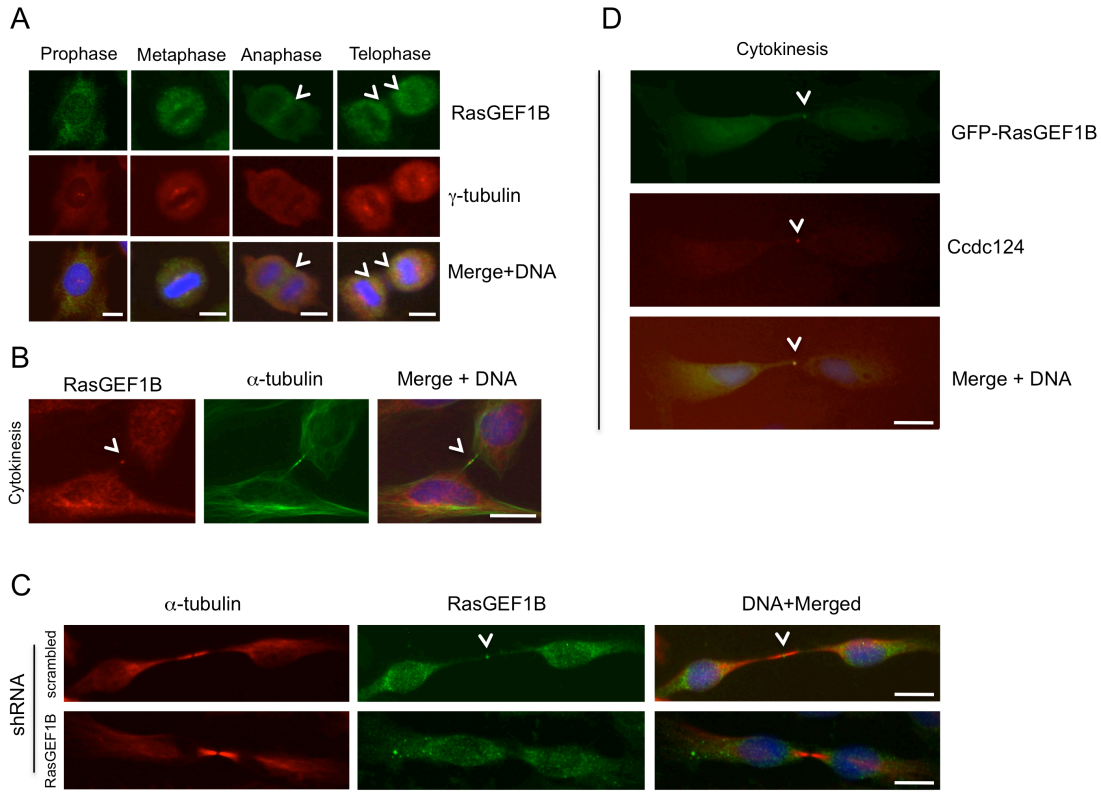
A
Prophase
Metaphase
Anaphase
Telophase
RasGEF1B
γ-tubulin
Merge+DNA
B
RasGEF1B
α-tubulin
Merge + DNA
Cytokinesis
C
α-tubulin
RasGEF1B
DNA+Merged
shRNA
scrambled
RasGEF1B
D
Cytokinesis
GFP-RasGEF1B
Ccdc124
Merge + DNA

**Figure 7**

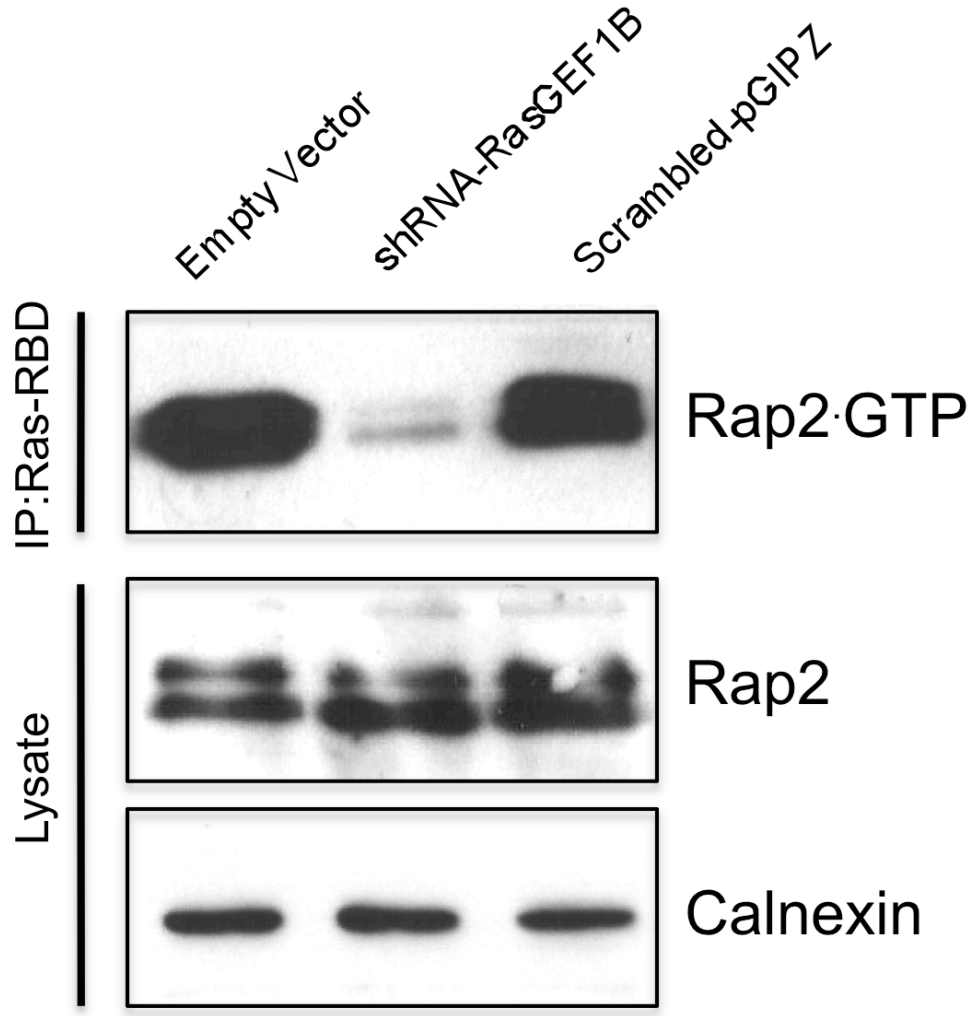
Empty Vector
shRNA-RasGEF1B
Scrambled-pGIPZ
IP:Ras-RBD
Rap2·GTP
Lysate
Rap2
Calnexin

## Figure 8

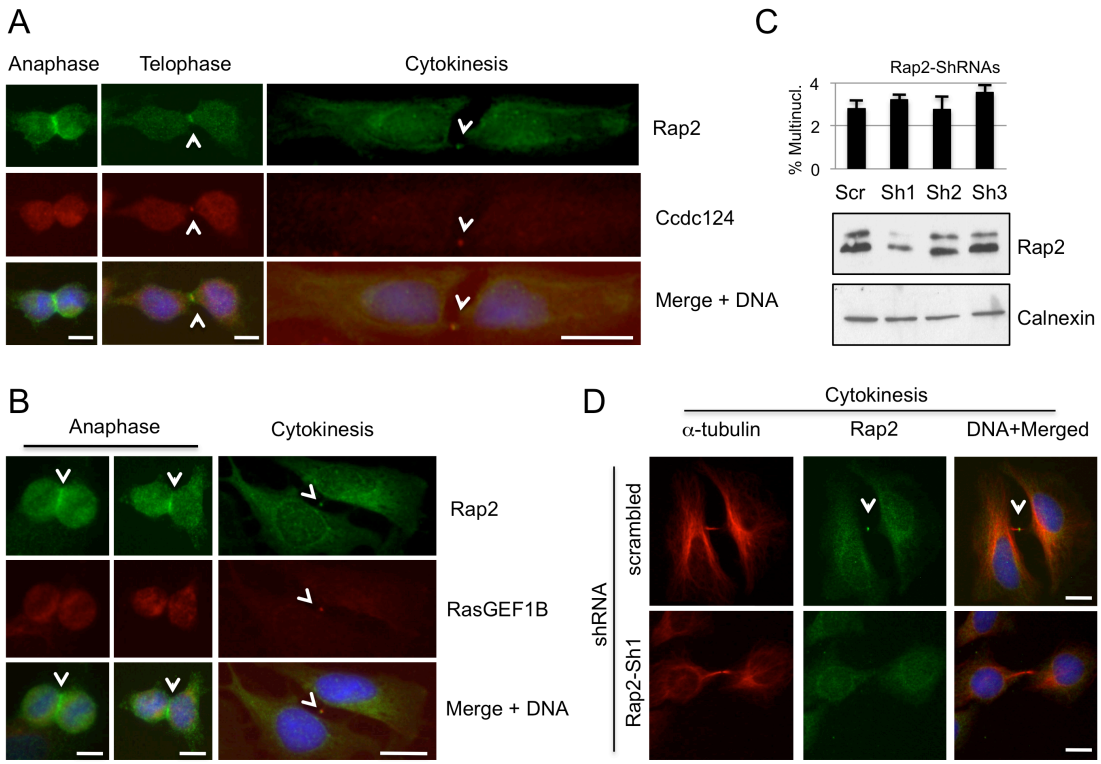
A
Anaphase
Telophase
Cytokinesis
Rap2
Ccdc124
Merge + DNA
C
Rap2-ShRNAs
% Multinucl.
4
2
0
Scr
Sh1
Sh2
Sh3
Rap2
Calnexin
B
Anaphase
Cytokinesis
Rap2
RasGEF1B
Merge + DNA
D
Cytokinesis
α-tubulin
Rap2
DNA+Merged
shRNA
scrambled
Rap2-Sh1

**Figure 9**

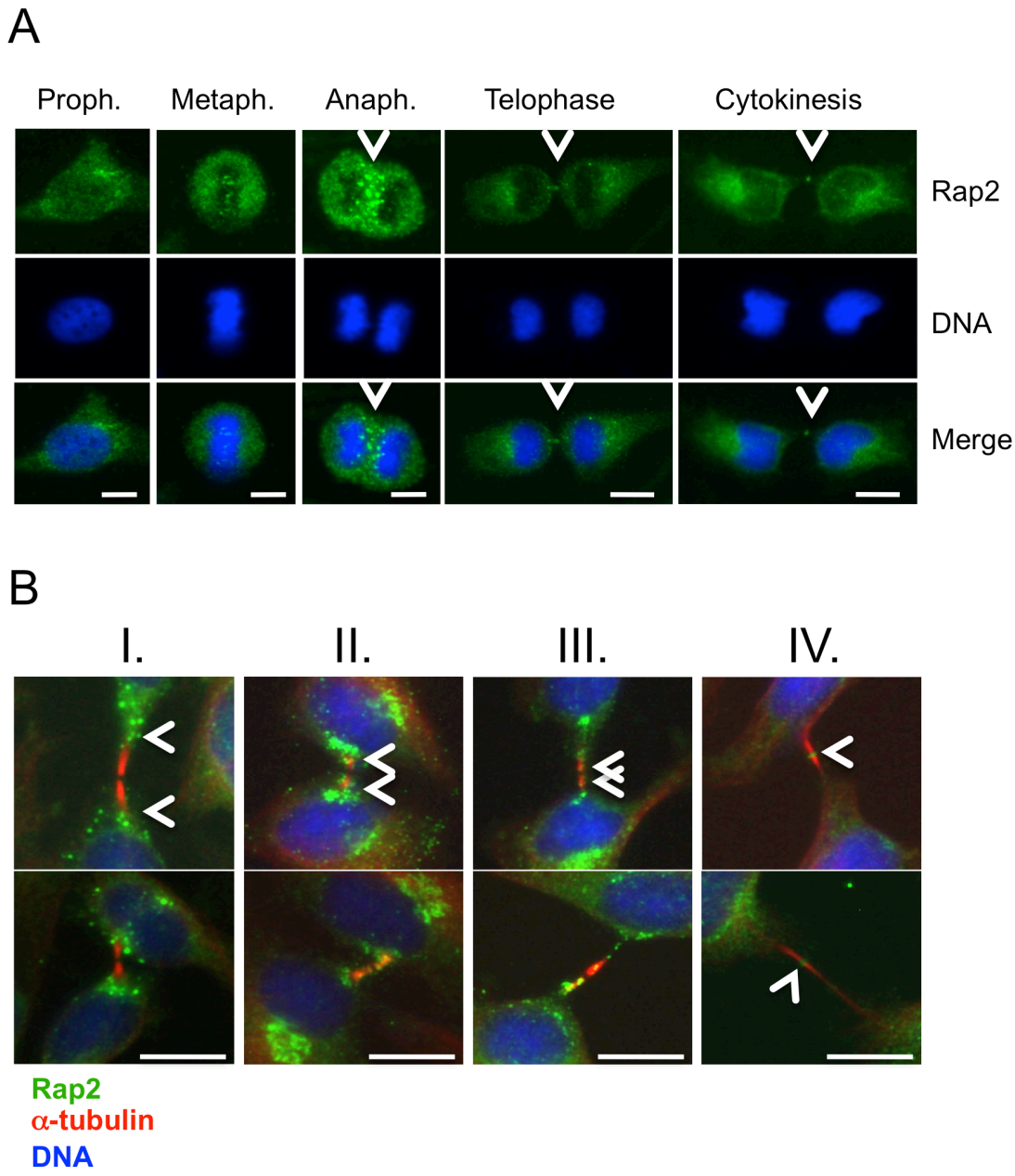
A
Proph.
Metaph.
Anaph.
Telophase
Cytokinesis
Rap2
DNA
Merge
B
I.
II.
III.
IV.
Rap2
α-tubulin
DNA

**Figure 10**

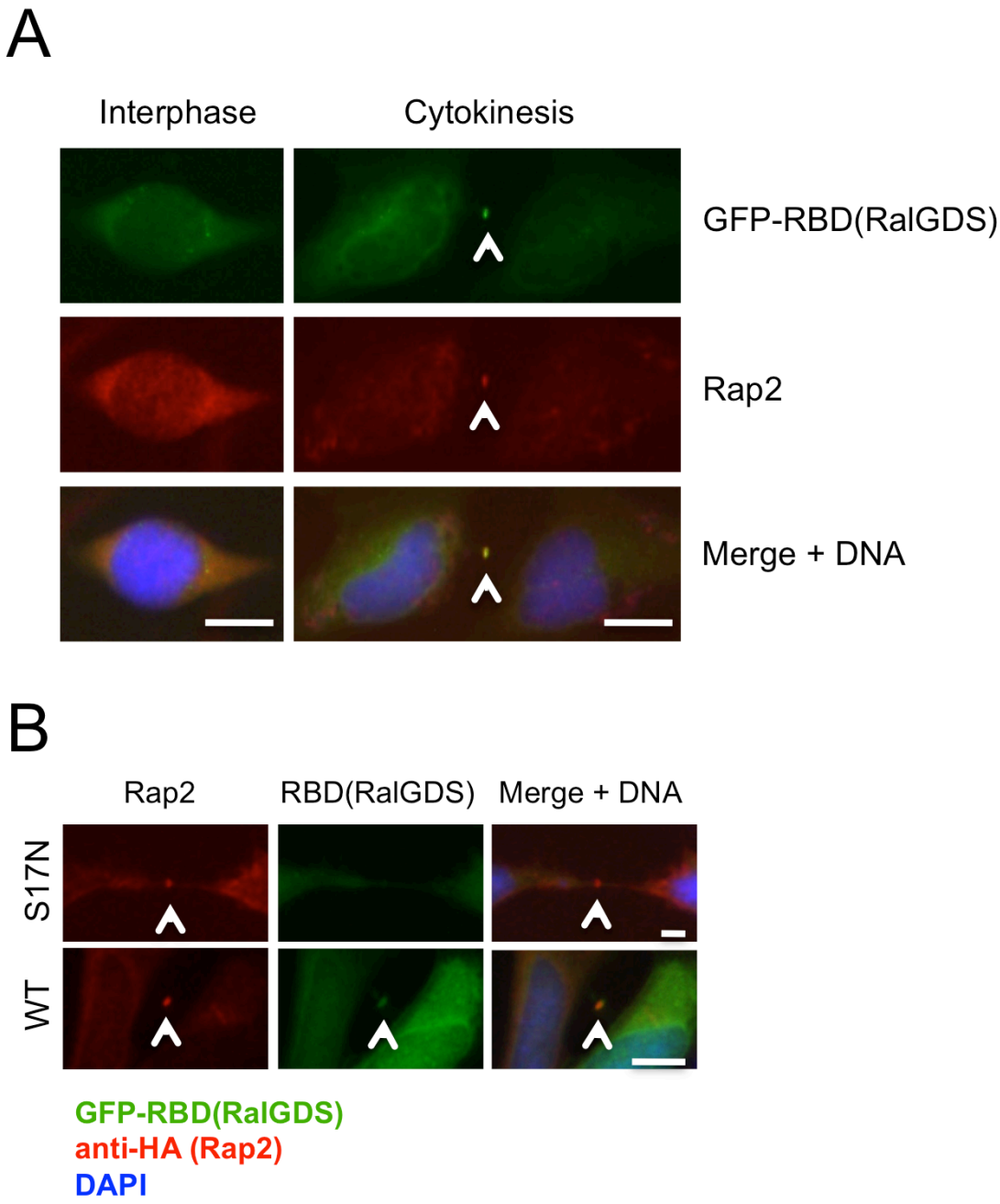
A
Interphase
Cytokinesis
GFP-RBD(RalGDS)
Rap2
Merge + DNA
B
Rap2
RBD(RalGDS)
Merge + DNA
S17N
WT
GFP-RBD(RalGDS)
anti-HA (Rap2)
DAPI

*3172–3185* *Nucleic Acids Research, 2010, Vol. 38, No. 10* *Published online 31 January 2010*
*doi:10.1093/nar/gkq023*

# Intronic elements in the Na+/I- symporter gene (NIS) interact with retinoic acid receptors and mediate initiation of transcription

**Hani Alotaibi[1], Elif Yaman[1], Domenico Salvatore[2], Valeria Di Dato[3], Pelin Telkoparan[1], Roberto Di Lauro[3,4] and Uygar H. Tazebay[1,*]**

[1]Department of Molecular Biology and Genetics, Bilkent University, 06800 Bilkent, Ankara, Turkey, [2]Department of Endocrinology and Molecular and Clinical Oncology, University of Naples 'Federico II', Via S. Pansini 5, 80131 Naples, [3]Stazione Zoologica Anton Dohrn (SZAD), Villa Communale, Naples and [4]BIOGEM, Biotechnology and Molecular Genetics in Southern Italy, 83031 Ariano Irpino, Avellino, Italy

Received November 19, 2009; Revised January 7, 2010; Accepted January 8, 2010

## ABSTRACT

**Activity of the sodium/iodide symporter (NIS) in lactating breast is essential for iodide ($I^-$) accumulation in milk. Significant NIS upregulation was also reported in breast cancer, indicating a potential use of radioiodide treatment. All-*trans*-retinoic acid (tRA) is a potent ligand that enhances *NIS* expression in a subset of breast cancer cell lines and in experimental breast cancer models. Indirect tRA stimulation of *NIS* in breast cancer cells is very well documented; however, direct upregulation by tRA-activated nuclear receptors has not been identified yet. Aiming to uncover *cis*-acting elements directly regulating *NIS* expression, we screened evolutionary-conserved non-coding genomic sequences for responsiveness to tRA in MCF-7. Here, we report that a potent enhancer in the first intron of *NIS* mediates direct regulation by tRA-stimulated nuclear receptors. *In vitro* as well as *in vivo* DNA–protein interaction assays revealed direct association between retinoic acid receptor-α (RARα) and retinoid-X-receptor (RXR) with this enhancer. Moreover, using chromatin immunoprecipitation (ChIP) we uncovered early events of NIS transcription in response to tRA, which require the interaction of several novel intronic tRA responsive elements. These findings indicate a complex interplay between nuclear receptors, RNA Pol-II and multiple intronic RAREs in NIS gene, and they establish a novel mechanistic model for tRA-induced gene transcription.**

## INTRODUCTION

In alveolar cells of the lactating mammary gland, the activity of $Na^+/I^-$ symporter (NIS) is required for the secretion of $I^-$ in mother's milk (1,2). $I^-$ in milk is then used by the newborn in thyroid hormone biosynthesis, and therefore it has an essential role in postnatal development of the baby (3). The timing of *NIS* expression in mammary epithelia is precisely synchronized with the onset of gestation and with lactation, and it ends when newborns stop suckling (2). NIS is not expressed in non-lactating mammary gland tissue unless experimental animals were treated with combinations of steroid and lactogenic hormones (2,4,5). Yet, a functional overexpression of NIS was detected in transgenic mice bearing experimental mammary tumors induced by mouse mammary tumor virus (MMTV) promoter-driven activated *Ras* and *Erb-B2/neu* oncogenes, polyoma middle-T antigen (PyMT), or cyclooxygenase-2 gene (2,6,7).

Relevant with the human breast cancer, increased NIS expression was also detected in about 70–80% of ductal carcinoma *in situ* and invasive breast cancer samples, as compared to the absence of NIS expression in healthy breast samples obtained in reductive mammoplasty operations (2,8). On the one hand, these results have raised the possibility that radioiodide may be used for diagnosis and treatment of breast cancer, as it is routinely used against thyroid cancer and its metastasis (9). On the other hand, only a small fraction of these NIS-positive tumors has the capacity to accumulate radio-labeled substrates of the symporter (2,4,8), suggesting that further enhancement of *NIS* expression or post-translational activation of NIS are required for an effective use of radio-labeled substrates for imaging and/or treatment of malignant breast disease.

*To whom correspondence should be addressed. Tel: +90 312 2902419; Fax: +90 312 2665097; Email: tazebay@fen.bilkent.edu.tr
Present addresses:
Hani Alotaibi, Department of Molecular Embryology, Max-Planck Institute of Immunobiology, Stuebeweg 51, D-79108 Freiburg, Germany.
Valeria Di Dato, Ceinge – Biotecnologie Avanzate s.c. a r.l. Via Comunale Margherita, 482, 80145, Naples, Italy.

Related with this, a number of hormones or ligands, such as retinoids (natural or synthetic analogs of vitamin A), human chorionic gonadotropin (hCG), dexamethasone (Dex) and troglitazone (a PPAR-γ ligand), were identified as molecules having an upregulatory effect on *NIS* expression and $I^-$ transport in the ERα-positive (ERα+) breast cancer cell model, MCF-7 (6,10–12). Retinoids have the most robust effect on *NIS* transcription, and among this group of ligands, all-*trans*-retinoic acid (tRA) is the most potent as it leads to an increase up to 10-fold both at the transcriptional level, as well as at the level of $I^-$ transport (10–12). Moreover, in immunodeficient mice model with MCF-7 cell xenografts, systemic tRA treatment stimulated NIS expression and radioiodide uptake around 15-fold in the implemented graft (7).

We have previously shown that, tRA induces *NIS* expression only in ERα+ mammary cell line models, and neither basal nor inducible *NIS* transcription is observed in ERα-negative (ERα−) mammary cell lines (13). ERα directly interacts with a responsive element in *NIS* promoter, and independent from the presence of estradiols the presence of ERα is important for maximal tRA induced *NIS* transcription (13). tRA stimulates *NIS* transcription also in human follicular thyroid carcinoma cell lines FTC-133 and FTC-238, and in these cells the effect of tRA is mediated by a RA response element (RARE) that is located at position –1375 relative to human *NIS* start codon (14). Dentice *et al.* (15) have shown that the cardiac homeobox transcription factor Nkx2.5 is induced by tRA, and this factor is involved in the upregulation of *NIS* transcription by binding to two *cis*-acting elements in *NIS* promoter.

Conserved transcriptional expression patterns of orthologous and paralogous genes could reflect common molecular regulatory mechanisms, as well as the presence of conserved regulatory *cis*-acting elements. Results supporting this view have previously been published for the *Drosophila* homeotic (hox) gene complex (16), and similar observations were reported for *NIS* (17). For instance, when the entire 5′-flanking sequences starting from *NIS* coding region up to the upstream neighboring gene (*RPL18A*) were compared, it was found that the similarity between rat and human sequences is only 11.8%. Yet, the similarity ratios of previously established *cis*-acting elements that are located in the same sequence are remarkably high, for example, in the NIS upstream enhancer (NUE), which is a strong thyroid-stimulating hormone (TSH) responsive enhancer that is localized between −9470 and −9046 on the human *NIS* and −2611 and −2230 on the rat *Nis* is 70% similar (18,19). Again, as expected, the basal promoter of the human *NIS* (–475 to −393) has ∼72% similarity with the rat *Nis* promoter (17). In this study, we initially undertook a comparative genomics approach in order to identify evolutionary conserved sequences that could play a role in tRA-dependent *NIS* regulation. Subsequently, our experimental studies resulted in the identification of a potent intronic enhancer, which binds RARα and RXR, and upon stimulation by tRA activates *NIS* promoter both *in vitro* and *in vivo*. We also show that the initiation of transcription by tRA involves interactions between several identical RARE sequences found in multiple introns of the gene and RA stimulated nuclear receptors *in vivo*. We present a novel as well as a rather complex and dynamic interplay between putative RA responsive *cis*-acting elements, RNA Pol-II and RA-stimulated nuclear receptors during *NIS* transcription.

## MATERIALS AND METHODS

### Sequence information and databases

Genomic DNA sequences to be analyzed for DNA conservation in non-coding sequences were obtained from the Genome Browser database at the University of California Santa Cruz (20). The analysis was performed on 90-kb sequences from *Homo sapiens* (Release July 2003; Chr. 19: 17816282-17906905), *Rattus norvegicus* (release June 2003; Chr. 16: 19018698-19107000) and from *Mus musculus* (Release October 2003; Chr. 8: 71152446-71242000). Annotations for the human sequence were obtained from the Genome Vista database, and sequences were aligned with the mVista tool using the human sequence at the *x*-axis and at 50% conservation level and a window length of 75 bp.

### Polymerase chain reaction amplification of conserved regions

Conserved regions clustered within about 1 kb were amplified by polymerase chain reaction (PCR) as one larger fragment and subsequently cloned into the reporter vector. PCR amplification was performed in 25-μl reaction volumes containing 0.8 × PCR buffer, 3 mM $MgCl_2$, 200 μM dNTP, 10 pmol of each primer (see Supplementary Table S1 for primer sequences), 5% DMSO, 1 U of *Taq* DNA polymerase (Roche) and 100 ng of human genomic DNA. Thermal cycler conditions were an initial denaturation step at 94°C for 4 min; a loop cycle of 94°C, 30 s/62°C, 30 s/72°C, 40 s; and a final extension at 72°C for 7 min.

### Reporter vector constructs

The reporter pGL3-E1b is a modified version of the original plasmid pGL3-Basic (Promega), which contains the E1b TATA element (5′-TCG AGT CTA GAG GGT ATA TAA TGG ATC-3′) between XhoI/BglII sites of pGL3-Basic; destroying the BglII site while keeping the XhoI site intact. PCR products containing conserved regions were cloned into MluI/XhoI sites of pGL3-E1b to produce the reporter plasmids named clusters (Cl) 1, 2, 3, 4, 5, 6 and 7.

Cluster 3 derivatives containing individual or combined conserved regions were prepared by restriction endonuclease digestion of internal sequences, or by PCR. The plasmid Cl3-1 was prepared by removing EspI/XhoI fragment from cluster 3, likewise plasmids Cl3-pm, Cl3 Δ3-4, Cl3-xp and Cl3-4 were prepared by removing the PvuII/MluI, the PstI/SmaI, the XhoI/PvuII and the SacI fragments, respectively. The plasmids Cl.3-2 and Cl3-3 were prepared by cloning PCR product containing each

conserved region using the primers shown in Supplementary Table S2. Subsequently, PCR products were cloned into MluI/XhoI sites of pGL3-E1b.

The plasmid DR2-1del was created by introducing a 490-bp deletion in Cl4Wt, deletion was created using restriction enzyme digestion with MluI and BalI. MluI digested overhangs were filled by incubating the digestion products with 5 U of Klenow fragment of DNA polymerase I (Fermentas) in the presence of 50 μM dNTP at 37°C for 1 h prior to ligation.

The plasmid Cl4-R was prepared by cloning the insert from Cl4Wt into BamHI and SalI sites downstream of the luciferase reporter. Cl3-pm was created by removing the sequence between PvuII and MluI from Cl3. The reporter Cl4-pm was created by replacing the MluI/PvuII fragment from Cl3 with KpnI/XhoI fragment containing Cl4 insert. Finally, Cl34-pm was prepared by cloning the insert from Cl4 into BamHI/SalI of Cl3-pm.

### Site-directed mutagenesis

Site-directed mutagenesis was performed on constructs harboring the retinoic acid response elements in clusters 3 and 4. Summary of the oligonucleotides used in this procedure is presented in Supplementary Table S2. PCR-based mutagenesis was performed in 50-μl reaction volumes containing 40 ng of target plasmid DNA, 1× Pfu buffer, 200 μM dNTP mix, 100 ng of each primer and 2.5 U of *Pfu*-Turbo DNA polymerase (Stratagene). Reaction conditions were an initial denaturation step at 95°C for 30 s followed by 15 cycles of 95°C for 30 s/55°C for 1 min/68°C for 6 min and 20 s. Following the PCR reaction the tubes were cooled to 37°C on ice and then 1 μl of DpnI (10 U/μl; Fermentas) was added and incubated at 37°C for 1 h. Following the DpnI digestion of the parental (methylated) strand, 5 μl were used for transformation of super-competent *E. coli* (DH5α) cells. Plasmids were rescued from single colonies and checked for the presence of the mutation by automated DNA sequencing.

### Luciferase reporter assay

MCF-7 cells were maintained in high glucose DMEM (Gibco) supplemented with 10% fetal bovine serum (FBS), 1% penicillin/streptomycin (P/S) and 1% L-glutamine (Biochrom), at 37°C in a 5% $CO_2$ incubator. Cells were transfected with plasmid DNAs using FuGENE-6 reagent (Roche). FuGENE:DNA ratios were determined experimentally to be 3:1. Cells were seeded in 24-well plates in DMEM; so that they would reach confluence at the time of the assay. Two days later, and 1 h prior to transfection, cells were washed twice with phosphate-buffered saline (PBS), and the medium was replaced with DMEM lacking antibiotics. Transfection was carried out with 200 ng of reporter vector plus 3 ng phRL-TK (Promega) to normalize for transfection efficiency. Two days post-transfection, medium was changed with fresh DMEM containing 1 μM tRA (Sigma) and continued incubation for 24 h, dimethyl sulfoxide (DMSO) was used as vehicle control. Then the cells were harvested and luciferase reporter assays were performed using the Dual-Glo Luciferase Assay system (Promega). Luciferase values for all samples were normalized by first subtracting the background of untransfected control, and then dividing firefly luciferase values over those of *Renilla* luciferase. Fold induction is relative to the value of the empty vector. Fold stimulation was calculated by dividing the values of the tRA-stimulated sample by the DMSO control sample and relative to the vector containing promoter only control. Experiments were performed at least three times in duplicates.

### Electrophoretic mobility shift assay

Nuclear extracts were prepared using the NE-PER solution (Nuclear and Cytoplasmic Extraction Reagents – Pierce Biotechnology). Sub-confluent MCF-7 cells grown in 150-mm plates were treated with 10-nM E2 (for maximal RARα expression) for 6 h and then harvested by trypsinization and collected by centrifugation at 1200 r.p.m. Nuclear protein extraction was performed using 50 μl packed cell volume samples according to the manufacturer's procedure. Oligonucleotide labeling was performed using the Biotin 3′ End Labeling Kit (Pierce Biotechnology). The labeling reactions contained 1× TdT reaction buffer, 100 nM unlabeled oligo, 0.5 μM Biotin-11-UTP and 10 U TdT in 50-μl reaction volumes. Electrophoretic mobility shift assay (EMSA) experiments were performed using the Lightshift Chemiluminescent EMSA kit (Pierce Biotechnology) according to the protocols provided. In brief, binding reactions included 1 × binding buffer, 2.5% glycerol, 5 mM $MgCl_2$, 50 ng/μl Poly (dI•dC), 0.05% NP-40, 4 pmol of unlabeled oligo, 5 μl nuclear extract and 20 fmol of biotin labeled oligo. For the super shift reaction 1 μg of anti-RARα (C-20, Santa Cruz) or anti-RXR (F-1, Santa Cruz) antibodies were included to the reaction just before adding the Biotin labeled oligos (Supplementary Table S2). Binding reactions were incubated at room temperature for 40 min and then resolved on a 6% native polyacrylamide gel in 0.5× TBE in a minigel electrophoresis apparatus (dimensions 8 × 8 × 0.1 cm). After electrophoresis, complexes were electro-transferred to Hybond-N+ nylon membranes (Amersham), and then cross-linked in the GS Gene Linker (Bio-Rad) at an energy level of 150 mJ. Chemiluminescent detection of biotin-labeled DNA was performed according to the supplier's protocol (Pierce Biotechnology).

### Chromatin immunoprecipitation

MCF-7 cells (in 6-well plates) grown in steroid-free and phenol-red-free DMEM (Gibco) were treated with 1 μM tRA (Sigma) in the presence of 10 nM estradiol (Sigma). Formaldehyde cross-linking [1% (w/v)] was performed for 10 min at room temperature. Cross-linking was terminated by the addition of glycine to a final concentration of 125 mM. Cells were scraped in PBS, divided into two tubes and lysed in 400 μl lysis buffer [1% SDS, 10 mM EDTA, 50 mM Tris–HCl (pH 8.0) and 1 × protease inhibitor cocktail]. Cell lysates were then sonicated twice in the

ultrasonic processor VCX-500 (Sonics and Materials, INC.), each for 15 min at 4°C using a pulse of 30 s and 80% amplitude. Cell lysates were cleared by centrifugation at 13 000 r.p.m. for 10 min, diluted to 6.1 ml in dilution buffer [0.01% SDS, 1.1% Triton X-100, 1.2 mM EDTA, 16.7 mM Tris–HCl (pH 8.0), 167 mM NaCl and 1× protease inhibitor cocktail]. At this point, 100 µl of chromatin solution was removed and labeled as 'Input'. Chromatin solution was precleared by adding 50 µl of protein A-Sepharose CL-4B (GE Healthcare) as 50% slurry containing 0.5 mg/ml BSA (Sigma), 200 µg/ml sonicated salmon sperm DNA (Sigma) in TE (pH 8.0) for 60 min. at 4°C. Immunoprecipitation was performed at 4°C for 16 h using chromatin immunoprecipitation (ChIP)-grade antibodies against RARα (H1920, Abcam), RXR (F-1, Santa Cruz), Pol-II (N-20, Santa Cruz) and FGFR1 (C-15, Santa Cruz). Then, immunocomplexes were incubated with 50 µl protein A-Sepharose (50% slurry) for at least 16 h at 4°C. Afterwards, beads were collected, washed four times in wash buffer I [0.1% SDS, 1% Triton X-100, 2 mM EDTA, 20 mM Tris–HCl (pH 8.0) and 150 mM NaCl], and twice in wash buffer II (0.1% SDS, 1% Triton X-100, 2 mM EDTA, 20 mM Tris–HCl (pH 8.0) and 500 mM NaCl]. Precipitated DNA (as well as the inputs) was recovered using a solution of 10% Chelex (Bio-Rad) and Proteinase K, and was used for qPCR amplification. Primers used for qPCR amplification are presented in the Supplementary Table S3. Quantitative real-time PCR was performed using iQ™ SYBR® Green Supermix (BioRad) and amplification was performed in the Mx3005P® QPCR System (Stratagene) using the following cycling parameters: 95°C for 10 min, then 45 cycles of 95°C for 15 s followed by 64°C for 15 s and 72°C for 20 s, and a melt curve starting at 55°C with 0.5°C increments for 80 cycles, except for intron 8 element, annealing temperature was 58°C. Data was normalized to the background (No Ab) and calculated as fold enrichment over the control IgG (FGFR1) applying the formula $[2^{-(\text{normalized Ct sample - normalized Ct IgG})}]$. Parallel PCR reactions were performed for agarose gel electrophoresis analysis, PCR parameters were an initial denaturation at 95°C for 5 min and 19 cycles of 15 s at 95°C, 15 s at 64°C and 20 s at 72°C. PCR products were resolved on a 2% agarose gel stained with ethidium bromide. At least three qPCR reactions in triplicates were performed on two independent ChIP experiments.

### mRNA expression analysis

A small fraction of the cells used for ChIP analysis was used for expression analysis. RNA was prepared using the Nucleospin RNA II kit (Macherey-Nagel) as recommended by the manufacturer. RNA quality was checked spectrophotometrically and quantified using NanoDrop 2000 (Thermo Scientific). Two micrograms of total RNA were used for cDNA synthesis using the Revert-Aid First Strand cDNA Synthesis Kit (Fermentas). NIS and GAPDH primers used for real-time PCR quantification are presented in Supplementary Table S3. Quantitative real-time PCR was performed as described above. Cycling parameters were similar with annealing temperature of 60°C. Quantification was performed using the ΔΔCt method. Data represent three qPCR experiments in triplicates from two independent samples.

### Statistical analysis

Statistical significance was determined by performing the Student's *t*-test (Figures 4D, 6 and 7A) or paired Student's *t*-test (Figures 2, 3, 4C and 7C) using a 95% confidence interval; *P*-values $<0.05$ were considered significant.

## RESULTS

### Comparative genomics identifies potential *cis*-acting elements controlling *NIS* transcription

We analyzed the conservation of non-coding DNA sequences of NIS by comparing genomic sequences in three species, *R. norvegicus*, *M. musculus* and *H. sapiens*. Conserved sequences at non-coding regions (defined as windows of 75 bp with 50% nucleotide identity) were identified in pair-wise alignments using the VISTA program (21). Figure 1 shows the results of the VISTA alignment in which the short conserved regions that are localized in non-coding sequences and that meet the selected criteria were highlighted in pink. Conserved regions clustered within 1 kb were later studied as single blocks and they were named as cluster 1, cluster 2, cluster 3 and so forth (Supplementary Table S1). This grouping of conserved regions facilitated subsequent functional analyses.

### Conserved clusters 3 and 4 respond to tRA in MCF-7 cells

Identified individual conserved regions that were located in clusters varied between 13 (as in cluster 6) and 244 bp (as in cluster 3) in length (Figure 1). We studied tRA responsive transcriptional activation capacities of these regions in MCF-7 cells in which, induction of NIS gene by tRA was previously reported (7,10,13). We amplified clusters of interest by PCR using human genomic DNA as a template, and we cloned these fragments into the luciferase reporter vector pGL3-E1b as described in 'Materials and Methods' section. Previously characterized NIS upstream enhancer, which contributes to the regulation of this gene in thyroid cells (18,19), was located in the coding sequence of the neighboring upstream gene, *RPL18A*. This region, named as 'cluster 1', was also included in our analysis in order to assess a possible function of this enhancer in a mammary cell system. All vector constructs were transiently transfected into MCF-7 cells, which were subsequently treated with either DMSO (as vehicle control) or 1 µM tRA for 24 h, and the regulatory potentials of these conserved clusters were assessed by luciferase reporter assays. As a result, we found that only clusters 3 and 4 significantly responded to the tRA stimulus (Figure 2).

Cluster 3 is a 1.1-kb sequence upstream of the human *NIS*, located from -1138 to -42 relative to the transcription start site (22,23). In a previous study, the tRA responsiveness of the human *NIS* promoter was attributed

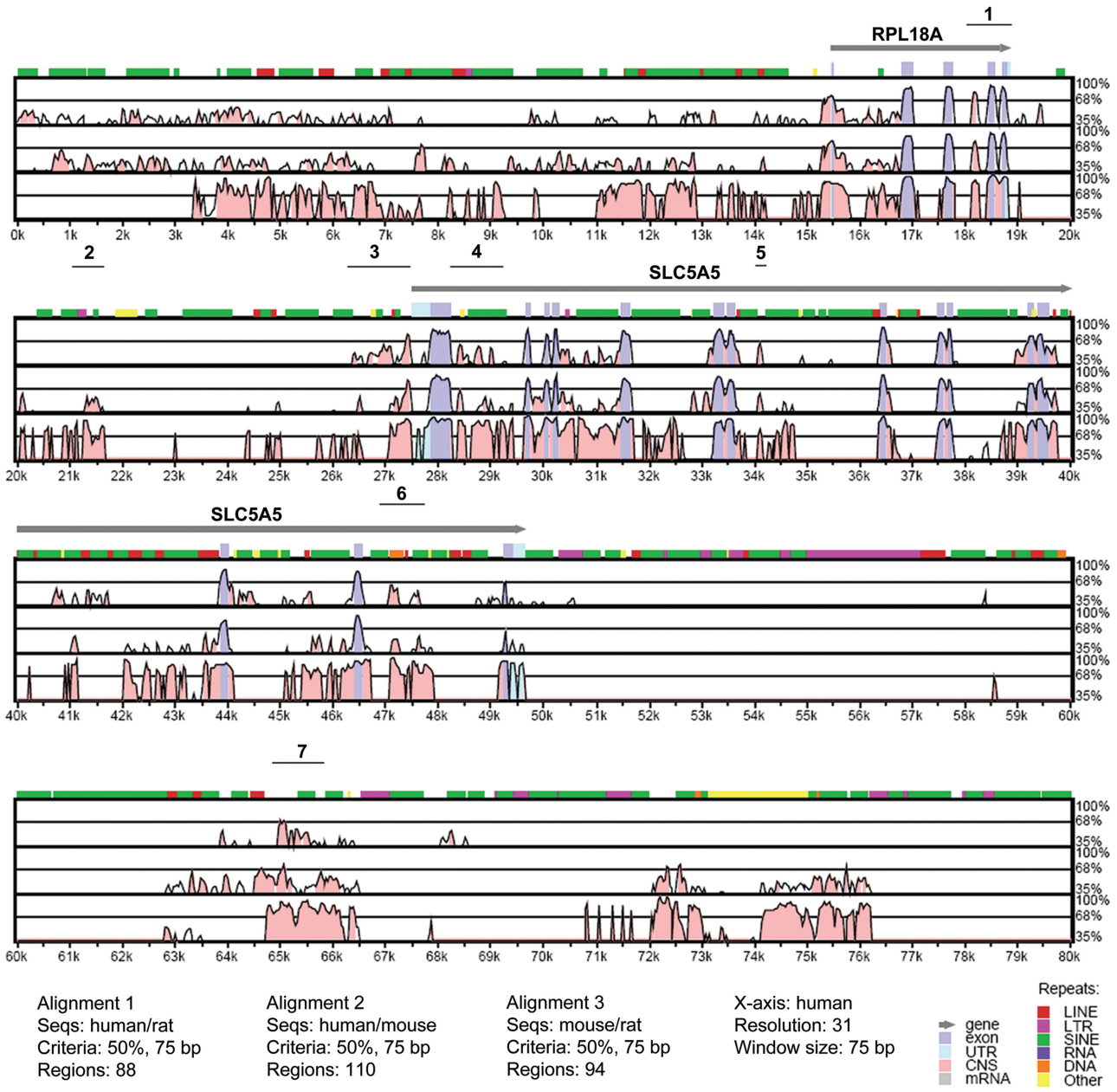


**Figure 1.** VISTA plot of sequence conservation in a 90-kb genomic DNA in human, mouse and rat. Percent nucleotide identities between human, mouse and rat DNA sequences are plotted as a function of position along the human sequence. Peaks of evolutionary conservation in overlapping exonic sequences are shaded blue. Aligned regions of >50% identity over 75 bases are shaded pink. Lines above each alignment indicate the position of the conserved cluster selected for PCR amplification. Only 80 kb of the alignment is shown.

to a RARE which is located between bases 125 and 146 of this cluster [at −1375 relative to the ATG, (14)]. In order to assess the functionality of this RARE in MCF-7 cells, we created a mutant version of Cl3, in which we introduced the same mutation (Figure 3A) that completely abolished tRA response from this sequence in thyroid cell lines (14). Interestingly, this mutation had a minor effect on tRA stimulation of Cl3, reducing the tRA stimulation by only 7% (Figure 3B), indicating that this RARE is not the major RA responsive site in MCF-7. This result suggests the presence of an alternative site for tRA responsiveness in mammary cell systems. To this end, we created deletion mutants of Cl3 in reporter plasmids, which contained individual as well as combined conserved regions (Figure 3C and results not shown). These constructs were then tested for tRA responsiveness using luciferase reporter assays in MCF-7. Despite intensive analysis on a relatively large number of overlapping deletion mutants, a tRA responsive region other than the previously identified RARE could not be found in Cl3 (see Figure 3C for a summary of our results). On the other hand, removal of conserved region 3–4 (~100 bp) has significantly reduced the magnitude of tRA response and the overall transcriptional potential

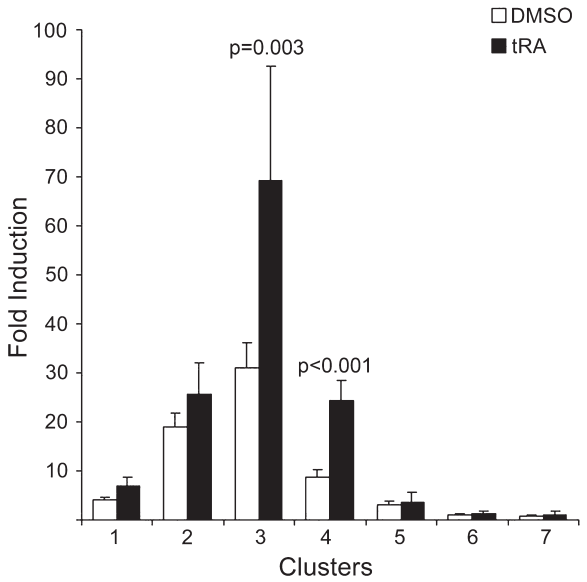


**Figure 2.** Conserved clusters 3 and 4 respond to tRA in MCF-7. Conserved clusters were amplified by PCR and cloned into the luciferase reporter plasmid pGL3-E1b. MCF-7 cells were transfected with all conserved clusters and treated with tRA or DMSO for 24 h. Of the seven clusters analyzed, only clusters 3 and 4 were significantly responsive to tRA treatment. *P*-values for the tRA-induced samples were calculated using paired Student's *t*-test with 95% confidence interval, values <0.05 were considered significant.

of this construct (Figure 3C), indicating the presence of elements essential for maximum levels of transcription. These results suggest that tRA responsiveness of Cl3 requires a synergistic effect of multiple regulatory elements.

### A functional RARE is present in the first intron of *NIS*

Cluster 4 is a 774-bp sequence located in the first intron of the human *NIS*. This cluster is composed of three conserved regions numbered from 4-1 to 4-3 (Figure 4A). A closer look at the sequence composition of this cluster revealed the presence of three putative RAREs. The first is a perfect DR2-type consensus RARE sequence (24) (DR2-1: AGGTCAggAGTTCA) located in the second conserved region (region 4-2) and starting at +927 relative to the ATG. The second is a DR10-type sequence [DR10: AGGTGG$_{(n_{10})}$AGGTCA], located just after the third conserved region (region 4-3) and starting at +1206 relative to the ATG. The third is, again, a DR2-type sequence identical to DR2-1 (DR2-2: A GGTCAggAGTTCA) and is located at +1222 relative to the start codon, overlapping with the DR10-type sequence described above (Figure 4A). A series of pGL3-E1b-based luciferase reporter constructs containing different fragments of this intronic region, as well as *in vitro* mutagenized versions of putative RARE sequences were constructed. A summary of mutations created is presented in Figure 4B. Functional activity of these RARE sequences was assessed by transient transfections followed by luciferase reporter assays in MCF-7 cells treated either with DMSO (as vehicle control) or with 1 μM tRA for 24 h. In MCF-7 cells transfected with the wild-type construct, tRA treatment results in an increase of about 4-fold when compared to cells treated with DMSO. This result confirmed once again that the intronic region contains tRA responsive sequences (Figure 4C; Cl4Wt), which have the capacity to activate the transcription of the reporter gene. A very small deletion (3 bp) that changed the second half-site of DR2-2 but left the DR2-1 and DR10 sequences intact abolished entirely the tRA responsive activity (Figure 4C; DR2-2del), indicating that DR2-2 has a functional role in ligand responsive activation of reporter expression. Moreover, when single or double point mutations were introduced by *in vitro* mutagenesis in each half site of the DR2-2, the tRA response was completely lost (Figure 4C; DR2-2mut1 and DR2-2mut2). However, removal of the DR2-1 region from the construct by introducing a 490-bp deletion did not make any effect at all on tRA responsive activity of the reporter, showing that DR2-1 is fully dispensable for tRA response (Figure 4C; DR2-1del). Absence of the DR10 element both in an otherwise wild-type intronic fragment context, and in the context of a fragment missing the DR2-1 element (DR2-1del) did not abolish tRA responsiveness coming from this region (Figure 4C; DR10mut and DR2-1del/DR10mut), but they had a minor effect on the magnitude of the response (2- to 3-fold stimulation).

We also investigated the potential of this intronic RARE to activate transcription through the native *NIS* minimal promoter. For this purpose, we constructed reporter plasmids containing the minimal *NIS* promoter (218 bp of *NIS* upstream region between −260 bp and −42 bp relative to transcription start site, and capable of initiating transcription as assessed by functional reporter assays, Figure 3C) controlled by Cl4 sequence either upstream of the promoter element or downstream of the reporter sequence (mimicking its location in the intron of *NIS*). Similar constructs were also prepared using the viral TATA element, E1b. As anticipated, Cl4 significantly activated *NIS* promoter in response to tRA when positioned either at the 5′ ($P < 0.0001$, $n = 8$) or at 3′ of the reporter ($P = 0.005$, $n = 8$), in agreement with the function of an enhancer (Figure 4D). On the other hand, regarding E1b promoter activation, Cl4 responded to the tRA stimulus only when positioned at the 5′ of the promoter element. Altogether these findings clearly indicate that the DR2-2 sequence can act as a RA responsive element, and it is the major RARE that is present in the first intron of human *NIS*.

### RARα and RXR physically interact with the intronic response element DR2-2 both *in vitro* and *in vivo*

Retinoids exert their effects by binding to nuclear retinoic acid receptors (RARs) and retinoid-X-receptors (RXRs), which in turn interact with *cis*-acting regulatory elements, or RAREs, and stimulate transcription of target genes. Consistently, previous work of Kogai *et al.* (12) has indicated that tRA stimulation of human *NIS* is mediated by RAR and RXR. In the presence of tRA, RAR could form homo- or hetero-dimers with RXR,

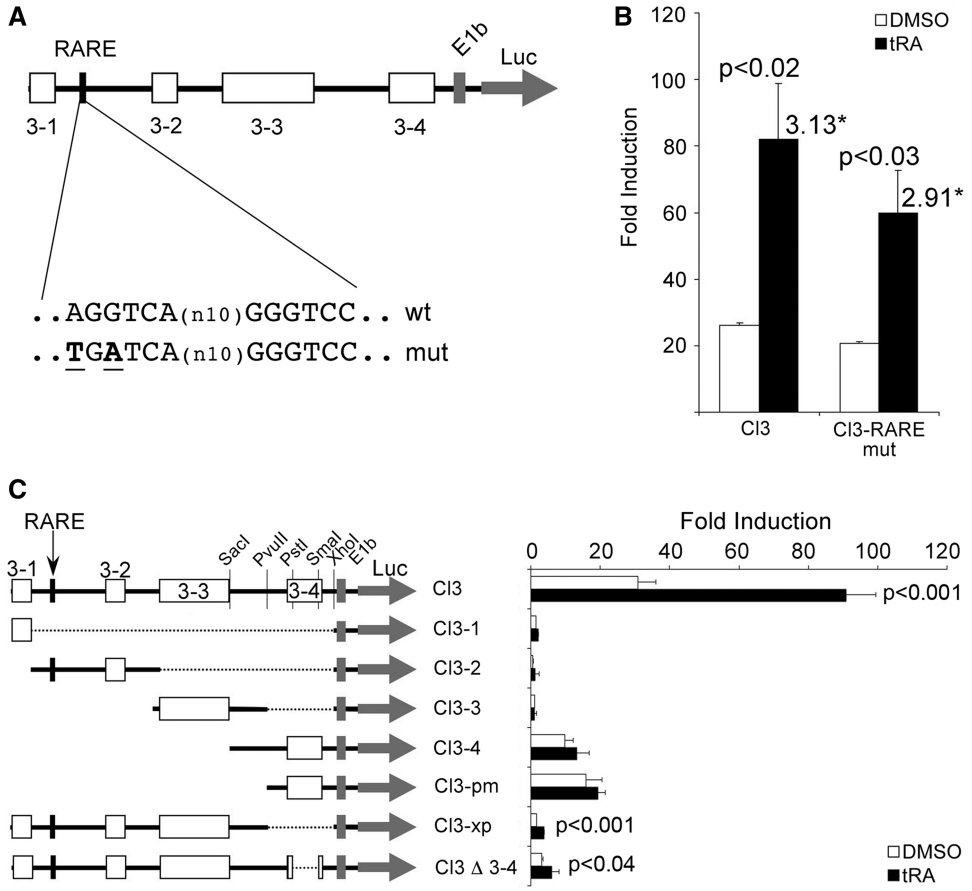


**Figure 3.** Stimulation of conserved cluster 3 is indirect and distinct from that in thyroid cells. (**A**) Map of Cl3, conserved regions are represented by boxes labeled 3-1 to 3-4, the previously characterized RARE is indicated by the black box, the wild type and the mutant sequences are shown below the map. (**B**) MCF-7 cells were transiently transfected with either the wild type or the mutant construct, cells were treated with tRA or DMSO and luciferase assays were performed. (**C**) Several deletion mutants were prepared to study the transcriptional potential in response to tRA stimulation of individual or combined conserved regions of Cl3. Plasmids were transfected to MCF-7 cells, followed by tRA (or the vehicle DMSO) treatment for 24 h, then luciferase assays were performed. The luciferase values were normalized to those of *Renilla* luciferase; fold induction was calculated relative to the empty vector. *Numbers above bars indicate the overall fold stimulation by tRA. *P*-values for the tRA-induced samples were calculated using paired Student's *t*-test with 95% confidence interval, values <0.05 were considered significant.

and the dimer mediates ligand-dependent gene activation by physically interacting with RAREs in RA responsive genes. In order to establish whether RAR and/or RXR have the potential to bind the DR2-2 element, we designed oligonucleotide probes corresponding to the wild-type DR2-2 sequence, or a variant of DR2-2 where single-point mutations were introduced in each half-site (Supplementary Table S2). We then studied *in vitro* binding capacities of the two nuclear receptors (RARα and RXR) to these probes by EMSA experiments (Figure 5). Initially, we have prepared nuclear extracts from 17-β-estradiol (E2)-treated MCF-7 cells, and we determined the abundance of both RARα and RXR in nuclear extracts by immunoblotting (data not shown). Subsequently, we incubated nuclear extracts with biotin-labeled probes containing either a consensus RARE that was known to interact with RARα and RXR, the wild-type DR2-2 sequences, or the mutant form of DR2-2. As expected, we have clearly observed retarded complexes when nuclear extracts were incubated with probes carrying the consensus RARE, or the novel element, DR2-2 (Figure 5, lanes 2 and 7). On the other hand, the introduction of point mutations into DR2-2 half-sites abolished this shift (Figure 5, compare lanes 7 and 12), unequivocally proving that these band shifts were observed as a result of direct interactions between the nuclear factors and the DR2-2 element (Figure 5, shown with bold arrows). A retarded band marked by an asterisk has indicated a DR2-2 independent interaction between nuclear proteins and the DNA probe. All bands were appropriately competed or shifted, confirming the specificity of the interactions (Figure 5, lanes 3, 8 and 13). In order to test whether the two nuclear transcription factors of interest, RARα and RXR, interact with DR2-2, we have added factor-specific monoclonal antibodies to our binding reactions. Both RARα and RXR antibodies caused a super shift in the consensus RARE and in DR2-2 probe (arrowheads), while they failed to do so when probes carrying point mutations on DR2-2 were used (Figure 5, for RARα compare lanes 4, 9 and 14; for RXR see lanes 5, 10 and 15). These results clearly indicate direct interactions between the nuclear

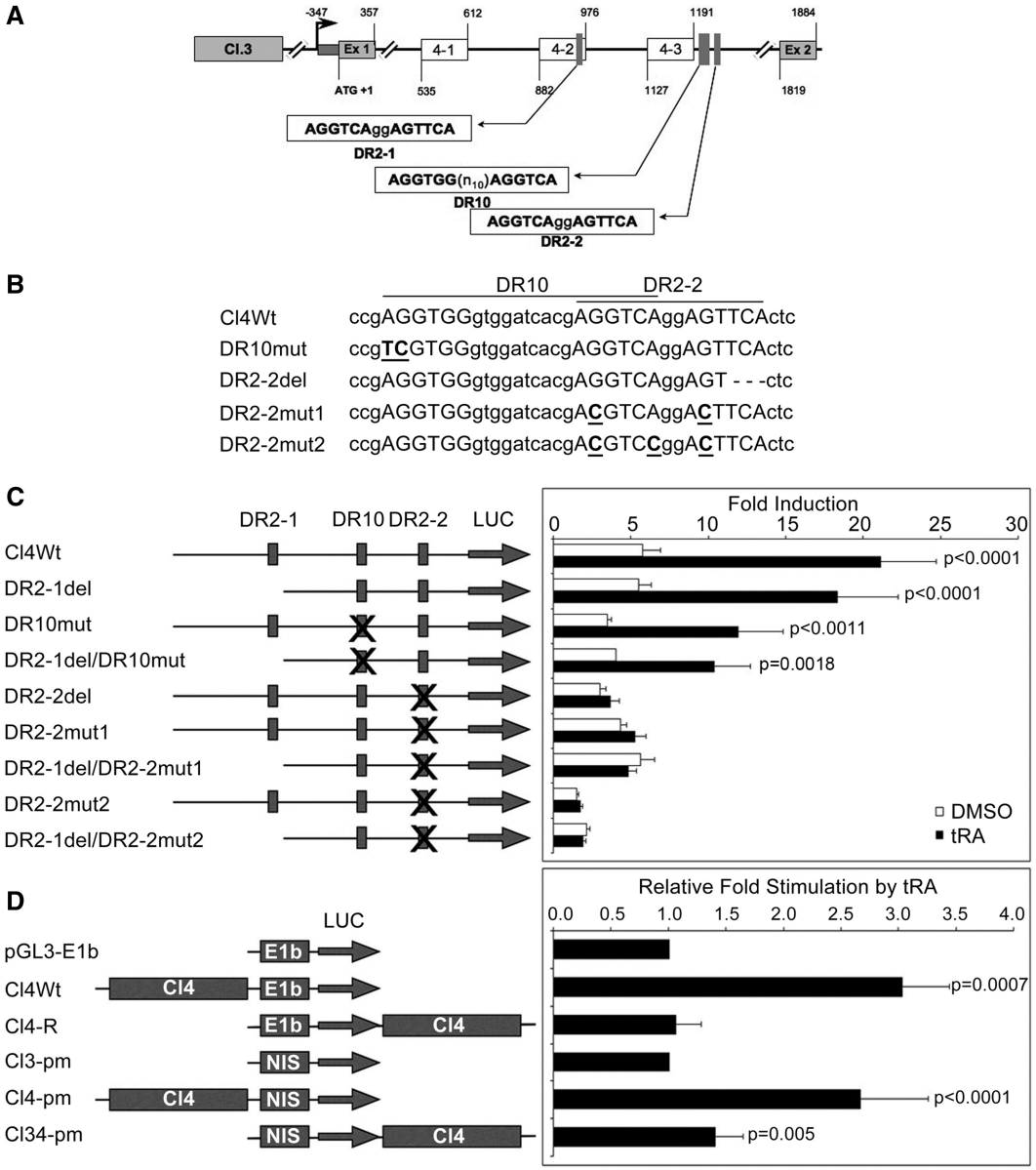


**Figure 4.** A Functional RARE (DR2-2) is present in the first intron of *NIS*. (**A**) Representation of conserved regions and putative RARE sequences in cluster 4. The boxes labeled 4-1 to 4-3 represent the position of the three conserved regions; the positions of putative RARE sequences, transcription start site and the ATG are indicated. Ex 1 and Ex 2 indicate positions of exons 1 and 2, respectively. (**B**) Sequence representation of the Cl4 variants used, RARE half sites are capitalized and mutated nucleotides are underlined and bolded, deleted nucleotides are replaced with dashes. (**C**) MCF-7 cells were transiently transfected with Cl4Wt or its mutant derivatives, cells were treated with tRA (or DMSO) for 24 h and luciferase reporter assays were performed. Luciferase values were normalized to those of *Renilla* luciferase and the fold induction is represented relative to the empty vector. Reporter constructs are presented in the drawing on the left; putative RAREs are indicated by vertical boxes, an X on a box indicates the RARE being altered. *P*-values were calculated using paired Student's *t*-test with 95% confidence interval, values $<0.05$ were considered significant. (**D**) MCF-7 cells were transfected with Cl4 controlling either the viral E1b promoter or the native *NIS* promoter (fragment NIS in Cl3-pm, see 'Materials and Methods' section). The sequence for Cl4 was located either 5′ of the promoter, or 3′ of the luciferase reporter. Luciferase assays were performed as mentioned above. Fold stimulation by tRA was calculated relative to the vector containing only the promoter element. *P*-values were calculated using Student's *t*-test with 95% confidence interval, values $<0.05$ were considered significant. Drawings are not to scale.

transcription factors RARα/RXR and the novel intronic RARE, DR2-2.

Subsequently, in order to assess whether RARα and/or RXR occupies the DR2-2 element in response to tRA *in vivo*, we carried out a series of ChIP experiments in MCF-7 cells. In the presence of RARα or RXR antibodies, a DNA fragment containing the DR2-2 element was precipitated from formaldehyde cross-linked total cell lysates (Figure 6). In contrast, the unrelated control IgG against fibroblast growth factor receptor 1 (FGFR1) did not precipitate the DR2-2 element above background levels (No Ab) of protein-A Sepharose beads (Figure 6A). We also investigated the presence of the two nuclear receptors on DR2-1 using the same

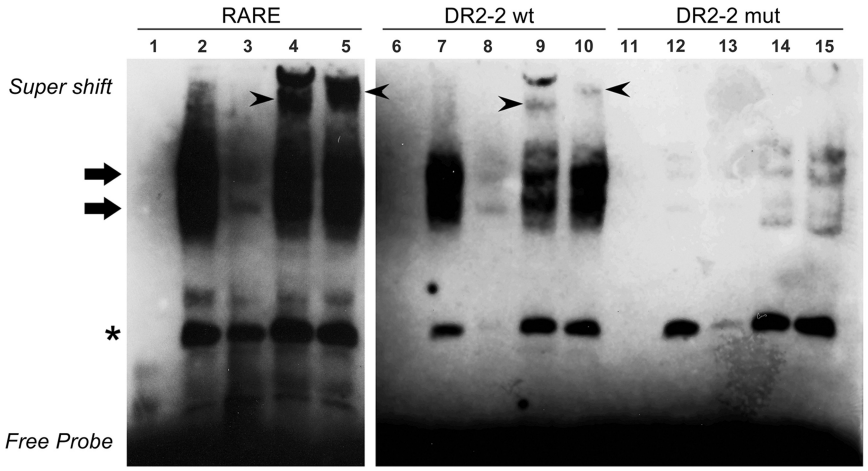


**Figure 5.** RARα and RXR interacts with the novel intronic RARE in gel retardation assays. Nuclear extracts from E2-treated MCF-7 cells were incubated with biotin labeled oligonucleotide probes representing a consensus RARE, the wild-type DR2-2 or the mutant variant DR2-2mut (DR2-2-Mut1-S in Supplementary Table S2). Samples were resolved on a 6% non-denaturing polyacrylamide gel in TBE, transferred to Hybond N+ membranes and then incubated with streptavidin, and biotin-labeled DNA probes were detected by chemiluminescence. The name of the probe used in each binding reaction is indicated on the top of each panel. All binding reactions were competed with 200-fold molar excess of the corresponding unlabeled probe. Arrows point out the nuclear receptor–DNA complexes, while arrowheads point out the super shift. The asterisk indicates a DR2-2 independent interaction with nuclear proteins. Labeled probes were incubated in the absence of nuclear extract (lanes 1, 6 and 11), in the presence of nuclear extract alone (lanes 2, 7 and 12), nuclear extract together with an excess of competing unlabeled probe (lanes 3, 8 and 13), in the presence of RARα antibodies (lanes 4, 9 and 14), or in the presence of RXR antibodies (lanes 5, 10 and 15). Experiments were repeated at least three times and a representative result is shown.

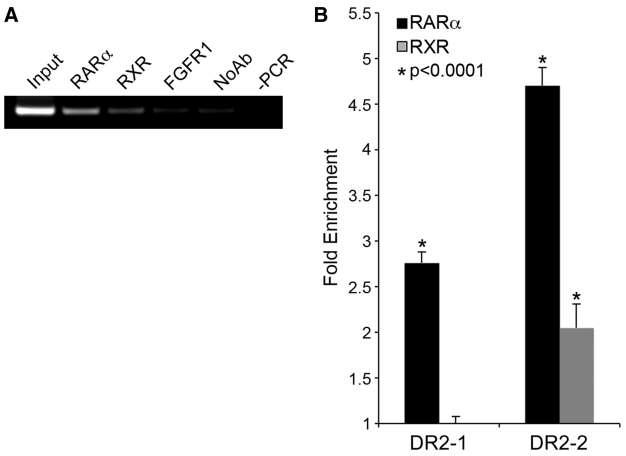


**Figure 6.** RARα and RXR occupy the novel intronic element *in vivo*. MCF-7 cells grown in DMEM were treated with 1 μM tRA and used for ChIP analysis using RARα and RXR specific antibodies. (**A**) DNA isolated from immunocomplexes was used as a template for PCR amplification using primers specific for DR2-2. PCR products were resolved on a 2% agarose gel (containing Ethidium bromide) and visualized on a UV transilluminator, RARα; anti-RAR-α Ab precipitated DNA, RXR; anti-RXR Ab precipitated DNA, FGFR1; anti-FGFR1 Ab precipitated DNA, No Ab; bead-only control, and -PCR is a negative control with $H_2O$ as a template. (**B**) Quantitative PCR was performed using immunoprecipitated DNA using DR2-1 and DR2-2 specific primers. Ct values were normalized to background levels of bead-only controls (No Ab) using $2^{(\delta Ct)}$. Data are represented as fold enrichment compared to IgG control. *$P$-values were calculated using Student's $t$-test (average of three experiments) with 95% confidence interval, values <0.05 were considered significant.

immunoprecipitated samples. Despite being non-responsive to tRA stimulation in reporter assays (Figure 4C), we found that DR2-1 is actually occupied by both nuclear receptors in MCF-7 cells (Figure 6B), but with lower abundance when compared to DR2-2 (~50% less). These findings demonstrate that, endogenous RARα and RXR bind to both DR2-1 and DR2-2 that are present in the first intron of *NIS in vivo*, thereby strongly suggesting that at least part of the regulatory effects of the two nuclear receptors, RARα and RXR, on *NIS* expression in MCF-7 cells were due to a direct interaction between the receptors and the intronic RAREs (Figure 6).

### Initiation of NIS transcription in response to tRA involves dynamic interactions between multiple intronic elements, nuclear receptors and the RNA Pol-II

Besides the intronic enhancer identified above (DR2-2 in intron 1), there exists several other putative intronic RARE sequences within NIS gene (25). As we found a functional RARE in intron 1, we were intrigued to study a possible involvement of other intronic putative RARE sequences in NIS gene transcription. As nuclear receptors interact with cognate response elements in a dynamic manner (26), we decided to study the dynamics of interactions taking place between *cis*- and *trans*-acting factors. To this end, we used ChIP assays to screen for the involvement of intronic sequences in NIS transcription in response to tRA treatment in MCF-7 cells (Figure 7).

MCF-7 cells were cultured in charcoal-treated steroid-free medium lacking phenol-red, and they were either treated with DMSO, or with tRA for 15, 30 or 60 min, and interactions of RARα, RXR and/or RNA Pol-II with sequences located in introns 1, 5, 7, 8, 12, 13 and 14 (Figure 7) were investigated. Prior to tRA stimulation (time point 0) all intronic sequences, except the one in intron 8, were engaged in an interaction with basal transcriptional machinery (based on precipitation of these sequences with RNA Pol-II, Figure 7A). By 15 min

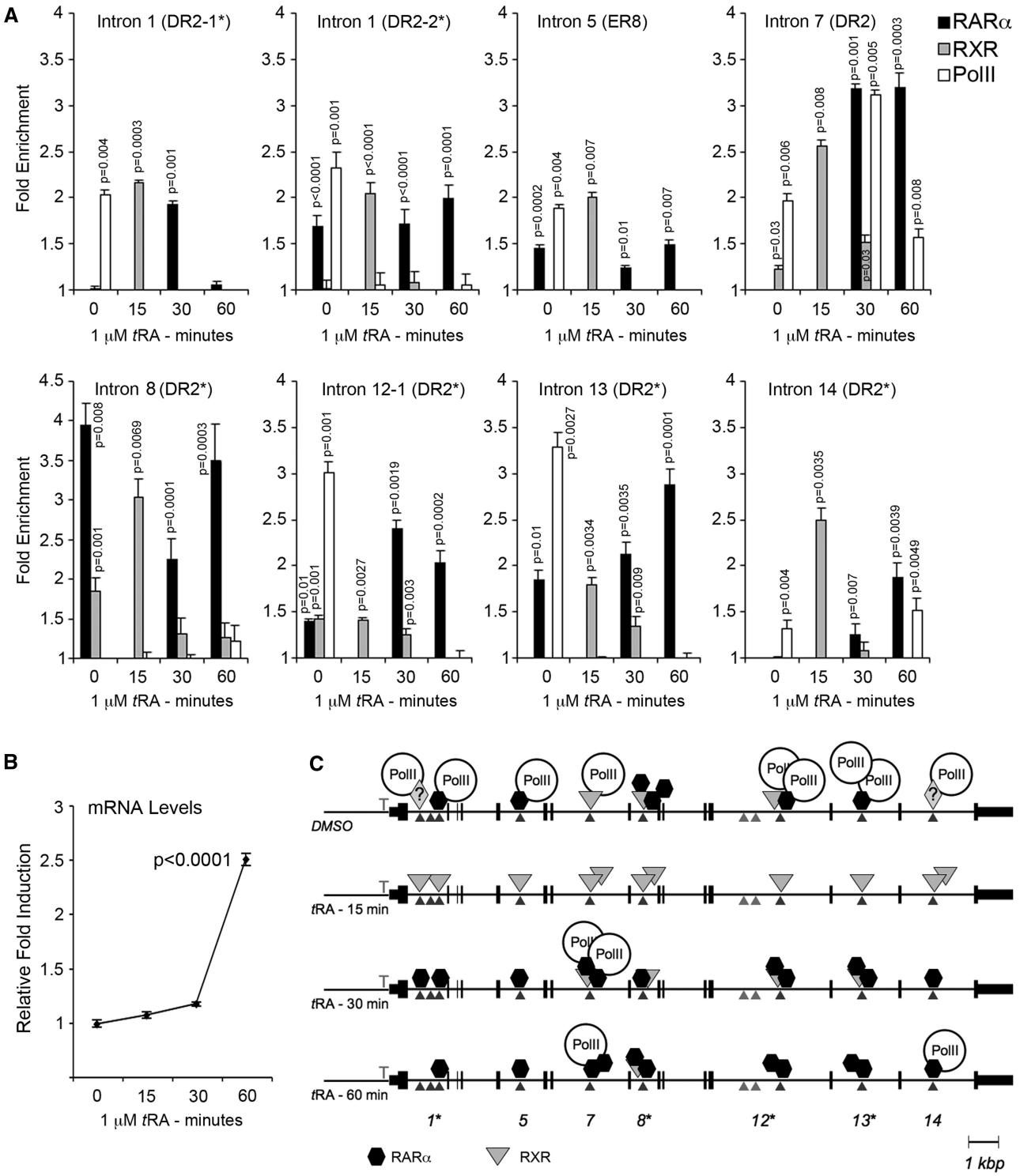


**Figure 7.** Nuclear receptors and RNA Pol-II interact with NIS intronic elements in a dynamic manner during the initiation of transcription. MCF-7 cells grown in steroid-free and phenol-red-free DMEM were treated either with DMSO (time 0) or with 1 μM tRA for 15, 30 and 60 min and used for ChIP analysis using RARα and RXR and RNA Pol-II specific antibodies. (**A**) DNA isolated from immunocomplexes was used for quantitative PCR using primers described in Supplementary Table S3. Ct values were normalized to background levels of bead-only controls. Data are represented as fold enrichment compared to IgG control. (**B**) mRNA was isolated from a fraction of the cells used for ChIP analysis above. Two micrograms of total RNA was converted to cDNA and used for quantitative real-time PCR. Expression was normalized to the levels of GAPDH using the ΔΔCt method and presented as relative fold induction compared to DMSO-treated samples. (**C**) Schematic representation of ChIP data depicting the events of transcription initiation of NIS in response to tRA stimulation. Arrow heads indicate the position of the intronic element investigated, vertical small lines represent NIS exons, numbers below indicate introns studied, asterisks above numbers indicate identical sequences. Parallelograms with question mark represent unidentified interacting proteins. DR, direct repeat; ER, everted repeat. Statistical significance was determined by performing the Student's *t*-test (Figure 7A) or paired Student's *t*-test (Figure 7C) using a 95% confidence interval; *P*-values <0.05 were considered significant.

of stimulation, interactions were limited to RXR but then they were replaced by RARα (30 min), with strong appearance together with RNA Pol-II on the element from intron 7 (Figure 7A). This presence of RARα persists at 60 min post-stimulation in the absence of RXR, accompanied by an acute increase in mRNA levels (Figure 7B). It appears that interactions with transcription machinery are sustained by sequences in intron 7 (30 and 60 min.) and in intron 14 (60 min.). Figure 7C recapitulates the dynamic events taking place during initiation of transcription in response to tRA stimulation.

## DISCUSSION

The identification of elements that control *NIS* regulation in mammary gland cells is of particular importance in the context that mammary-tumor-specific stimulation of NIS activity followed by radioiodide substrate ($^{131}I$, $^{123}I$ or $^{99m}TcO_4$) administration could have an important potential as a novel alternative in the diagnosis and treatment of breast tumors (2,7,8,17,27). Yet, in a recent publication (28), it was reported that NIS-related intracellular staining in immunohistochemistry experiments on thyroid cancers was due to non-specific binding of the antibodies. These authors also conclude that the intracellular signal in breast tumors might not always be specific. Therefore, in our opinion, establishing clinical methods of increasing expression levels of NIS would be essential if the activity of this symporter is to be used for a radio-labeled substrate-based diagnosis and therapy of a large set of breast tumors (29,30). In a series of publications, Kogai *et al.* (7,17,25,31) has demonstrated that tRA stimulates *NIS* expression and the selective cytotoxic effect of radioiodide both in MCF-7 cells as well as in MCF-7-derived xenografts in nude mice. Yet, the molecular mechanisms of tRA effect on *NIS* in mammary gland cells are not completely revealed. Although tRA upregulates both rodent and human NIS expression at the transcriptional level in a variety of thyroid and mammary gland cell lines, molecular mechanisms and elements that were reported to mediate tRA responsive *NIS* regulation varied depending on the organism and the cell origin. A better understanding of molecular determinants, mechanisms and ligands that have a role in NIS regulation would be essential for successful implementation of possible NIS-activity-based novel methods for the management of malignant breast diseases. In this respect, our description regarding the molecular interplay between retinoid receptors, intronic *cis*-acting elements and RNA Pol-II brings important clarifications about precise molecular mechanisms and interactions controlling tRA-dependent NIS gene upregulation (see below).

In an initial effort to identify mammary-gland-specific enhancers of *NIS*, we adopted a comparative genomics approach followed by functional assays of conserved DNA sequences in different cell types (data not shown). As widely appreciated, interspecies genome comparisons were in general very useful for a rather accurate prediction of protein encoding genes in different organisms (32). On the other hand, prediction of gene regulatory regions by genome comparisons tends to be relatively more difficult as they tolerate much more sequence divergence than coding sequences while retaining their original function. Yet, several reports have indicated that interspecies genome comparisons of close relatives could lead to correct predictions of regulatory sequences (33–35). A similar comparative analysis of a 90-kb region, including and flanking NIS loci in mice, rat and human genomes, followed by functional tests in MCF-7 cells, has led us to identify a novel tRA responsive region in the first intron of the human *NIS*.

A conserved 5′ upstream region of the human *NIS* (referred to as cluster 3 in this work) contains a tRA responsive element that was previously identified as a RARE in human follicular thyroid carcinoma cell lines, FTC-133 and FTC-238 (14). As expected, we have observed that this region has a remarkable tRA responsive regulatory capacity (Figure 2) in MCF-7 cells. Surprisingly, point mutations that were shown to abolish tRA responsiveness of this element in thyroid cells (14) had no significant suppressive effect on tRA stimulation in MCF-7 cells (Figure 3B). Our intensive search both by bioinformatics and by experimental methods, as well as studies carried out by other groups (25), did not reveal another RARE in this region. This could imply that first, the mechanism of RA stimulation of human *NIS* expression in mammary cell models is distinct from that of thyroid cells; and, second, the stimulatory effect of RA on this sequence is actually an indirect one. Moreover, analysis of overlapping deletion mutations in Cl3 did not reveal any RA responsive sequence (Figure 3C), suggesting that RA stimulation of the human NIS gene requires the synergistic effect of multiple factors.

Indirect stimulation of *NIS* by tRA was previously reported; tRA was shown to upregulate the rat *Nis* promoter in MCF-7 cells by activating the homeobox-containing transcription factor, Nkx2.5 (15). In this cell line, tRA treatment stimulates the expression of this NK2-type transcription factor, which in turn, activates *Nis* promoter by binding to two *cis*-acting elements located at −446 and −154 relative to ATG (15). Despite extensive search for similar binding sites in the human *NIS* locus, Nkx2.5 responsive *cis*-acting sequences were not found (data not shown). In a more recent study, Kogai *et al.* (25) described an indirect effect of RA on *NIS* expression that is mediated by IGF-1/PI3K signaling pathways in MCF-7 but not in the rat normal thyroid cell line FRTL-5. In MCF-7 cells, RA exerts its effect by activating PI3K signaling pathways, which result in the activation of an unknown transcription factor, leading to an enhanced *NIS* expression (36). It would be interesting to find out whether the binding site of this yet-uncharacterized factor maps in Cl3 or not.

Intronic sequences could contain motifs and *cis*-acting elements with varying functions, such as exon/intron recognition, regulation of alternative splicing events, activation of transcription, stimulation of polyadenylation and, surprisingly enough, in certain cases elements regulating the stability of encoded proteins (37–42). In this report, we describe a novel enhancer that is located in intron 1, and that mediates retinoic acid responsive NIS gene

expression. We have initially shown evidences for a direct interaction between RARα/RXR and a novel RARE within the first intron of the human *NIS* in MCF-7 cells (Figures 5–7). This DR-2 type RARE (DR2-2) was functional in reporter assays and had the capacity to activate both the native *NIS* promoter (regardless of position or orientation) as well as the viral E1b TATA element (Figure 4D). Recently, Kogai *et al.* (25) reported putative RARE sequences present within several introns of the human *NIS*, including elements found in the first intron, but they could not attribute a functional role to these elements (25). Thus, it seems that other than its native promoter, NIS intronic enhancer could activate only a subset of heterologous promoters. Interestingly, another DR-2-type element (DR2-1) of identical sequence in the same intron was occupied by tRA stimulated nuclear receptors *in vivo* despite being non-responsive to tRA in reporter assays. The difference in the regulatory potential of these sequence-wise identical elements in intron 1 could be related to initial (time 0) and persistent (60 min) interactions with RARα that we observe in DR2-2 but not DR2-1 (Figure 7A). This temporal regulation of RARα interaction with its cognate response elements could well be governed by epigenetic factors modifying local chromatin structure of this region. Related to this, we have clearly observed tri-methylation of H3K4 residues both on DR2-1, DR2-2 as well as on other intronic RAREs (see below, and also Supplementary Figure S1), a characteristic histone H3 modification found at enhancer regions of transcriptionally active genes (43). We have previously shown that tRA-upregulated NIS expression is restricted to ERα-positive mammary gland cell lines. In the absence of ERα, neither NIS promoter, nor the luciferase reporter gene under control of cluster 3 were stimulated in response to tRA stimulation, even though tRA signaling was operative in these cells (13, and Supplementary Figure S2). Re-introduction of ERα in previously ERα (−) cells was required for the recovery of NIS expression (13). It is therefore plausible to anticipate that intronic elements that were described in this work could only stimulate initiation of NIS gene transcription only in the presence of active ERα.

Our ChIP assays have revealed that at the onset of NIS gene transcription, sequences located in introns 1, 5, 7, 8, 12, 13 and 14 (Figure 7) interact temporally with nuclear receptors and with RNA Pol-II. Interestingly, all intronic elements (except the one in intron 8) were found to interact intensively with RNA Pol-II in the absence of ligand, tRA (Figure 7A and C), which might keep the polymerase ready for the initiation. With the tRA-dependent onset of transcription, interactions between *cis*-acting sequences and RNA Pol-II become undetectable in our assay system, and in the first 15 min of tRA induction RXR solely occupies all intronic positions (Figure 7C), indicating the early role of this *trans*-acting factor in tRA dependent transcription. At later time points (30 and 60 min) while mRNA levels increase in a steady manner (Figure 7B), interactions between sequences in intron 7 and RNA Pol-II (and later in intron 14 and RNA Pol-II) becomes detectable once again, suggesting frequent interactions between general transcription apparatus and elements in intron 7 and 14 during maximal levels of transcription (Figure 7A–C). At the same time points, RARα replaces RXR and dominates interactions in intronic sites, which implies the principal role of RARα at relatively late stages of tRA-dependent transcription initiation. Positions of intronic sequences found to interact with the RNA Pol-II and tRA-stimulated nuclear receptors matches exactly with locations where H3K4 tri-methylations were observed (Supplementary Figure S1). In fact, in most cases, persistent RARα interactions at later stages (30–60 min) with intronic elements coincide with increased H3K4 tri-methylation (Figures 7 and S1). Nuclear receptors, including RARα and RXR, are well known to recruit histone-modifying co-regulators facilitating conversion of chromatin regions to transcriptionally permissive states (44). For instance, MLL5, which is a histone lysine methyltransferase, was recently described to be one of the H3K4 modifying enzymes enhancing RARα-dependent gene transcription (45); one of the epigenetic mechanisms that could also operate during NIS expression.

Earlier work and results presented in this manuscript clearly indicate that molecular mechanisms presiding NIS expression involve a number of classical and intronic elements that regulate temporal and spatial expression, and they are likely to be more complex than previously anticipated. Future experiments will show whether the activities of intronic enhancers lead also to a tissue- or cell-type-specific regulation of NIS. A better understanding of this mechanism of regulation, as well as the ability to selectively enhance NIS expression in tumor cells will, eventually, be of great importance for potential future applications in breast cancer diagnosis and treatment.

## SUPPLEMENTARY DATA

Supplementary Data are available at NAR Online.

## ACKNOWLEDGEMENTS

We thank Prof. Mehmet Öztürk and Dr. Khemais Benhaj for valuable discussions.

## FUNDING

The EU 7th Framework Program Project UNAM-REGPOT Grant no: 203953 and by an EMBO Short Term Fellowship (to H.A.); Associazione Italiana per la Ricerca sul Cancro (to R.D.L. and D.S.); Turkish Scientific and Technical Research Council (104-T-231 to U.H.T); the Turkish Academy of Sciences-Young Scientist Award (GEBIP/2001-2-18 to U.H.T); Bilkent University Research Funds; DPT-KANILTEK Project Funds; Feyzi Akkaya Research Fund for Scientific Activities (FABED; to U.H.T.). Funding for open access charge: partially waived by Oxford University Press.

*Conflict of interest statement*. None declared.

## REFERENCES


1. Spitzweg,C., Joba,W., Eisenmenger,W. and Heufelder,A.E. (1998) Analysis of human sodium iodide symporter gene expression in extrathyroidal tissues and cloning of its complementary deoxyribonucleic acids from salivary gland, mammary gland, and gastric mucosa. *J. Clin. Endocrinol. Metab.*, **83**, 1746–1751.
2. Tazebay,U.H., Wapnir,I.L., Levy,O., Dohan,O., Zuckier,L.S., Zhao,Q.H., Deng,H.F., Amenta,P.S., Fineberg,S., Pestell,R.G. *et al*. (2000) The mammary gland iodide transporter is expressed during lactation and in breast cancer. *Nat. Med.*, **6**, 871–878.
3. Stubbe,P., Schulte,F.J. and Heidemann,P. (1986) Iodine deficiency and brain development. *Bibl. Nutr. Dieta.*, 206–208.
4. Cho,J.Y., Leveille,R., Kao,R., Rousset,B., Parlow,A.F., Burak,W.E. Jr, Mazzaferri,E.L. and Jhiang,S.M. (2000) Hormonal regulation of radioiodide uptake activity and Na+/I- symporter expression in mammary glands. *J. Clin. Endocrinol. Metab.*, **85**, 2936–2943.
5. Perron,B., Rodriguez,A.M., Leblanc,G. and Pourcher,T. (2001) Cloning of the mouse sodium iodide symporter and its expression in the mammary gland and other tissues. *J. Endocrinol.*, **170**, 185–196.
6. Knostman,K.A., Cho,J.Y., Ryu,K.Y., Lin,X., McCubrey,J.A., Hla,T., Liu,C.H., Di Carlo,E., Keri,R., Zhang,M. *et al*. (2004) Signaling through 3′,5′-cyclic adenosine monophosphate and phosphoinositide-3 kinase induces sodium/iodide symporter expression in breast cancer. *J. Clin. Endocrinol. Metab.*, **89**, 5196–5203.
7. Kogai,T., Kanamoto,Y., Che,L.H., Taki,K., Moatamed,F., Schultz,J.J. and Brent,G.A. (2004) Systemic retinoic acid treatment induces sodium/iodide symporter expression and radioiodide uptake in mouse breast cancer models. *Cancer Res.*, **64**, 415–422.
8. Wapnir,I.L., van de Rijn,M., Nowels,K., Amenta,P.S., Walton,K., Montgomery,K., Greco,R.S., Dohan,O. and Carrasco,N. (2003) Immunohistochemical profile of the sodium/iodide symporter in thyroid, breast, and other carcinomas using high density tissue microarrays and conventional sections. *J. Clin. Endocrinol. Metab.*, **88**, 1880–1888.
9. Mazzaferri,E.L. (1999) An overview of the management of papillary and follicular thyroid carcinoma. *Thyroid*, **9**, 421–427.
10. Kogai,T., Curcio,F., Hyman,S., Cornford,E.M., Brent,G.A. and Hershman,J.M. (2000) Induction of follicle formation in long-term cultured normal human thyroid cells treated with thyrotropin stimulates iodide uptake but not sodium/iodide symporter messenger RNA and protein expression. *J. Endocrinol.*, **167**, 125–135.
11. Tanosaki,S., Ikezoe,T., Heaney,A., Said,J.W., Dan,K., Akashi,M. and Koeffler,H.P. (2003) Effect of ligands of nuclear hormone receptors on sodium/iodide symporter expression and activity in breast cancer cells. *Breast Cancer Res. Treat.*, **79**, 335–345.
12. Kogai,T., Kanamoto,Y., Li,A.I., Che,L.H., Ohashi,E., Taki,K., Chandraratna,R.A., Saito,T. and Brent,G.A. (2005) Differential regulation of sodium/iodide symporter gene expression by nuclear receptor ligands in MCF-7 breast cancer cells. *Endocrinology*, **146**, 3059–3069.
13. Alotaibi,H., Yaman,E.C., Demirpençe,E. and Tazebay,U.H. (2006) Unliganded estrogen receptor-alpha activates transcription of the mammary gland Na+/I- symporter gene. *Biochem. Biophys. Res. Commun.*, **345**, 1487–1496.
14. Schmutzler,C., Schmitt,T.L., Glaser,F., Loos,U. and Köhrle,J. (2002) The promoter of the human sodium/iodide-symporter gene responds to retinoic acid. *Mol. Cell. Endocrinol.*, **189**, 145–155.
15. Dentice,M., Luongo,C., Elefante,A., Romino,R., Ambrosio,R., Vitale,M., Rossi,G., Fenzi,G. and Salvatore,D. (2004) Transcription factor Nkx-2.5 induces sodium/iodide symporter gene expression and participates in retinoic acid- and lactation-induced transcription in mammary cells. *Mol. Cell. Biol.*, **24**, 7863–7877.
16. Negre,B., Casillas,S., Suzanne,M., Sánchez-Herrero,E., Akam,M., Nefedov,M., Barbadilla,A., de Jong,P. and Ruiz,A. (2005) Conservation of regulatory sequences and gene expression patterns in the disintegrating Drosophila Hox gene complex. *Genome Res.*, **15**, 692–700.
17. Kogai,T., Taki,K. and Brent,G.A. (2006) Enhancement of sodium/iodide symporter expression in thyroid and breast cancer. *Endocr. Relat. Cancer*, **13**, 797–826.
18. Ohno,M., Zannini,M., Levy,O., Carrasco,N. and di Lauro,R. (1999) The paired-domain transcription factor Pax8 binds to the upstream enhancer of the rat sodium/iodide symporter gene and participates in both thyroid-specific and cyclic-AMP-dependent transcription. *Mol. Cell. Biol.*, **19**, 2051–2060.
19. Taki,K., Kogai,T., Kanamoto,Y., Hershman,J.M. and Brent,G.A. (2002) A thyroid-specific far-upstream enhancer in the human sodium/iodide symporter gene requires Pax-8 binding and cyclic adenosine 3′,5′-monophosphate response element-like sequence binding proteins for full activity and is differentially regulated in normal and thyroid cancer cells. *Mol. Endocrinol.*, **16**, 2266–2282.
20. Kent,W.J., Sugnet,C.W., Furey,T.S., Roskin,K.M., Pringle,T.H., Zahler,A.M. and Haussler,D. (2002) The human genome browser at UCSC. *Genome Res.*, **12**, 996–1006.
21. Mayor,C., Brudno,M., Schwartz,J.R., Poliakov,A., Rubin,E.M., Frazer,K.A., Pachter,L.S. and Dubchak,I. (2000) VISTA: visualizing global DNA sequence alignments of arbitrary length. *Bioinformatics*, **16**, 1046–1047.
22. Behr,M., Schmitt,T.L., Espinoza,C.R. and Loos,U. (1998) Cloning of a functional promoter of the human sodium/iodide-symporter gene. *Biochem. J.*, **331(Pt 2)**, 359–63.
23. Endo,T., Kaneshige,M., Nakazato,M., Ohmori,M., Harii,N. and Onaya,T. (1997) Thyroid transcription factor-1 activates the promoter activity of rat thyroid Na+/I- symporter gene. *Mol. Endocrinol.*, **11**, 1747–1755.
24. Giguère,V. (1994) Retinoic acid receptors and cellular retinoid binding proteins: complex interplay in retinoid signaling. *Endocr. Rev.*, **15**, 61–79.
25. Kogai,T., Ohashi,E., Jacobs,M.S., Sajid-Crockett,S., Fisher,M.L., Kanamoto,Y. and Brent,G.A. (2008) Retinoic acid stimulation of the sodium/iodide symporter in MCF-7 breast cancer cells is mediated by the insulin growth factor-I/phosphatidylinositol 3-kinase and p38 mitogen-activated protein kinase signaling pathways. *J. Clin. Endocrinol. Metab.*, **93**, 1884–1892.
26. Metivier,R., Penot,G., Hubner,M.R., Reid,G., Brand,H., Kos,M. and Gannon,F. (2003) Estrogen receptor-alpha directs ordered, cyclical, and combinatorial recruitment of cofactors on a natural target promoter. *Cell*, **115**, 751–763.
27. Wapnir,I.L., Goris,M., Yudd,A., Dohan,O., Adelman,D., Nowels,K. and Carrasco,N. (2004) The Na+/I- symporter mediates iodide uptake in breast cancer metastases and can be selectively down-regulated in the thyroid. *Clin. Cancer Res.*, **10**, 4294–4302.
28. Peyrottes,I., Navarro,V., Ondo-Mendez,A., Marcellin,D., Bellanger,L., Marsault,R., Lindenthal,S., Ettore,F., Darcourt,J. and Pourcher,T. (2009) Immunoanalysis indicates that the sodium iodide symporter is not overexpressed in intracellular compartments in thyroid and breast cancers. *Eur. J. Endocrinol.*, **160**, 215–225.
29. Daniels,G.H. and Haber,D.A. (2000) Will radioiodine be useful in treatment of breast cancer? *Nat. Med.*, **6**, 859–860.
30. Welcsh,P.L. and Mankoff,D.A. (2000) Taking up iodide in breast tissue. *Nature*, **406**, 688–689.
31. Kogai,T., Schultz,J.J., Johnson,L.S., Huang,M. and Brent,G.A. (2000) Retinoic acid induces sodium/iodide symporter gene expression and radioiodide uptake in the MCF-7 breast cancer cell line. *Proc. Natl Acad. Sci. USA*, **97**, 8519–8524.
32. Dolinski,K. and Botstein,D. (2007) Orthology and functional conservation in eukaryotes. *Annu. Rev. Genet.*, **41**, 465–507.
33. Dubchak,I., Brudno,M., Loots,G.G., Pachter,L., Mayor,C., Rubin,E.M. and Frazer,K.A. (2000) Active conservation of noncoding sequences revealed by three-way species comparisons. *Genome Res.*, **10**, 1304–1306.
34. Boffelli,D., McAuliffe,J., Ovcharenko,D., Lewis,K.D., Ovcharenko,I., Pachter,L. and Rubin,E.M. (2003) Phylogenetic shadowing of primate sequences to find functional regions of the human genome. *Science*, **299**, 1391–1394.

35. Haubold,B. and Wiehe,T. (2004) Comparative genomics: methods and applications. *Naturwissenschaften*, **91**, 405–421.
36. Ohashi,E., Kogai,T., Kagechika,H. and Brent,G.A. (2009) Activation of the PI3 kinase pathway by retinoic acid mediates sodium/iodide symporter induction and iodide transport in MCF-7 breast cancer cells. *Cancer Res.*, **69**, 3443–3450.
37. Lou,H., Gagel,R.F. and Berget,S.M. (1996) An intron enhancer recognized by splicing factors activates polyadenylation. *Genes Dev.*, **10**, 208–219.
38. Müller,F., Chang,B., Albert,S., Fischer,N., Tora,L. and Strähle,U. (1999) Intronic enhancers control expression of zebrafish sonic hedgehog in floor plate and notochord. *Development*, **126**, 2103–2116.
39. Noé,V., MacKenzie,S. and Ciudad,C.J. (2003) An intron is required for dihydrofolate reductase protein stability. *J. Biol. Chem.*, **278**, 38292–38300.
40. Khandekar,M., Brandt,W., Zhou,Y., Dagenais,S., Glover,T.W., Suzuki,N., Shimizu,R., Yamamoto,M., Lim,K.C. and Engel,J.D. (2007) A Gata2 intronic enhancer confers its pan-endothelia-specific regulation. *Development*, **134**, 1703–1712.
41. Feng,W., Huang,J., Zhang,J. and Williams,T. (2008) Identification and analysis of a conserved Tcfap2a intronic enhancer element required for expression in facial and limb bud mesenchyme. *Mol. Cell. Biol.*, **28**, 315–325.
42. Hertel,K.J. (2008) Combinatorial control of exon recognition. *J. Biol. Chem.*, **283**, 1211–1215.
43. Barski,A., Cuddapah,S., Cui,K., Roh,T.Y., Schones,D.E., Wang,Z., Wei,G., Chepelev,I. and Zhao,K. (2007) High-resolution profiling of histone methylations in the human genome. *Cell*, **129**, 823–837.
44. McEwan,I.J. (2000) Gene regulation through chromatin remodelling by members of the nuclear receptor superfamily. *Biochem. Soc. Trans.*, **28**, 369–373.
45. Fujiki,R., Chikanishi,T., Hashiba,W., Ito,H., Takada,I., Roeder,R.G., Kitagawa,H. and Kato,S. (2009) GlcNAcylation of a histone methyltransferase in retinoic-acid-induced granulopoiesis. *Nature*, **459**, 455–459.

OPEN ACCESS Freely available online

PLoS one

# The Ability to Generate Senescent Progeny as a Mechanism Underlying Breast Cancer Cell Heterogeneity

**Mine Mumcuoglu[1], Sevgi Bagislar[1,2], Haluk Yuzugullu[1,2], Hani Alotaibi[1], Serif Senturk[1], Pelin Telkoparan[1], Bala Gur-Dedeoglu[1], Burcu Cingoz[1], Betul Bozkurt[3], Uygar H. Tazebay[1], Isik G. Yulug[1], K. Can Akcali[1], Mehmet Ozturk[1,2]***

**1** BilGen Genetics and Biotechnology Center, Department of Molecular Biology and Genetics, Bilkent University, Ankara, Turkey, **2** INSERM - Université Joseph Fourrier, CRI U823, Grenoble, France, **3** Department of Surgery, Ankara Numune Research and Teaching Hospital, Ankara, Turkey

## Abstract

***Background:*** Breast cancer is a remarkably heterogeneous disease. Luminal, basal-like, "normal-like", and ERBB2+ subgroups were identified and were shown to have different prognoses. The mechanisms underlying this heterogeneity are poorly understood. In our study, we explored the role of cellular differentiation and senescence as a potential cause of heterogeneity.

***Methodology/Principal Findings:*** A panel of breast cancer cell lines, isogenic clones, and breast tumors were used. Based on their ability to generate senescent progeny under low-density clonogenic conditions, we classified breast cancer cell lines as senescent cell progenitor (SCP) and immortal cell progenitor (ICP) subtypes. All SCP cell lines expressed estrogen receptor (ER). Loss of ER expression combined with the accumulation of $p21^{Cip1}$ correlated with senescence in these cell lines. $p21^{Cip1}$ knockdown, estrogen-mediated ER activation or ectopic ER overexpression protected cells against senescence. In contrast, tamoxifen triggered a robust senescence response. As ER expression has been linked to luminal differentiation, we compared the differentiation status of SCP and ICP cell lines using stem/progenitor, luminal, and myoepithelial markers. The SCP cells produced CD24+ or ER+ luminal-like and ASMA+ myoepithelial-like progeny, in addition to CD44+ stem/progenitor-like cells. In contrast, ICP cell lines acted as differentiation-defective stem/progenitor cells. Some ICP cell lines generated only CD44+/CD24-/ER-/ASMA- progenitor/stem-like cells, and others also produced CD24+/ER- luminal-like, but not ASMA+ myoepithelial-like cells. Furthermore, gene expression profiles clustered SCP cell lines with luminal A and "normal-like" tumors, and ICP cell lines with luminal B and basal-like tumors. The ICP cells displayed higher tumorigenicity in immunodeficient mice.

***Conclusions/Significance:*** Luminal A and "normal-like" breast cancer cell lines were able to generate luminal-like and myoepithelial-like progeny undergoing senescence arrest. In contrast, luminal B/basal-like cell lines acted as stem/progenitor cells with defective differentiation capacities. Our findings suggest that the malignancy of breast tumors is directly correlated with stem/progenitor phenotypes and poor differentiation potential.

**Citation:** Mumcuoglu M, Bagislar S, Yuzugullu H, Alotaibi H, Senturk S, et al. (2010) The Ability to Generate Senescent Progeny as a Mechanism Underlying Breast Cancer Cell Heterogeneity. PLoS ONE 5(6): e11288. doi:10.1371/journal.pone.0011288

**Editor:** Syed A. Aziz, Health Canada, Canada

**Received** March 16, 2010; **Accepted** June 4, 2010; **Published** June 24, 2010



**Funding:** This work was supported by TUBITAK (The Scientific and Technological Research Council of Turkey), DPT (State Planning Office of Turkey) and TUBA (Turkish Academy of Sciences). Additional funding was from Institut National de Cancer and INSERM of France. The funders had no role in study design, data collection and analysis, decision to publish, or preparation of the manuscript.

**Competing Interests:** The authors have declared that no competing interests exist.

* E-mail: ozturkm@ujf-grenoble.fr

## Introduction

Human breast tumors are heterogeneous, both in their pathology and in their molecular profiles. Gene expression analyses classify breast tumors into distinct subtypes, such as luminal A, luminal B, ERBB2-positive (ERBB2+) and basal-like [1,2,3]. The prognosis and therapeutic response of each subtype is different. Luminal A cancers are mostly estrogen receptor-α-positive (ER+) and sensitive to anti-estrogen therapy, with the best metastasis-free and overall survival rates. Luminal B tumors have an incomplete anti-estrogen response and lower survival rates. Basal-like and ERBB2+ tumors are ER- and display the worst survival rates [2,3]. The patterns of genetic changes such as chromosomal aberrations and gene mutations observed in breast tumors indicate that breast tumorigenesis does not follow a stepwise linear progression from well-differentiated to poorly differentiated tumors with cumulative genetic aberrations [4]. This suggests that different breast tumor subtypes do not represent different stages of tumor progression, but rather represent the cells from which they initiate [4]. The mammary gland is composed of differentiated luminal and myoepithelial cells that are generated from multi-lineage, luminal-restricted, and myoepithelial-restricted progenitors originating from a hypothetical breast epithelial stem cell. Thus, different types of breast cancers might originate from such stem or progenitor cells at a given stage of commitment and differentiation, as observed in hematological malignancies [4,5]. Without compromising the author's hypothesis, it is also possible that the molecular heterogeneity of breast cancer is due to subtle differences in the ability of tumor-initiating cells to generate differentiated progeny.

Epithelial cells isolated from mammary gland cells undergo two successive senescence states in cell culture, termed "stasis" and "agonescence" [6,7]. In contrast to normal mammary epithelial cells, established breast cancer cells are immortal by definition. They may owe this phenotype of immortalization to genetic and epigenetic inactivation of senescence checkpoints and reactivation of telomerase reverse transcriptase expression [7]. Either in relation to these changes or independently, breast cancer cells may also present a stem/progenitor phenotype that is less subjected or resistant to senescence barriers. However, the abundance of non-tumorigenic and differentiated cells both in breast tumors and cell lines strongly suggests that replicative immortality cannot be assigned to all cells within a tumor or a cancer cell line, and that spontaneous senescence after a limited number of population doublings (PD) is likely to occur. If this hypothesis is correct, then the rate of generation of senescent progeny may reflect the potential of a cancer stem/progenitor cell to produce terminally differentiated progeny. We tested this hypothesis using a panel of luminal and basal-like breast cancer cell lines (Table S1). Although a single cell line is not representative of breast tumor heterogeneity, a panel of cell lines might reproduce the heterogeneity that is observed in primary breast tumors, albeit with some limitations [5,8]. Therefore, we hoped that in vitro studies with a panel of cell lines might help to better understand breast tumor heterogeneity.

Our senescence tests allowed us to classify breast cancer cell lines as senescent cell progenitor (SCP) and immortal cell progenitor (ICP) subtypes. We also show that senescent progeny are observed exclusively in ER-positive cells, as a result of ER inactivation, partly mediated with $p21^{Cip1}$ protein. The ability to produce senescent progeny was associated with the ability to produce luminal-like and myoepithelial-like progeny from stem/progenitor-like cells. In contrast, most of the cell lines lacking senescent progeny were also unable to generate differentiated progeny. Finally, we show that SCP-subtype cells cluster with luminal A and "normal-like" breast tumor types and are less tumorigenic, whereas ICP-subtype cell lines cluster with luminal B and basal-like tumor types and are more tumorigenic.

## Materials and Methods

### Ethics Statement

We used archival tumor samples remaining from a previous study by BB and IGY described in Gur-Dedeoglu et al. [9], for which the use of the tissue material was approved by the Research Ethics Committee of Ankara Numune Research and Teaching Hospital (decision date: 04/07/2007). The tumor samples in this study were used anonymously. All animals received care according to the Guide for the Care and Use of Laboratory Animals. All animal experiments have been pre-approved by the Bilkent University Animal Ethics Committee (Decision No: 2006/1; Decision date: 10/5/2006).

### Clinical samples and cell lines

Freshly frozen tumor specimens were collected at Ankara Numune Hospital. Breast cancer cell lines used in this study were obtained from ATCC (http://www.atcc.org) and listed in Table S1. Cell line authenticity was verified by short tandem repeat profiling, as recommended by ATCC (Dataset S1). Isogenic clones from the T47D (n = 20) cell line were obtained from single cell-derived colonies. Briefly, cells were plated in 96-well plates to obtain single colonies in fewer than 70% of the wells. Isolated colonies were then transferred to progressively larger wells, and to T25 flasks. Clones were subcultivated weekly at 1:4 dilution ratios, and maintained in culture for 25–30 passages to reach >60 PD before testing.

### Primary antibodies

The following antibodies were used: anti-CD44 (559046; BD Pharmingen), anti-CD24 (sc53660; Santa Cruz,), anti-ASMA (ab7817; Abcam), anti-CK19 (sc6278; Santa Cruz,), anti-$p21^{Cip1}$ (OP64; Calbiochem), anti-$p16^{Ink4a}$ (NA29, Calbiochem), anti-ERα (sc8002; Santa Cruz).

### Low-density clonogenic assays

Cells were seeded as low-density on coverslips in six-well plates (500–2000 cells, according to plating efficiency) and allowed to grow in DMEM supplemented with 10% fetal calf serum (FCS), with medium change every three days, until they formed colonies of a few hundred cells. Depending on the cell line, this took one to two weeks. For bromodeoxyuridine (BrdU) incorporation assays, cells were labeled for 24 h prior to immunocytochemistry, as described previously [10].

### Immunocytochemistry

For simple immunoperoxidase assays, cells were fixed with cold methanol for five minutes, then blocked with 10% FCS in phosphate-buffered saline (PBS) for 1 hour. This was followed by incubation with a primary antibody for 1 h. Cells were then washed with PBS three times and subjected to immunostaining using the Dako-Envision-dual-link system and the liquid diaminobenzidine (DAB) substrate chromogen system (Dako, CA, USA), according to the manufacturer's instructions. Hematoxylin was used as a counter-stain when the visualization of cells was necessary. For SABG-immunoperoxidase co-staining studies, unfixed cells were first subjected to SABG assay, and then fixed prior to immunostaining assays. Hematoxylin counter-staining was omitted for co-staining experiments, unless cells were negative for SABG staining.

### Immunoblot analyses

Cell pellets were incubated in an NP-40 lysis buffer containing 50 mM Tris–HCl, pH 8.0, 250 mM NaCl, 0.1% Nonidet P-40, and a protease inhibitor cocktail (Roche) for 30 minutes in a cold room. Cell lysates were then cleared by centrifugation, and a Bradford assay was performed to quantify their protein concentration. 30 µg of protein was denatured and resolved by SDS-PAGE using 10% or 12% gels. The proteins were then transferred to the PVDF or nitrocellulose membranes. Membranes were treated for 1 h with a blocking solution of TRIS-buffered saline containing 0.1% Tween-20 and 5% non-fat milk powder (TBS-T) and probed with a primary antibody for 1 h. Next, membranes were washed three times with TBS-T and incubated with an HRP-conjugated secondary antibody for 1 h. Immunocomplexes were then detected by an ECL-plus (Amersham) kit on the membrane. α-tubulin was used as an internal control.

### SABG assay and BrdU/SABG co-staining

SABG activity was detected as described [11], except that cells were counterstained with eosin or nuclear fast red following SABG staining. For BrdU/SABG co-staining, cells were first labeled with BrdU (10 µg/ml) for 24 h in a freshly added culture medium as described [10]. Next, cells were subjected to a SABG assay, fixed in 70% methanol, and subjected to BrdU immunostaining.

### Estrogen and tamoxifen treatment

Cells were seeded under low-density clonogenic conditions onto coverslips in six-well plates, and cultivated in a standard culture

medium for seven to eight days. Then, cells were fed with phenol red-free DMEM (Gibco) supplemented with 5% charcoal-stripped FCS for 48 h, followed by two successive 48 h treatments with $10^{-9}$ M estrogen (E2; 17β-estradiol; Sigma), $10^{-6}$ to $10^{-9}$ M 4-hydroxytamoxifen (4OHT; Sigma) or an ethanol vehicle, under the same conditions. Colonies were then subjected to a SABG assay. Each experimental condition was conducted in triplicate and experiments were repeated three times.

### Generation of estrogen receptor-overexpressing clones

T47D-iso23 cells were transfected with the expression vector pCMV- ERα [12] or an empty vector, using FuGENE-6 (Roche). ER overexpressing and control clones were selected with 500 μg/ml G418 for three weeks. Isolated single cell-derived colonies were picked and expanded in the presence of G418.

### Lentiviral infection and generation of $p21^{Cip1}$ knockdown clones

We used mission shRNA plasmid pLKO.1<-puro-p21 (NM_000389.2-640s1c1, Sigma) for $p21^{cip1}$ knockdown experiments. The Control vector shRNA-pGIPz-SCR-puro and a helper packaging mix (Invitrogen) were also used. HEK293T was co-transfected with the appropriate vector and packaging mix, using the CalPhos Mammalian Transfection Kit (Clontech) and following the manufacturer's instructions. After 48 h of culture, virus-containing culture media were collected, filtered, and used to infect T47D-iso23 cells. After 4 h of infection, stable cells were selected with 1 μg/ml puromycin for seven days.

### *Nude* mice tumorigenicity and in vivo senescence assays

T47D and MDA-MB-231 cells ($5\times10^6$) were injected subcutaneously into CD-1 *nude* mice (Charles River). Females (n = 5 for each cell line) and males (n = 4 for each cell line) were used. Tumor sizes were measured up to 47 days post-injection. In addition, four tumors from each cell line were analyzed for the presence of senescent cells by SABG staining, as described previously [10].

### Cluster analysis

The two-channel microarray data containing 8102 cDNA genes/clones generated by Sorlie et al. [2] were downloaded from the Stanford Microarray Database (SMD) (http://genome-www.stanford.edu/MicroArray/). In the downloading process, the "log (base 2) of R/G Normalized Ratio (median)" parameter was used for data filtering. We have median-centered expression values for each array. We selected arrays and genes with greater than 75% good data (representing the amount of data passing the spot criteria). Sixty-eight tissue samples were obtained according to this criterion and annotated with the subtypes described by the authors, found in the "Supplementary Information" of the data set in SMD. The expression values of "500 gene signature," defined by the authors, were extracted from the data. Gene expression profiles of 31 breast cancer cell lines performed by Charafe-Jauffret et al. [13], using the whole-genome cDNA microarray Affymetrix HGU-133 plus 2, was obtained from the "Supplementary Table" of the article. The authors filtered genes with low and poorly measured expression, and with low expression variation, retaining 15, 293 genes. After log transformation of the data, we median normalized the data arrays in R language, using the Bioconductor biostatistical package (www.r-project.org/ and www.bioconductor.org/). The "500 gene signature" tumor data [2] and the normalized breast-cancer cell line data [13] were combined with respect to probe IDs using a set of customized perl routines (source codes are available upon request). A set of 175 genes was common. "Median center" normalization of genes was done for the merged data set for the total samples. We performed unsupervised hierarchical clustering with the 99 samples (the 31 breast cell line [13] and 68 breast tumor [2] samples) by the pair-wise complete-linkage hierarchical clustering parameter, using the Gene-Pattern program. The Pearson correlation method was used for distance measurements. Clustering was visualized by java treeview, again using Gene-Pattern (http://www.broad.mit.edu/cancer/software/genepattern/).

### Statistical analyses

Significant differences were evaluated using unpaired Student's t test for compared samples sizes of 10 or higher. Otherwise, one-tailed Fisher's exact test was used with 2×2 tables; $P<0.05$ was considered statistically significant. On the graphical representation of the data, y-axis error bars indicate the standard deviation for each point on the graph.

## Results

### Classification of breast cancer cell lines as senescent-cell progenitor and immortal-cell progenitor subtypes

Clonogenic assays have been successfully used to test the generation and self-renewal abilities of phenotypically distinct progeny of mammary stem/progenitor cells [14]. We previously applied this technique to test the ability of cancer cells to produce progeny with replication-dependent senescence arrest [10]. Cells were plated under low-density clonogenic conditions and cultivated for one to two weeks until individual cells performed eight to ten PDs and generated isolated colonies composed of several hundred cells. This method permits tracing progeny generated by a few hundred cells under the same experimental conditions. We explored a panel of 12 breast cancer cell lines, composed of luminal (n = 7) and basal (n = 5) subtypes (Table S1). Cell lines formed two groups, according to the presence of senescent cells in isolated colonies. One group of cell lines generated colonies with high rates of senescence, while others did not produce appreciable amounts of senescent cells. Representative pictures of colonies subjected to the SABG assay are shown in Fig. 1A. The percent of SABG+ progeny was calculated by manual counting of at least 10 different colonies for each cell line. Colonies derived from five cell lines generated SABG+ cells at high rates (means: 5-40%) Senescence rates were negligible (means <5%) in the progeny of the remaining seven cell lines. The first group, the senescent cell progenitor subtype, included T47D, BT-474, ZR-75-1, MCF-7, and CAMA-1 cell lines. The second group, the immortal cell progenitor subtype, included MDA-MB-453, BT-20, SK-BR-3, MDA-MB-468, HCC1937, MDA-MB-231 and MDA-MB-157 (Fig. 1B).

In order to verify whether the occurrence of senescent cells in the SCP group was intrinsic to each cell line or due to the presence of a side population, we generated clones from the T47D (n = 20) cell line, and subjected them to the SABG assay at different intervals. All clones acted similarly to the parental T47D cell line with similar rates of SABG+ progeny. No clone gained the ICP phenotype. More importantly, none of the clones tested over a long period of time (>60 PDs) entered full senescence (data not shown), unlike normal mammary epithelial cells that undergo two stages of senescence arrest over a period of ~20 PDs [7]. The SABG assay can provide false-positive responses, especially when cells remain under confluence for a long period [15]. Although all our tests used low-density clonogenic conditions, we wanted to confirm the senescence arrest by a long-term (24 h) BrdU labeling assay under mitogenic

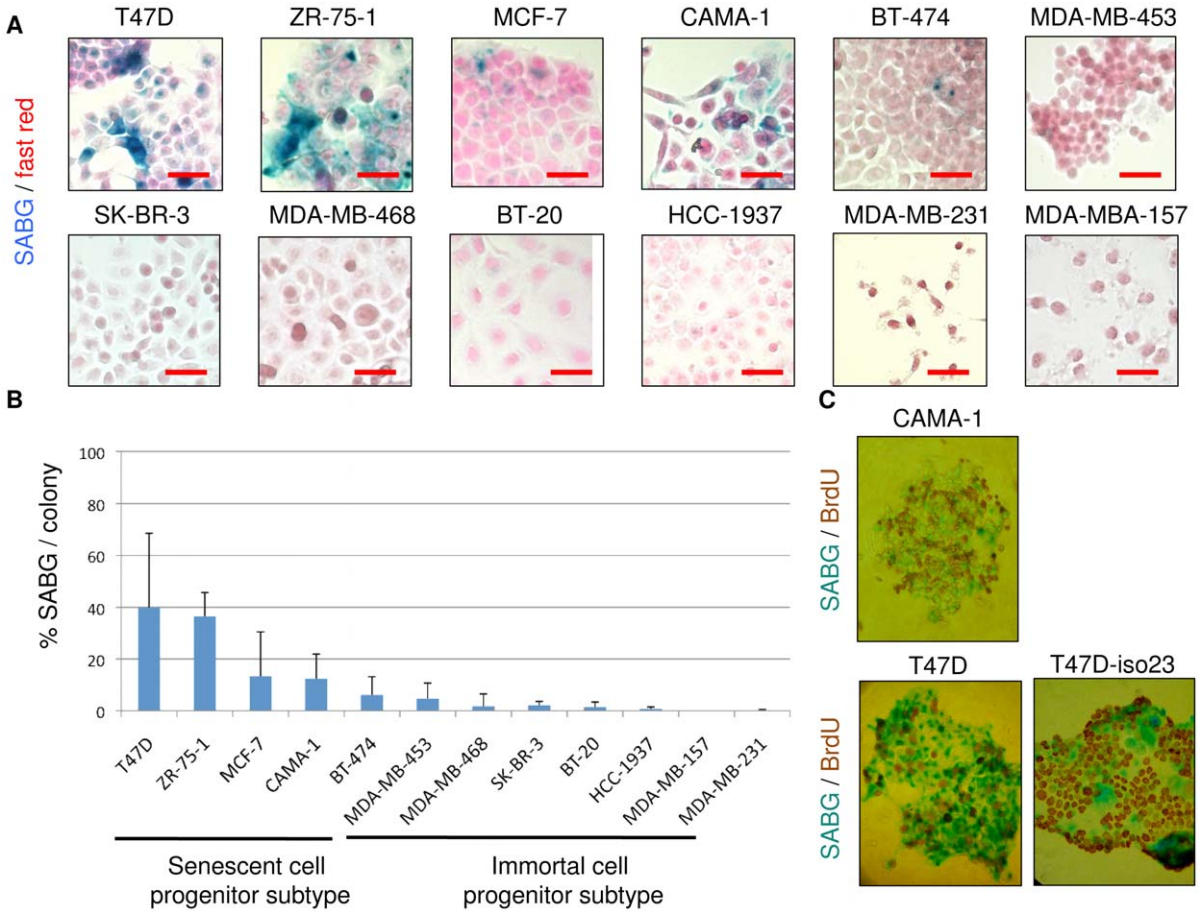


**Figure 1. Classification of breast cancer cell lines as senescent cell progenitor and immortal cell progenitor subtypes.** (**A**) Examples of SABG staining for senescence of breast cancer cell line colonies obtained after plating at low-density clonogenic conditions. Breast cancer cell lines (Table S1) were plated to obtain a few hundred colonies with 1–2 weeks of cell culturing and were subjected to SABG assay, followed by counterstaining with nuclear fast red. T47D, ZR-75-1, MCF-7, CAMA-1 and BT-474 generated heterogeneous colonies composed of with SABG+ and SABG- cells (shown here), but also fully negative and/or fully positive colonies. All other cell lines produced only SABG- colonies (<5% SABG+ cells). Scale bar: 50 μm. (**B**) Classification of breast cancer cell lines as senescent cell progenitor (SCP) and immortal cell progenitor (ICP) subtypes by quantification of the ability to generate senescent progeny. Cell lines with a mean of SABG+ cells higher than 5% were termed SCP, and the other cell lines as ICP. Colonies that were generated and stained as described in (**A**) were counted manually to calculate % SABG+ cells. At least 10 colonies were counted for each cell line. Error bars represent mean ± SD. (**C**) SABG+ senescent cells displayed terminal growth arrest. CAMA-1, T47D and T47D-iso23 colonies were generated as described in (**A**), labeled with BrdU for 24 h in the presence of freshly added culture medium, and subjected to SABG/BrdU double-staining. SABG+ cells are BrdU-, and *vice versa*. T47D-iso23 is a clone derived from T47D. Note that parental T47D and T47D-iso23 clones displayed similar staining features.
doi:10.1371/journal.pone.0011288.g001

conditions, as senescent cells in permanent cell cycle arrest cannot incorporate BrdU under these conditions [16]. Co-staining of cells for SABG and BrdU from CAMA-1, T47D, and T47D-iso23 colonies provided clear indication that the great majority of SABG+ senescent cells were BrdU-, whereas non-senescent BrdU+ cells were usually SABG- (Fig. 1C). These findings indicated that SABG+ senescent cells were at the terminal differentiation stage with an irreversible loss of DNA synthesis ability. Our observations also indicated that SABG and BrdU tests could be used alternatively to identify senescent (SABG+/BrdU-) and immortal (SABG-/BrdU+) cells under our experimental conditions.

## Senescent cell progenitor phenotype association with $p21^{Cip1}$ expression

$p16^{Ink4a}$ and $p21^{Cip1}$ (in a p53-dependent manner or independently) have been shown to be mediators of senescence arrest in different cells, including mammary epithelial cells [6,15,17,18,19]. We therefore analyzed the expression of $p16^{Ink4a}$ and $p21^{Cip1}$ in the cell line panel. Heterogeneously positive nuclear $p21^{Cip1}$ immunoreactivity was observed in four of the five SCP cell lines, but not in any of the seven ICP cell lines (Fig. 2A). The association of $p21^{Cip1}$ expression with the SCP subtype was statistically significant ($P = 0.01$). We also compared the expression of $p16^{Ink4a}$. Three of five SCP cell lines displayed heterogeneously positive immunostaining, whereas three of seven ICP cell lines displayed homogenously positive staining (Fig. S1). The difference of $p16^{Ink4a}$ expression between the two groups was not significant ($P = 1$). These observations indicated that the SCP phenotype was associated with $p21^{Cip}$ expression in breast cancer cell lines.

To test whether $p21^{Cip1}$ was directly involved in the senescence observed in SCP cells, we first performed $p21^{Cip1}$/SABG staining in T47D-iso23 cells (hereafter termed T47D). $p21^{Cip1}$, but not $p16^{Ink4a}$ staining, was associated with SABG staining (Fig. S2). Next, we generated two derivative cell lines following infection of T47D with lentiviral vectors encoding $p21^{Cip1}$ shRNA (T47D-p21sh) or a scrambled control (T47D-scr). Following the

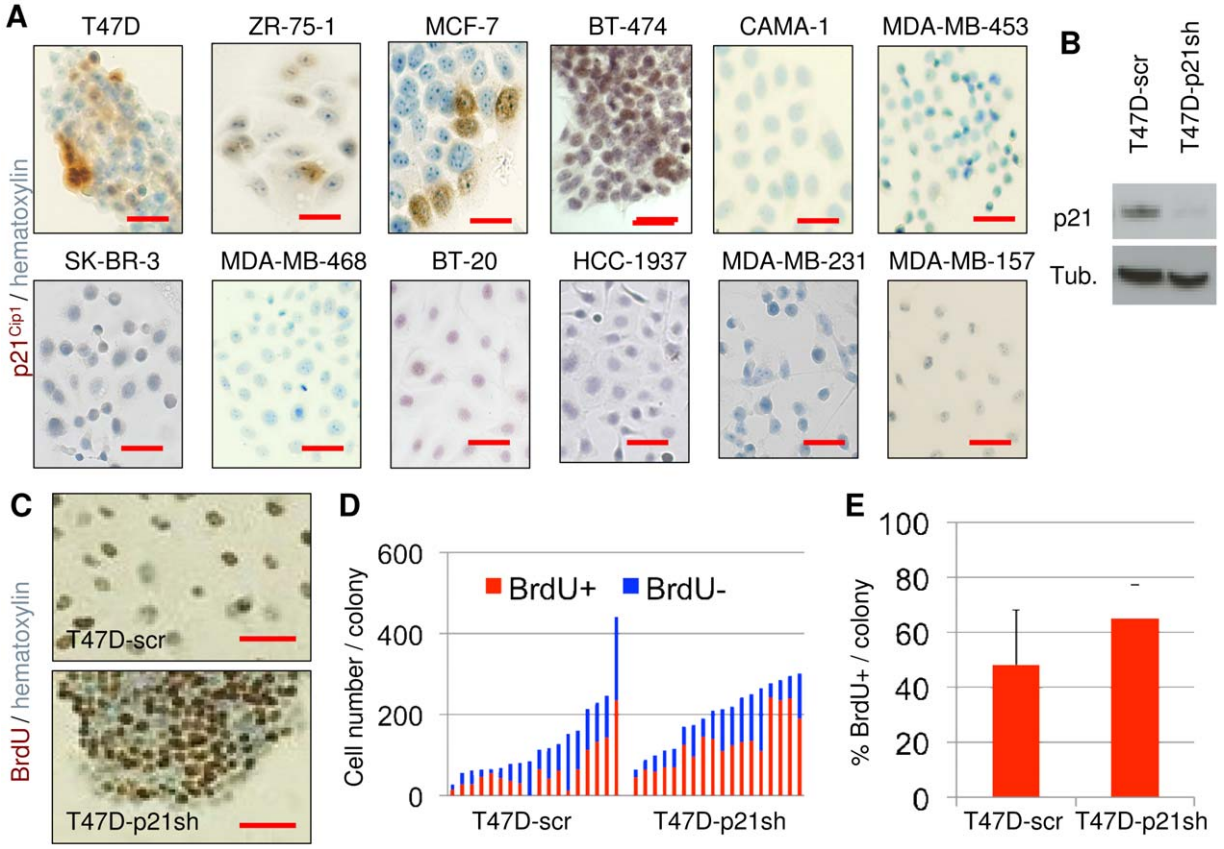


**Figure 2. Growth arrest observed in senescent cell progenitors was inhibited by $p21^{Cip1}$ silencing.** (**A**) Four of five senescent SCP cell lines (top four from left) generated colonies with heterogeneous expression of $p21^{Cip1}$; in contrast none of seven ICP cell lines generated $p21^{Cip1}$ cells. Colonies were immunostained for $p21^{Cip1}$, with hematoxylin used as counterstain. Scale bar: 50 μm. (**B–E**) $p21^{Cip1}$ silencing inhibited the production of the terminally arrested progeny of SCP cells. (**B**) shRNA-mediated inhibition of $p21^{Cip1}$ expression. T47D cells were infected with lentiviral vectors encoding $p21^{Cip1}$ shRNA or scrambled shRNA to generate T47D-p21sh and T47D-scr stable cell lines, and tested for $p21^{Cip1}$ knockdown by western blotting. (**C–E**) The ability to generate growth-arrested cells was inhibited by $p21^{Cip1}$ knockdown. Colonies were generated from respective cell lines, labeled with BrdU for 24 h, immunostained for BrdU, and slightly counterstained with hematoxylin to visualize BrdU+ and negative cells. Scale bar: 50 μm. (**C**). Individual colonies were manually counted for quantification of % BrdU cells. Each bar represents one colony (**D**). The silencing of $p21^{Cip1}$ caused a significant increase ($P = 0.0043$) in % ratios of BrdU+ cells (**E**). Mean % BrdU+ cells (± SD) values were calculated from data presented in (**D**). Error bars represent mean ± SD. Tub.; α-tubulin.
doi:10.1371/journal.pone.0011288.g002

demonstration of $p21^{Cip1}$ knockdown in T47D-p21sh cells by western blot assay (Fig. 2B), both cell lines were plated under low-density plating conditions, colonies were grown for 10 days, and subjected to SABG and BrdU staining. It was not possible to quantify SABG+ cells in T47D-p21sh cells because they formed tight clusters in culture (data not shown). We therefore used BrdU staining as an alternative method for senescent cell quantification (Fig. 2C). Randomly selected colonies were counted for the number of BrdU+ and BrdU- cells (Fig. 2D). The T47D-scr cell line generated BrdU+ progeny at a rate of 48±20% per colony (n = 18). Under the same conditions, T47D-p21sh cells displayed BrdU+ progeny at a rate of 65±12% per colony (n = 18), with a significant ($P = 0.0043$) increase in the number of cells escaping terminal arrest (Fig. 2E). These results indicated that $p21^{Cip1}$ was responsible, at least partly, for inducing the senescence observed in the progeny of T47D cells.

## The control of senescent cell progeny generation by an estrogen receptor

As stated above, $p21^{Cip1}$ is a downstream target of p53 for senescence, but T47D cells do not express wild-type p53 (Table S1). Estrogen inhibits $p21^{Cip1}$ expression [20] by c-Myc-mediated repression [21], *MYC* gene being a direct target of ER complex [22]. We therefore tested whether ER could be involved in the senescence observed in T47D cells. The data shown in Fig. 3A indicates that T47D cells displayed nuclear ER immunoreactivity in their great majority, but some progeny was ER-. More interestingly, these ER- cells tended to be SABG+, suggesting that senescence occurred in T47D cells as a result of ER loss. Next, we tested whether experimentally modifying ER activity in T47D cells had any effect on senescence response. After plating at low-density clonogenic conditions, cells were grown in a regular cell culture medium that contained weakly estrogenic phenol red [23] for seven days in order to obtain visible colonies. The culture medium was then changed with phenol-free DMEM complemented with charcoal-treated FCS, grown for two more days, and then cultivated for four more days in the presence of E2 ($10^{-9}$ M), OHT ($10^{-9}$ M to $10^{-6}$ M), or an ethanol vehicle as control. Colonies were subjected to SABG staining (Fig. 3B). Total and SABG+ cells were counted from 20 randomly selected colonies for each treatment (Fig. 3C). Colonies grown in a phenol-free charcoal-treated control medium complemented with an ethanol vehicle only displayed 31±13% SABG+ cells. Complementing this medium with $10^{-9}$ M

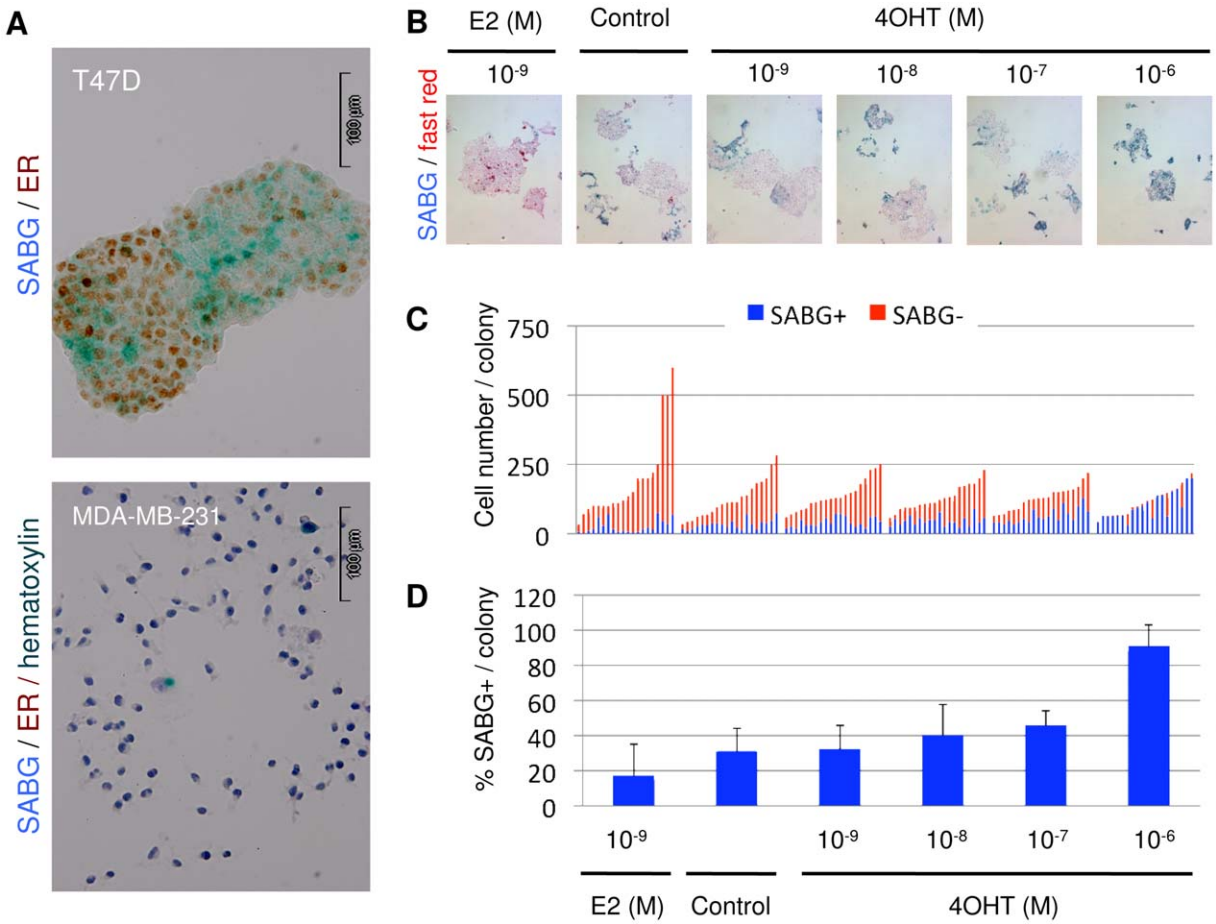


**Figure 3. Generation of senescent cell progeny was controlled by the estrogen receptor-α.** (**A**) SCP cells (T47D) expressed nuclear ER. Colonies were co-stained for senescence by SABG and for ER expression by immunoperoxidase. The MDA-MB-231 cell line was used as a negative control. (**B–D**) The production of senescent progeny in SCP cells was inhibited by estrogen (E2), but enhanced by tamoxifen (4OHT) treatment. After plating in low-density clonogenic conditions, T47D cells were grown in standard cell culture medium for seven days, followed by phenol-free DMEM complemented with charcoal-treated fetal calf serum for two days, and then cultivated for four days in the presence of E2, OHT, or an ethanol vehicle (control). Colonies were subjected to SABG staining (**B**). Total and SABG+ and SABG- cells were counted from 20 randomly selected colonies (**C**), and mean % SABG+ cells (± SD) values were calculated (**D**). Error bars represent mean ± SD. The inhibition of senescence by E2 and its activation by OHT was statistically significant when compared to ethanol-complemented control cells (*P* values 0.0093, 0.0002 and <0.0001 for $10^{-9}$ M E2, $10^{-7}$ M OHT and $10^{-6}$ M OHT, respectively).
doi:10.1371/journal.pone.0011288.g003

E2 generated colonies with 17±18% SABG+ cells. Senescence inhibition by E2 was nearly 50% and statistically significant when compared to the ethanol-complemented control cells ($P=0.0093$). In contrast to E2, OHT provoked a dose-dependent increase in the proportion of SABG+ cells. At the maximum dose used ($10^{-6}$ M OHT), 90±13% of colony-forming cells displayed a SABG+ signal (Fig. 3D), indicating that tamoxifen-mediated inactivation of ER can induce almost a complete senescence response in these cells ($P<0.0001$). The increase in senescence rate was also significant with $10^{-7}$ M OHT ($P=0.0002$).

Our findings strongly suggested that the senescence observed in the SCP T47D cell line was due to a loss of expression and/or function of ER in a subpopulation of the progeny of these cells. For confirmation, we constructed ER-overexpressing stable clones from T47D cells. The thhree clones with the highest ER expression were selected. In addition, three clones with endogenous expressions of ER were selected from stable clones obtained with an empty vector (Fig. 4A). Progeny obtained from these six clones were tested by BrdU assay (Fig. S3). Randomly selected colonies (n = 10) from each clone were evaluated for total and BrdU+ number of cells (Fig. 4B). Consistently higher levels of BrdU+ cells were observed with clones ectopically expressing the ER protein (Fig. 4C). Overexpression of ER resulted in a significant increase in the BrdU+ progeny ($P=0.034$). The protective effect of ER overexpression was not as important as the senescence-promoting effects of ER inhibition. This was not unexpected, since the parental cells used for the ER overexpression studies were already expressing high levels of endogenous ER (Fig. 4A), displaying a baseline anti-senescence activity due to the serum estrogen and phenol red found in the cell culture medium.

The close relationship between ER and senescence in the ER+ T47D cell line, and the highly effective treatment of ER+ breast tumors with tamoxifen, which induced senescence in our experimental model, suggested that senescence induction might be a relevant mechanism involved in anti-estrogen treatments. As fresh tumor tissues cannot be obtained from tamoxifen-treated patients for obvious ethical reasons, we analyzed untreated ER+ breast tumor samples for evidence of spontaneously occurring in vivo senescence. We screened a panel of 12 snap-frozen ER+ breast tumor tissues from 11 patients for senescence by an SABG

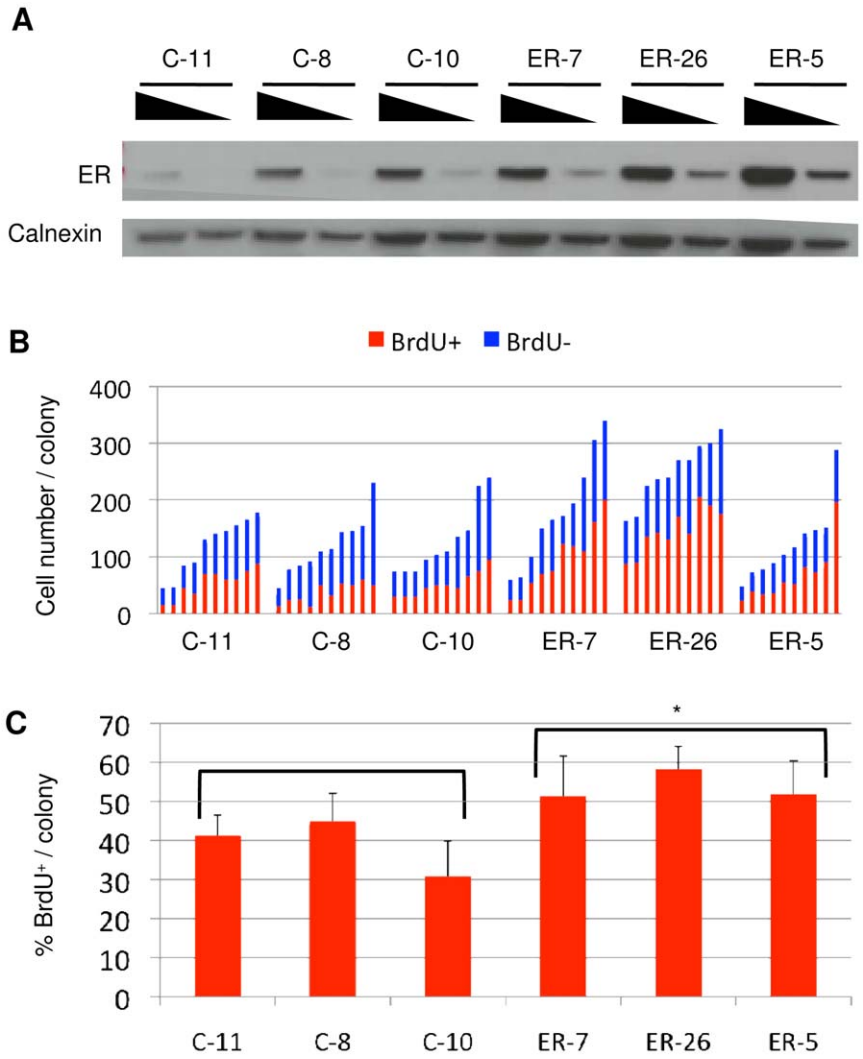


**Figure 4. Overexpression of estrogen receptor-α inhibited the production of terminally arrested progeny.** (**A**) ER-overexpressing (ER-5, ER-7, ER-26) and control (C-8, C-10, C-11) clones were established from T47D cells and tested for ER expression by western blotting using decreasing amounts of total proteins. Calnexin was used as loading control. (**B–C**). Colonies were generated, labeled with BrdU for 24 h and immunostained for BrdU (shown in Fig. S3). Individual colonies were manually counted for quantification of % BrdU cells (**B**), and mean % BrdU+ cells values were calculated (**C**). Error bars represent mean ± SD. ER overexpression caused a significant increase in % ratio of BrdU+ cells (*three ER clones *versus* three controls; $P = 0.034$).
doi:10.1371/journal.pone.0011288.g004

assay. The mean age of the patients was 58±12 yrs, with a mixed menopause status (Table S2). Two tumors (17%) displayed SABG+ cells that were scattered within the tumor area (Fig. S4). Thus, ER+ breast tumors also produced senescent progeny in vivo, but at a lower rate.

## Senescent cell progenitor and immortal cell progenitor subtypes' abilities to differentiate into luminal and myoepithelial cell types

The cellular specificity of ER expression in the mammary epithelial cell hierarchy is poorly understood. Previous data suggests that normal ER+ cells may represent either relatively differentiated luminal cells with limited progenitor capacity or primitive progenitors with stem cell properties in the luminal cell compartment [4,24,25]. Based on the close association between senescence (which can be considered a manifestation of terminal differentiation) and loss of ER positivity, we hypothesized that ER+ SCP cells may differ from ER- ICP cells by their differentiation potential. We surveyed a few hundred single-cell-derived colonies from each of the 12 cell lines for production of stem/progenitor-like, luminal-like, and myoepithelial-like cells. We used CD44 as a positive stem/progenitor cell marker [26,27], CD24, ER, and CK19 as luminal lineage markers [27,28,29], and ASMA as a myoepithelial lineage marker [29].

Representative examples of marker studies by immunoperoxidase staining in SCP and ICP cell lines are shown in Fig. 5. All five SCP cell lines displayed a heterogeneous pattern of positivity for CD44; some colonies were fully positive, some fully negative, and others were composed of both positive and negative cells. CD44/CD24 double immunofluorescence studies with the T47D cell line indicated that SCP cells produce also CD44+/CD24- stem/progenitor cells, as expected (data not shown). In sharp contrast, five of the seven ICP cell lines generated only fully positive CD44 colonies, indicating they do not produce CD44- cells. One cell line was totally CD44-. Only one cell line displayed

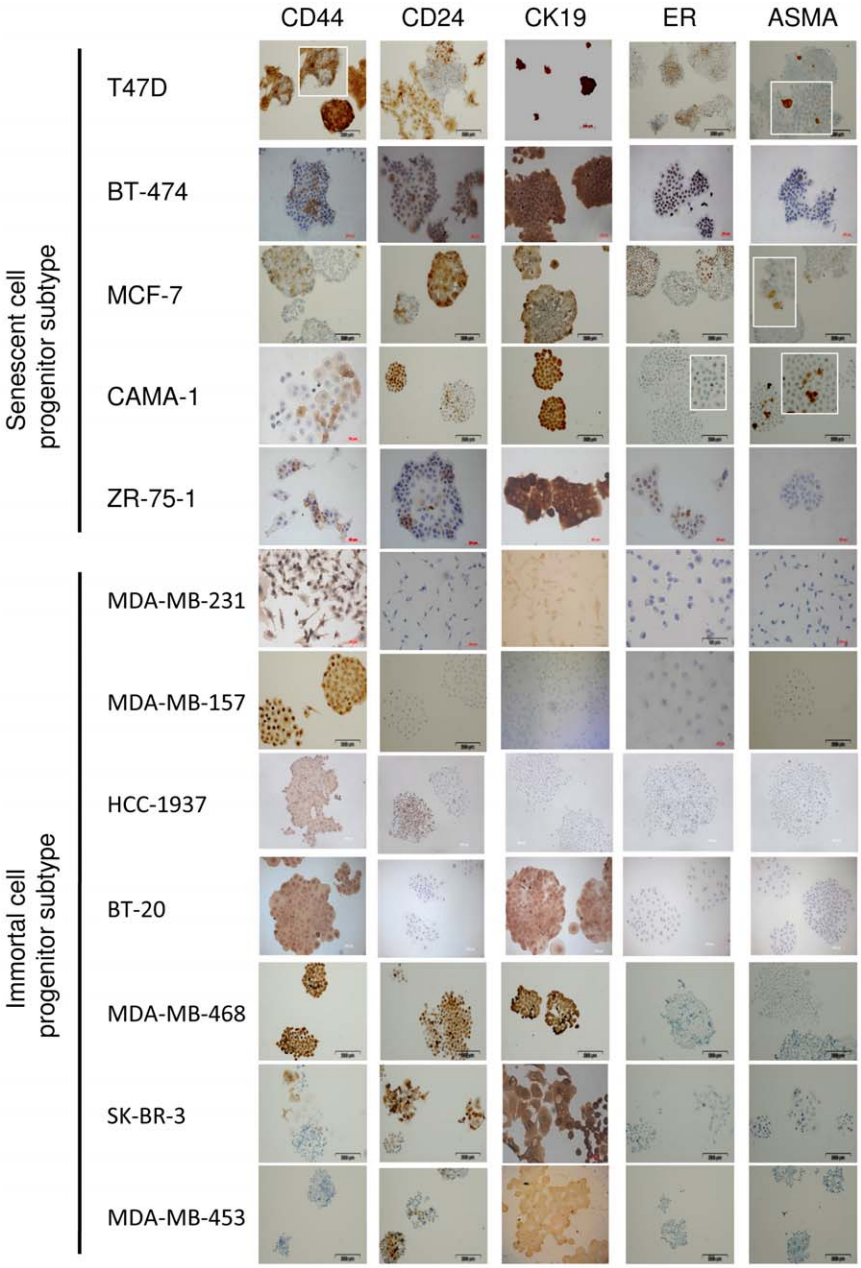


**Figure 5. Senescent cell progenitor and immortal cell progenitor subtypes greatly differed in their ability to differentiate into luminal and myoepithelial lineage cells.** Senescent cell progenitor and immortal cell progenitor subtype cell lines were studied by immunoperoxidase staining using CD44 and markers for luminal epithelial (CD24, CK19, ER) and myoepithelial (ASMA) lineages. Insets: magnified views of positive cells. Both subtypes have CD44+ cells. Senescent cell progenitor cell lines produced both progenitor-like (CD44+; CD24−), as well as ER+ luminal-like and ASMA+ myoepithelial-like cells (except ZR-75-1 for myoepithelial-like cells). Immortal cell progenitor cell lines were defective for generation of ER+ luminal-like or ASMA+ myoepithelial-like cells. Moreover, five of seven cell lines could not generate CD44- cells. The expression of CD24 and CK19 markers did not differ significantly between the two subgroups, except that some immortal cell progenitor subtype cell lines did not express CD24 or CK19.
doi:10.1371/journal.pone.0011288.g005

a pattern similar to that of SCP cell lines. A comparison of the two subtypes indicated that the ability to generate both CD44+ and CD44- progeny was significantly associated with the SCP phenotype ($P = 0.0046$). All five SCP cell lines displayed heterogeneous, but mostly positive ER immunostaining, whereas all seven ICP cell lines never generated ER+ cells. The expression of ER was also significantly associated with the SCP subtype ($P = 0.0012$), as well as the ability to produce ASMA+ progeny ($P = 0.0046$). The ICP cell lines did not generate ASMA+ cells, while four out of five SCP cell lines generated rare ASMA+ cells under low-density clonogenic conditions. Interestingly, the abundance of ASMA+ cells was much higher in the two SCP cell lines that were tested at high cell density (Fig. S5). This suggests that either the production of ASMA+ cells is enhanced at high cell density, or these myoepithelial-like cells display limited survival under long-term culture conditions. We did not find a strong association between the expression of CD24 and CK19 markers and cell subtype. All five SCP cell lines and three ICP cell lines

generated heterogeneously staining colonies for CD24 expression. Similarly, all five SCP cell lines, as well as three ICP cell lines, expressed CK19, but homogenously.

## Typical features of senescent progenitor and immortal progenitor breast cancer cell lines

As summarized in Fig. 6, SCP and ICP subtype cell lines displayed several subtype-specific features. All SCP cell lines produced differentiated and senescent cells, in addition to putative CD44+/CD24− stem/progenitor cells. Indeed, all of them produced ER+ and CD24+ luminal-like cells and most of them (n = 4/5) also produced ASMA+ myoepithelial-like cells. In contrast, five of the seven ICP cell lines never produced CD44- cells, suggesting they cannot generate differentiated progeny under the experimental conditions tested. In confirmation of this hypothesis, four ICP cell lines only produced CD44+/CD24−/ER-/CK19-/ASMA- stem/progenitor-like, but never differentiated cells. Furthermore, all seven ICP cell lines were unable to produce ASMA+ myoepithelial-like, ER+ luminal-like or SABG+ senescent cells. CD24 and CD19 luminal lineage markers were expressed in three cell lines, one of which was fully positive for the CD44 stem/progenitor marker.

## SCP and ICP subtype cell lines correlate with distinct breast tumor subtypes

Distinct cell-type features associated with SCP and ICP subtypes suggest that they may be phenocopies of molecularly defined breast tumor subtypes [1,2,3,30]. As the prognosis and therapeutic response of each subtype is different [2,3], we questioned whether we could assign SCP and ICP cell lines to known molecular subtypes of breast tumors. Using cell line and primary tumor gene expression datasets, we conducted a hierarchical clustering analysis. The "intrinsic gene set" data generated by Sorlie et al. [2] to classify breast tumors into five molecular subtypes was used to filter cell line data generated by Charafe-Jauffret et al. [13]. A set of 175 genes was common between the two data sets. Sixty-eight tumors and 31 cell lines were subjected to pair-wise complete-linkage hierarchical clustering and distance measurements. This tumor–cell line combined analysis produced two major clusters. One cluster was composed of basal and luminal B subtype tumors and five of six ICP cell lines. The other cluster included luminal A, ERBB2+, and "normal-like" subtype tumors and all five SCP subtype cells. Four cell lines clustered with the luminal A tumor subclass. Finally. one cell line clustered with the "normal-like" subclass (Fig. 7A). A full list of clustered tumors and cell lines is provided in Fig. S6.

Luminal A tumors clustering with our SCP subtype cell lines displayed the longest tumor-free, distant metastasis-free, and overall survival rates. In contrast, basal and luminal B tumors clustering with our ICP subtype cell lines had the worst prognosis, with shorter tumor-free, distant metastasis-free, and overall survival times [2]. Our cluster analysis suggested that the ability to generate differentiated and senescent progeny characterized breast cancers with poor tumorigenicity, and that resistance to differentiation and senescence was indicative of more aggressive tumorigenicity. We compared in vivo intrinsic tumorigenic behaviors of the SCP cell line T47D and the ICP cell line MDA-MB-231 in female (n = 5 for each cell line) and male (n = 4 for each cell line) CD1 *nude* mice Fig. 7B). MDA-MB-231 cells displayed higher tumorigenicity than T47D cells. In total, we observed progressively growing tumors in five of nine animals injected with MDA-MB-231. In contrast, T47D formed smaller and regressing tumors in nine of nine animals ($P<0.03$). Interestingly, the difference in tumorigenicity between these two cell lines was more pronounced in male animals ($P<0.05$ after 20 days post-injection). To test whether the difference in tumorigenicity between MDA-MB-231 and T47D cells was correlated with spontaneous in vivo senescence, we analyzed four tumors from each cell line. Two T47D tumors displayed positive SABG staining, whereas no positive staining was observed with all four MDA-MB-231 tumors (Fig. S7).

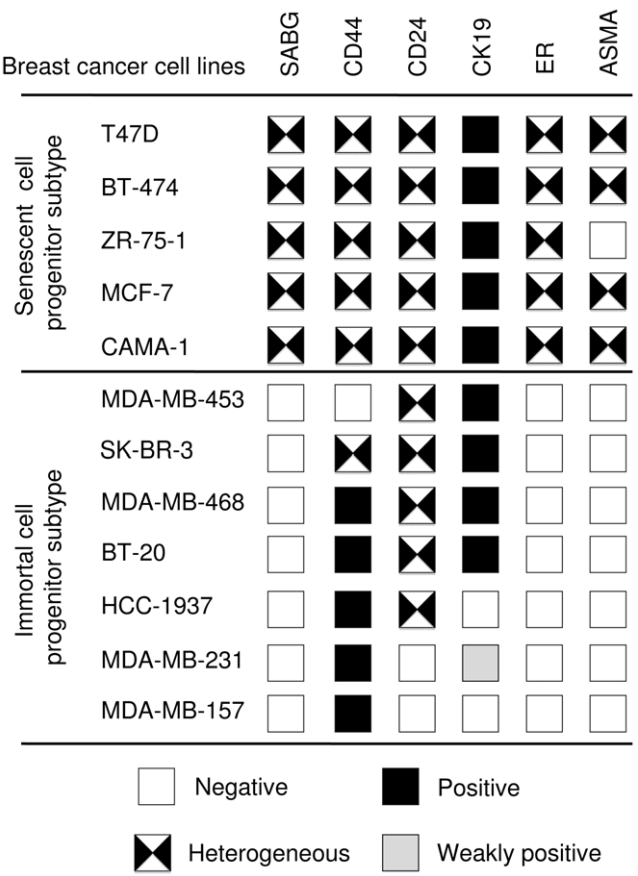


**Figure 6. Typical features of senescent progenitor and immortal progenitor breast cancer cell lines.**
doi:10.1371/journal.pone.0011288.g006

## Discussion

In recent years, phenotypic heterogeneity of breast cancers has been correlated with genetic and molecular heterogeneity [1,3]. Breast cancer subtypes may represent cancers originating from different progenitor cells. Molecular and phenotypic heterogeneity and associated clinical manifestations of breast tumor subtypes have been related to the type of hypothetical tumor progenitor cells originating from a hypothetical mammary epithelial stem cell or from downstream progenitor cells [4,5]. This hypothesis has not been fully validated, mainly because a hierarchical map of cells involved in mammary epitheliogenesis has not yet been established.

To better understand phenotypic differences between breast cancer subtypes, we applied senescence as a surrogate marker for the potential to generate terminally differentiated progeny. We completed these studies with markers for breast stem/progenitor and differentiated luminal and myoepithelial lineage cells. The use of low-density clonogenic conditions allowed us to follow the fate

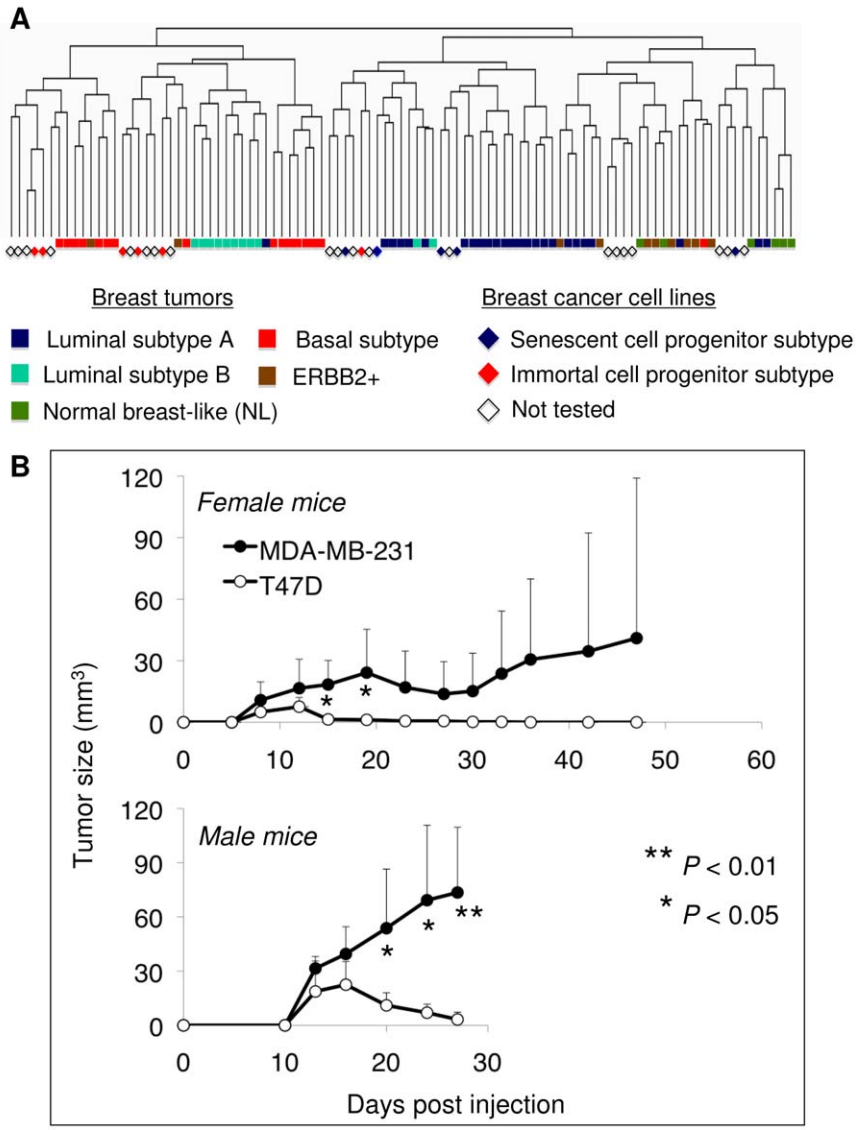


**Figure 7. Senescence cell progenitor and immortal cell progenitor subtype cell lines correlate with distinct breast tumor subtypes.** (**A**) Unsupervised hierarchical clustering of breast tumor and cell line gene expression data were obtained from Sorlie et al [2] and Charafe-Jauffret et al [25]. Dendrogram displaying the relative organization of tumor and cell line data demonstrated that ICP cell lines cluster with basal and luminal A tumors in the same branch, except for MDA-MB-453. In contrast, SCP cell lines clustered with luminal A (BT-474, CAMA-1, MCF-7, T47D) and "normal-like" tumors (ZR-75-1). No data was available for MDA-MB-468. A dendrogram with sample IDs was provided in Fig. S6. The "intrinsic gene set" data generated by Sorlie et al. [2] was used to filter cell line data generated by Charafe-Jauffret et al. [13]. A set of 175 genes was common between the two data sets. Sixty-eight tumors and 31 cell lines were subjected to pair-wise complete-linkage hierarchical clustering and distance measurements. (**B**) Immortal cell progenitor MDA-MB-231 was more tumorigenic than the SCP type T47D cell line. Female (n = 5 per cell line) and male (n = 4 per cell line) CD1*nude* mice received $5\times10^6$ cells by subcutaneous injection and observed up to 47 days for tumor formation. Chart displays mean tumor sizes (± S.D.) generated by MDA-MB-231 and T47D cell lines, respectively in female (top) and mala (bottom) mice. T47D cells formed smaller tumors that regressed and completely resolved within 30 days. Tumors formed by MDA-MB-231 were larger in size and did not show total resolution. Note that this cell line was more tumorigenic in male mice.
doi:10.1371/journal.pone.0011288.g007

of a large number of progeny for each cell line studied. From these approaches, we draw several important conclusions. First, breast cancer cell lines form two distinct groups: SCP and ICP subtypes. The SCP cell lines produce non-senescent and senescent progeny, whereas the ICP cell lines produce only non-senescent progeny. Second, SCP and ICP cell lines are exclusively ER+ and ER- cell lines, respectively. Senescence occurs as a result of ER loss associated with $p21^{Cip1}$ induction in SCP cells. Inversely, experimental activation of ER by E2 protects from senescence, whereas its inactivation by tamoxifen aggravates it. Thus, senescence in ER-dependent cells appears to result from the loss of survival signals generated by transcriptional activity of ER. A similar type of senescence has been reported for lymphoma, osteosarcoma, and hepatocellular carcinoma tumors upon c-*MYC* inactivation [31]. Third, SCP cells generate ER+, CD24+, or CK19+ luminal-like, as well as ASMA+ myoepithelial-like progeny. These findings strongly suggest that most, if not all, SCP cells have the capacity to give rise to two major types of differentiated cells that are found in normal mammary epithelium. In sharp contrast, ICP cells never produce ER+ luminal-like or

ASMA+ myoepithelial-like cells. Indeed, some ICP cells generate only CD44+ stem/progenitor-like cells and never CD44−, CD24+, CK19+, ER+, or ASMA+ cells. These findings indicate that ICP cells have limited differentiation ability, at least under in vitro conditions. The differentiation ability of ICP cells appears to be lost completely or partially, so that they do not differentiate fully while they self-renew as stem/progenitor-like cells. Fourth, SCP cell lines form the same molecular cluster with luminal A and "normal-like" breast tumors. This suggests that SCP cell lines are phenocopies of these relatively benign and/or anti-estrogen-responsive tumors. The poor tumorigenicity of SCP cells in *nude* mice correlates with better tumor-free and metastasis-free survival of patients with luminal A type tumors. In contrast, ICP cell lines cluster with luminal B and basal-like breast tumor subtypes, and they are more tumorigenic, as expected for luminal B and basal-like tumor cells. It is presently unknown whether breast tumor subtypes that cluster with SCP or ICP cell lines are also composed of either differentiating or mostly self-renewing stem/progenitor cells. Recent studies reported that breast tumors may contain only CD44+, or only CD24+ cells, as well as mixed cell populations, and that CD44+ tumor cells express many stem-cell markers [27,32]. In addition, an association between basal-like breast cancer and the presence of CD44+/CD24− cells has been established [32].

The mechanisms of the differentiation block observed in ICP cell lines are not known. One might argue that cell lines that produce only CD44+, but never differentiation marker-positive cells, cannot be defined as stem/progenitor cells. However, such cell lines are not completely inert to differentiation stimuli, and may undergo differentiation under special conditions. For example, MDA-MB-231 and MDA-MB-468 cells (identified as ICP cell lines here) can be induced to differentiate into ER+ cells by Wnt5a treatment, and MDA-MB-231 cells then become sensitive to tamoxifen [33].

Most of the findings reported here are derived from in vitro studies performed with established cancer cell lines. Presently, it is unknown to what extent these findings are also relevant for breast tumors. We provide here some promising data that supports in vivo relevance of our conclusions. First, our cluster analyses associated SCP cell types with luminal A and "normal-like" breast tumors, whereas ICP cell types shared similar gene expression profiles with luminal B and basal-like breast tumors. Second, ICP-type MDA-MB-231 cells were more tumorigenic than SCP-type T47D cells. T47D cells formed smaller tumors in some animals, and all tumors displayed regression between 10 and 15 days post-injection. Accordingly, we observed positive SABG staining in two out of four T47D tumors, but not in MDA-MB-231 tumors. Obviously, ICP-like and SCP-like tumors in affected women may or may not display similar tumorigenic potentials, depending on the women's hormonal status and treatment conditions. However, as most SCP-like luminal A or ER+ tumors are successfully treated with tamoxifen [34], their less aggressive behavior could be related to their highly effective senescence response to tamoxifen treatment, as shown here with T47D cells under in vitro conditions (Fig. 3). It will be interesting to examine whether the success of anti-estrogenic treatments is indeed associated with senescence induction in breast tumors. If this is the case, senescence-inducing treatments could be considered for breast cancer.

In conclusion, our analyses reveal that the in vitro ability to generate senescent progeny permits discrimination between cells that share molecular and tumorigenic similarities with luminal A subtype breast tumors from cells related to basal/luminal B subtype tumors. We also provide in vitro evidence for classifying breast cancers into two major groups based on the ability to generate differentiated progeny. Less-tumorigenic SCP cell lines generate both luminal- and myoepithelial-like cells. In contrast, more-tumorigenic ICP cell lines are defective in their ability to generate differentiated progeny. Our findings may have prognostic relevance and serve as a basis for therapeutically inducing differentiation and senescence in breast cancer.

## Supporting Information

**Dataset S1** STR analysis data that shows the authenticity of breast cancer cell lines used in this study.
Found at: doi:10.1371/journal.pone.0011288.s001 (1.50 MB XLS)

**Table S1** Gene clusters, genetic mutations and epigenetic changes of breast cancer cell lines used in this study.
Found at: doi:10.1371/journal.pone.0011288.s002 (0.05 MB DOC)

**Table S2** Estrogen receptor (ER) status, main pathological features of senescence staining (SABG) of breast tumors used in this study.
Found at: doi:10.1371/journal.pone.0011288.s003 (0.05 MB DOC)

**Figure S1** p16Ink4a expression in colonies obtained from breast cancer cell lines. There was no correlation between p16Ink4a expression and progenitor subtype.
Found at: doi:10.1371/journal.pone.0011288.s004 (3.39 MB TIF)

**Figure S2** Co-staining experiments indicate that SABG staining is associated with p21Cip1, but with p16Ink4a expression in SCP cells. Colonies were generated from T47D and MB-MDA-231 cells and subjected to SABG staining, followed by p21Cip1 or p16Ink4a immunoperoxidase (brown) staining. MDA-MB-231 cells were used as negative control.
Found at: doi:10.1371/journal.pone.0011288.s005 (2.74 MB TIF)

**Figure S3** Effect of estrogen receptor-overexpression on the production of BrdU-negative terminally arrested cell progeny. ER-overexpressing (ER-5, ER-7, ER-26) and control (C-8, C-10, C-11) stable clones were established from T47D cells. Following transfection with ER expression and control vectors, colonies were generated from respective cell lines, labeled with BrdU for 24 h, immunostained for BrdU (brown), and slightly counterstained with hematoxylin to visualize BrdU+ and BrdU- cells.
Found at: doi:10.1371/journal.pone.0011288.s006 (6.57 MB TIF)

**Figure S4** Detection of SABG+ senescent cells in estrogen receptor-positive breast tumors. Snap-frozen tumors were used to obtain 6 μ thick sections and used directly to detect SABG+ cells. H&E: hematoxylin-eosin staining.
Found at: doi:10.1371/journal.pone.0011288.s007 (9.45 MB TIF)

**Figure S5** ASMA+ myoepithelial-like cells are produced frequently in senescent cell progenitor T47D and MCF-7 cell lines under confluent conditions. ASMA was tested by immunoperoxidase.
Found at: doi:10.1371/journal.pone.0011288.s008 (4.08 MB TIF)

**Figure S6** Unsupervised hierarchical clustering of breast tumor and cell line gene expression data that is described in Fig. 7A. Dendrogram shown here includes tumor and cell line sample IDs.
Found at: doi:10.1371/journal.pone.0011288.s009 (1.05 MB TIF)

**Figure S7** Tumors derived from T47D but not from MDA-MB-231 display SABG (+) senescent cells. Two of four T47D tumors

displayed SABG+ cells. All four MDA-MB-231 tumors lacked SABG+ cells.
Found at: doi:10.1371/journal.pone.0011288.s010 (7.97 MB TIF)

## Acknowledgments

We thank Rana Nelson for editorial help.

## Author Contributions

Conceived and designed the experiments: MO. Performed the experiments: MM SB HY HA SS PT BGD BC. Analyzed the data: MM UHT IGY CA MO. Contributed reagents/materials/analysis tools: BB. Wrote the paper: MM MO.

## References


1. Perou CM, Sorlie T, Eisen MB, van de Rijn M, Jeffrey SS, et al. (2000) Molecular portraits of human breast tumours. Nature 406: 747–752.
2. Sorlie T, Tibshirani R, Parker J, Hastie T, Marron JS, et al. (2003) Repeated observation of breast tumor subtypes in independent gene expression data sets. Proc Natl Acad Sci U S A 100: 8418–8423.
3. Sotiriou C, Pusztai L (2009) Gene-expression signatures in breast cancer. N Engl J Med 360: 790–800.
4. Stingl J, Caldas C (2007) Molecular heterogeneity of breast carcinomas and the cancer stem cell hypothesis. Nat Rev Cancer 7: 791–799.
5. Vargo-Gogola T, Rosen JM (2007) Modelling breast cancer: one size does not fit all. Nat Rev Cancer 7: 659–672.
6. Romanov SR, Kozakiewicz BK, Holst CR, Stampfer MR, Haupt LM, et al. (2001) Normal human mammary epithelial cells spontaneously escape senescence and acquire genomic changes. Nature 409: 633–637.
7. Stampfer MR, Yaswen P (2003) Human epithelial cell immortalization as a step in carcinogenesis. Cancer Lett 194: 199–208.
8. Neve RM, Chin K, Fridlyand J, Yeh J, Baehner FL, et al. (2006) A collection of breast cancer cell lines for the study of functionally distinct cancer subtypes. Cancer Cell 10: 515–527.
9. Gur-Dedeoglu B, Konu O, Kir S, Ozturk AR, Bozkurt B, et al. (2008) A resampling-based meta-analysis for detection of differential gene expression in breast cancer. BMC Cancer 8: 396.
10. Ozturk N, Erdal E, Mumcuoglu M, Akcali KC, Yalcin O, et al. (2006) Reprogramming of replicative senescence in hepatocellular carcinoma-derived cells. Proc Natl Acad Sci U S A 103: 2178–2183.
11. Dimri GP, Lee X, Basile G, Acosta M, Scott G, et al. (1995) A biomarker that identifies senescent human cells in culture and in aging skin in vivo. Proc Natl Acad Sci U S A 92: 9363–9367.
12. Alotaibi H, Yaman EC, Demirpence E, Tazebay UH (2006) Unliganded estrogen receptor-alpha activates transcription of the mammary gland Na+/I− symporter gene. Biochem Biophys Res Commun 345: 1487–1496.
13. Charafe-Jauffret E, Ginestier C, Monville F, Finetti P, Adelaide J, et al. (2006) Gene expression profiling of breast cell lines identifies potential new basal markers. Oncogene 25: 2273–2284.
14. Stingl J (2009) Detection and analysis of mammary gland stem cells. J Pathol 217: 229–241.
15. Campisi J, d'Adda di Fagagna F (2007) Cellular senescence: when bad things happen to good cells. Nat Rev Mol Cell Biol 8: 729–740.
16. Wei W, Sedivy JM (1999) Differentiation between senescence (M1) and crisis (M2) in human fibroblast cultures. Exp Cell Res 253: 519–522.
17. Kiyono T, Foster SA, Koop JI, McDougall JK, Galloway DA, et al. (1998) Both Rb/p16INK4a inactivation and telomerase activity are required to immortalize human epithelial cells. Nature 396: 84–88.
18. Beausejour CM, Krtolica A, Galimi F, Narita M, Lowe SW, et al. (2003) Reversal of human cellular senescence: roles of the p53 and p16 pathways. EMBO J 22: 4212–4222.
19. Garbe JC, Holst CR, Bassett E, Tlsty T, Stampfer MR (2007) Inactivation of p53 function in cultured human mammary epithelial cells turns the telomere-length dependent senescence barrier from agonescence into crisis. Cell Cycle 6: 1927–1936.
20. Cariou S, Donovan JC, Flanagan WM, Milic A, Bhattacharya N, et al. (2000) Down-regulation of p21WAF1/CIP1 or p27Kip1 abrogates antiestrogen-mediated cell cycle arrest in human breast cancer cells. Proc Natl Acad Sci U S A 97: 9042–9046.
21. Mukherjee S, Conrad SE (2005) c-Myc suppresses p21WAF1/CIP1 expression during estrogen signaling and antiestrogen resistance in human breast cancer cells. J Biol Chem 280: 17617–17625.
22. Dubik D, Shiu RP (1992) Mechanism of estrogen activation of c-myc oncogene expression. Oncogene 7: 1587–1594.
23. Berthois Y, Katzenellenbogen JA, Katzenellenbogen BS (1986) Phenol red in tissue culture media is a weak estrogen: implications concerning the study of estrogen-responsive cells in culture. Proc Natl Acad Sci U S A 83: 2496–2500.
24. Booth BW, Smith GH (2006) Estrogen receptor-alpha and progesterone receptor are expressed in label-retaining mammary epithelial cells that divide asymmetrically and retain their template DNA strands. Breast Cancer Res 8: R49.
25. Shyamala G, Chou YC, Cardiff RD, Vargis E (2006) Effect of c-neu/ErbB2 expression levels on estrogen receptor alpha-dependent proliferation in mammary epithelial cells: implications for breast cancer biology. Cancer Res 66: 10391–10398.
26. Al-Hajj M, Wicha MS, Benito-Hernandez A, Morrison SJ, Clarke MF (2003) Prospective identification of tumorigenic breast cancer cells. Proc Natl Acad Sci U S A 100: 3983–3988.
27. Shipitsin M, Campbell LL, Argani P, Weremowicz S, Bloushtain-Qimron N, et al. (2007) Molecular definition of breast tumor heterogeneity. Cancer Cell 11: 259–273.
28. Sleeman KE, Kendrick H, Ashworth A, Isacke CM, Smalley MJ (2006) CD24 staining of mouse mammary gland cells defines luminal epithelial, myoepithelial/basal and non-epithelial cells. Breast Cancer Res 8: R7.
29. Yeh IT, Mies C (2008) Application of immunohistochemistry to breast lesions. Arch Pathol Lab Med 132: 349–358.
30. Sotiriou C, Neo SY, McShane LM, Korn EL, Long PM, et al. (2003) Breast cancer classification and prognosis based on gene expression profiles from a population-based study. Proc Natl Acad Sci U S A 100: 10393–10398.
31. Wu CH, van Riggelen J, Yetil A, Fan AC, Bachireddy P, et al. (2007) Cellular senescence is an important mechanism of tumor regression upon c-Myc inactivation. Proc Natl Acad Sci U S A 104: 13028–13033.
32. Honeth G, Bendahl PO, Ringner M, Saal LH, Gruvberger-Saal SK, et al. (2008) The CD44+/CD24− phenotype is enriched in basal-like breast tumors. Breast Cancer Res 10: R53.
33. Ford CE, Ekstrom EJ, Andersson T (2009) Wnt-5a signaling restores tamoxifen sensitivity in estrogen receptor-negative breast cancer cells. Proc Natl Acad Sci U S A 106: 3919–3924.
34. (1998) Tamoxifen for early breast cancer: an overview of the randomised trials. Early Breast Cancer Trialists' Collaborative Group. Lancet 351: 1451–1467.

# APPENDIX IV

Copyright and reprint permissions

## Order Completed

Thank you very much for your order.

This is a License Agreement between Pelin Telkoparan ("You") and AlphaMed Press ("AlphaMed Press") The license consists of your order details, the terms and conditions provided by AlphaMed Press, and the payment terms and conditions.

| | |
|---|---|
| License number | Reference confirmation email for license number |
| License date | May 08, 2013 |
| Licensed content publisher | AlphaMed Press |
| Licensed content title | The oncologist |
| Licensed content date | Jan 1, 1996 |
| Type of use | Thesis/Dissertation |
| Requestor type | Academic institution |
| Format | Print, Electronic |
| Portion | image/photo |
| Number of images/photos requested | 1 |
| Title or numeric reference of the portion(s) | Chapter 1, Figure 1.1. |
| Editor of portion(s) | N/A |
| Author of portion(s) | Israels and Israels, 2000 |
| Volume of serial or monograph | 5 |
| Page range of portion | 510-513 |
| Publication date of portion | jun/2013 |
| Rights for | Main product |
| Duration of use | Life of current edition |
| Creation of copies for the disabled | no |
| With minor editing privileges | no |
| For distribution to | Other territories and/or countries |
| Territory/Countries where you intend to distribute new product | TURKEY |
| In the following language(s) | Original language of publication |
| With incidental promotional use | no |
| Lifetime unit quantity of new product | 0 to 499 |
| Made available in the following markets | Education |

| | |
|---|---|
| The requesting person/organization | Pelin Telkoparan |
| Order reference number | |
| Author/Editor | Pelin Telkoparan |
| The standard identifier | PT14031982 |
| Title | Characterization of the coiled-coil domain-containing protein 124 (Ccdc124) as a novel centrosome and midbody component involved in cytokinesis. |
| Publisher | Bilkent University |
| Expected publication date | Jun 2013 |
| Estimated size (pages) | 120 |
| Billing Type | Invoice |
| Billing address | Bilkent Universitesi Fen Fakultesi<br>Molekuler Biyologi ve Genetik Bolumu<br>ANKARA, 06680<br>Turkey |
| Total (may include CCC user fee) | 0.00 USD |

CLOSE WINDOW

# NATURE PUBLISHING GROUP LICENSE TERMS AND CONDITIONS

May 03, 2013

This is a License Agreement between Pelin Telkoparan ("You") and Nature Publishing Group ("Nature Publishing Group") provided by Copyright Clearance Center ("CCC"). The license consists of your order details, the terms and conditions provided by Nature Publishing Group, and the payment terms and conditions.

**All payments must be made in full to CCC. For payment instructions, please see information listed at the bottom of this form.**

| | |
|---|---|
| License Number | 3141480960172 |
| License date | May 03, 2013 |
| Licensed content publisher | Nature Publishing Group |
| Licensed content publication | Nature Cell Biology |
| Licensed content title | Re-staging mitosis: a contemporary view of mitotic progression |
| Licensed content author | Jonathon PinesandConly L. Rieder |
| Licensed content date | Jan 1, 2001 |
| Volume number | 3 |
| Issue number | 1 |
| Type of Use | reuse in a thesis/dissertation |
| Requestor type | non-commercial (non-profit) |
| Format | print and electronic |
| Portion | figures/tables/illustrations |
| Number of figures/tables/illustrations | 1 |
| Figures | Figure 1.2 |
| Author of this NPG article | no |
| Your reference number | |
| Title of your thesis / dissertation | Characterization of the coiled-coil domain-containing protein 124 (Ccdc124) as a novel centrosome and midbody component involved in cytokinesis |
| Expected completion date | Jun 2013 |
| Estimated size (number of pages) | 120 |
| Total | 0.00 USD |
| Terms and Conditions | |

## Terms and Conditions for Permissions

Nature Publishing Group hereby grants you a non-exclusive license to reproduce this

material for this purpose, and for no other use, subject to the conditions below:

1. NPG warrants that it has, to the best of its knowledge, the rights to license reuse of this material. However, you should ensure that the material you are requesting is original to Nature Publishing Group and does not carry the copyright of another entity (as credited in the published version). If the credit line on any part of the material you have requested indicates that it was reprinted or adapted by NPG with permission from another source, then you should also seek permission from that source to reuse the material.

2. Permission granted free of charge for material in print is also usually granted for any electronic version of that work, provided that the material is incidental to the work as a whole and that the electronic version is essentially equivalent to, or substitutes for, the print version. Where print permission has been granted for a fee, separate permission must be obtained for any additional, electronic re-use (unless, as in the case of a full paper, this has already been accounted for during your initial request in the calculation of a print run). NB: In all cases, web-based use of full-text articles must be authorized separately through the 'Use on a Web Site' option when requesting permission.

3. Permission granted for a first edition does not apply to second and subsequent editions and for editions in other languages (except for signatories to the STM Permissions Guidelines, or where the first edition permission was granted for free).

4. Nature Publishing Group's permission must be acknowledged next to the figure, table or abstract in print. In electronic form, this acknowledgement must be visible at the same time as the figure/table/abstract, and must be hyperlinked to the journal's homepage.

5. The credit line should read:
   Reprinted by permission from Macmillan Publishers Ltd: [JOURNAL NAME] (reference citation), copyright (year of publication)
   For AOP papers, the credit line should read:
   Reprinted by permission from Macmillan Publishers Ltd: [JOURNAL NAME], advance online publication, day month year (doi: 10.1038/sj.[JOURNAL ACRONYM].XXXXX)

   **Note: For republication from the *British Journal of Cancer*, the following credit lines apply.**
   Reprinted by permission from Macmillan Publishers Ltd on behalf of Cancer Research UK: [JOURNAL NAME] (reference citation), copyright (year of publication) For AOP papers, the credit line should read:
   Reprinted by permission from Macmillan Publishers Ltd on behalf of Cancer Research UK: [JOURNAL NAME], advance online publication, day month year (doi: 10.1038/sj.[JOURNAL ACRONYM].XXXXX)

6. Adaptations of single figures do not require NPG approval. However, the adaptation should be credited as follows:

Adapted by permission from Macmillan Publishers Ltd: [JOURNAL NAME] (reference citation), copyright (year of publication)

**Note: For adaptation from the *British Journal of Cancer*, the following credit line applies.**
Adapted by permission from Macmillan Publishers Ltd on behalf of Cancer Research UK: [JOURNAL NAME] (reference citation), copyright (year of publication)

7. Translations of 401 words up to a whole article require NPG approval. Please visit http://www.macmillanmedicalcommunications.com for more information.
Translations of up to a 400 words do not require NPG approval. The translation should be credited as follows:

   Translated by permission from Macmillan Publishers Ltd: [JOURNAL NAME] (reference citation), copyright (year of publication).

   **Note: For translation from the *British Journal of Cancer*, the following credit line applies.**
   Translated by permission from Macmillan Publishers Ltd on behalf of Cancer Research UK: [JOURNAL NAME] (reference citation), copyright (year of publication)

We are certain that all parties will benefit from this agreement and wish you the best in the use of this material. Thank you.

Special Terms:

v1.1

**If you would like to pay for this license now, please remit this license along with your payment made payable to "COPYRIGHT CLEARANCE CENTER" otherwise you will be invoiced within 48 hours of the license date. Payment should be in the form of a check or money order referencing your account number and this invoice number RLNK501013977.**
**Once you receive your invoice for this order, you may pay your invoice by credit card. Please follow instructions provided at that time.**

**Make Payment To:**
**Copyright Clearance Center**
**Dept 001**
**P.O. Box 843006**
**Boston, MA 02284-3006**

**For suggestions or comments regarding this order, contact RightsLink Customer Support: customercare@copyright.com or +1-877-622-5543 (toll free in the US) or +1-978-646-2777.**

**Gratis licenses (referencing $0 in the Total field) are free. Please retain this printable license for your reference. No payment is required.**

# ELSEVIER LICENSE
# TERMS AND CONDITIONS

May 03, 2013

This is a License Agreement between Pelin Telkoparan ("You") and Elsevier ("Elsevier") provided by Copyright Clearance Center ("CCC"). The license consists of your order details, the terms and conditions provided by Elsevier, and the payment terms and conditions.

**All payments must be made in full to CCC. For payment instructions, please see information listed at the bottom of this form.**

| | |
|---|---|
| Supplier | Elsevier Limited<br>The Boulevard,Langford Lane<br>Kidlington,Oxford,OX5 1GB,UK |
| Registered Company Number | 1982084 |
| Customer name | Pelin Telkoparan |
| Customer address | Bilkent Universitesi Fen Fakultesi<br>ANKARA, 06680 |
| License number | 3141481267245 |
| License date | May 03, 2013 |
| Licensed content publisher | Elsevier |
| Licensed content publication | Seminars in Cell & Developmental Biology |
| Licensed content title | Cytokinetic abscission in animal cells |
| Licensed content author | Julien Guizetti,Daniel W. Gerlich |
| Licensed content date | December 2010 |
| Licensed content volume number | 21 |
| Licensed content issue number | 9 |
| Number of pages | 8 |
| Start Page | 909 |
| End Page | 916 |
| Type of Use | reuse in a thesis/dissertation |
| Intended publisher of new work | other |
| Portion | figures/tables/illustrations |
| Number of figures/tables/illustrations | 2 |
| Format | both print and electronic |
| Are you the author of this Elsevier article? | No |

| | |
|---|---|
| Will you be translating? | No |
| Order reference number | |
| Title of your thesis/dissertation | Characterization of the coiled-coil domain-containing protein 124 (Ccdc124) as a novel centrosome and midbody component involved in cytokinesis |
| Expected completion date | Jun 2013 |
| Estimated size (number of pages) | 120 |
| Elsevier VAT number | GB 494 6272 12 |
| Permissions price | 0.00 USD |
| VAT/Local Sales Tax | 0.0 USD / 0.0 GBP |
| Total | 0.00 USD |
| Terms and Conditions | |

## INTRODUCTION

1. The publisher for this copyrighted material is Elsevier. By clicking "accept" in connection with completing this licensing transaction, you agree that the following terms and conditions apply to this transaction (along with the Billing and Payment terms and conditions established by Copyright Clearance Center, Inc. ("CCC"), at the time that you opened your Rightslink account and that are available at any time at http://myaccount.copyright.com).

## GENERAL TERMS

2. Elsevier hereby grants you permission to reproduce the aforementioned material subject to the terms and conditions indicated.

3. Acknowledgement: If any part of the material to be used (for example, figures) has appeared in our publication with credit or acknowledgement to another source, permission must also be sought from that source. If such permission is not obtained then that material may not be included in your publication/copies. Suitable acknowledgement to the source must be made, either as a footnote or in a reference list at the end of your publication, as follows:

"Reprinted from Publication title, Vol /edition number, Author(s), Title of article / title of chapter, Pages No., Copyright (Year), with permission from Elsevier [OR APPLICABLE SOCIETY COPYRIGHT OWNER]." Also Lancet special credit - "Reprinted from The Lancet, Vol. number, Author(s), Title of article, Pages No., Copyright (Year), with permission from Elsevier."

4. Reproduction of this material is confined to the purpose and/or media for which permission is hereby given.

5. Altering/Modifying Material: Not Permitted. However figures and illustrations may be altered/adapted minimally to serve your work. Any other abbreviations, additions, deletions and/or any other alterations shall be made only with prior written authorization of Elsevier Ltd. (Please contact Elsevier at permissions@elsevier.com)

6. If the permission fee for the requested use of our material is waived in this instance, please be advised that your future requests for Elsevier materials may attract a fee.

7. Reservation of Rights: Publisher reserves all rights not specifically granted in the combination of (i) the license details provided by you and accepted in the course of this licensing transaction, (ii) these terms and conditions and (iii) CCC's Billing and Payment terms and conditions.

8. License Contingent Upon Payment: While you may exercise the rights licensed immediately upon issuance of the license at the end of the licensing process for the transaction, provided that you have disclosed complete and accurate details of your proposed use, no license is finally effective unless and until full payment is received from you (either by publisher or by CCC) as provided in CCC's Billing and Payment terms and conditions. If full payment is not received on a timely basis, then any license preliminarily granted shall be deemed automatically revoked and shall be void as if never granted. Further, in the event that you breach any of these terms and conditions or any of CCC's Billing and Payment terms and conditions, the license is automatically revoked and shall be void as if never granted. Use of materials as described in a revoked license, as well as any use of the materials beyond the scope of an unrevoked license, may constitute copyright infringement and publisher reserves the right to take any and all action to protect its copyright in the materials.

9. Warranties: Publisher makes no representations or warranties with respect to the licensed material.

10. Indemnity: You hereby indemnify and agree to hold harmless publisher and CCC, and their respective officers, directors, employees and agents, from and against any and all claims arising out of your use of the licensed material other than as specifically authorized pursuant to this license.

11. No Transfer of License: This license is personal to you and may not be sublicensed, assigned, or transferred by you to any other person without publisher's written permission.

12. No Amendment Except in Writing: This license may not be amended except in a writing signed by both parties (or, in the case of publisher, by CCC on publisher's behalf).

13. Objection to Contrary Terms: Publisher hereby objects to any terms contained in any purchase order, acknowledgment, check endorsement or other writing prepared by you, which terms are inconsistent with these terms and conditions or CCC's Billing and Payment terms and conditions. These terms and conditions, together with CCC's Billing and Payment terms and conditions (which are incorporated herein), comprise the entire agreement between you and publisher (and CCC) concerning this licensing transaction. In the event of any conflict between your obligations established by these terms and conditions and those established by CCC's Billing and Payment terms and conditions, these terms and conditions shall control.

14. Revocation: Elsevier or Copyright Clearance Center may deny the permissions described in this License at their sole discretion, for any reason or no reason, with a full refund payable to you. Notice of such denial will be made using the contact information provided by you. Failure to receive such notice will not alter or invalidate the denial. In no event will Elsevier or Copyright Clearance Center be responsible or liable for any costs, expenses or damage

incurred by you as a result of a denial of your permission request, other than a refund of the amount(s) paid by you to Elsevier and/or Copyright Clearance Center for denied permissions.

## LIMITED LICENSE

The following terms and conditions apply only to specific license types:

15. **Translation**: This permission is granted for non-exclusive world **English** rights only unless your license was granted for translation rights. If you licensed translation rights you may only translate this content into the languages you requested. A professional translator must perform all translations and reproduce the content word for word preserving the integrity of the article. If this license is to re-use 1 or 2 figures then permission is granted for non-exclusive world rights in all languages.

16. **Website**: The following terms and conditions apply to electronic reserve and author websites:
**Electronic reserve**: If licensed material is to be posted to website, the web site is to be password-protected and made available only to bona fide students registered on a relevant course if:
This license was made in connection with a course,
This permission is granted for 1 year only. You may obtain a license for future website posting,
All content posted to the web site must maintain the copyright information line on the bottom of each image,
A hyper-text must be included to the Homepage of the journal from which you are licensing at http://www.sciencedirect.com/science/journal/xxxxx or the Elsevier homepage for books at http://www.elsevier.com , and
Central Storage: This license does not include permission for a scanned version of the material to be stored in a central repository such as that provided by Heron/XanEdu.

17. **Author website** for journals with the following additional clauses:

All content posted to the web site must maintain the copyright information line on the bottom of each image, and the permission granted is limited to the personal version of your paper. You are not allowed to download and post the published electronic version of your article (whether PDF or HTML, proof or final version), nor may you scan the printed edition to create an electronic version. A hyper-text must be included to the Homepage of the journal from which you are licensing at http://www.sciencedirect.com/science/journal/xxxxx . As part of our normal production process, you will receive an e-mail notice when your article appears on Elsevier's online service ScienceDirect (www.sciencedirect.com). That e-mail will include the article's Digital Object Identifier (DOI). This number provides the electronic link to the published article and should be included in the posting of your personal version. We ask that you wait until you receive this e-mail and have the DOI to do any posting.

Central Storage: This license does not include permission for a scanned version of the material to be stored in a central repository such as that provided by Heron/XanEdu.

18. **Author website** for books with the following additional clauses:
Authors are permitted to place a brief summary of their work online only.

A hyper-text must be included to the Elsevier homepage at http://www.elsevier.com . All content posted to the web site must maintain the copyright information line on the bottom of each image. You are not allowed to download and post the published electronic version of your chapter, nor may you scan the printed edition to create an electronic version.

Central Storage: This license does not include permission for a scanned version of the material to be stored in a central repository such as that provided by Heron/XanEdu.

19. **Website** (regular and for author): A hyper-text must be included to the Homepage of the journal from which you are licensing at http://www.sciencedirect.com/science/journal/xxxxx. or for books to the Elsevier homepage at http://www.elsevier.com

20. **Thesis/Dissertation**: If your license is for use in a thesis/dissertation your thesis may be submitted to your institution in either print or electronic form. Should your thesis be published commercially, please reapply for permission. These requirements include permission for the Library and Archives of Canada to supply single copies, on demand, of the complete thesis and include permission for UMI to supply single copies, on demand, of the complete thesis. Should your thesis be published commercially, please reapply for permission.

21. **Other Conditions**:

v1.6

**If you would like to pay for this license now, please remit this license along with your payment made payable to "COPYRIGHT CLEARANCE CENTER" otherwise you will be invoiced within 48 hours of the license date. Payment should be in the form of a check or money order referencing your account number and this invoice number RLNK501013978.**
**Once you receive your invoice for this order, you may pay your invoice by credit card. Please follow instructions provided at that time.**

**Make Payment To:**
**Copyright Clearance Center**
**Dept 001**
**P.O. Box 843006**
**Boston, MA 02284-3006**

**For suggestions or comments regarding this order, contact RightsLink Customer Support: customercare@copyright.com or +1-877-622-5543 (toll free in the US) or +1-978-646-2777.**

**Gratis licenses (referencing $0 in the Total field) are free. Please retain this printable license for your reference. No payment is required.**

## NATURE PUBLISHING GROUP LICENSE TERMS AND CONDITIONS

May 03, 2013

This is a License Agreement between Pelin Telkoparan ("You") and Nature Publishing Group ("Nature Publishing Group") provided by Copyright Clearance Center ("CCC"). The license consists of your order details, the terms and conditions provided by Nature Publishing Group, and the payment terms and conditions.

**All payments must be made in full to CCC. For payment instructions, please see information listed at the bottom of this form.**

| | |
|---|---|
| License Number | 3141481486419 |
| License date | May 03, 2013 |
| Licensed content publisher | Nature Publishing Group |
| Licensed content publication | Nature Reviews Molecular Cell Biology |
| Licensed content title | Re-evaluating centrosome function |
| Licensed content author | Stephen Doxsey |
| Licensed content date | Sep 1, 2001 |
| Volume number | 2 |
| Issue number | 9 |
| Type of Use | reuse in a thesis/dissertation |
| Requestor type | academic/educational |
| Format | print and electronic |
| Portion | figures/tables/illustrations |
| Number of figures/tables/illustrations | 1 |
| Figures | Figure 1.4 |
| Author of this NPG article | no |
| Your reference number | |
| Title of your thesis / dissertation | Characterization of the coiled-coil domain-containing protein 124 (Ccdc124) as a novel centrosome and midbody component involved in cytokinesis |
| Expected completion date | Jun 2013 |
| Estimated size (number of pages) | 120 |
| Total | 0.00 USD |
| Terms and Conditions | |

### Terms and Conditions for Permissions

Nature Publishing Group hereby grants you a non-exclusive license to reproduce this

material for this purpose, and for no other use, subject to the conditions below:

1. NPG warrants that it has, to the best of its knowledge, the rights to license reuse of this material. However, you should ensure that the material you are requesting is original to Nature Publishing Group and does not carry the copyright of another entity (as credited in the published version). If the credit line on any part of the material you have requested indicates that it was reprinted or adapted by NPG with permission from another source, then you should also seek permission from that source to reuse the material.

2. Permission granted free of charge for material in print is also usually granted for any electronic version of that work, provided that the material is incidental to the work as a whole and that the electronic version is essentially equivalent to, or substitutes for, the print version. Where print permission has been granted for a fee, separate permission must be obtained for any additional, electronic re-use (unless, as in the case of a full paper, this has already been accounted for during your initial request in the calculation of a print run). NB: In all cases, web-based use of full-text articles must be authorized separately through the 'Use on a Web Site' option when requesting permission.

3. Permission granted for a first edition does not apply to second and subsequent editions and for editions in other languages (except for signatories to the STM Permissions Guidelines, or where the first edition permission was granted for free).

4. Nature Publishing Group's permission must be acknowledged next to the figure, table or abstract in print. In electronic form, this acknowledgement must be visible at the same time as the figure/table/abstract, and must be hyperlinked to the journal's homepage.

5. The credit line should read:
   Reprinted by permission from Macmillan Publishers Ltd: [JOURNAL NAME] (reference citation), copyright (year of publication)
   For AOP papers, the credit line should read:
   Reprinted by permission from Macmillan Publishers Ltd: [JOURNAL NAME], advance online publication, day month year (doi: 10.1038/sj.[JOURNAL ACRONYM].XXXXX)

   **Note: For republication from the *British Journal of Cancer*, the following credit lines apply.**
   Reprinted by permission from Macmillan Publishers Ltd on behalf of Cancer Research UK: [JOURNAL NAME] (reference citation), copyright (year of publication) For AOP papers, the credit line should read:
   Reprinted by permission from Macmillan Publishers Ltd on behalf of Cancer Research UK: [JOURNAL NAME], advance online publication, day month year (doi: 10.1038/sj.[JOURNAL ACRONYM].XXXXX)

6. Adaptations of single figures do not require NPG approval. However, the adaptation should be credited as follows:

Adapted by permission from Macmillan Publishers Ltd: [JOURNAL NAME] (reference citation), copyright (year of publication)

**Note: For adaptation from the *British Journal of Cancer*, the following credit line applies.**
Adapted by permission from Macmillan Publishers Ltd on behalf of Cancer Research UK: [JOURNAL NAME] (reference citation), copyright (year of publication)

7. Translations of 401 words up to a whole article require NPG approval. Please visit http://www.macmillanmedicalcommunications.com for more information.
Translations of up to a 400 words do not require NPG approval. The translation should be credited as follows:

   Translated by permission from Macmillan Publishers Ltd: [JOURNAL NAME] (reference citation), copyright (year of publication).

   **Note: For translation from the *British Journal of Cancer*, the following credit line applies.**
   Translated by permission from Macmillan Publishers Ltd on behalf of Cancer Research UK: [JOURNAL NAME] (reference citation), copyright (year of publication)

We are certain that all parties will benefit from this agreement and wish you the best in the use of this material. Thank you.

Special Terms:

v1.1

**If you would like to pay for this license now, please remit this license along with your payment made payable to "COPYRIGHT CLEARANCE CENTER" otherwise you will be invoiced within 48 hours of the license date. Payment should be in the form of a check or money order referencing your account number and this invoice number RLNK501013982.**
**Once you receive your invoice for this order, you may pay your invoice by credit card. Please follow instructions provided at that time.**

**Make Payment To:**
**Copyright Clearance Center**
**Dept 001**
**P.O. Box 843006**
**Boston, MA 02284-3006**

**For suggestions or comments regarding this order, contact RightsLink Customer Support: customercare@copyright.com or +1-877-622-5543 (toll free in the US) or +1-978-646-2777.**

**Gratis licenses (referencing $0 in the Total field) are free. Please retain this printable license for your reference. No payment is required.**

# ELSEVIER LICENSE
# TERMS AND CONDITIONS

May 03, 2013

This is a License Agreement between Pelin Telkoparan ("You") and Elsevier ("Elsevier") provided by Copyright Clearance Center ("CCC"). The license consists of your order details, the terms and conditions provided by Elsevier, and the payment terms and conditions.

**All payments must be made in full to CCC. For payment instructions, please see information listed at the bottom of this form.**

| | |
|---|---|
| Supplier | Elsevier Limited<br>The Boulevard,Langford Lane<br>Kidlington,Oxford,OX5 1GB,UK |
| Registered Company Number | 1982084 |
| Customer name | Pelin Telkoparan |
| Customer address | Bilkent Universitesi Fen Fakultesi<br>ANKARA, 06680 |
| License number | 3141490144868 |
| License date | May 03, 2013 |
| Licensed content publisher | Elsevier |
| Licensed content publication | Cell |
| Licensed content title | Cytokinesis: Placing and Making the Final Cut |
| Licensed content author | Francis A. Barr,Ulrike Gruneberg |
| Licensed content date | 30 November 2007 |
| Licensed content volume number | 131 |
| Licensed content issue number | 5 |
| Number of pages | 14 |
| Start Page | 847 |
| End Page | 860 |
| Type of Use | reuse in a thesis/dissertation |
| Intended publisher of new work | other |
| Portion | figures/tables/illustrations |
| Number of figures/tables/illustrations | 1 |
| Format | both print and electronic |
| Are you the author of this Elsevier article? | No |

| | |
|---|---|
| Will you be translating? | No |
| Order reference number | |
| Title of your thesis/dissertation | Characterization of the coiled-coil domain-containing protein 124 (Ccdc124) as a novel centrosome and midbody component involved in cytokinesis |
| Expected completion date | Jun 2013 |
| Estimated size (number of pages) | 120 |
| Elsevier VAT number | GB 494 6272 12 |
| Permissions price | 0.00 USD |
| VAT/Local Sales Tax | 0.0 USD / 0.0 GBP |
| Total | 0.00 USD |
| Terms and Conditions | |

## INTRODUCTION

1. The publisher for this copyrighted material is Elsevier. By clicking "accept" in connection with completing this licensing transaction, you agree that the following terms and conditions apply to this transaction (along with the Billing and Payment terms and conditions established by Copyright Clearance Center, Inc. ("CCC"), at the time that you opened your Rightslink account and that are available at any time at http://myaccount.copyright.com).

## GENERAL TERMS

2. Elsevier hereby grants you permission to reproduce the aforementioned material subject to the terms and conditions indicated.

3. Acknowledgement: If any part of the material to be used (for example, figures) has appeared in our publication with credit or acknowledgement to another source, permission must also be sought from that source. If such permission is not obtained then that material may not be included in your publication/copies. Suitable acknowledgement to the source must be made, either as a footnote or in a reference list at the end of your publication, as follows:

"Reprinted from Publication title, Vol /edition number, Author(s), Title of article / title of chapter, Pages No., Copyright (Year), with permission from Elsevier [OR APPLICABLE SOCIETY COPYRIGHT OWNER]." Also Lancet special credit - "Reprinted from The Lancet, Vol. number, Author(s), Title of article, Pages No., Copyright (Year), with permission from Elsevier."

4. Reproduction of this material is confined to the purpose and/or media for which permission is hereby given.

5. Altering/Modifying Material: Not Permitted. However figures and illustrations may be altered/adapted minimally to serve your work. Any other abbreviations, additions, deletions and/or any other alterations shall be made only with prior written authorization of Elsevier Ltd. (Please contact Elsevier at permissions@elsevier.com)

6. If the permission fee for the requested use of our material is waived in this instance, please be advised that your future requests for Elsevier materials may attract a fee.

7. Reservation of Rights: Publisher reserves all rights not specifically granted in the combination of (i) the license details provided by you and accepted in the course of this licensing transaction, (ii) these terms and conditions and (iii) CCC's Billing and Payment terms and conditions.

8. License Contingent Upon Payment: While you may exercise the rights licensed immediately upon issuance of the license at the end of the licensing process for the transaction, provided that you have disclosed complete and accurate details of your proposed use, no license is finally effective unless and until full payment is received from you (either by publisher or by CCC) as provided in CCC's Billing and Payment terms and conditions. If full payment is not received on a timely basis, then any license preliminarily granted shall be deemed automatically revoked and shall be void as if never granted. Further, in the event that you breach any of these terms and conditions or any of CCC's Billing and Payment terms and conditions, the license is automatically revoked and shall be void as if never granted. Use of materials as described in a revoked license, as well as any use of the materials beyond the scope of an unrevoked license, may constitute copyright infringement and publisher reserves the right to take any and all action to protect its copyright in the materials.

9. Warranties: Publisher makes no representations or warranties with respect to the licensed material.

10. Indemnity: You hereby indemnify and agree to hold harmless publisher and CCC, and their respective officers, directors, employees and agents, from and against any and all claims arising out of your use of the licensed material other than as specifically authorized pursuant to this license.

11. No Transfer of License: This license is personal to you and may not be sublicensed, assigned, or transferred by you to any other person without publisher's written permission.

12. No Amendment Except in Writing: This license may not be amended except in a writing signed by both parties (or, in the case of publisher, by CCC on publisher's behalf).

13. Objection to Contrary Terms: Publisher hereby objects to any terms contained in any purchase order, acknowledgment, check endorsement or other writing prepared by you, which terms are inconsistent with these terms and conditions or CCC's Billing and Payment terms and conditions. These terms and conditions, together with CCC's Billing and Payment terms and conditions (which are incorporated herein), comprise the entire agreement between you and publisher (and CCC) concerning this licensing transaction. In the event of any conflict between your obligations established by these terms and conditions and those established by CCC's Billing and Payment terms and conditions, these terms and conditions shall control.

14. Revocation: Elsevier or Copyright Clearance Center may deny the permissions described in this License at their sole discretion, for any reason or no reason, with a full refund payable to you. Notice of such denial will be made using the contact information provided by you. Failure to receive such notice will not alter or invalidate the denial. In no event will Elsevier or Copyright Clearance Center be responsible or liable for any costs, expenses or damage

incurred by you as a result of a denial of your permission request, other than a refund of the amount(s) paid by you to Elsevier and/or Copyright Clearance Center for denied permissions.

## LIMITED LICENSE

The following terms and conditions apply only to specific license types:

15. **Translation**: This permission is granted for non-exclusive world **English** rights only unless your license was granted for translation rights. If you licensed translation rights you may only translate this content into the languages you requested. A professional translator must perform all translations and reproduce the content word for word preserving the integrity of the article. If this license is to re-use 1 or 2 figures then permission is granted for non-exclusive world rights in all languages.

16. **Website**: The following terms and conditions apply to electronic reserve and author websites:
**Electronic reserve**: If licensed material is to be posted to website, the web site is to be password-protected and made available only to bona fide students registered on a relevant course if:
This license was made in connection with a course,
This permission is granted for 1 year only. You may obtain a license for future website posting,
All content posted to the web site must maintain the copyright information line on the bottom of each image,
A hyper-text must be included to the Homepage of the journal from which you are licensing at http://www.sciencedirect.com/science/journal/xxxxx or the Elsevier homepage for books at http://www.elsevier.com , and
Central Storage: This license does not include permission for a scanned version of the material to be stored in a central repository such as that provided by Heron/XanEdu.

17. **Author website** for journals with the following additional clauses:

All content posted to the web site must maintain the copyright information line on the bottom of each image, and the permission granted is limited to the personal version of your paper. You are not allowed to download and post the published electronic version of your article (whether PDF or HTML, proof or final version), nor may you scan the printed edition to create an electronic version. A hyper-text must be included to the Homepage of the journal from which you are licensing at http://www.sciencedirect.com/science/journal/xxxxx . As part of our normal production process, you will receive an e-mail notice when your article appears on Elsevier's online service ScienceDirect (www.sciencedirect.com). That e-mail will include the article's Digital Object Identifier (DOI). This number provides the electronic link to the published article and should be included in the posting of your personal version. We ask that you wait until you receive this e-mail and have the DOI to do any posting.

Central Storage: This license does not include permission for a scanned version of the material to be stored in a central repository such as that provided by Heron/XanEdu.

18. **Author website** for books with the following additional clauses:
Authors are permitted to place a brief summary of their work online only.

A hyper-text must be included to the Elsevier homepage at http://www.elsevier.com . All content posted to the web site must maintain the copyright information line on the bottom of each image. You are not allowed to download and post the published electronic version of your chapter, nor may you scan the printed edition to create an electronic version.

Central Storage: This license does not include permission for a scanned version of the material to be stored in a central repository such as that provided by Heron/XanEdu.

19. **Website** (regular and for author): A hyper-text must be included to the Homepage of the journal from which you are licensing at http://www.sciencedirect.com/science/journal/xxxxx. or for books to the Elsevier homepage at http://www.elsevier.com

20. **Thesis/Dissertation**: If your license is for use in a thesis/dissertation your thesis may be submitted to your institution in either print or electronic form. Should your thesis be published commercially, please reapply for permission. These requirements include permission for the Library and Archives of Canada to supply single copies, on demand, of the complete thesis and include permission for UMI to supply single copies, on demand, of the complete thesis. Should your thesis be published commercially, please reapply for permission.

21. **Other Conditions**:

v1.6

**If you would like to pay for this license now, please remit this license along with your payment made payable to "COPYRIGHT CLEARANCE CENTER" otherwise you will be invoiced within 48 hours of the license date. Payment should be in the form of a check or money order referencing your account number and this invoice number RLNK501013984.**
**Once you receive your invoice for this order, you may pay your invoice by credit card. Please follow instructions provided at that time.**

**Make Payment To:**
**Copyright Clearance Center**
**Dept 001**
**P.O. Box 843006**
**Boston, MA 02284-3006**

**For suggestions or comments regarding this order, contact RightsLink Customer Support: customercare@copyright.com or +1-877-622-5543 (toll free in the US) or +1-978-646-2777.**

**Gratis licenses (referencing $0 in the Total field) are free. Please retain this printable license for your reference. No payment is required.**

## Order Completed

Thank you very much for your order.

This is a License Agreement between Pelin Telkoparan ("You") and Annual Reviews, Inc ("Annual Reviews, Inc") The license consists of your order details, the terms and conditions provided by Annual Reviews, Inc, and the payment terms and conditions.

| | |
|---|---|
| License number | Reference confirmation email for license number |
| License date | May 03, 2013 |
| Licensed content publisher | Annual Reviews, Inc |
| Licensed content title | ANNUAL REVIEW OF CELL AND DEVELOPMENTAL BIOLOGY |
| Licensed content date | Jan 1, 1995 |
| Type of use | Thesis/Dissertation |
| Requestor type | Author of requested content |
| Format | Print, Electronic |
| Portion | image/photo |
| Number of images/photos requested | 1 |
| Title or numeric reference of the portion(s) | Chapter 1 Figure 1.7 |
| Editor of portion(s) | N/A |
| Author of portion(s) | Pelin Telkoparan |
| Volume of serial or monograph | N/A |
| Page range of portion | 120 |
| Publication date of portion | Jun/2013 |
| Rights for | Main product |
| Duration of use | Life of current edition |
| Creation of copies for the disabled | no |
| With minor editing privileges | no |
| For distribution to | Other territories and/or countries |
| Territory/Countries where you intend to distribute new product | TURKEY |
| In the following language(s) | Original language of publication |
| With incidental promotional use | no |
| Lifetime unit quantity of new product | 0 to 499 |
| Made available in the following markets | education |

| | |
|---|---|
| The requesting person/organization | Pelin Telkoparan |
| Order reference number | |
| Author/Editor | Pelin Telkoparan |
| The standard identifier | PT14031982 |
| Title | Characterization of the coiled-coil domain-containing protein 124 (Ccdc124) as a novel centrosome and midbody component involved in cytokinesis |
| Publisher | Bilkent University |
| Expected publication date | Jun 2013 |
| Estimated size (pages) | 120 |
| Billing Type | Invoice |
| Billing address | Bilkent Universitesi Fen Fakultesi<br>Molekuler Biyologi ve Genetik Bolumu<br>ANKARA, 06680<br>Turkey |
| Total (may include CCC user fee) | 0.00 USD |

CLOSE WINDOW